

# A biophysical model for the Marlborough Sounds

Part 1: Queen Charlotte Sound and Tory Channel

*Prepared for Marlborough District Council*

*September 2014*

Prepared by:  
Mark Hadfield  
Niall Broekhuizen  
David Plew

For any information regarding this report please contact:

Niall Broekhuizen  
Ecological Modeller  
Coastal & Estuarine Processes  
+64-7-856 1798  
niall.broekhuizen@niwa.co.nz

National Institute of Water & Atmospheric Research Ltd  
10 Kyle Street  
Riccarton  
Christchurch 8011

Phone +64 3 348 8987

NIWA CLIENT REPORT No: CHC2014-116  
Report date: September 2014  
NIWA Project: MDC13301

---

© All rights reserved. This publication may not be reproduced or copied in any form without the permission of the copyright owner(s). Such permission is only to be given in accordance with the terms of the client's contract with NIWA. This copyright extends to all forms of copying and any storage of material in any kind of information retrieval system.

Whilst NIWA has used all reasonable endeavours to ensure that the information contained in this document is accurate, NIWA does not give any express or implied warranty as to the completeness of the information contained herein, or that it will be suitable for any purpose(s) other than those specifically contemplated during the Project or agreed by NIWA and the Client.

# Contents

<b>Executive summary .....</b>	<b>8</b>
<b>1 Introduction .....</b>	<b>13</b>
1.1 Background .....	13
1.2 Definition of a biophysical model .....	13
1.3 Scope of the project.....	14
1.4 Outline of this report .....	14
<b>2 Hydrodynamic model: Methods .....</b>	<b>16</b>
2.1 Model description.....	16
2.2 Model grids and bathymetry .....	16
2.3 Initial and boundary conditions.....	19
2.4 Hydrodynamic field data.....	22
<b>3 Hydrodynamic model: Results .....</b>	<b>24</b>
3.1 Model vs observations: temperature and salinity.....	24
3.2 Model vs observations: tidal height fluctuations .....	30
3.3 Model vs observations: tidal currents .....	31
3.4 Model vs observations: sub-tidal currents .....	34
3.5 Currents and volume fluxes .....	39
3.6 Effect of model resolution on Tory Channel tidal flow.....	46
3.7 Flushing.....	48
3.8 Hydrodynamic model summary.....	55
<b>4 Biophysical model: Methods .....</b>	<b>58</b>
4.1 Model description.....	58
4.2 Representing the spatial distribution of the mussel crop .....	60
4.3 Representing the spatial distribution of fish farms .....	62
4.4 Water quality data .....	64
4.5 Initial conditions .....	66
4.6 Model calibration.....	66
4.7 Cook Strait boundary data .....	66
4.8 Catchment Boundary Conditions.....	68
4.9 Simulation scenarios.....	68

4.10	Analysis and presentation of biophysical model simulation results.....	68
<b>5</b>	<b>Biophysical model: Results .....</b>	<b>72</b>
5.1	Biophysical results: existing conditions .....	72
5.2	Comparisons of simulation results with calibration field data.....	73
5.3	Simulations of the influence of existing mussel farming and existing mussel+fish farming (with benthic denitrification) .....	78
5.4	Simulations of the influence of combined mussel & fish farming activities under 2012 occupation and approved occupation .....	83
5.5	Influence of denitrification .....	86
5.6	Total nitrogen under each scenario.....	91
<b>6</b>	<b>Biophysical model: Discussion .....</b>	<b>93</b>
6.1	Performance of the biophysical model.....	93
6.2	Limitations of the biophysical model.....	94
6.3	Implications of the biophysical modelling results: putting the changes in context.....	96
6.4	Biophysical modelling: summary of conclusions .....	98
<b>7</b>	<b>Deposition modelling.....</b>	<b>100</b>
7.1	Methods.....	100
7.2	Analysis and presentation of deposition model results .....	101
7.3	Deposition modelling: Results .....	101
7.4	Summary & Conclusions .....	103
<b>8</b>	<b>Acknowledgements .....</b>	<b>104</b>
<b>9</b>	<b>Glossary of abbreviations and terms .....</b>	<b>105</b>
<b>10</b>	<b>References.....</b>	<b>106</b>
<b>Appendix A</b>	<b>Mathematical description of the Fennel NPZD model .....</b>	<b>110</b>
<b>Appendix B</b>	<b>Mathematical description of the mussel farm model .....</b>	<b>115</b>
<b>Appendix C</b>	<b>Mathematical description of the fish farm model .....</b>	<b>119</b>
<b>Appendix D</b>	<b>Fish feed inputs .....</b>	<b>125</b>
<b>Appendix E</b>	<b>Hydrodynamic model vs observations: additional graphs and tables .....</b>	<b>126</b>
<b>Appendix F</b>	<b>Time-series of simulated water quality at the Marlborough District Council sampling sites under differing scenarios. ....</b>	<b>134</b>

<b>Appendix G</b>	<b>Enlarged images of simulation results .....</b>	<b>139</b>
	<b>Comparison of <i>no farms, existing mussel farms</i> and <i>existing mussel+fish farms</i> (with denitrification) .....</b>	<b>141</b>
	Winter .....	141
	Summer .....	148
	<b>Comparison of <i>no farms, existing farms</i> and <i>approved mussel+fish farms</i> (with denitrification) .....</b>	<b>155</b>
	Winter .....	155
	Summer .....	162
	<b>Comparison of <i>no farms, existing farms</i> and <i>approved farms</i> (without denitrification) .....</b>	<b>169</b>
	Winter .....	169
	Summer .....	176

## Tables

Table 2-1:	Grid resolution and execution time.	18
Table 3-1:	Comparison of M2 tidal sea level parameters.	31
Table 3-2:	Equilibrium flushing times and dilution rates for Queen Charlotte Sound.	51
Table 4-1:	Water-quality variables measured for Marlborough District Council.	65
Table 4-2:	Means by which the field-data were used to derive analogue values for the model state-values.	69
Table 7-1:	Assumptions regarding composition of fish feed and assimilation of fish feed for deposition modelling.	100
Table 10-1:	Coefficients of the Fennel module.	111
Table 10-2:	Coefficients required to link the Fennel NPZD model and the Ren mussel physiology model.	114
Table 10-3:	Coefficients for the fish physiology module.	122
Table E-1:	S2 tidal height parameters.	128
Table E-2:	N2 tidal height parameters.	128
Table E-3:	O1 tidal height parameters.	128
Table E-4:	Comparison of M2tidal ellipse parameters.	132
Table E-5:	Comparison of S2 tidal ellipse parameters.	132
Table E-6:	Comparison of N2 tidal ellipse parameters.	132
Table E-7:	Comparison of O1 tidal ellipse parameters.	133
Table E-8:	Sub-tidal velocity comparison.	133

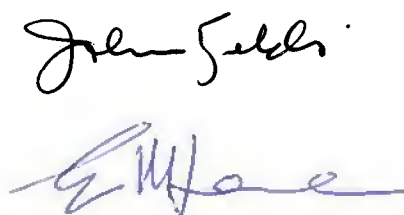
## Figures

Figure 2-1:	The Queen Charlotte Sound model domain and bathymetry.	17
Figure 2-2:	The Queen Charlotte Sound and Cook Strait model boundaries.	20

Figure 2-3:	Surface freshwater flux.	22
Figure 2-4:	Location of moorings and sampling stations for hydrodynamic measurements.	23
Figure 3-1:	Observed and modelled temperature time series.	25
Figure 3-2:	Observed and modelled temperature profiles.	27
Figure 3-3:	Observed and modelled salinity time series.	28
Figure 3-4:	Observed and modelled salinity profiles.	30
Figure 3-5:	M2 tidal velocity comparison (Queen Charlotte Outer).	32
Figure 3-6:	M2 tidal velocity comparison (Tory Channel).	33
Figure 3-7:	M2 tidal velocity profile comparison (Queen Charlotte Outer).	33
Figure 3-8:	M2 tidal velocity profile comparison (Tory Channel).	34
Figure 3-9:	Sub-tidal velocity vector comparison (Queen Charlotte Outer).	35
Figure 3-10:	Sub-tidal along-channel and across-channel velocity comparisons (Queen Charlotte Outer).	36
Figure 3-11:	Sub-tidal velocity vector comparison (Tory Channel).	37
Figure 3-12:	Sub-tidal along-channel and across-channel velocity comparisons (Tory Channel).	38
Figure 3-13:	Along-channel mean velocity profile comparison (Queen Charlotte Outer).	39
Figure 3-14:	Model mean current speed.	40
Figure 3-15:	Location of sections used for volume-flux calculations.	41
Figure 3-16:	Tidal volume fluxes.	42
Figure 3-17:	Sub-tidal volume fluxes.	43
Figure 3-18:	Sub-tidal volume flux <i>versus</i> surface stress.	44
Figure 3-19:	Sub-tidal volume flux compared with the prediction from the surface stress.	44
Figure 3-20:	Velocity through cross-channel sections.	45
Figure 3-21:	Semi-major amplitude of M2 tidal currents in Tory Channel vs model resolution.	47
Figure 3-22:	Mean currents forced by rectification of the M2 tide in Tory Channel vs model resolution.	48
Figure 3-23:	Location of passive tracer sources in the flushing simulations.	49
Figure 3-24:	Accumulation of tracer from the 200 m flushing simulation.	51
Figure 3-25:	Effect of model resolution on flushing.	52
Figure 3-26:	Equilibrium concentration for Grove Arm tracers.	53
Figure 3-27:	Equilibrium concentration for Outer Queen Charlotte Sound tracers.	54
Figure 3-28:	Equilibrium concentration for Tory Channel tracers.	55
Figure 4-1:	Map showing the depiction of mussel farms within the biophysical model grid.	62
Figure 4-2:	Map showing the locations of the five fish farms.	64
Figure 4-3:	Map illustrating the locations of Marlborough District Council (green) and New Zealand King Salmon (blue) water-quality sampling sites.	67
Figure 5-1:	Time-series of measured and simulated water-quality characteristics at station QCS-1.	74
Figure 5-2:	Time-series of measured and simulated water-quality characteristics at station QCS-2.	75

Figure 5-3:	Time-series of measured and simulated water-quality characteristics at station QCS-3.	76
Figure 5-4:	Time-series of measured and simulated water-quality characteristics at station QCS-4.	77
Figure 5-5:	Time-series of measured and simulated water-quality characteristics at station QCS-5.	78
Figure 5-6:	Winter-period time averaged absolute and relative concentration for the no farms, existing mussel farms and existing mussel+fish farms scenarios.	80
Figure 5-7:	Summer-period time averaged absolute and relative concentration for the no farms, existing mussel farms and existing mussel+fish farms scenarios.	82
Figure 5-8:	Winter-period time averaged absolute and relative concentration for the no farms, existing mussel+fish farms and the approved mussel+fish farms scenarios.	84
Figure 5-9:	Summer-period time averaged absolute and relative concentration for the no farms, existing mussel+fish farms and the approved mussel+fish farms scenarios.	85
Figure 5-10:	Winter-period time averaged absolute and relative concentration for the <i>no farms with denitrification, no farms without denitrification and approved farms without denitrification scenarios.</i>	89
Figure 5-11:	Summer-period time averaged absolute and relative concentration for the <i>no farms with denitrification, no farms without denitrification and approved farms without denitrification scenarios.</i>	90
Figure 5-12:	Time averaged concentration of total nitrogen TN under some of the scenarios that we have simulated.	92
Figure 7-1:	False colour plots of the simulated rates of fish faeces deposition ( $\text{g C m}^{-2} \text{d}^{-1}$ ) around each farm.	103
Figure D-1:	Histogram of monthly feed inputs provided by New Zealand King Salmon for their existing farms.	125
Figure E-1:	Temperature comparison.	126
Figure E-2:	Salinity comparison.	127
Figure E-3:	S2 tidal velocity comparison.	129
Figure E-4:	N2 tidal velocity comparison.	130
Figure E-5:	O1 tidal velocity comparison.	131

Reviewed by



Approved for release by



## Executive summary

The Marlborough District Council commissioned NIWA to undertake biophysical modelling of the Queen Charlotte and Pelorus Sounds. The purpose of the modelling was to describe effects of existing and proposed mussel and fish farms on water quality. This report presents results for Queen Charlotte Sound and Tory Channel. Results for Pelorus Sound will be presented in a subsequent report.

The biophysical model consists of a three-dimensional hydrodynamic model (with 20 layers in the vertical) coupled to a biogeochemical model (which models water quality, plankton, and other biological and chemical attributes). We used the ROMS hydrodynamic model with the Fennel biogeochemical model, with additional components added to simulate mussel and fish farms. The biogeochemical model includes: (a) the inorganic nutrients ammonium and nitrate, (b) a single phytoplankton class, (c) a single zooplankton class and (d) two classes of particulate organic detritus (slow and fast sinking). The abundances of most of these are characterized by means of nitrogen concentration, but the phytoplankton is characterized by two variables: nitrogen concentration and chlorophyll concentration.

Three farming/biogeochemical scenarios were modelled:

- *Present day/existing farms scenario*: mussel farms in operation in 2012 (counted by aerial-surveys), and New Zealand King Salmon Ltd. Salmon farms that operated during 2012/2013.
- *Approved farms*: as for the *present day* scenario, but also including the one newly approved salmon farm in Tory channel (*Ngamahau*) and mussel farms which have been approved (or which existed, but were not occupied) at the time of the aerial survey.
- *Worst case*: as for *approved farms*, but ignoring the losses of nitrogen from the marine system that arise from denitrification. The *present day* and *approved farms* scenarios both assume that 75% of any particulate organic nitrogen (from any source) which settles to the bed will be lost from the system through denitrification (whilst the remaining 25% is returned to the water column as ammonium). In the *worst-case* scenario, none of the sedimenting particulate organic nitrogen is lost from the system. It is all returned to the water column as ammonium.

Additional scenarios were modelled with *no farms* and with *mussel farms only* in order to provide a baseline for assessing farm impact, and for comparing the relative influence of mussel farms and fish farms.

Simulations spanned 500 days (24 May 2012 to 6 October 2013), consisting of a 135 day spin-up period followed by 365 days (1 year) over which the model outputs were analysed.

Horizontal grid resolutions from 50 m to 400 m were tested. Finer resolution grids provide greater detail of the spatial distributions of both physical (hydrodynamic) and biogeochemical properties, but the simulations take significantly more time to run (halving the size between grid points increases the computation time by a factor of approximately 8). The 200 m model reproduces the essential aspects of the hydrodynamics of Queen Charlotte Sound with acceptable accuracy and allows simulations with the full biophysical model for periods of over one year. The 200 m resolution grid was used when making the biophysical simulations reported within this document.



The hydrodynamic model was compared to current meter data from Tory Channel and Outer Queen Charlotte Sound. Modelled temperature and salinity are compared with time-series measured at two depths from these sites and also in Inner Queen Charlotte Sound, as well as with monthly profiles of temperature and salinity collected by Marlborough District Council.

Analysis of the hydrodynamic model output allows us to make the following conclusions about the physical behaviour of the Sound.

- The Inner and Outer Queen Charlotte Sound exhibit a seasonal stratification, while Tory Channel remains well mixed year round.
- The tidal volume fluxes through Tory Channel are large, at around 20,000 m<sup>3</sup>s<sup>-1</sup> at neap tide and 30,000 m<sup>3</sup>s<sup>-1</sup> at spring tide. The large tidal flows through Tory Channel maintain a vertically well-mixed state and allow it to act as a conduit for bi-directional exchange between central Queen Charlotte Sound and Cook Strait.
- There is a sub-tidal flow, typically inwards through Tory Channel and outwards through the outer Queen Charlotte Sound (i.e. clockwise around Arapawa Island) that varies from extremes of -2000 m<sup>3</sup> s<sup>-1</sup> to +6000 m<sup>3</sup> s<sup>-1</sup>. Short term (5–10 day) fluctuations in this flow are largely driven by wind, with winds from the SSW driving a positive (clockwise around Arapawa Island) flow. This sub-tidal inflow through Tory Channel will aid the movement of water from Cook Strait into central Queen Charlotte Sound.
- The sub-tidal flow described above averaged over the final year of the simulation is 660 m<sup>3</sup> s<sup>-1</sup> but there is a slow variation between less than 500 m<sup>3</sup> s<sup>-1</sup> in winter to 1800 m<sup>3</sup> s<sup>-1</sup> in early autumn. This variation does not appear to be related to wind, but might be related to the seasonal variation in temperature and salinity.
- The model produces a well-defined estuarine circulation in Queen Charlotte Sound consistent with observations from mooring data from the Outer Queen Charlotte Sound. No estuarine circulation is seen in Tory Channel.
- Particularly in summer, Tory Channel water is cooler and more saline – and hence denser – than surface water in the Queen Charlotte Sound. Tory Channel water will therefore tend to move into the lower, inflowing layer of the estuarine circulation in Queen Charlotte Sound and move into the inner Sound before it is mixed to the surface and transported back outwards through inner and outer Queen Charlotte Sound.
- The flushing behaviour of Queen Charlotte Sound has been investigated with idealised tracer sources in three locations. Flushing time is an indication of how long it takes for water within a region to be replaced. The flushing time (Table 3-2) varies from ~40 days for tracer released in Inner QCS to only 10.9 days for tracer released in central Tory Channel. The flushing time for the tracers released in Inner and Outer QCS varies seasonally, being larger in winter than summer, owing to a seasonally varying estuarine circulation taking surface water out of the Sound.

We calibrated the biophysical model against three years of water-quality data which have been collected from five stations in the Marlborough Sounds by Marlborough District Council. The calibrated model reproduces the annual average water-quality characteristics at all stations very well. It also reproduces the amplitude of the annual phytoplankton cycles well, but at the two inner-

most stations (in Inner QCS), it suggests that the phytoplankton have a single (mid-summer) abundance maximum. In contrast, the field data suggest that there are two maxima during the year, in late winter/early spring and in late summer/early autumn. In Tory Channel and outer Queen Charlotte (where the farms are, and where the farm effects are likely to be most marked) the model reproduces the phase of the seasonal cycles better. There, however the model shows peak phytoplankton abundance in early/mid-summer, whereas the field data show it occurs in late summer/early autumn.

Under the assumption that benthic denitrification removes 75% of all sedimenting particulate organic nitrogen, the biophysical model predicts that:

- Mussel farming induces bay-scale effects where the concentrations of phytoplankton and detritus decrease whilst the concentration of ammonium tends to be elevated. These effects amount to a few percent (up to circa 15%) of *background* concentrations. In summer, the remineralized ammonium from the mussels can stimulate moderate (a few percent) increases in phytoplankton and detrital abundances in the far-field (beyond the bays in which the farms are found).
- Fish farming induces effects which extend through the entire Queen Charlotte Sound system during the summer, but are of more limited spatial extent during winter. Except very close to the farms, the effects do not exceed 20% of background in summer and 30% in winter. These are smaller than natural variability.
- The majority of the farm-derived nutrient is predicted to be lost from the system by export to Cook Strait rather than by denitrification in the seabed.

In simulations when we assumed that there is no denitrification in the *worst case* scenario) (i.e. that all sedimenting particulate organic nitrogen is returned to the water column as ammonium), the model shows:

- *no-farms, no denitrification* – summertime phytoplankton concentrations increase by a margin of approximately 10% (outer Queen Charlotte) – 40% (inner Queen Charlotte) relative to the *no-farms+denitrification* baseline. Summertime zooplankton concentrations increase by a margin of 20–100%.
- *approved mussel and fish farms, no denitrification* – summertime phytoplankton increase by margins of 20-60% (relative to *no farms with denitrification*) whilst zooplankton increase by 50-300%. Changes (of smaller magnitude) are also evident in the concentrations of nutrients and detritus.

Given that denitrification is a benthic process, the fact that the relative changes in concentrations tend to be greatest in the shallow side bays and shallow inner Queen Charlotte is not surprising.

Whilst the model does predict that fish farming will yield increased nutrient and phytoplankton concentrations, the resultant elevated concentrations are not alarmingly high. They are not atypical of New Zealand coastal waters and the time-averaged simulated concentrations do not exceed levels that have been measured in the Sounds on some occasions. Similarly, whilst mussel-induced plankton depletion is larger than we initially anticipated, we do not regard it as alarmingly severe.

The changes in nutrient and plankton concentrations are small in comparison to natural variability but are chronic in nature. We cannot entirely discount the possibility of a longer-term evolution

towards eutrophy whether by persistent and substantially increased phytoplankton or changes elsewhere in the food-web. However, the modelling indicates that winter-time light limitation acts as a 'bottleneck', which combined with relatively rapid flushing and benthic denitrification make it unlikely that the system will undergo extreme changes in response to the levels of farming presently permitted in this system.

The Board of Inquiry which approved the new Ngamahau salmon farm imposed numerous consent conditions. Amongst these was a ruling that the Sounds water quality should not be allowed to move significantly towards a eutrophic state. In that context, eutrophy was defined to be chlorophyll concentrations that were persistently (annual average) above 5 mg chl m<sup>-3</sup> over a large area. The model indicates that this threshold will not be exceeded even under our worst-case scenario (*approved farms, no denitrification*).

Whilst we believe that the inferences that we draw from our modelling are robust, we caution that almost no sensitivity trials have been undertaken to justify that belief. We therefore recommend that further sensitivity trials be undertaken to determine the degree to which the model predictions are robust against assumptions regarding:

- Sinking speed of fish and mussel faeces (introduce a third detrital class specifically for these very fast sinking materials)
- Light attenuation (what happens if we take better account of the differential attenuation of different wavelengths, and topographic shading?)
- Formulation of the zooplankton mortality term
- Our decision to assume that real-world dissolved organic nitrogen is biologically inert
- Sensitivity to Cook Strait boundary conditions

We described the deposition footprints of the five fish farms in Tory Channel/Queen Charlotte (namely: Te Pangu, Clay Point, Ngamahau, Ruakaka & Otanerau) using a particle-tracking model driven by the 3D hydrodynamic simulations on a 100 m horizontal resolution grid. The model predicted that farm-derived particulates settle to the seabed rapidly (within minutes). Thus, dispersal of the farm-derived waste is driven by tidal currents rather than longer-term residual flow patterns.

Tidal speeds are higher around the three farms in Tory Channel (Clay Point, Te Pangu and Ngamahau) than around Ruakaka or Otanerau. Thus, the benthic footprints of the latter two farms are less extensive. At present, there are no direct measurements of deposition rates at any of these farms, but the predicted rates at the pen perimeter are similar to those that have been measured at Waihinau.

The predicted rates of deposition are similar to those which have been predicted by the Cawthron Institute using an entirely independent model (DEPOMOD). To a first approximation, the spatial patterns are also similar, but it is noteworthy that our deposition footprints around Te Pangu and Clay Point farms are crescent-shaped whereas the DEPOMOD ones are more nearly elliptical. By visual comparison (only), we believe that our crescent-shaped footprints better reproduce the measured shapes of the benthic environmental footprints (inferred from measurements of the composition and abundance of the benthic fauna) at these sites. We believe that the differences stem from the fact that our modelling includes the effects of horizontal variations in flow whereas DEPOMOD assumes that the current field is spatially uniform in the horizontal. In this instance, we

do not believe that the discrepancies between the predictions of the two models are sufficiently large to raise any concerns. Nonetheless, we believe that the discrepancies provide some evidence that DEPOMOD (in its present release variant) is not the most suitable tool for predicting benthic deposition when farms are situated in locations where eddy activity will be significant (i.e. close to headlands which interrupt tidal currents).

# 1 Introduction

## 1.1 Background

The Marlborough District Council is the regional authority overseeing the Marlborough Sounds, where approximately 80% of New Zealand's aquaculture production occurs. The majority of the area used for aquaculture is occupied by mussel farms, however there are also a small number of salmon farms, particularly in Queen Charlotte Sound. At the commencement of this project, applications had been submitted to the Environmental Protection Authority for additional finfish farm sites. In light of these applications and the possibility of future proposals to expand finfish aquaculture, the Marlborough District Council desired an improved range of tools to enable them to predict ecological implications with more certainty. They commissioned NIWA to undertake biophysical modelling of the Queen Charlotte and Pelorus Sounds in order to help them understand potential effects of future aquaculture developments. The information provided from the modelling will be used to help plan for longer term, and identify both risks and opportunities.

The primary motivation for the biophysical modelling is to assess the influence of aquaculture. In the later part of the project, the Marlborough District Council has expressed interest in whether the models can be used for assessing the effects of other activities, such as catchment land-use changes. This is possible (indeed the models incorporate freshwater flows and nutrients from rivers and runoff) but modelling the effects of land-use change or changes in nutrient loads other than from aquaculture is outside the scope of the current project.

The two sounds (Queen Charlotte and Pelorus) are modelled separately in this project. This report describes the results for the Queen Charlotte Sound. Results for Pelorus Sound will be presented in a second report.

## 1.2 Definition of a biophysical model

In this report, we use the term 'biophysical model' to describe a numerical (computer) model that couples physical (hydrodynamic) processes with biological and chemical processes.

The biophysical model is comprised of several component 'sub-models'.

- The ROMS (Regional Ocean Model) hydrodynamic model, which simulates the physical behaviour of water including currents, salinity and temperature.
- A nutrient/phytoplankton/zooplankton/detritus (NPZD) model. The particular model that we have adopted includes a simple description of the benthic mineralization of sedimented detritus. For that reason, we will refer to it as the *biogeochemical model*.
- A mussel farm model which focuses upon feeding, respiration and excretion.
- A fish farm model which also focuses upon feeding, respiration and excretion.

The four sub-models are implemented within a single code-base and we will refer to the collective implementation as the *biophysical model*. The biogeochemical model component relies on accurate predictions of transport by water currents by the hydrodynamic model, thus the accuracy of the biogeochemical modelling component depends greatly on the hydrodynamic model adequately

capturing the physical behaviour of the region to be modelled. The hydrodynamics affect the biogeochemical modelling, but we do not allow for the presence of mussel and fish farms to influence hydrodynamics since we believe any such feedback will be negligible at the regional scale. Consequently this report first focuses on describing the performance of the hydrodynamic model before considering the biogeochemical predictions of the complete biophysical model.

### 1.3 Scope of the project

The scope of this project is to

1. Conduct 3D hydrodynamic simulations of the Queen Charlotte Sound and Pelorus Sound that accurately simulate tidal, wind-driven and residual currents; and model the changes in stratification over seasonal and annual time periods.
2. Couple the hydrodynamic model with a water quality/biogeochemical model to simulate the influence of present day aquaculture activities on nutrient concentrations, phytoplankton and zooplankton. We will refer to this as the *existing conditions* or *present day* scenario. This scenario contains: (a) those mussel farms which were shown to have backbones in the water during aerial-survey operations flown in 2012; and (b) the New Zealand King Salmon Ltd Salmon farms that operated during the 2012/2013 period.
3. Simulate two alternative scenarios.
  - *Approved Farms*: as for the *present day* scenario, but also including the one newly approved salmon farm in Tory channel (*Ngamahau*) and a small number of mussel farms which have been approved (or which existed, but were not yet occupied) at the time of the 2012 aerial survey.
  - *Worst case*: as for the *approved farms* scenario, but with benthic denitrification processes turned off (such that all particulate organic nitrogen, from any source, which settles to the seabed is returned to the bottom-most layer of the water-column as ammonium).
4. Simulate the deposition of waste matter (faeces) emanating from the fish farms.

Note that the future scenarios described here apply to Queen Charlotte Sound. The scenarios for Pelorus Sound will be described in the report to be presented when the modelling of Pelorus Sound has been completed.

In addition to the scenarios described above, we also ran simulations with no mussel or fish farms present (with and without benthic denitrification), and with existing mussel farms only (with denitrification). While these scenarios were not required under the agreed scope, we included them as they provide useful information on the relative effects of mussel and fish farms both with respect to each other, and also to the background (no marine farms) conditions of Queen Charlotte Sound.

### 1.4 Outline of this report

In the following sections of this report, we describe

- Section 2: The hydrodynamic model, the area modelled, and the data used as input to this model.
- Section 3: Results from the hydrodynamic modelling, including a comparison to observed data.
- Section 4: The biogeochemical components of the biophysical model and its parameterisation.
- Section 5: Results from the biophysical modelling. Specifically, the following results are presented:
  - *No farms with benthic denitrification.*
  - *Existing mussel farms only with benthic denitrification.*
  - *Existing mussel and fish farms with benthic denitrification.*
  - *All approved mussel and fish farms with denitrification.*
  - *No farms without benthic denitrification.*
  - *All approved mussel and fish farms without denitrification.*
- Section 6: A discussion of the performance, limitations, and implications of the biophysical modelling.
- Section 7: A description of and results from the deposition model used to simulate finfish farm benthic footprints.

## 2 Hydrodynamic model: Methods

### 2.1 Model description

The hydrodynamic model used in this project was ROMS (Haidvogel, Arango et al. 2008), a widely accepted ocean/coastal model. ROMS has a number of optional sub-models, including several alternative biological models. The current project uses the Fennel biological model as described in Section 4.1.

ROMS is a fully 3 dimensional model and is able to simulate the currents forced by tides and wind, as well as the effects of density differences caused by variations in temperature and salinity. In the vertical, ROMS uses a terrain-following coordinate system, i.e. a fixed number of levels (here 20) is fitted between the bottom and the surface; this system is well suited to coastal situations and copes well with large tidal variations in sea level. In the horizontal, ROMS uses a structured rectangular (as used in this project) or curvilinear grid. There are several aspects of the ROMS structure that relate to its suitability for the present application.

1. The ROMS grid cannot be fitted around complicated coastlines: instead land is represented by masking out grid cells. This leads to some inefficiency, because in the model grids used for this project less than 50% of the area is occupied by water.
2. The horizontal spacing of a ROMS grid cannot be reduced for better resolution in specific areas, e.g. around a fish farm or in a small bay.
3. ROMS uses a time splitting scheme for the equations of motion, i.e. it solves for the depth-average velocity on a short time step and for the vertical variations from that depth average on a longer time step. For the 200 m simulations described here the short time step was 1.5 s and the long time step was 12 s. The time-splitting scheme is computationally efficient when the maximum depth in the model domain is large (a few hundred metres or more) but has no advantage in shallower water.
4. ROMS uses an explicit time-stepping scheme, which means that the time step is constrained to a maximum that depends on the grid spacing and the flow speed.

There is another class of hydrodynamic models, examples of which are SELFE and Delft3D, that use more flexible grid layouts, permit large variations in grid spacing, do not employ time splitting and use implicit rather than explicit time stepping. (These different aspects are inter-related. For example, implicit time stepping relaxes the grid-size-dependent constraints on time step and so are compatible with large variations in grid spacing.) There are trade-offs between these approaches, some of them not obvious. For example, implicit time stepping and flexible grid geometry both tend to increase numerical diffusion (i.e. fine details of the flow are smeared out) and this can mean that the areas with fine grid spacing are not as well resolved as the grid spacing would suggest. The question of which is the most appropriate type of model for the current problem is not settled, in our opinion. We consider that a carefully focussed inter-comparison would be valuable.

### 2.2 Model grids and bathymetry

The Queen Charlotte Sound model domain (that is the area over which the calculations are performed) is shown in Figure 2-1. It was chosen to cover all of the Sound, plus the area immediately



outside in Cook Strait. The domain axes were rotated by 22° anticlockwise from true north/east to better align the domain with the Sound. The exact placement of the boundaries was fine-tuned to avoid instabilities caused by the strong Cook Strait tidal currents interacting with the land or with bathymetric features.

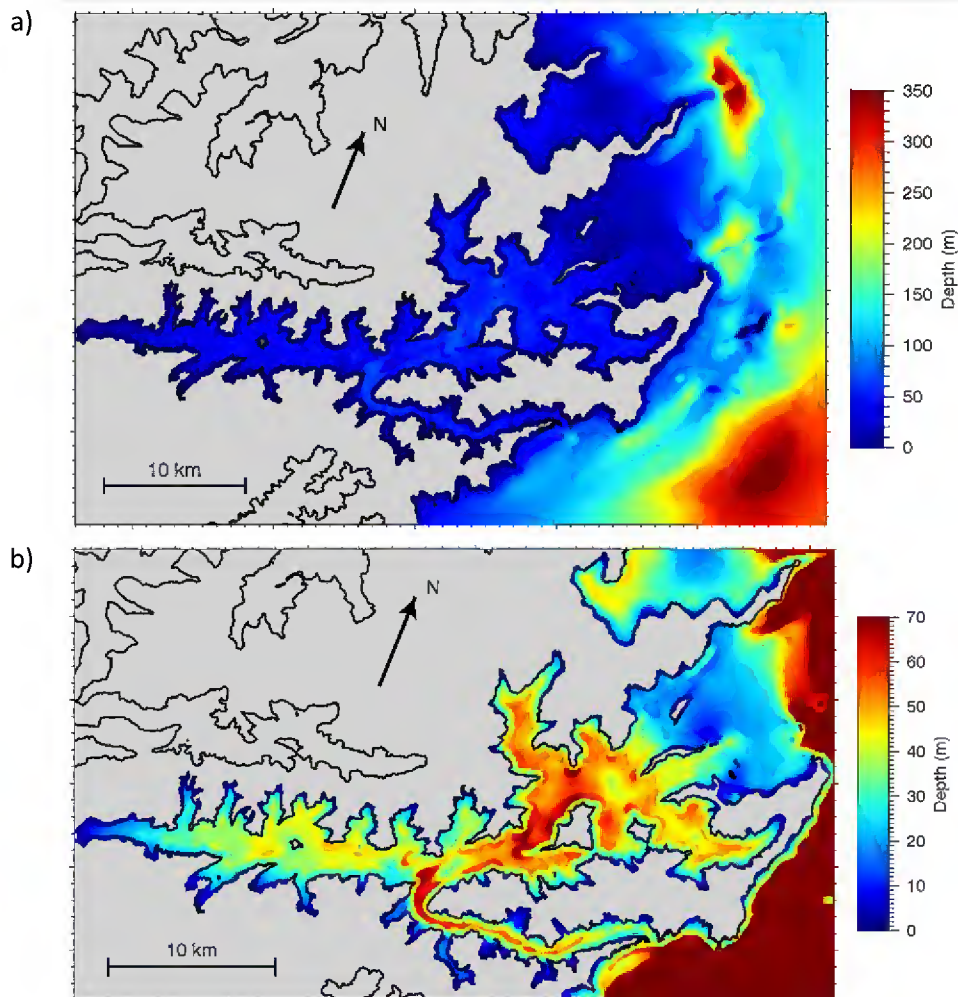


**Figure 2-1: The Queen Charlotte Sound model domain and bathymetry.** a) A map showing the model bathymetry and land mask (100 m grid) with LINZ coastline data (black). Note that while parts of the neighbouring Pelorus Sound and Port Underwood are within the domain, these regions were blanked out (shown as grey in the above figures) and were not modelled here. b) The same Queen Charlotte Sound bathymetry in more detail.

The majority of model simulations described in this report have been for a period of 500 days (24 May 2012 to 6 October 2013) which allows for 135 days to spin-up various components of the model (notably the biogeochemical model) followed by 365 days over which the model output is analysed. Given the short model time steps that are required in coastal situations, a simulation of this duration can be very expensive computationally. Running the model on finer resolution grids allows spatial variability in both physical and biological properties to be better represented, but this comes at the cost of the model taking longer to execute. There is a balance to strike between sufficiently fine resolution and manageable execution time. To exam this issue we set up a series of model grids on the same domain, with different horizontal grid spacing. We employed four such grids: 400 m, 200 m, 100 m and 50 m.

The execution time (Table 2-1) increases by a factor of approximately 8 with each halving of the resolution, except that between 400 m and 200 m the factor is somewhat smaller because the 400 m grid is not large enough to use the computer efficiently.

**Table 2-1: Grid resolution and execution time.** Time required to execute the Queen Charlotte Sound model for 500 days at four different grid resolutions on a single node of the NIWA supercomputer, Fitzroy. Values in italics have been estimated by extrapolation.

Execution time (days)	400 m	200 m	100 m	50 m
Hydrodynamics only	0.4	2.1	18.8	<i>150</i>
Hydrodynamics plus 6 tracers	0.6	2.8	<i>26.1</i>	<i>210</i>
Hydrodynamics plus biogeochemical model, mussel farms and fish farms	1.1	4.2	<i>39.2</i>	<i>313</i>

The four grids were used for different purposes in our simulation strategy as follows:

- The 400 m grid was used during development of the hydrodynamic, biogeochemical, mussel-farm and fish-farm models (i.e., configuring and tuning the model parameters), but with the expectation that the coarse resolution would limit the accuracy of the hydrodynamics significantly.
- The 200 m grid was used for production simulations, once the model configuration was settled.
- The 100 m grid was used for simulations of less than the full 500 days, to check for any consistent differences from the 200 m grid.
- The 50 m grid was used only for an idealised 6-day simulation, to investigate the resolution dependence of tidal flow in Tory Channel.

Bathymetry data were taken from multiple sources and gridded with the GMT mapping tools<sup>1</sup>. The sources were:

- a Marlborough Sounds digital terrain model (DTM) at a resolution of 25 m generated from NIWA bathymetric contour data by NIWA staff in 2003;
- high-resolution coastline position data from LINZ;
- a New Zealand land elevation digital terrain model at 200 m resolution (this has some effect on the bathymetry because it affects the interpolation near the coast);
- NIWA bathymetric contour data (this is used in the deeper areas in Cook Strait, beyond the coverage of the 25 m DTM).

Each of the ROMS gridded bathymetries was smoothed as necessary to remove areas where the slope parameter—a measure of the fractional change in depth between adjacent grid cells (Beckmann and Haidvogel 1993)—exceeded 0.25. Wetting & drying of intertidal areas was not represented in the model—though this option is available in ROMS—because the intertidal areas in Queen Charlotte Sound are small. In other words, areas occupied by land and sea are specified by a

<sup>1</sup> <http://gmt.soest.hawaii.edu/>

land mask in the model grid file and do not change during the simulation. The land mask was calculated directly from the LINZ coastline data and then manually adjusted in a few places to avoid spurious features like “channels” cutting through narrow peninsulas and “lakes” at the head of bays.

## 2.3 Initial and boundary conditions

The simulations described in this report were all carried out in forward mode, i.e. the model’s temperature, salinity, velocity, sea surface height and biochemical variables were set to a plausible initial state and then stepped forward in time subject to various forcings from the surface (wind stress, heat flux, freshwater fluxes), the bottom (bottom drag), the open ocean lateral boundaries (specified temperature, salinity, velocity, etc.) and inflows from point sources like rivers. There is no process of adjustment towards observations during the model run (i.e. data assimilation), as there is in a forecasting model, for instance.

The initial and boundary data for the hydrodynamic variables were taken from a larger-scale model covering Cook Strait (Figure 2-2) at a resolution of 2 km. The purpose of the Cook Strait model in this instance was to generate a realistic temperature, salinity and currents at the entrances to Queen Charlotte Sound. The Cook Strait model itself required lateral boundary data, which was taken from a global ocean analysis and prediction system operated by the US Naval Research Laboratory, using the HYCOM<sup>2</sup> ocean model. (The specific dataset used here is called Glba08.) The HYCOM system provides daily snapshots of the three-dimensional state of the global ocean on a 1/12° grid; at NIWA we have archived a subset of this data around New Zealand since 2003.

The Cook Strait model was run for the same period as the Queen Charlotte Sound simulations, with model fields saved as consecutive six-hour averages. These data were then interpolated to the boundaries of the Queen Charlotte Sound model and written to data files that were read by the latter model. This process is known as one-way, off-line nesting.

---

<sup>2</sup> <http://hycom.org/>

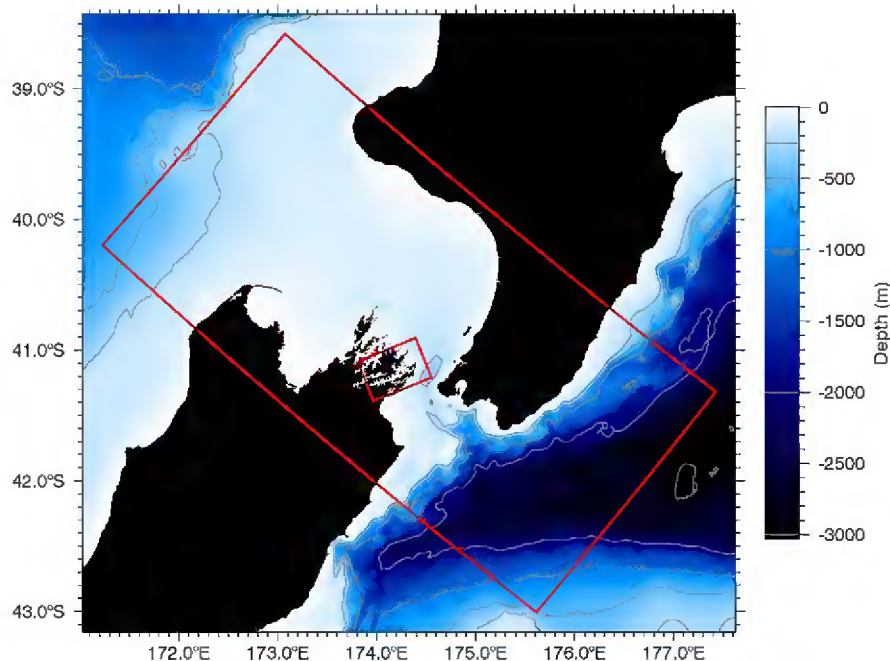


**Figure 2-2: The Queen Charlotte Sound and Cook Strait model boundaries.**

In principle, the Cook Strait model could include tides and the tidal fluctuations in sea-surface height and velocity, which would then be passed into the Queen Charlotte Sound model through its lateral boundaries. However this would require outer model data to be saved at intervals of ~30 minutes, which would require very large output files. Therefore tides were not represented in the Cook Strait model but were applied at the boundaries of the Queen Charlotte model. Amplitude and phase data for 8 tidal constituents (M2, S2, N2, K2, K1, O1, P1, Q1, 2N2, MU2, NU2, L2, T2) were interpolated from the output of the NIWA New Zealand region tidal model (Walters, Goring et al. 2001). The ROMS tidal forcing scheme then calculated tidal sea surface height and depth-averaged velocity at each time step and added them at the boundaries.

Surface stresses generated by the wind are an important factor in forcing currents in Cook Strait and (we expect) in Queen Charlotte Sound. These stresses were calculated from 3-hourly winds from the NZLAM 12 km regional atmospheric model<sup>3</sup>. Surface stress was calculated from wind speed using an equation of the form  $\tau = \rho_{air} C_D U_h^2$ , where  $\tau$  is the stress,  $\rho_{air}$  the density of the air,  $U_h$  the wind speed and  $C_D$  a wind-speed-dependent term called the drag coefficient (Smith, S.D. 1988). For the larger Cook Strait model, it was found in a previous modelling exercise (Hadfield 2013) that the modelled currents agreed well with measurements, but only when the drag coefficient was multiplied by a factor of 1.4. A similar adjustment has been found to be necessary in previous coastal modelling exercises around New Zealand by us (Hadfield and Zeldis 2012) and others (e.g. P. McComb *pers. comm.*). For the Queen Charlotte Sound model the drag coefficient was not increased. The relatively coarse spatial resolution of the atmospheric model means that it will not reproduce the topographic channelling of the wind that is seen in Marlborough Sounds and this can be expected to limit the accuracy of the hydrodynamic model. It is possible to run an atmospheric model at much finer resolution to generate more detailed wind fields, but this is outside of the scope of the current work. We note that from mid-2014 NIWA have an atmospheric model running at 1.5 km resolution

<sup>3</sup> NZLAM is part of the NIWA Ecoconnect environmental forecasting system: <http://EcoConnect.niwa.co.nz/>

which may give improved results in the Marlborough Sounds compared to the 12 km model. Unfortunately this could not be used for the present study but could be considered in the future.

Surface heat fluxes in both the Cook Strait and Queen Charlotte Sound models were calculated using data (6-hourly averages) from a global atmospheric analysis system called the NCEP Reanalysis (Kalnay, Kanamitsu et al. 1996), with a heat flux correction term that causes the model sea surface temperature (SST) to be nudged towards observed SST (the NOAA Optimum Interpolation 1/4° daily SST dataset (Reynolds, Smith et al. 2007)). The heat flux correction prevents the modelled SST from departing too far from reality due to any biases in the surface fluxes, but has a negligible effect on day-to-day variability.

The surface freshwater flux (precipitation minus evaporation) was calculated from a combination of NCEP Reanalysis 6-hourly evaporation data and daily rainfall from the Crail Bay climatological station (NIWA Climate Database<sup>4</sup> agent number 4232). The average annual rainfall at Crail Bay is 1675 mm. Applied over the area of Queen Charlotte Sound (inside the boundaries shown in Figure 3-23 below) of 304 km<sup>2</sup>, this implies a mean rainfall input of  $5.1 \times 10^8$  m<sup>3</sup> per year, or  $16.1 \text{ m}^3 \text{ s}^{-1}$ .

Regarding riverine input of freshwater into Queen Charlotte Sound, there are many small streams, but no rivers with flows much larger than  $1 \text{ m}^3 \text{ s}^{-1}$ . Monthly flow data are available since mid-2011 for three streams—the Waitohi, Duncan and Graham—that suggests their combined mean flow is  $\sim 1.8 \text{ m}^3 \text{ s}^{-1}$  and there is daily data for a short period in the past (1999–2000) for the Waitohi. However there are also several ungauged catchments that drain into the Sound and can be expected from their area to yield comparable flows. Given the absence of high-quality flow data for most of the catchment, the riverine freshwater input was estimated from the rainfall. It was assumed that the catchment area of Queen Charlotte Sound (not including the Sound itself) is 243 km<sup>2</sup> (Heath 1974) and that of the rainfall falling on that area every day, 20% is lost to evaporation and the remainder is immediately delivered to the sea at the coastline. This was achieved by applying an increment to the surface freshwater flux (i.e. an extra input of freshwater, see Figure 2-3) of an appropriate amount in all model grid cells that are adjacent to the land mask and inside the boundaries of Queen Charlotte Sound. The annual mean input by this mechanism is  $3.3 \times 10^8$  m<sup>3</sup> per year, or  $10.3 \text{ m}^3 \text{ s}^{-1}$ .

---

<sup>4</sup> <http://cliflo.niwa.co.nz/>

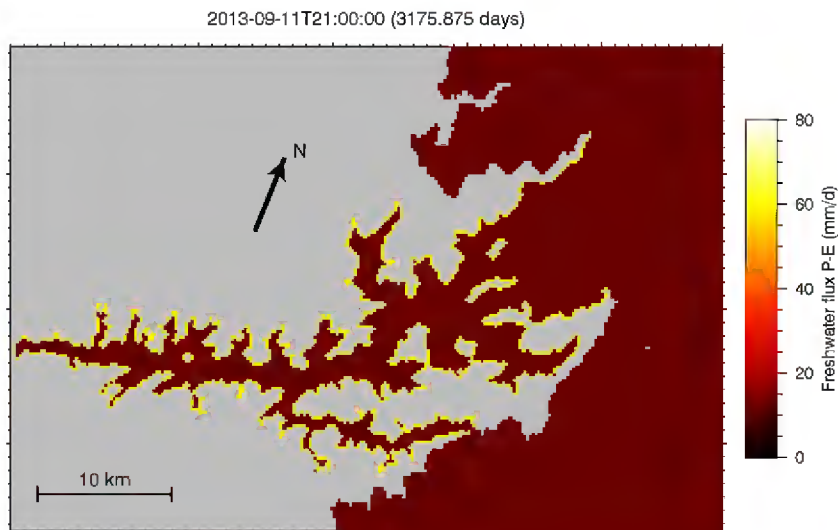


**Figure 2-3: Surface freshwater flux.** A colour plot showing a snapshot of the surface freshwater flux on the 200 m grid during a moderate rain event ( $\sim 10 \text{ mm d}^{-1}$ ), illustrating the extra input of freshwater in a band next to the coast in Queen Charlotte Sound.

The other freshwater source that was taken into account in the model was the Picton Wastewater Treatment Plant, which was assigned a seasonally varying value of between  $0.10$  and  $0.25 \text{ m}^3 \text{ s}^{-1}$  (annual mean  $0.13 \text{ m}^3 \text{ s}^{-1}$ ). This was negligible in terms of its effect on the hydrodynamics, but was included because it is associated with an input of nutrients and detritus into the biogeochemical model.

## 2.4 Hydrodynamic field data

Hydrodynamic data (time-series of currents, and profiles of temperature and salinity) were obtained from two sources.

1. NIWA deployed moorings at 3 sites (Figure 2-4) from 28 June 2012 to 10 May 2013. These moorings were equipped with acoustic Doppler current profilers, and temperature and conductivity (salinity) sensors at two depths, one 5 m above the bottom and the other as close as possible to the surface. However it is worth noting that for the Queen Charlotte Sound Inner and Outer sites, the upper sensor needed to be 11–13 m below the surface to avoid interference with navigation. At the Tory Channel site, the upper sensor was placed on a second mooring near the side of the channel and was much closer to the surface, at 2 m depth. Locations of the moorings are indicated in Figure 2-4. Data were not always continuous over the entire deployment period due to instrument malfunction or, in one case, loss of the instrument.
2. Monthly vertical profiles of temperature and salinity collected with a CTD (conductivity, temperature, depth profiler) at 11 sites (Figure 2-4). These data were collected by Marlborough District Council, using a NIWA supplied instrument, as part of a sampling programme that started in July 2011 and continued through to June 2014.

The CTD was also equipped with a PAR (photosynthetically active radiation) sensor for many of the monthly samples. This data has been used to calculate light attenuation, which is used in the biogeochemical model.

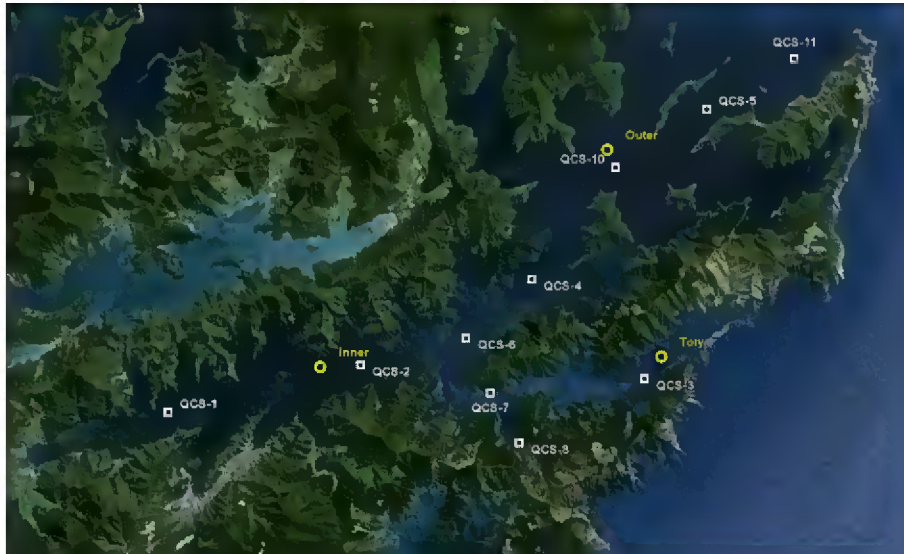


**Figure 2-4: Location of moorings and sampling stations for hydrodynamic measurements.** The three mooring sites are indicated by yellow circles, and the 11 sites for monthly temperature and salinity profiles by the white squares. The moorings were deployed from 28 June 2012 to 10 May 2013, and the monthly profiles collected from July 2011 to June 2014.

## 3 Hydrodynamic model: Results

### 3.1 Model vs observations: temperature and salinity

Unless otherwise stated, model results reported here are from 200 m resolution grid. While finer resolution grids give better detail particularly in the Tory Channel (see section 3.6), the 200 m grid captures the behaviour of the sounds sufficiently well for the purposes of this investigation. Further comparisons of the effect of grid resolution are given in sections 3.6 and 3.7.

Figure 3-1 shows time series of temperature measured at the three mooring sites (Figure 2-4) in comparison with co-located model output. As described previously, the measurements were made at two depths at each mooring, one 5 m above the bottom and the other as close as possible to the surface (2 m depth at the Tory Channel site, and 11–13 m at the Queen Charlotte Sound Inner and Outer sites). Note that data from the observations and the model are plotted on different axes which are offset to allow each time series to be distinguished. The observed data (the lower blue and red lines) are plotted against the temperature scale on left of the figure, and the modelled data (upper blue and red lines) against the temperature scale on the right.

Taking the QCS Inner site first (Figure 3-1a), the measured lower temperature varies from  $\sim 12$  °C in winter (minimum in July–August) to  $\sim 16$  °C in late summer (maximum in February–March). At the upper sensor, the temperature is higher than at the bottom sensor by approximately 0.8 °C from the beginning of November to the end of March, but in July the upper temperature is slightly lower than the near-bed temperature. The modelled temperature time series at the same locations are similar to the measured ones. The maximum near-bed temperature is a little higher than measured. The same difference of about 0.8 °C between upper and lower locations is seen from November–March. The model has somewhat more variability in temperature during the summer than during the winter, with a few sharp drops in the lower temperature (e.g. the one at 2013-02-05) that are not as pronounced in the measurements. However, overall the model matches the measurements reasonably well in their nature and their magnitude.

At the QCS Outer mooring site (Figure 3-1b), the temperature time series are basically similar to those at the Inner site, though with more short-term variability at the lower sensor at the Outer site and a somewhat smaller seasonal temperature range. Again the model matches the measurements reasonably well.

At the Tory Channel mooring site (Figure 3-1c) the appearance of the time series is rather different from the other two sites. There is very little difference in temperature between upper and lower sensors, this despite the fact that the upper sensor is at a depth of only 2 m, which would allow it to capture any shallow surface warming. The seasonal temperature variation is smaller at this site, e.g. the measured temperature varies from typical values of  $\sim 12.5$  °C in winter to  $\sim 15.5$  °C in late summer. The seasonal variation is punctuated by several sharp drops of  $\sim 1$  °C and there is considerable short-term variability which appears as a blur on this time scale but has a period of 12–13 hours and is clearly tidal. The model matches the measurements reasonably well and reproduces the character of the measured time series which is very different from the other two sites.



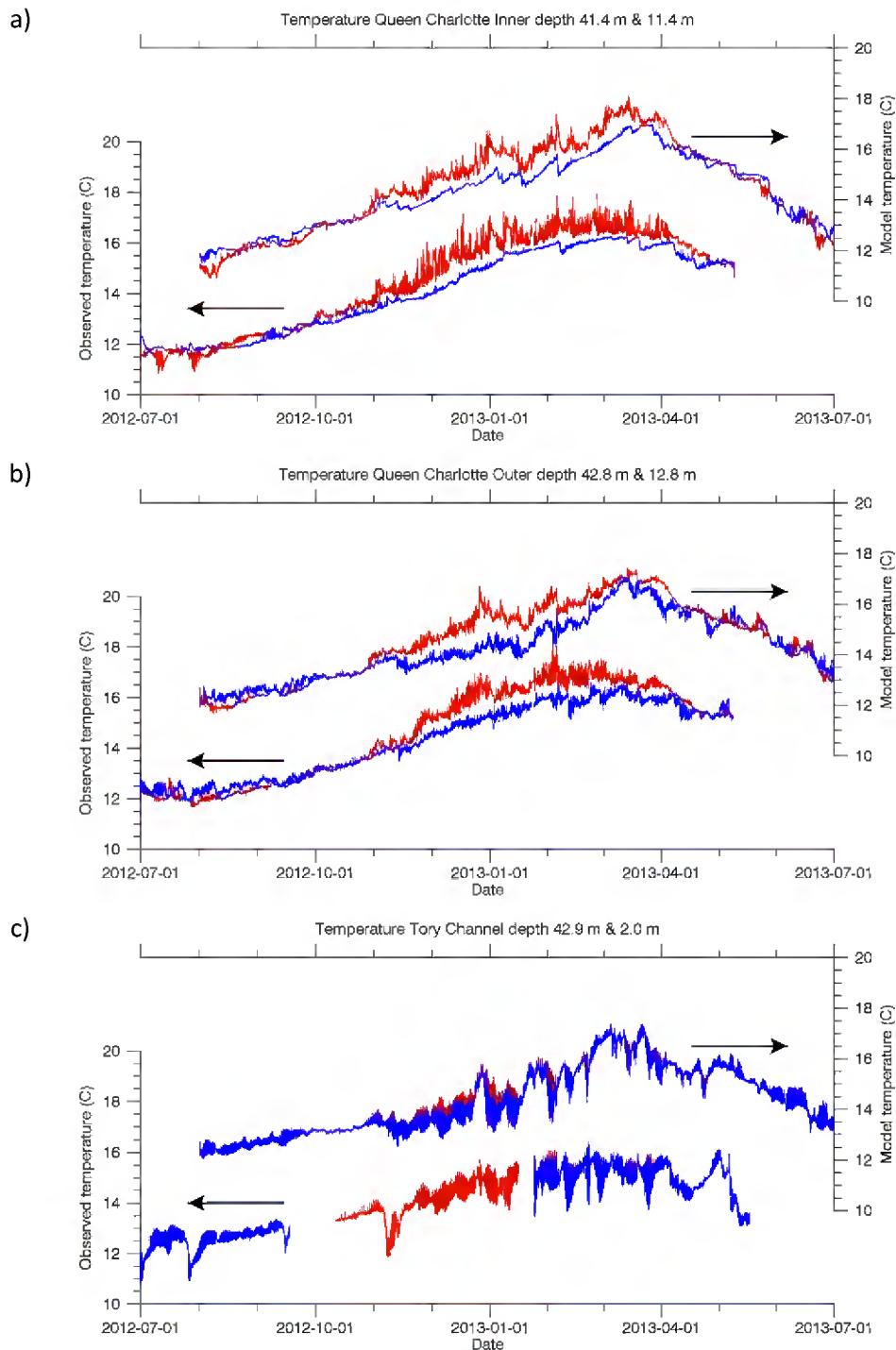


**Figure 3-1: Observed and modelled temperature time series.** Temperature at two depths (blue lower, red upper) at the 3 conductivity-temperature mooring sites shown in Figure 2-4: a) Inner QCS; b) Outer QCS; c) Tory Channel. The lower pair of curves in each panel shows measurements (left-hand axis) and the upper pair shows modelled values (right-hand axis).

The time series plots in Figure 3-1 are good for comparing the modelled and observed temporal variation, but the offset vertical axes make it difficult to compare values directly. Therefore Appendix E presents scatter plots (Figure E-1) for each of the three sites showing temperatures at the upper and lower sensors along with the difference (upper minus lower). These scatter plots indicate good quantitative agreement, with little bias and with modelled temperatures generally agreeing with

observed temperatures to within  $\pm 2^\circ\text{C}$  and differences between upper and lower sensors to within  $\pm 1^\circ\text{C}$ .

The monthly CTD casts provide a complementary picture of the dependence of water temperature on time and depth, with measurements over a full range of depths at more locations, but only at monthly intervals. Figure 3-2 shows the observed CTD temperature data as a colour plot against time and depth axes, along with comparable model data. (However note that the way the CTD data are graphed suggests the temperature is uniform throughout the month, but in fact it only applies to a period of an hour or so, and—as we saw from the time series plots in Figure 3-1—there is considerable within-month variability in the actual temperatures, just as there is in the model.) The four panels of Figure 3-2 show four sites: QCS-1 (Christy's Bay) in Grove Arm, QCS-3 (Tio Point) in eastern Tory Channel; QCS-6 (Dieffenbach Island) near the junction of Queen Charlotte Sound and Tory Channel; and QCS-10 (Blumine Island) in outer Queen Charlotte Sound.

At QCS-1 (Figure 3-2a), the observed surface temperature warms from a winter minimum of  $\sim 12^\circ\text{C}$  to a late-summer maximum of above  $\sim 18^\circ\text{C}$  and then cools again in autumn. The temperature rise starts at the surface in October–November but lags behind this at depth, leading to a temperature difference between the surface and the deeper layers of  $2\text{--}3^\circ\text{C}$  that develops in spring and drops away from about March, when the entire water column has warmed up. The model reproduces this behaviour very well, bearing in mind that the coarse temporal resolution of the CTD data precludes an exact match.

At QCS-3 (Figure 3-2b), there is a modest seasonal variation ( $\sim 3^\circ\text{C}$ ) in temperature with no perceptible vertical variations. QCS-6 (Figure 3-2c) and QCS-10 (Figure 3-2d) are intermediate between QCS-1 and QCS-3. In all cases the model matches the observations reasonably well, and the model reproduces the observed variation between the different sites.

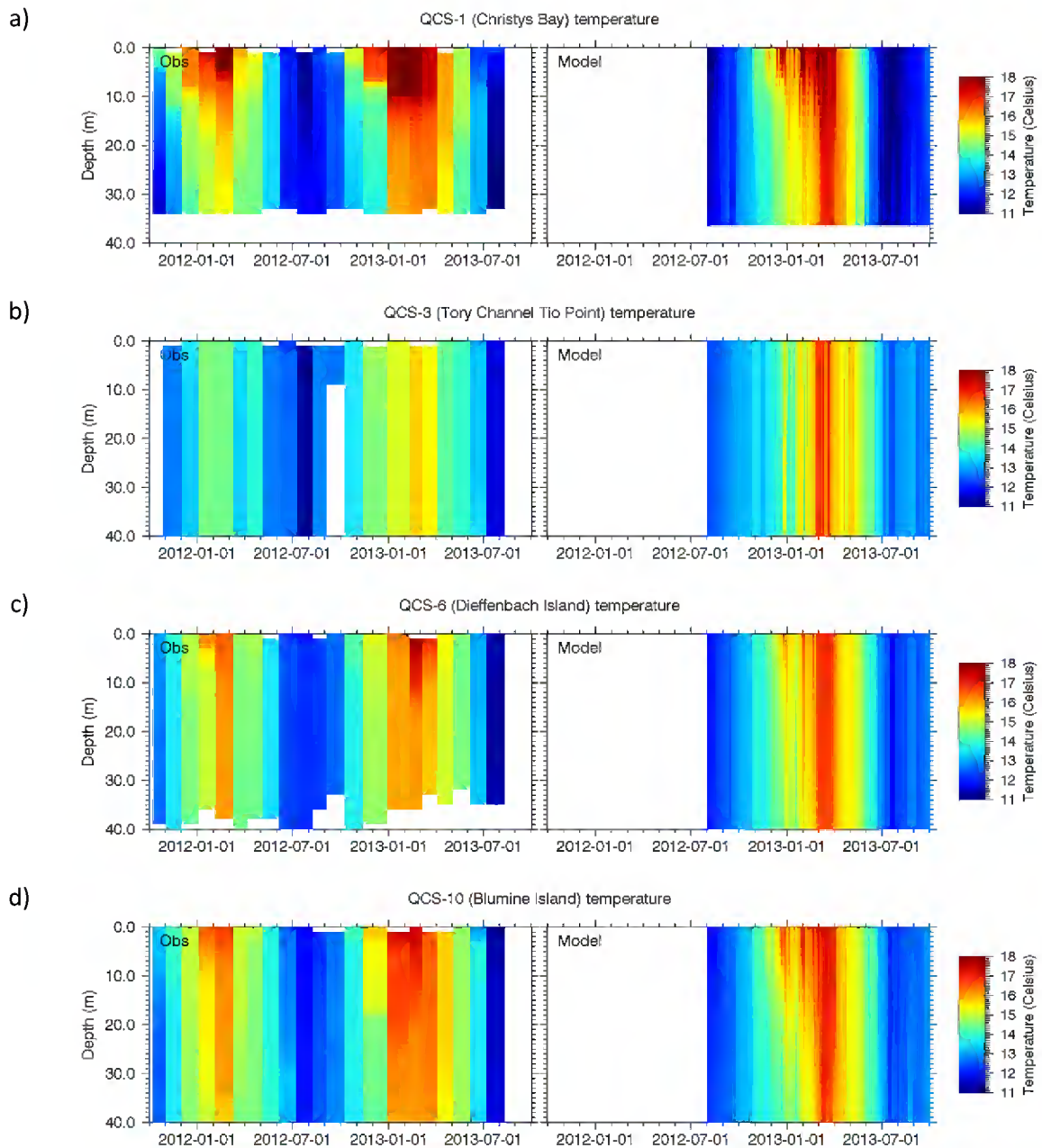


**Figure 3-2: Observed and modelled temperature profiles.** Temperature versus time and depth from monthly CTD casts (left) and model (right) for 4 sampling locations shown in Figure 2-4: a) QCS-1; b) QCS-3; c) QCS-6; d) QCS-10.

Salinity<sup>5</sup> time series at the mooring sites are shown in Figure 3-3. One of the difficulties in comparing modelled and measured salinity data is that stable measurements of salinity for periods of several months in a coastal environment are difficult to obtain due to fouling and contamination. Several sections of the measured data have been rejected as implausible and omitted from the figure. The monthly CTD casts were used in this quality control process. Of the remaining data, not all can be assumed to be completely reliable. Note that the observed and modelled salinity data are plotted on separate offset axes similar to the previously shown temperature data.

<sup>5</sup> The term "salinity" in this report implies absolute salinity as defined by the TEOS-10 standard (Pawlowicz 2010).

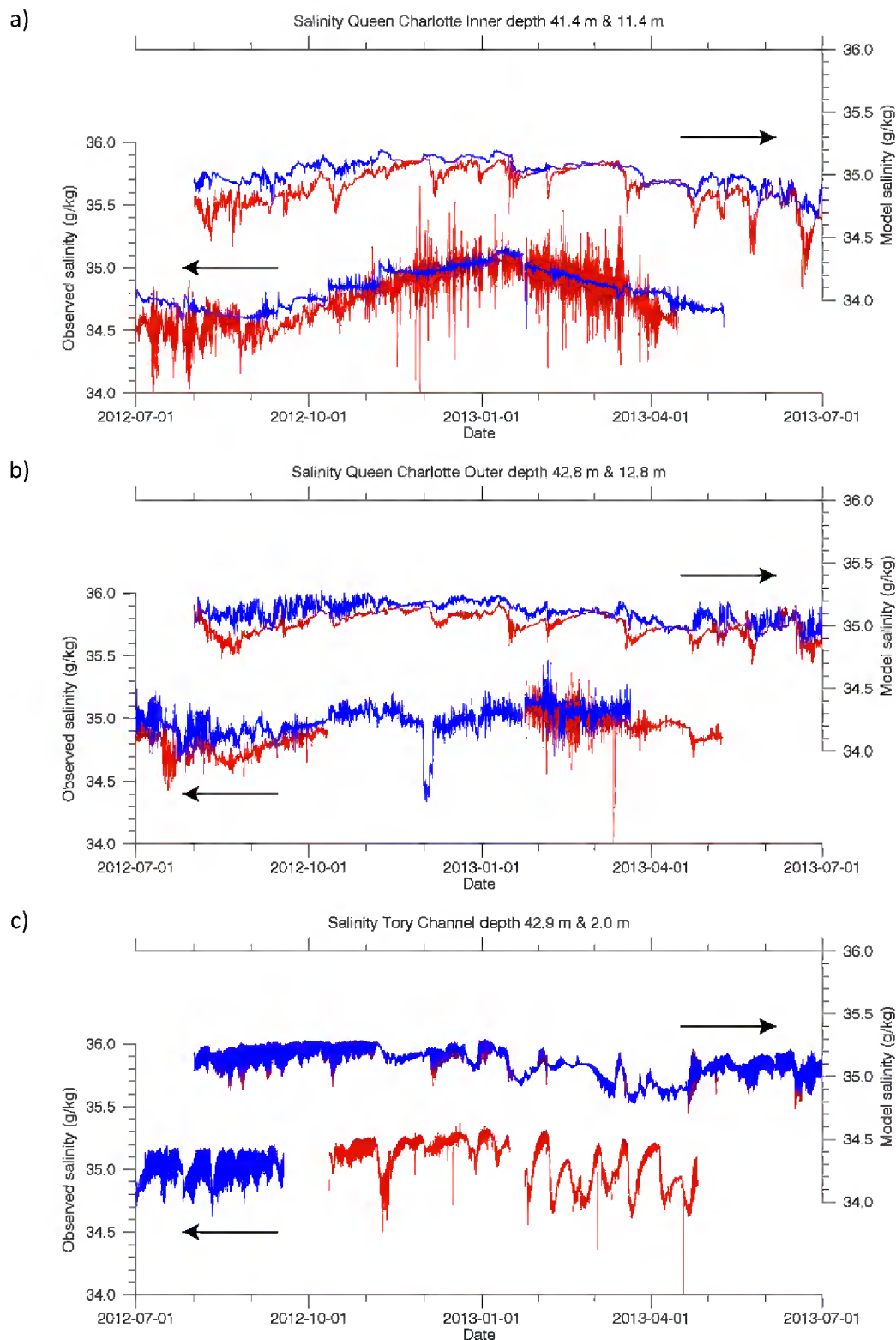


**Figure 3-3: Observed and modelled salinity time series.** As Figure 3-1 but for salinity.

With that caveat in mind, the salinity at the lower sensor at the QCS Inner mooring (Figure 3-3a) has a seasonal variation from about  $34.6 \text{ g kg}^{-1}$  in August to  $35.1 \text{ g kg}^{-1}$  in January. For comparison, the salinity in Cook Strait is  $35.1\text{--}35.2 \text{ g kg}^{-1}$ . The salinity at the upper sensor is about  $0.2 \text{ g kg}^{-1}$  lower than at the lower sensor in winter, but similar in summer. There is a lot of short-term variability in

the upper sensor from late November: this may be spurious. The modelled salinity shows a slight decreasing trend over the course of the simulation, which may indicate that the adjustment of salinity in Inner QCS is a slow process. On top of this decreasing trend there is a seasonal variation, but weaker than the measured seasonal variation. Modelled salinity at the upper sensor location is about  $0.2 \text{ g kg}^{-1}$  lower than at the lower sensor. Agreement between the model and measurements is not perfect but is reasonably good.

The picture at the Queen Charlotte Outer mooring (Figure 3-3b) is similar, though salinities (measured and modelled) are generally somewhat higher. There are a couple of negative spikes in measured salinity that we believe are spurious.

At the Tory Channel mooring (Figure 3-3c) we see very little difference between upper and lower sensors, as for temperature, and salinities are generally close to the Cook Strait value. Tidal variations of up to  $\sim 0.3 \text{ g kg}^{-1}$  peak-to-peak are apparent in some parts of the time series. From late January to late April 2013, the measured time series (from the upper sensor only) shows relatively low salinities with a fluctuation of up to  $\sim 0.5 \text{ g kg}^{-1}$  peak-to-peak with a period of around 14 days. This, if it is real, suggests some sort of spring-neap modulation of salinity in Tory Channel. The model does not really reproduce this, though modelled salinities in this period are lower than they are before and after, in agreement with the measurements.

As was done for temperature, the salinity time series data are compared by means of scatter plots in Appendix E (Figure E-2). Modelled salinities generally agree with observed salinities to within  $\pm 0.5 \text{ g kg}^{-1}$ , as do the differences. There are some rather large differences (eg. QCS Outer upper sensor) which may indicate a problem with the measurements rather than the model.

Figure 3-4 shows salinity versus time and depth at the same four CTD stations as Figure 3-2. The contrast in the degree of stratification between QCS-1 at one extreme and QCS-3 at the other has been commented on before. On the whole, the model agrees reasonably well with the observations. At QCS-1 several surface freshening events are observed that are also seen in the model, though not so pronounced. (Note, again, that the way the monthly observed CTD data are presented in these plots may be misleading.) There is a freshening observed in July 2013 at all sites (though not strongly at QCS-3). This also appears in the model output, but is somewhat underestimated.

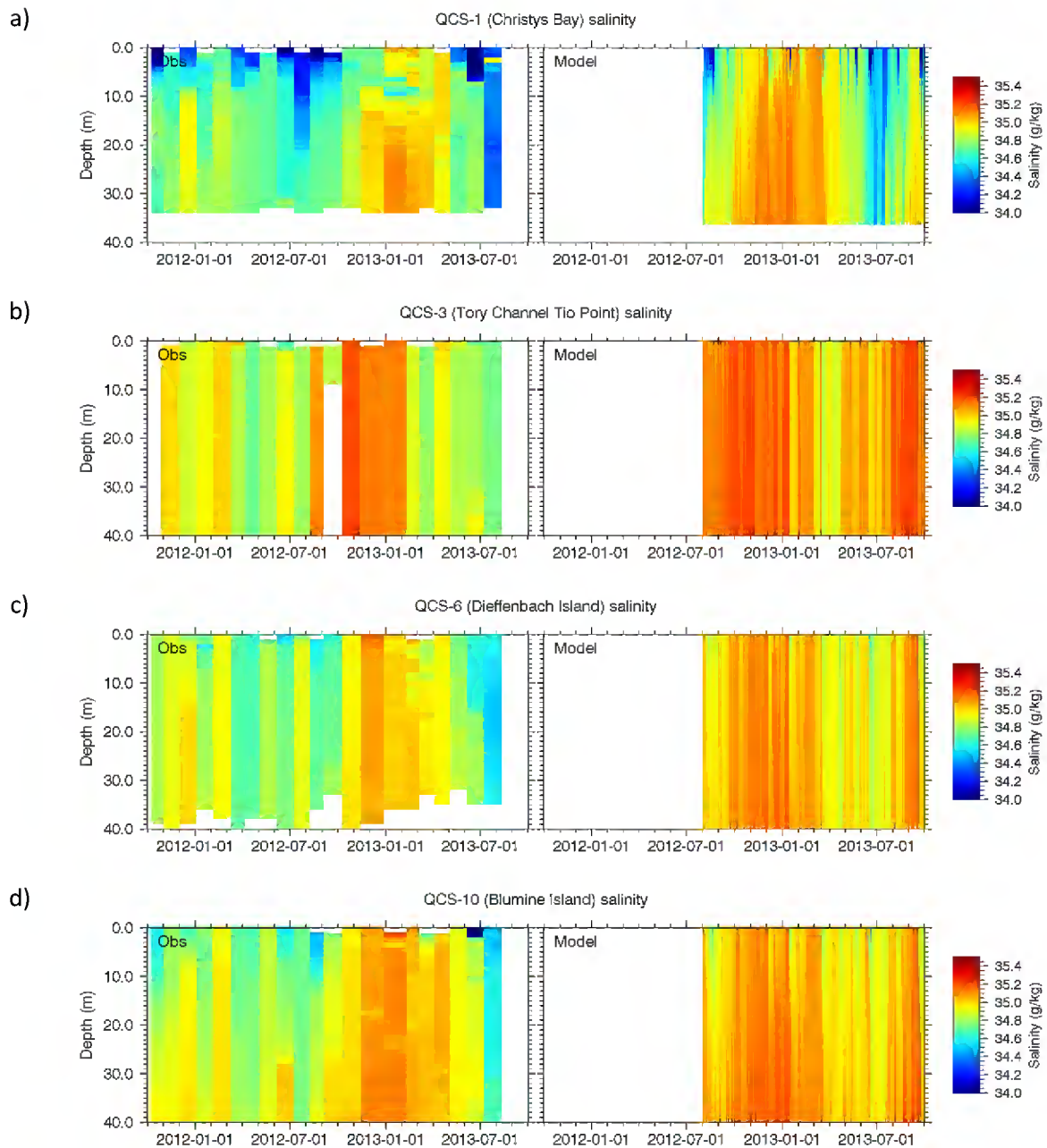


**Figure 3-4: Observed and modelled salinity profiles.** As Figure 3-2 but for salinity.

### 3.2 Model vs observations: tidal height fluctuations

This section considers the accuracy of the model's representation of tidal fluctuations in sea surface height. These are estimated by fitting tidal harmonics of specified frequencies to the data. As is the case elsewhere around New Zealand, the dominant tidal constituent in the area is the lunar, semi-diurnal constituent (M2). The tidal variation is defined by two parameters: the amplitude (metres) and the phase (degrees) in time of the sinusoidal oscillation. A phase difference of  $1^\circ$  corresponds to a time difference of  $1/360^{\text{th}}$  of the tidal period: for the M2 tide, the period is 12.42 hours (0.5 lunar days) so a phase difference of  $1^\circ$  corresponds to a shift of 2.1 minutes.

Table 3-1 compares measured and modelled M2 tidal parameters at the QCS Outer and Tory Channel ADCP sites (Figure 2-4). The model over-predicts the amplitude by 20% and the modelled phase differs from the measured phase by 8–13°, the negative sign implying that the modelled tides *precede* the measured tides by 17–27 minutes. One would normally expect a model like this to predict the amplitude to within 10% and the phase to within 5–10°. Table 3-1 shows that the model does not achieve that degree of agreement, though it should be adequate for the model’s intended purpose. The most likely reason is a bias in the tides specified at the model’s boundary, as the Cook Strait Narrows region has large horizontal gradients in the amplitude and phase of the M2 tide and is therefore challenging for the NZ region tidal model.

**Table 3-1: Comparison of M2 tidal sea level parameters.** M2 tidal sea level parameters from ADCP pressure data and model. Here “ratio” means model value divided by observed value and “difference” means model value minus observed value.

ADCP Site/Deployment	Amplitude (m)			Phase (°)		
	Obs.	Model	Ratio	Obs.	Model	Difference
QCS Outer Deployment 1	0.508	0.607	<b>1.19</b>	105.5	96.1	<b>-9.4</b>
QCS Outer Deployment 2	0.515	0.615	<b>1.19</b>	103.9	95.7	<b>-8.2</b>
Tory Channel Deployment 1	0.375	0.457	<b>1.22</b>	115.6	102.8	<b>-12.8</b>
Tory Channel Deployment 2	0.369	0.464	<b>1.26</b>	114.5	102.3	<b>-12.2</b>

Similar comparisons are presented in Appendix E for the S2, N2 and O1 tidal constituents (Table E-1 to Table E-3). The S2 (solar, semi-diurnal) constituent has a period of 12 hours and is the largest constituent after M2. Superposition, or “beating”, of the M2 and S2 constituents accounts for most of the spring-neap cycle in the semi-diurnal tide. N2 is a smaller semi-diurnal constituent that further modifies the spring-neap cycle and O1 is the largest of the diurnal constituents, but is still small relative to M2 or S2. For the S2 constituent, the model over-predicts the amplitude by 9–18% and matches the phase to within 7.5°, i.e. a little better than it does for the M2 constituent. For the smaller N2 and O1 constituents the model matches the observations less well.

### 3.3 Model vs observations: tidal currents

Tidal velocity variations are conventionally characterised by tidal ellipses, a representation indicating the path taken by the tip of a tidal current vector, which rotates at a constant angular frequency and changes in length (current speed) through a tidal cycle. A tidal ellipse is defined by four parameters:

- **Semi-major amplitude ( $m s^{-1}$ ):** The semi-major axes are lines from the origin to the two most distant points on the ellipse perimeter. The two axes are equal in length, and this length represents the amplitude of the velocity along the semi-major direction.
- **Eccentricity:** At right angles to the semi-major axes are the semi-minor axes, which connect the origin to the two closest points on the ellipse perimeter. The eccentricity, or “fatness”, of the ellipse is the ratio of semi-minor to semi-major axis lengths. The eccentricity can be positive (vector rotates anti-clockwise) or negative (clockwise).
- **Inclination (°T):** The inclination is the orientation of one of the semi-major axes. The choice between the two is arbitrary: here we take the semi-major axis directed

towards the northeastern or southeastern quadrant and express the inclination as the orientation in degrees clockwise from true north ( $^{\circ}$ T).

- **Phase ( $^{\circ}$ ):** The phase relates to the time at which the rotating tidal current vector passes through the semi-major axis. A phase difference of  $1^{\circ}$  corresponds to a time difference of  $1/360^{\text{th}}$  of the tidal period.

Figure 3-5 compares measured and modelled M2 tidal ellipses at the Queen Charlotte Outer ADCP site. The ellipses match very well in orientation, but the model clearly under-predicts the amplitude somewhat. A tabular comparison (Appendix E, Table E-4) shows that the model under-predicts the semi-major amplitude by 20% (cf. the over-prediction of M2 height variations at the same location) and the phase leads the observations by  $16\text{--}21^{\circ}$ .

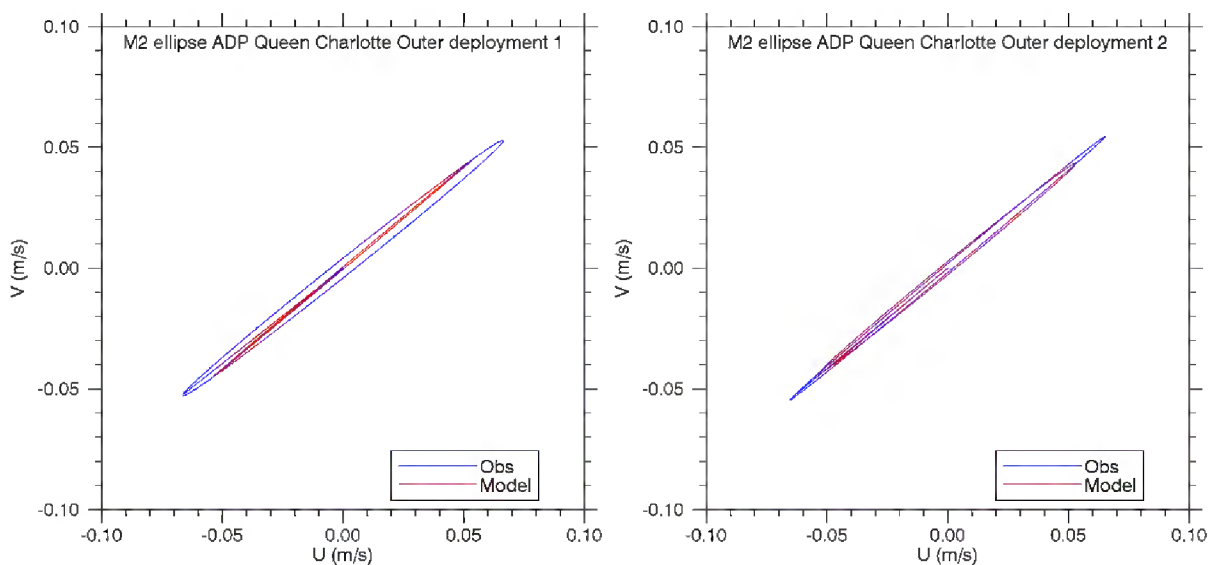


**Figure 3-5: M2 tidal velocity comparison (Queen Charlotte Outer).** Mid-depth M2 tidal ellipses from ADCP (blue) and model (red). The axes correspond to the velocity components towards due east ( $u$ ) and due north ( $v$ ). The ellipses represent the magnitude and orientation of the tidal velocity variations (see text) and the straight line from the origin to the ellipse represents the phase. The left- and right-hand panels are for Deployments 1 (2012-06-28 to 2012-10-10) and 2 (2012-10-11 to 2013-01-22).

Figure 3-6 shows a similar comparison for the Tory Channel ADCP. The modelled and observed amplitudes agree very well, as does the inclination of the ellipse for Deployment 1, but less so for Deployment 2. The comparison of tabulated parameters in Table E-4 indicates good agreement—much better than for the QCS Outer ADCP—with the most obvious disagreement being a difference of  $7.9^{\circ}$  in inclination for Deployment 2. Differences between observed data for deployments 1 and 2 may be due to the instrument not being located in exactly the same location – a difficult feat to achieve in such strong tidal currents – and as section 3.6 illustrates the currents vary quickly across the channel.



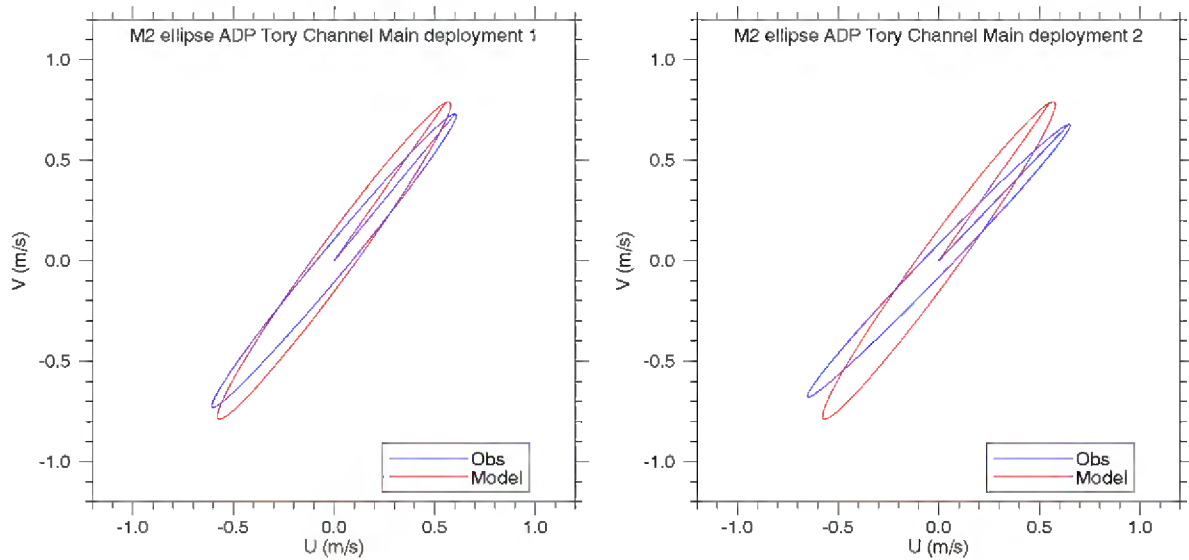


**Figure 3-6: M2 tidal velocity comparison (Tory Channel).** As Figure 3-5 but for the Tory Channel ADCP. Note the large difference in velocity scales.

Table E-5 to Table E-7 also shows comparisons for the smaller S2 and N2 semi-diurnal constituents and the O1 diurnal constituent. Agreement is about as good for S2 and N2 as for M2. The agreement is not so good for O1, however this constituent is very small and has only a small influence on current speeds.

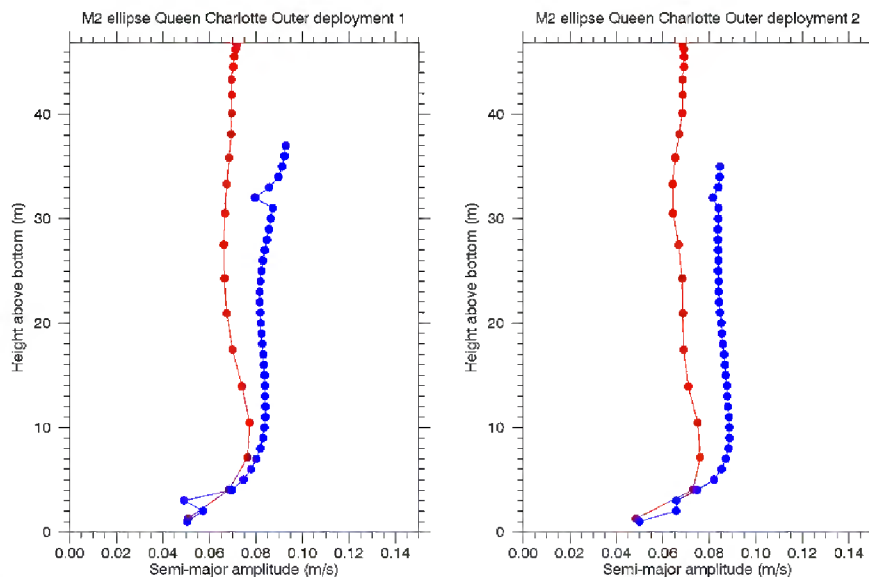


**Figure 3-7: M2 tidal velocity profile comparison (Queen Charlotte Outer).** M2 semi-major amplitude versus depth from ADCP (blue) and model (red) for Deployment 1 (left) and 2 (right).

The tidal current amplitude normally decreases towards the bottom due to friction. Figure 3-7 shows the variation of the M2 semi-major amplitude with height for the QCS Outer ADCP and Figure 3-8 shows a similar plot for the Tory Channel ADCP. In the QCS Outer plot (Figure 3-7) the model's under-prediction of tidal currents in the middle of the water column is evident. The model and observations show a slight maximum in amplitude at about 10 m above the bottom and then a reduction over the lowest 5 m or so of the water column, where they agree reasonably well. The maximum at 10 m is

probably related to the bathymetry in the area of the ADCP (Figure 2-1b), specifically to the presence of a sill at the entrance to Queen Charlotte Sound. At the Tory Channel ADCP site (Figure 3-8), the modelled and measured profiles agree, with the amplitude dropping off smoothly towards the bottom (except for a step in observed profile at 3 m depth).

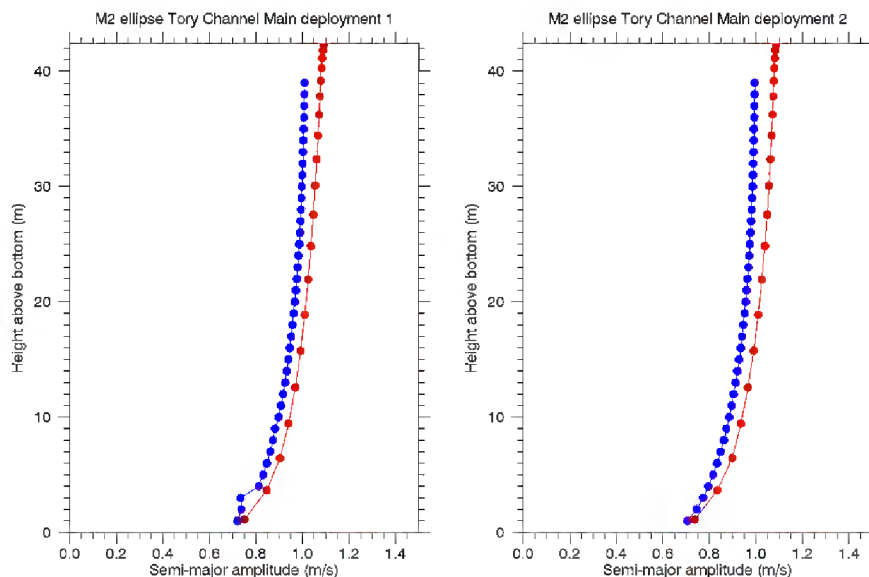


**Figure 3-8: M2 tidal velocity profile comparison (Tory Channel).** As Figure 3-7 but for Tory Channel.

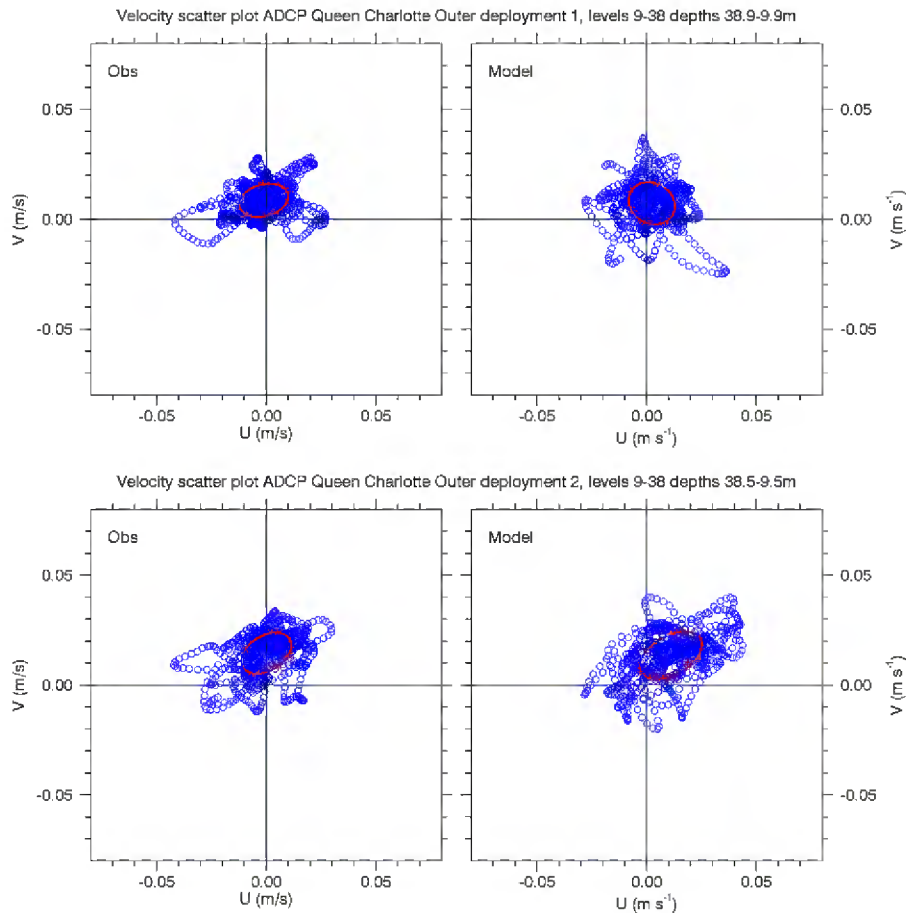
### 3.4 Model vs observations: sub-tidal currents

This section considers the accuracy of the model's representation of sub-tidal currents, i.e. fluctuations in the currents with frequencies below the tidal frequencies. The comparison is presented graphically in Figure 3-9 to Figure 3-12 with tabular data shown in Table E-8. Sub-tidal currents were estimated by applying a low-pass temporal filter to the data, an operation known as detiding. The filter was the 24G113 filter from Thompson (1983), applied to hourly values; see Figure 1 of that article for its frequency response. The filter removes essentially all fluctuations with a period of less than 2 days from the data and yields rather smooth time series as a result. Note that a comparison between model and measurements, as here, should not be particularly sensitive to the filter characteristics as long as the same filter is applied to both.

Figure 3-9 compares measured and modelled scatter plots of the sub-tidal velocities at the Queen Charlotte Outer mooring site. The red ellipse in each scatter plot is a variance ellipse, a conventional representation of the magnitudes of variability in velocity data. A variance ellipse can be characterised by its semi-major axis (in this context called a principal axis), eccentricity and inclination, like a tidal ellipse. However a variance ellipse does not have a phase (since it says nothing about the timing of the variability) and its eccentricity has no sign (since it says nothing about the rotation of velocity vectors). Also, the centres of the variance ellipses in Figure 3-9 are offset from the origin by an amount representing the mean current over the period of the deployment.

The variance ellipses in Figure 3-9 are quite round, i.e. currents are not strongly aligned along the direction of the channel, which is  $50^\circ$  T at this site. Magnitudes are typically  $\sim 0.02 \text{ m s}^{-1}$  (cf. the semi-major axis of the  $M_2$  tidal current, which is  $\sim 0.08 \text{ m s}^{-1}$ ) and the mean current is generally directed

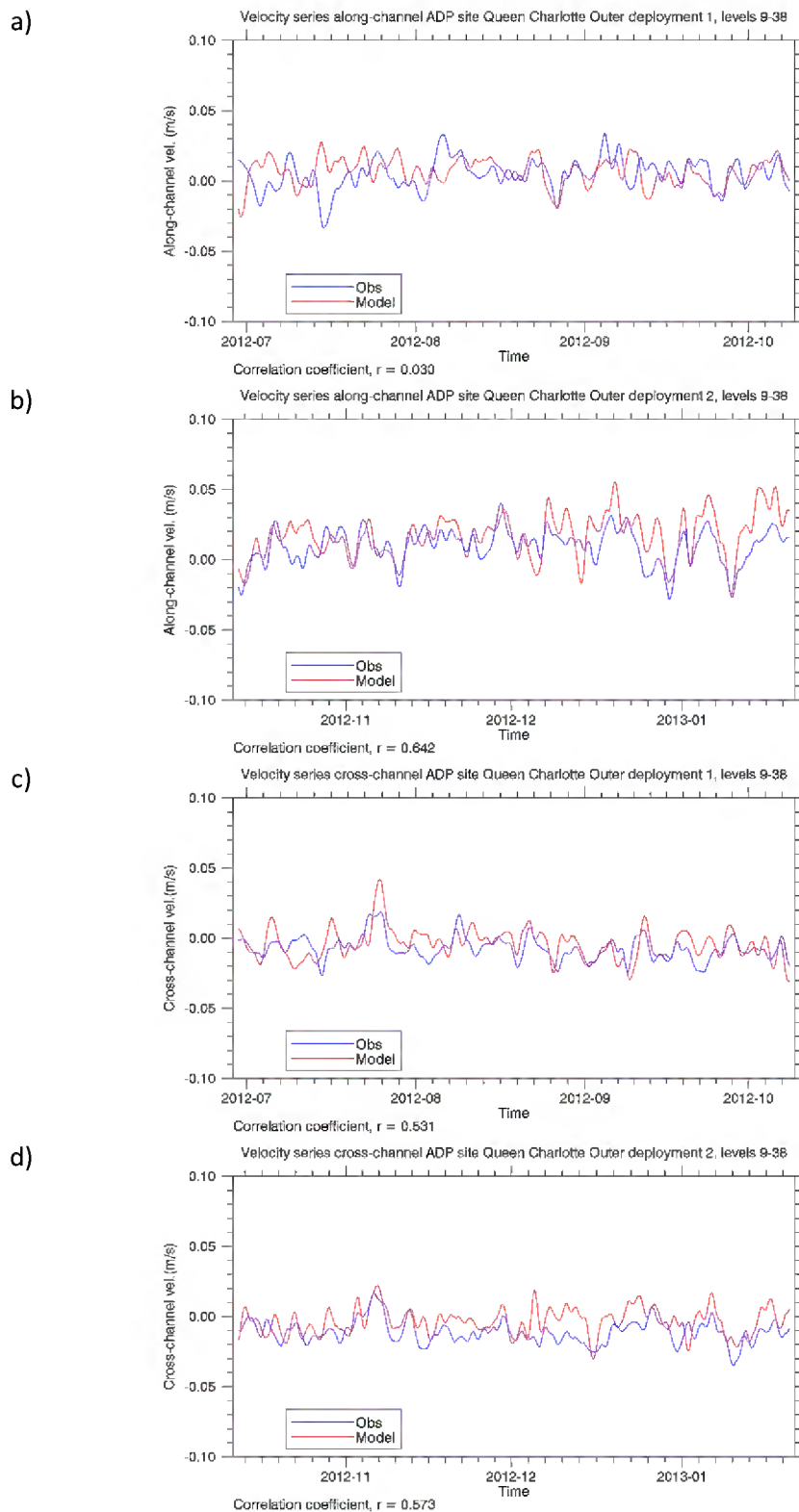
towards the north at  $\sim 0.01\text{--}0.02\text{ m s}^{-1}$ . Agreement between the model and measurements is reasonably good.



**Figure 3-9: Sub-tidal velocity vector comparison (Queen Charlotte Outer).** Scatter plots of measured (left) and modelled (right) sub-tidal velocity at the Queen Charlotte Outer ADCP site. The axes correspond to the velocity components towards due east ( $u$ ) and due north ( $v$ ). The red lines are variance ellipses, representing the magnitude and orientation of the sub-tidal velocity variations (see text). The upper and lower panels are for Deployments 1 (2012-06-28 to 2012-10-10) and 2 (2012-10-11 to 2013-01-22).

Figure 3-10 compares time series of measured and modelled along-channel and across-channel velocities. The along-channel direction was estimated by eye from a map to be  $50^\circ$  T; the across-channel direction is perpendicular to this at  $140^\circ$  T. The correlation coefficient ( $r$ ) between the two time series is shown on each plot.

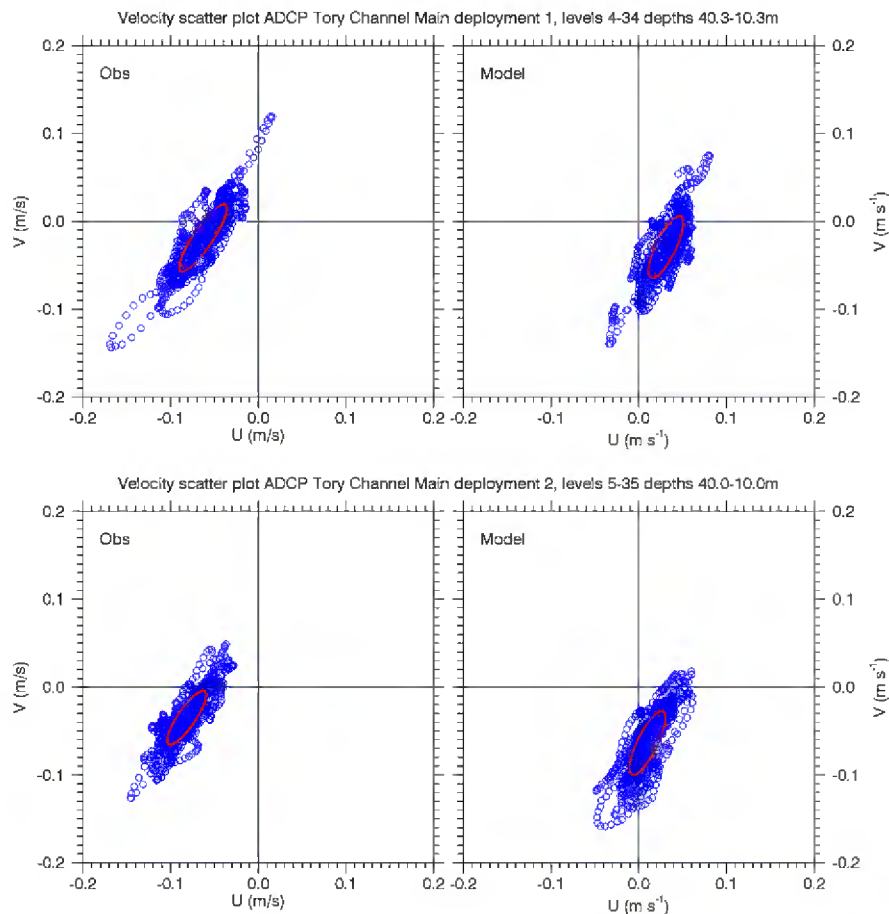
Our experience of ROMS in open-coast situations (Hadfield and Zeldis 2012; Hadfield 2013) is that along-channel or coast-parallel currents, which are primarily wind-driven, are well-predicted by the model with  $r$  between 0.8 and 0.9, but that across-channel or coast-perpendicular currents are less well predicted, with  $r \sim 0.6$  or less, sometimes zero. For the time series in Figure 3-10 the correlation coefficient varies between  $+0.03$  and  $+0.64$ , which indicates negligible to modest correlation: some peaks in the measured time series are duplicated rather well by the model, but many are not.



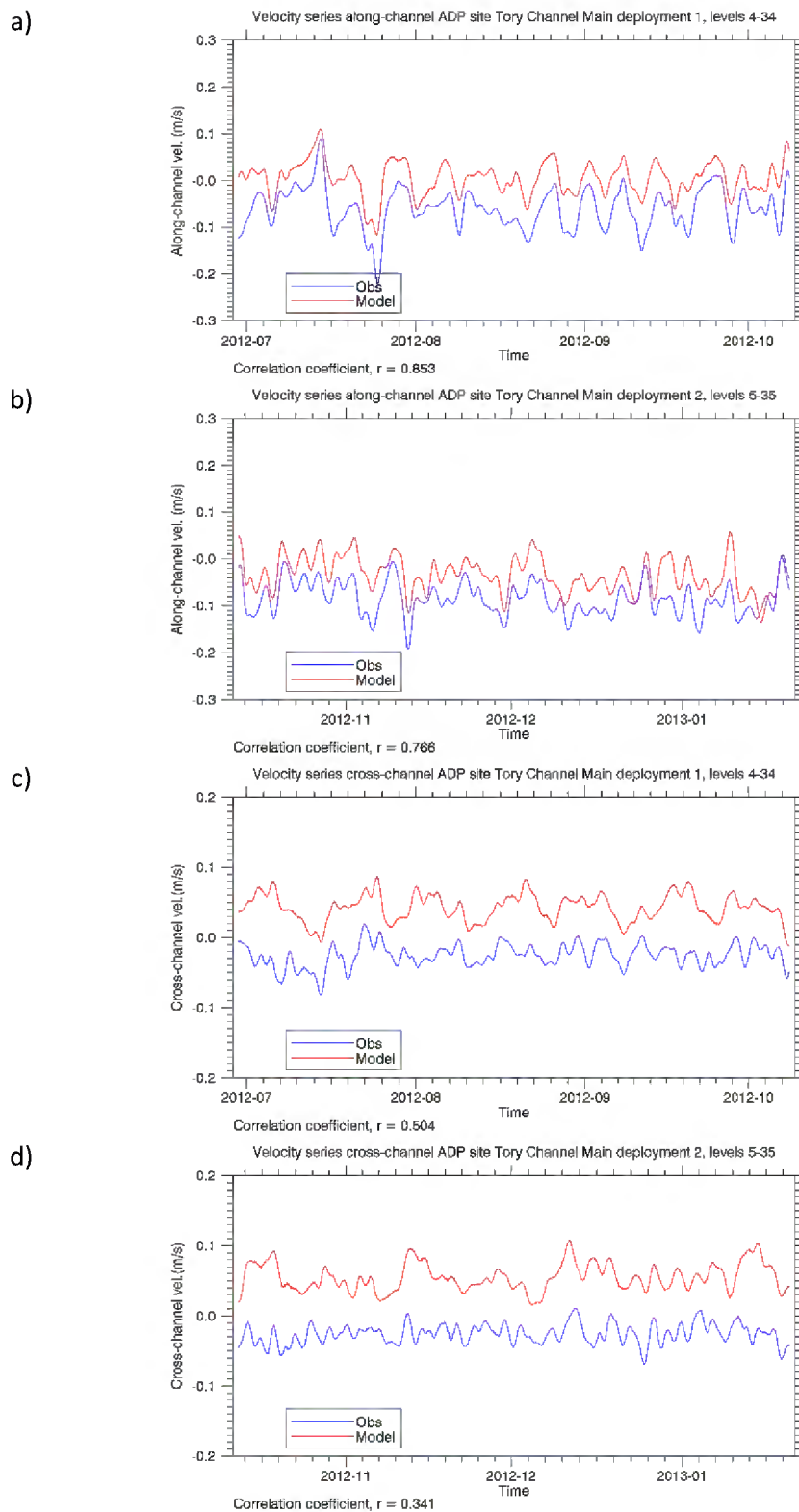
**Figure 3-10: Sub-tidal along-channel and across-channel velocity comparisons (Queen Charlotte Outer).** Time series of measured (blue) and modelled (red) sub-tidal velocity components in the along-channel (towards 50° T) and across-channel (towards 140° T) for Queen Charlotte Outer mooring deployments 1 and 2: a) along-channel deployment 1; b) along-channel deployment 2; c) across-channel deployment 1; d) across-channel deployment 2.

Figure 3-11 and Figure 3-12 show a similar comparison for the Tory Channel ADCP. The along-channel direction was again estimated by eye to be  $50^\circ$  T. The inclination and magnitude (semi-major axis) of the variance ellipses are similar between all the plots in Figure 3-11 at values of  $\sim 30^\circ$  T and  $0.04 \text{ m s}^{-1}$  (c.f. the M2 tidal semi-major axis of  $\sim 1.0 \text{ m s}^{-1}$ ). However there is a substantial difference between the measured and modelled mean current vectors. The measured mean current in both deployments is directed towards  $250^\circ$  T at  $\sim 0.08 \text{ m s}^{-1}$ . The modelled mean current is a little smaller in magnitude ( $\sim 0.05 \text{ m s}^{-1}$ ) but directed towards  $120^\circ$  T in Deployment 1 and  $160^\circ$  T in Deployment 2. In other words the measured mean current at the Tory Channel ADCP site is directed along the channel towards its junction with Queen Charlotte Sound, but the modelled current is directed across the channel towards its southern shore.

From the time series plots in Figure 3-12 the model reproduces the observed fluctuations in along-channel current reasonably well ( $r$  values are 0.85 and 0.77) and the fluctuations in across-channel currents less well ( $r$  values are 0.50 and 0.34). The mean offset between the measured and modelled across-channel currents is very apparent.



**Figure 3-11: Sub-tidal velocity vector comparison (Tory Channel).** Scatter plots of measured (left) and modelled (right) sub-tidal velocity as Figure 3-9, but for the Tory Channel mooring.



**Figure 3-12: Sub-tidal along-channel and across-channel velocity comparisons (Tory Channel).** Time series measured and modelled velocity components, as Figure 3-10 but for Tory Channel. The along-channel and across-channel directions are the same as for the Queen Charlotte Outer site.

Finally, in connection with sub-tidal currents, Figure 3-13 shows the vertical profile of the mean, along-channel velocity from the ADCP (blue) and the model (red) for Deployments 1 and 2. In all

cases the velocity is positive (directed out of the Sound) at the surface and negative at the bottom. The profiles match rather well for Deployment 1, but for Deployment 2, the model has a stronger vertical variation than the ADCP data.

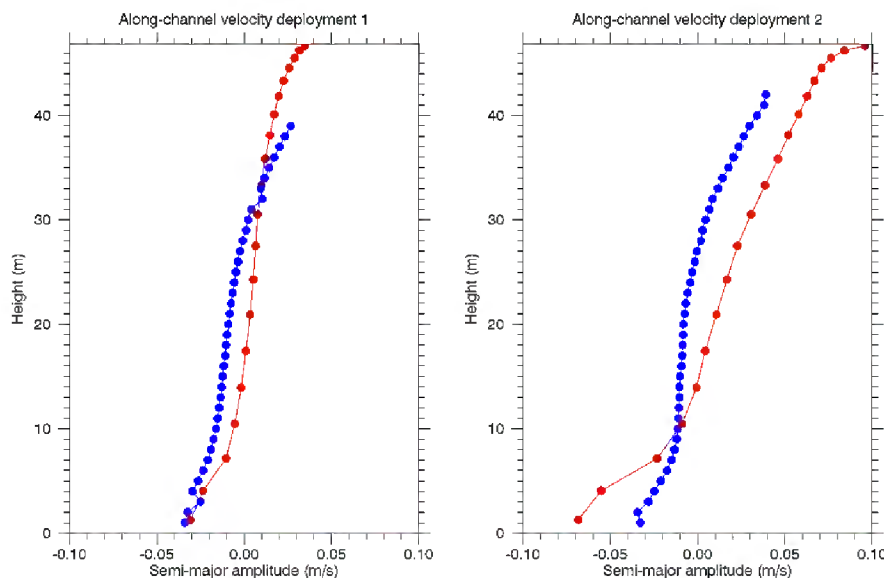


**Figure 3-13: Along-channel mean velocity profile comparison (Queen Charlotte Outer).** Mean along-channel velocity versus depth from ADCP (blue) and model (red), for Deployment 1 (left) and 2 (right).

Overall, the model generates sub-tidal currents at the ADCP sites with approximately the right magnitude, but the temporal correlation between modelled and measured fluctuations is not as good as one expects from a model on the open coast. At the Tory Channel site there is a consistent offset between the modelled and measured mean currents. These limitations are likely due to two reasons.

- The surface wind dataset was generated by an atmospheric model with a resolution of 12 km, which is too coarse to resolve the channelling of the wind by topography around Marlborough Sounds.
- For the Tory Channel site, there are strong tidal currents ( $\sim 1 \text{ m s}^{-1}$ ) which generate—through non-linear effects like ebb-flood symmetry—significant, spatially complex mean currents that are comparable to or larger than the measured sub-tidal currents ( $\sim 0.05 \text{ m s}^{-1}$ ). It is challenging to simulate these tidal currents accurately without high spatial resolution in the model (which we cannot afford) and an accurate description of the bathymetry (which we don't have). The effect of model resolution on the simulated flows in Tory Channel is discussed in more detail in Section 3.6 below.

### 3.5 Currents and volume fluxes

The capacity of the environment to dilute and disperse additional dissolved material—whether it be fish farm wastes or substances from other sources—is clearly central to the present project. Before moving directly to the biophysical model and its results, the remainder of this section presents some relevant analyses of the currents in the main channels of the Queen Charlotte Sound system. A later

section (Section 3.7) looks specifically at the transport of dissolved material through and out of the Sound.

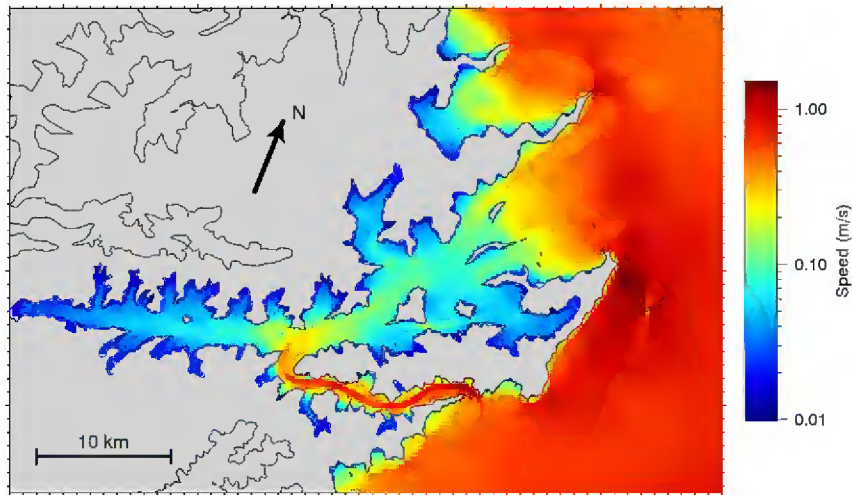


**Figure 3-14: Model mean current speed.** Mean current speed at 5 m depth, based on one year's hourly data from the 200 m model.

As an approximate indicator of near-field dispersal of nutrients or waste from a mussel farm or fish farm, Figure 3-14 shows the mean current speed at 5 m depth. The largest mean speeds are associated with the strong tidal currents through Tory Channel and in Cook Strait. The mean speed is above  $0.7 \text{ m s}^{-1}$  along Tory Channel,  $1.2 \text{ m s}^{-1}$  through Tory Channel entrance (which is not resolved very well at this model resolution, however) and up to  $1.5 \text{ m s}^{-1}$  between Arapawa Island and The Brothers. Throughout much of the interior of Queen Charlotte Sound the mean speed is  $\sim 0.05 \text{ m s}^{-1}$  but it increases above this at the junction with Tory Channel and in the Sound entrance area beyond Long Island.

The analyses in the remainder of this section deal with several sections across Tory Channel and Queen Charlotte Sound (Figure 3-15).



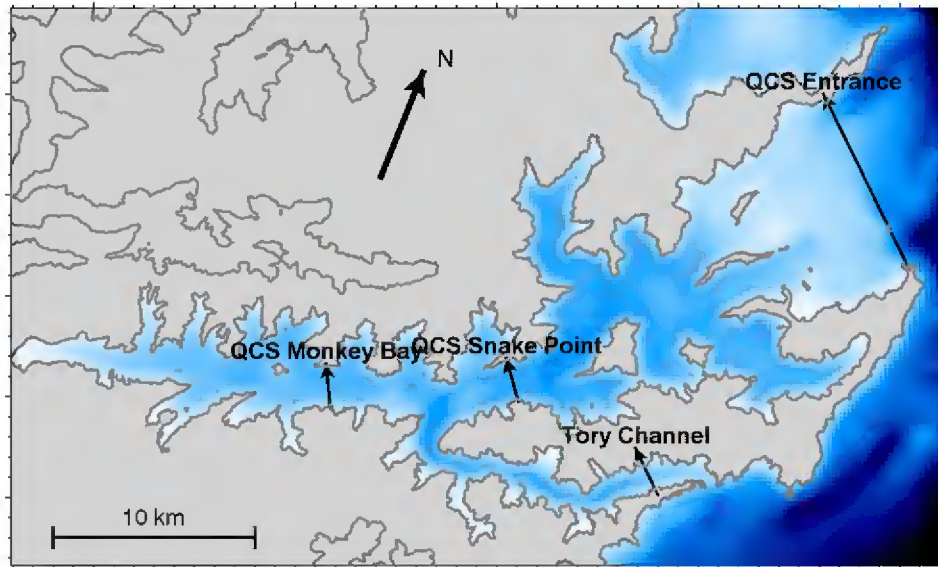


**Figure 3-15: Location of sections used for volume-flux calculations.** A map showing the model bathymetry and land mask (200 m grid), with labelled cross-sections.

Figure 3-16 shows the volume flux across two of these sections based on hourly model output. The flux through QCS Entrance is typically  $10\text{--}15,000\text{ m}^3\text{ s}^{-1}$  at spring tide and  $0\text{--}5,000\text{ m}^3\text{ s}^{-1}$  at neap tide. The flux through Tory Channel is larger at  $30,000\text{ m}^3\text{ s}^{-1}$  (spring) and  $20,000\text{ m}^3\text{ s}^{-1}$  (neap). Given that the volume of Queen Charlotte Sound (in the region defined for the flushing calculations of Section 3.7) is around  $9900 \times 10^6\text{ m}^3$ , the peak spring-tide volume flux through Tory Channel would be large enough to replace all the water in the Sound in 3.8 days, if it were maintained for long enough. Of course, the peak tidal transports are not maintained for several days, but this calculation nonetheless gives some context to the magnitude of these volume fluxes. Another interesting implication of these graphs is that, of the water filling and draining Queen Charlotte Sound on each tide, the volume coming through Tory Channel is much larger (particularly at neap tide) than the volume coming through the main entrance of Queen Charlotte Sound, despite the smaller width of Tory Channel.

The black lines in Figure 3-16 are based on a moving-window analysis for the semi-diurnal tide, with the central black line indicating the sub-tidal part of the volume flux. Figure 3-17a shows this sub-tidal flux (outflow positive) through the QCS Entrance (blue) and Tory Channel (red) sections. The two time series tend to be opposite in sign and approximately equal in magnitude, as confirmed by plotting the sum (black) which is small at  $\sim\pm 100\text{ m}^3\text{ s}^{-1}$ . (Note that this sum has to be small because otherwise water would progressively accumulate in or drain from Queen Charlotte Sound.)

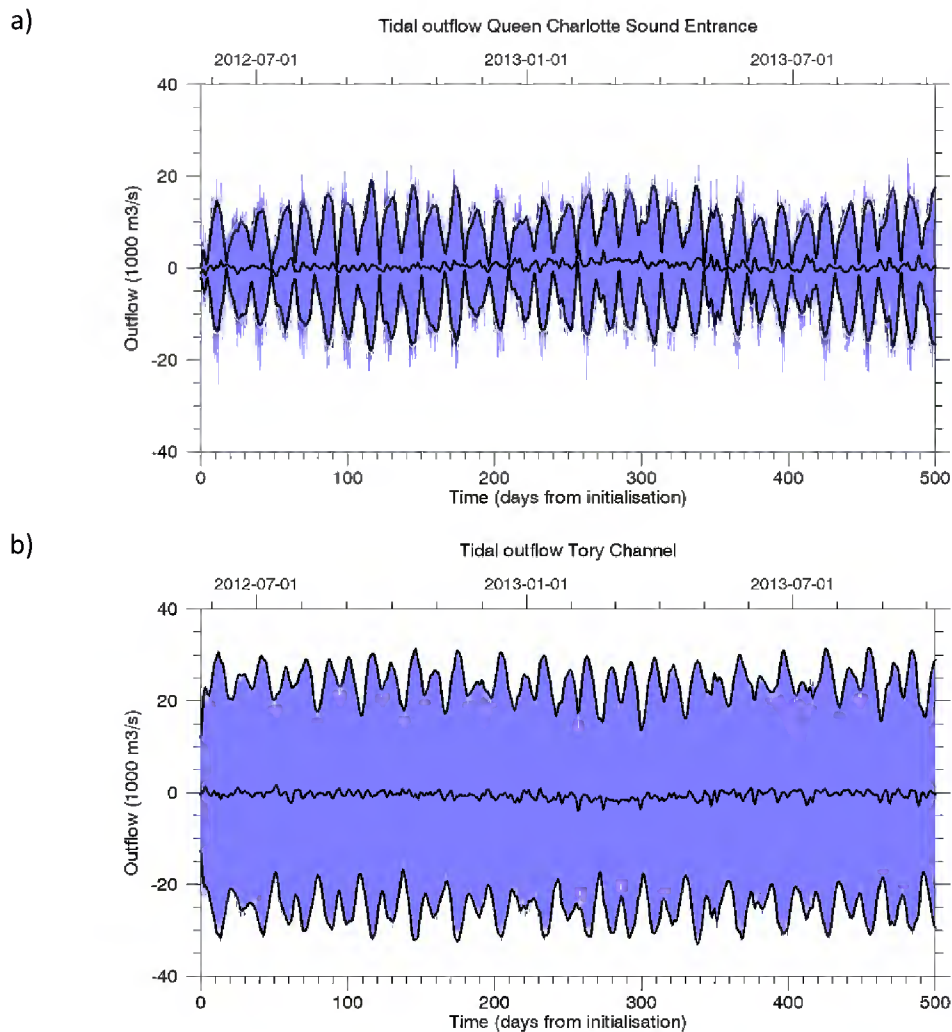


**Figure 3-16: Tidal volume fluxes.** Time series of volume flux for sections across: a) Queen Charlotte Sound Entrance; b) Tory Channel. The light blue line represents the hourly volume flux (outflow positive) and the thick black lines represent the mean plus & minus the amplitude of the semi-diurnal tidal flux as estimated by a moving-window tidal harmonic analysis (window width 3.5 days).

Figure 3-17b shows just the QCS Entrance sub-tidal flux, which can be identified as the sub-tidal flow *through* Tory Channel and Outer Queen Charlotte Sound, with a positive value indicating *clockwise* flow around Arapawa Island. The thick blue line is a 20-day moving average. It is small ( $< 500 \text{ m}^3 \text{ s}^{-1}$ ) at the start of the simulation, rises fairly smoothly to a peak of  $1800 \text{ m}^3 \text{ s}^{-1}$  at the beginning of March 2013 and then drops back to less than  $500 \text{ m}^3 \text{ s}^{-1}$  or so by the beginning of August 2013. The average over the final 365 days of the simulation is  $660 \text{ m}^3 \text{ s}^{-1}$ . Around the 20-day average line there are positive and negative fluctuations—with the positive ones being apparently a little larger than the negative ones—with magnitudes up to  $\sim 2000 \text{ m}^3 \text{ s}^{-1}$  and typical durations of 5–10 days.

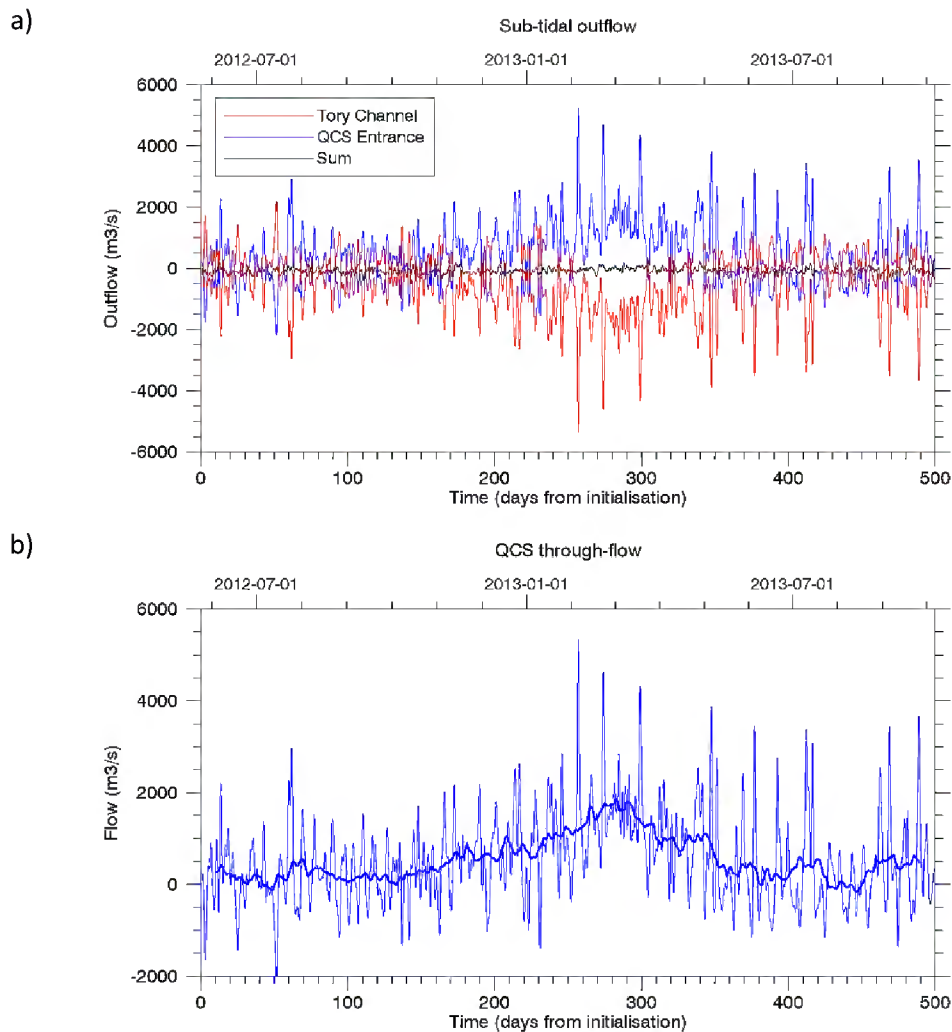


**Figure 3-17: Sub-tidal volume fluxes.** a) Sub-tidal outflow through QCS Entrance (blue) and Tory Channel (red) sections, with the sum in black; b) Sub-tidal outflow through QCS Entrance (thin blue line) with 20-day moving average (thick blue line). Sub-tidal fluxes are estimated from hourly data with the same Thompson (1983) 24G113 filter that was applied in Section 3.4.

A comparison of the sub-tidal volume flux with the surface stress (Figure 3-18) identifies the latter as a major driver of the short-term variability in the volume flux. The figure indicates a positive correlation between the sub-tidal volume flux and the component of the surface stress directed towards  $15^\circ$  T, the direction having been chosen to maximise the correlation. The relationship is physically reasonable, as a surface stress directed towards  $15^\circ$  T acting on Outer Queen Charlotte Sound will tend to push water out of the Sound. There will also be an opposing effect from the same surface stress acting on Tory Channel, but the latter has a much smaller area so this effect will be smaller.

The dashed blue line and blue text in Figure 3-18 indicate a linear regression relationship by which the volume flux can be predicted from the surface stress. Figure 3-19 shows how good this prediction is. The linear regression prediction reproduces the short-term fluctuations in the volume flux from the hydrodynamic model very well, as one would expect with a correlation coefficient of 0.70. However the linear regression prediction does not reproduce the peak in the 20-day-average volume flux in early March 2013 and instead produces a broader maximum centred on June 2013.

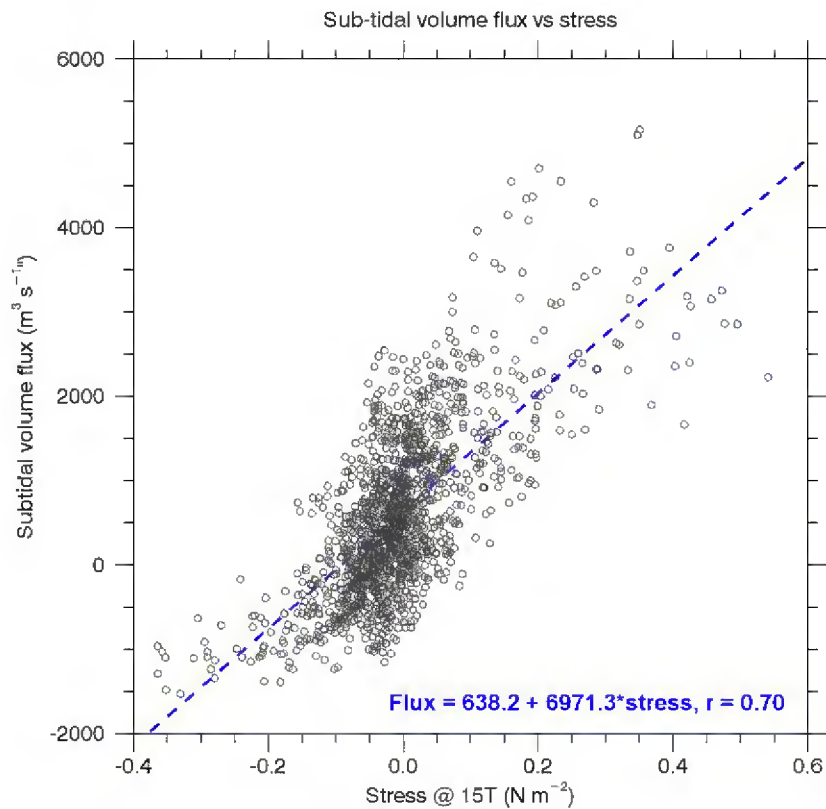


**Figure 3-18: Sub-tidal volume flux versus surface stress.** A scatter plot of sub-tidal volume flux (as plotted in Figure 3-17b) against the surface stress component directed towards 15° T. Data are shown for the final 365 days of the simulation. The surface stress values are daily averages calculated from the 3-hourly model forcing at a location in Outer QCS. The dashed blue line indicates a linear regression relationship, with coefficients given in the blue text. The direction of 15° T has been chosen to maximise the correlation.

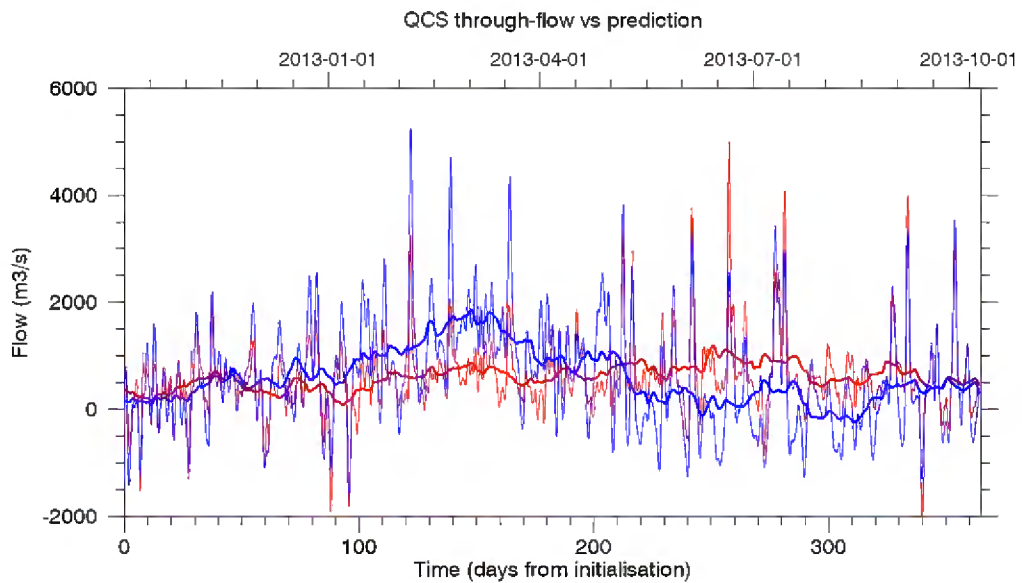


**Figure 3-19: Sub-tidal volume flux compared with the prediction from the surface stress.** Sub-tidal volume flux (blue) through Queen Charlotte Sound (cf. Figure 3-17b) compared with the prediction (red) of the regression relation given in Figure 3-18. The thin lines represent unfiltered values and thick lines represent 20-day moving averages.

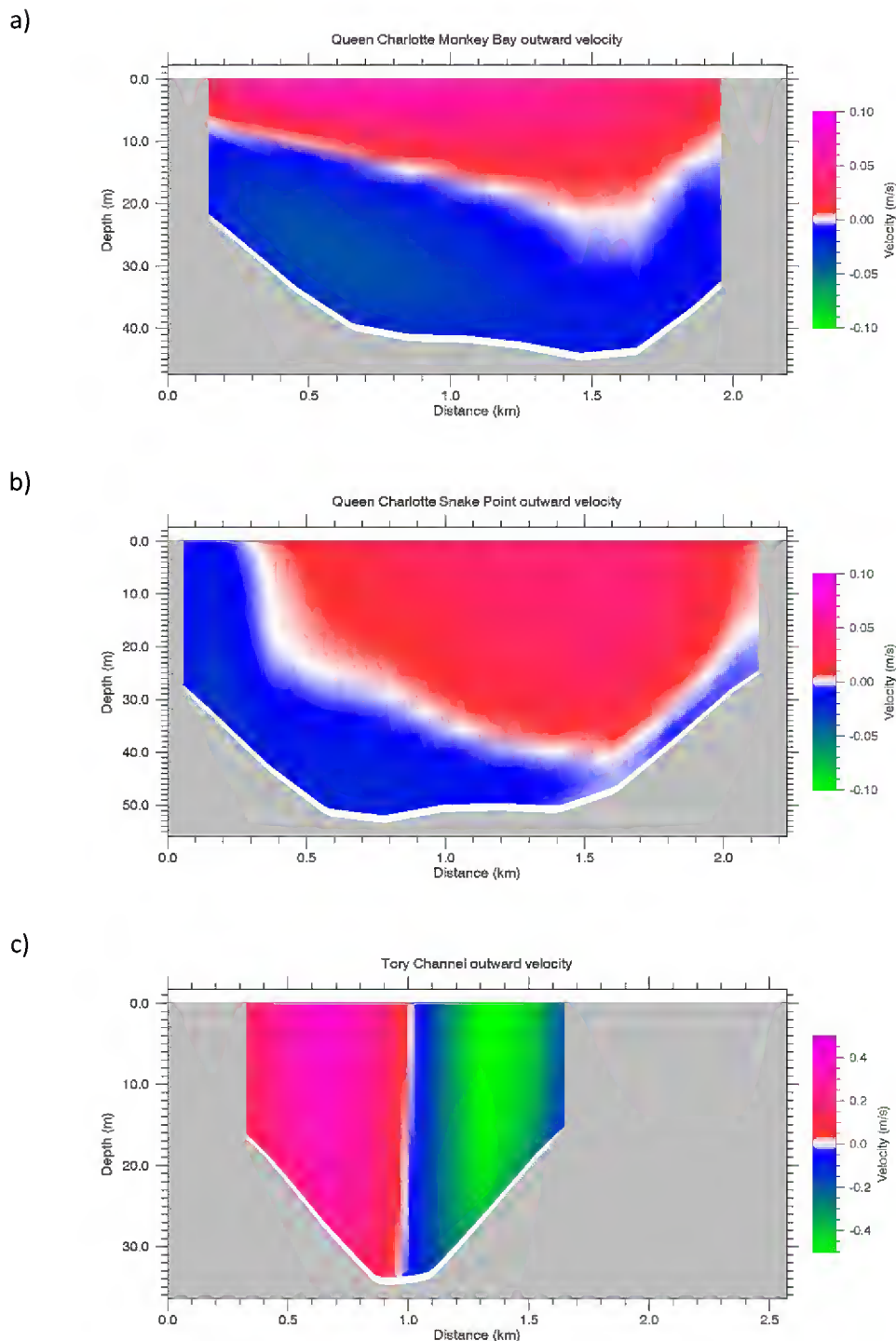


**Figure 3-20: Velocity through cross-channel sections.** One-year mean modelled velocity perpendicular to sections across Queen Charlotte Sound and Tory Channel as shown in Figure 3-15: a) Queen Charlotte Monkey Bay (Inner QCS); b) Queen Charlotte Snake Point (Outer QCS); c) Tory Channel. Velocity is positive outwards and the view is looking from the seaward side of the section, looking inwards.

The information on volume fluxes presented in this section relates to the vertically-averaged currents. Another important aspect of the currents in Queen Charlotte Sound is the vertical variation.

Figure 3-20 shows plots of time-averaged velocity (positive outwards) through three sections across Queen Charlotte Sound and Tory Channel (see Figure 3-15 for these locations). For Inner QCS (Figure 3-20a) there is an outward flow at the surface (up to  $0.06 \text{ m s}^{-1}$ ) overlying an inward flow below (up to  $0.04 \text{ m s}^{-1}$ ), with the boundary between at 10–20 m depth. This is the vertical structure expected for an estuarine circulation, generated by the freshwater input into the Sound. Animations (not shown) of this graph with monthly average data indicate that this vertical structure is set up within 60 days or so of the beginning of the simulation and continues with relatively little change throughout. For Outer QCS at Snake Point (Figure 3-20b) there is a similar circulation, but with the core of the outward flow displaced towards the right-hand (north-western) end of the section and the inwards flow displaced towards the left. For the Tory Channel section (Figure 3-20c) the mean flow is almost uniform with outwards flow on the left-hand (south-western) side of the channel and inwards flow on the right-hand side. (Note the different scale for the Tory Channel figure, required by the much larger mean currents.) The structure of the mean flow in Tory Channel is discussed again in the following section.

### 3.6 Effect of model resolution on Tory Channel tidal flow

Tory Channel plays an important role in transporting material into and out of Queen Charlotte Sound and is a relatively narrow ( $\sim 1 \text{ km}$  along most of its length, but narrower at the entrance) and sinuous channel with strong ( $\geq 1 \text{ m s}^{-1}$ ) tidal currents. Modelling the flow through the Channel is arguably the biggest challenge in modelling the Sound as a whole. As discussed in Section 2.2 we used models at several different grid resolutions, with the coarsest grids allowing speedy model development and the finest grids allowing us to explore the effect of grid resolution on the results. Figure 3-21 and Figure 3-22 show the effect of grid resolution on the model's treatment of tides in Tory Channel. The simulation here was 3-dimensional but with uniform density and forced only by the M2 tide (no surface stresses or fluxes, zero mean currents at the boundary). It was run for 6 lunar days<sup>6</sup>, with 3 lunar days to spin up the tides and 3 lunar days for analysis. The short period allowed the use of a 50 m grid, which is too expensive for simulations of a few months or longer.

Figure 3-21 shows the semi-major tidal amplitude. At the coarsest resolution, 400 m, there is a broad, relatively sluggish band of tidal flow across the channel, with no mid-channel maximum, which is not surprising as there are only 3–4 grid cells across the width of the channel. At the finer resolutions, there is a progressively better resolved mid-channel maximum in the tidal current, with more along-channel variation, sharper gradients in some places along the edges and a more “fluid” appearance to the graph.

Examination of animations (not shown) from these simulations shows that the current tends to meander in the channel, taking a somewhat different path on the flood (incoming) tide than on the ebb (outgoing tide). For example, in the curved section of the channel between the ADCP location and the entrance, the inflowing current pushes against the northern side of the channel, but the outgoing current is closer to the southern side. This process, which is a form of tidal rectification (generation of mean currents from fluctuating tidal forcing), results in a gyre pattern in the mean currents (Figure 3-22). The magnitude of the gyre currents is of the order of  $0.2 \text{ m s}^{-1}$  and they change in nature as they are better resolved by the model at finer resolutions. The Tory Channel ADCP site is near the south-western edge of an anti-clockwise gyre. The mean current at the ADCP

---

<sup>6</sup> One lunar day equals two M2 tidal periods, or 24.84 hours.

location is sensitive to the grid resolution and would also be sensitive to any changes in the gyre pattern, for whatever reason. In other words, it is very challenging for a model to reproduce mean currents at the location of the current meter.

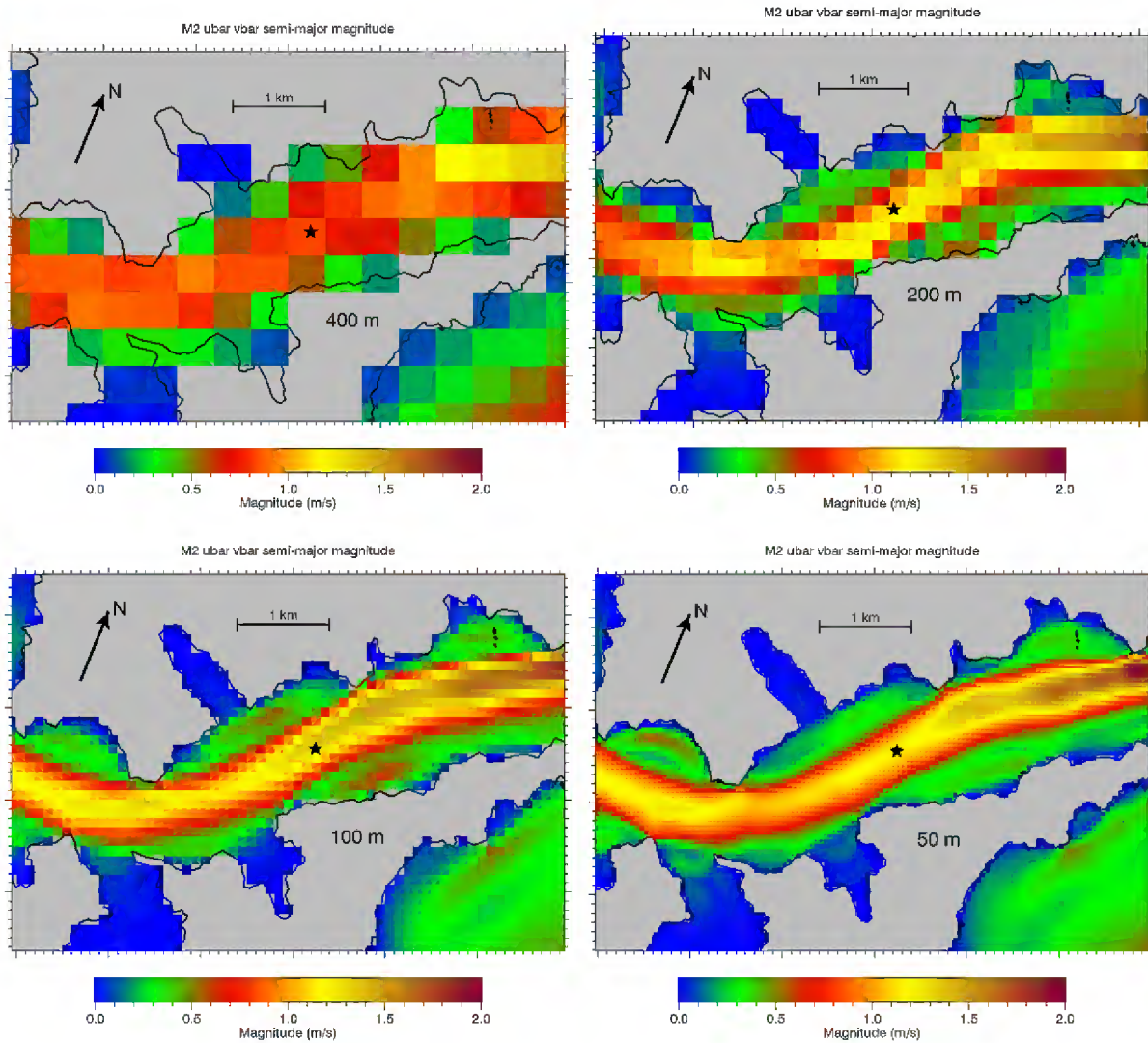


**Figure 3-21: Semi-major amplitude of M2 tidal currents in Tory Channel vs model resolution.** Map of modelled semi-major amplitude in Tory Channel from simulations forced by the M2 tide only. Results are shown from models at four different horizontal resolutions, from 400 m to 50 m. Data are calculated over 6 tidal cycles from the depth-average current saved at intervals of 30 lunar minutes. The star symbol indicates the position of the Tory Channel ADCP.

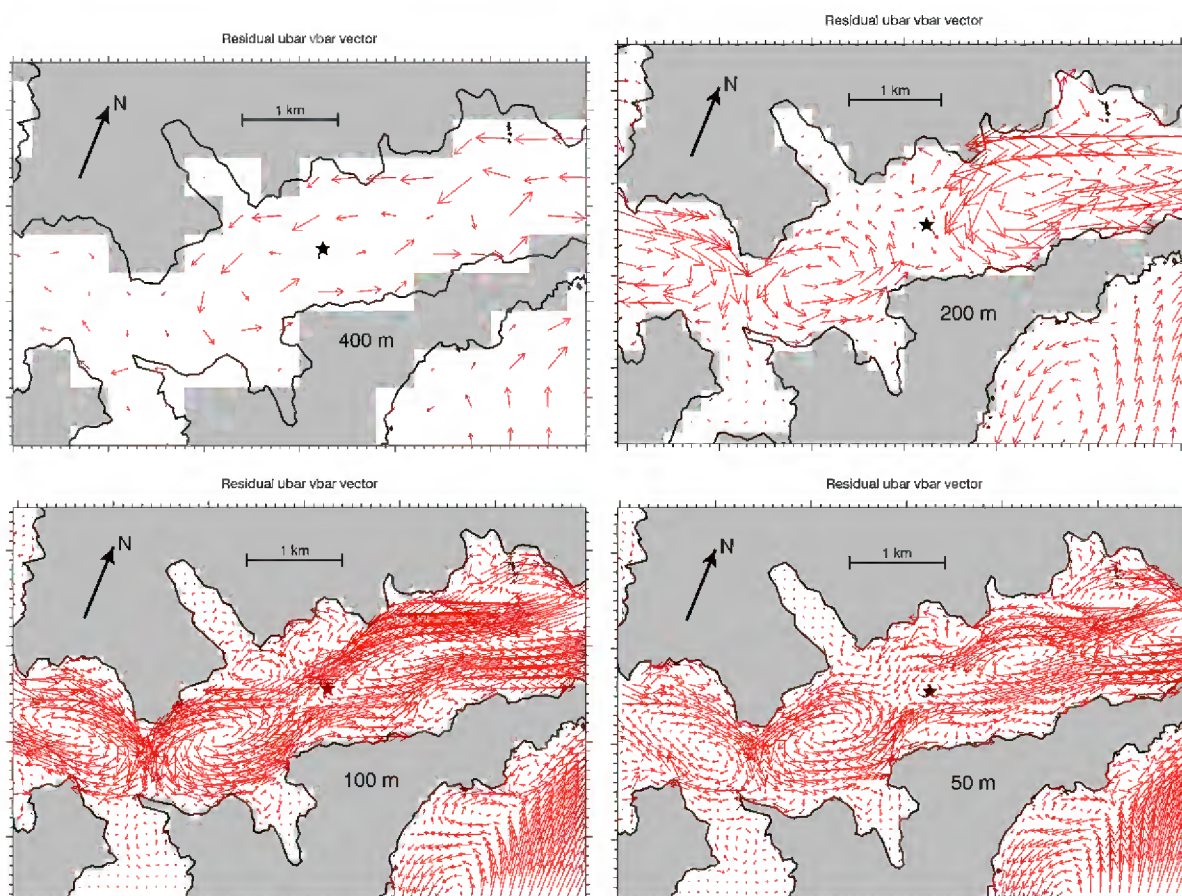


**Figure 3-22: Mean currents forced by rectification of the M2 tide in Tory Channel vs model resolution.** As Figure 3-21 but showing mean current vectors for the same simulation. Vectors are shown at every grid point for the 400, 200 and 100 m models, and at every second grid point for the 50 m model.

### 3.7 Flushing

A set of simulations was set up to investigate the dilutive capacity of Queen Charlotte Sound for idealised sources of dissolved material. Passive tracers, or virtual dyes, were injected into a hydrodynamic model of the Sound at three sites (Figure 3-23) representative of Inner QCS, Outer QCS and central Tory Channel. There were two releases at each site, one 5 m below the surface and another 5 m above the bottom, giving a total of 6 virtual dyes in each simulation. The model was run at three resolutions, 400 m, 200 m and 100 m, for the usual 500 days, except that the 100 m simulation (which would take approximately 26 days wall clock time to complete) has been run for only 200 days.



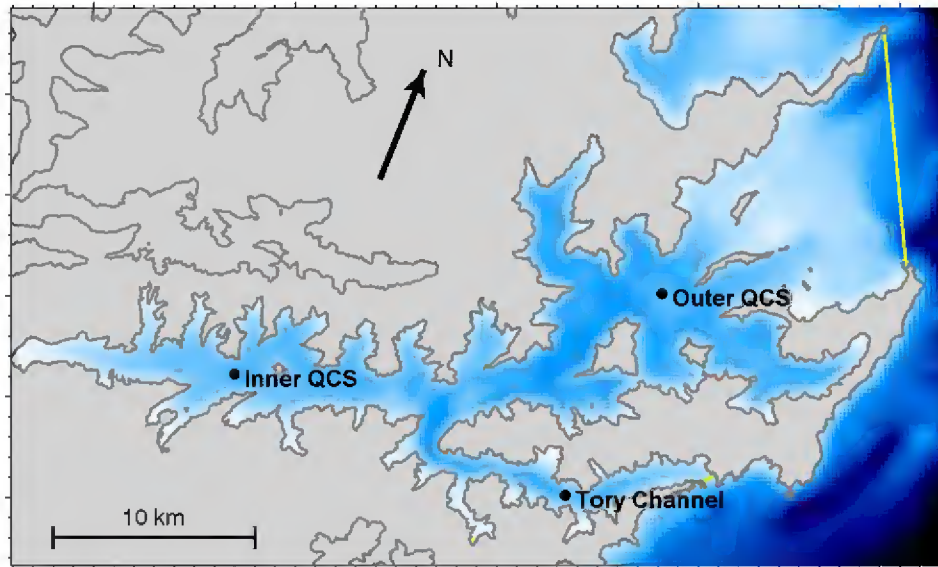


**Figure 3-23: Location of passive tracer sources in the flushing simulations.** A map showing the model bathymetry and land mask (200 m grid), with source locations for the flushing simulations (black circles and labels) and the boundaries for calculation of volume integrals (yellow lines across QCS and Tory Channel entrances).

The release rate  $Q$  of each dye was constant at a nominal  $1 \text{ kg s}^{-1}$ . The concentration  $C$  of the same dye at any location and time is measured in  $\text{kg m}^{-3}$  and should be proportional to  $Q$  (i.e. doubling the release rate should exactly double the concentration). Therefore the ratio between them,  $C/Q$ , can be called a normalised concentration: it has units of  $\text{s m}^{-3}$  and depends on the flow and the location of the source, but not on the release rate. It is convenient to represent this normalised concentration in terms of its reciprocal, called the dilution rate  $D$ , which has units of  $\text{m}^3 \text{ s}^{-1}$  (Equation 3-1).

**Equation 3-1: Definition of the instantaneous dilution rate**

$$D = Q/C$$

A simple physical example illustrates the significance of the dilution rate. Consider a source of passive tracer, or dye, in a river. The dye plume will initially be narrow, but within a few hundred metres (or kilometres for a large river, and assuming no major tributaries join in the meantime) the dye will become uniformly mixed across the river, with a concentration equal to the release rate divided by the river's flow rate. In other words, the dilution rate at large distances downstream is equal to the river flow rate. Closer to the source, the dilution rate within the dye plume is lower (the concentration is higher), because not all of the river flow has mixed into the plume. Note that for a medium-sized river like the Pelorus the mean flow rate is approximately  $50 \text{ m}^3 \text{ s}^{-1}$  and for the Clutha River, the largest river by volume in New Zealand, it is approximately  $500 \text{ m}^3 \text{ s}^{-1}$ .

Within the context of coastal inlets, it is common to introduce the concept of flushing time (Zimmerman 1988; Monsen, Cloern et al. 2002). Here we specify the boundaries of the inlet (as in Figure 3-23), calculate the volume  $V$  (in  $\text{m}^3$ ) and evaluate the mass (in kg) of the tracer inside this volume. If the release rate is kept steady for long enough, we expect the mass to reach a more or less steady equilibrium value  $M_e$ . The equilibrium flushing time  $T_e$  is then defined by Equation 3-2:

**Equation 3-2: Definition of flushing time.**

$$T_e = M_e/Q$$

This gives a result in seconds, which is normally converted to days for convenience.

From the equilibrium mass  $M_e$  and the volume  $V$  we can calculate the equilibrium mean concentration  $C_e = M_e/V$  and from that we can calculate an equilibrium dilution rate  $D_e$  (Equation 3-3), which is representative of the inlet as a whole and applies when there is a balance, more or less, between input of the tracer from the source and flushing through the boundaries.

**Equation 3-3: Definition of the equilibrium dilution rate**

$$D_e = \frac{Q}{C_e} = \frac{V}{T_e}$$

Although discussions of dilution in coastal inlets often concentrate on the flushing time, the equilibrium dilution rate is often a more pertinent measure, and it involves the volume of the inlet as well as the flushing time.

For an indication of how these concepts can be applied to Queen Charlotte Sound, Figure 3-24 shows the time series of the total tracer mass within the Sound for the six tracers in the 200 m simulation. The lower horizontal axis in the plot shows time in days from the beginning of the simulation (and the tracer release); the upper horizontal axis shows the date. As explained in connection with Figure 3-23, there are 3 release sites, with sources at two heights at each site. The vertical axis is the normalised mass of tracer within the Sound, i.e. it is the mass  $M$  (in kg) divided by the release rate  $Q$  (in  $\text{kg s}^{-1}$ ), yielding a value in seconds, which is converted to days for plotting.

If Queen Charlotte Sound were a simple, well-mixed volume, then all six lines in Figure 3-24 would follow the same path. They would have an initial linear portion with a slope of 1 (i.e. one day's accumulation of mass per one day of release) and would then tend exponentially towards a horizontal line, at a value equal to the flushing time of the inlet. The actual lines do exhibit some of this behaviour, but deviate in several important respects. For the (blue) lines representing tracer released in Grove Arm, the initial portion with a slope of 1 is present and the lines reach a maximum value of around 40 days at 150 days after the start time (October 2012). They then drop away somewhat to a minimum in January 2013 and rise again to a second, slightly higher, maximum in July 2013. It appears that there is a seasonal variation, with the lowest value (fastest flushing) in summer and the largest (slowest flushing) in winter.

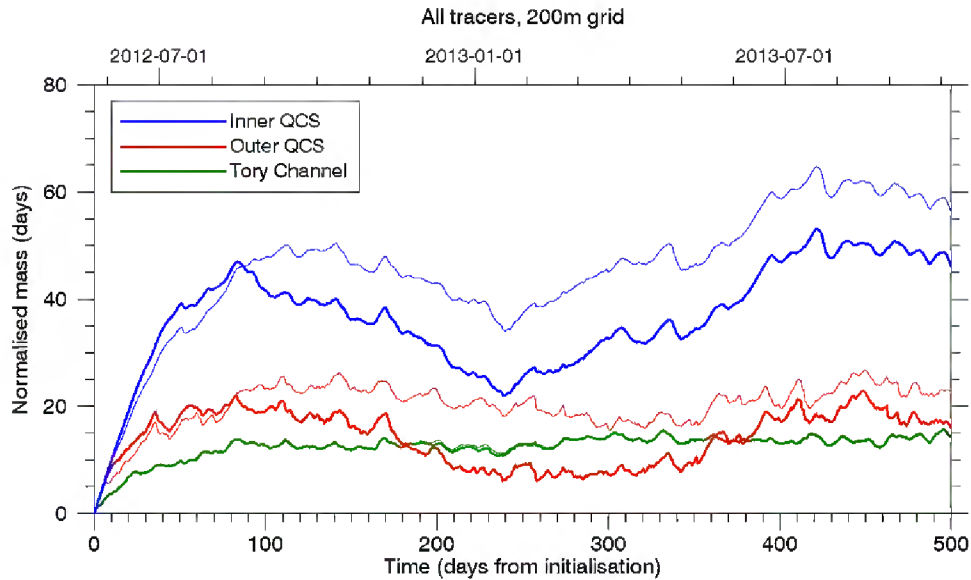


**Figure 3-24: Accumulation of tracer from the 200 m flushing simulation.** Normalised mass of tracer within Queen Charlotte Sound versus time in the 200 m flushing simulation for near-surface (thick line) and near-bottom (thin line) sources at the three tracer release sites: Inner QCS, blue; Outer QCS, red, Tory Channel, dark green.

To estimate an annual-average flushing time and dilution rate for the Grove Arm tracers in Queen Charlotte Sound, we have taken the average normalised mass for each tracer over the final 365 days of the simulation, i.e. from 2835 days (16 October 2012) to 3200 days (16 October 2013). The annual-average flushing time (Table 3-2) for the Grove Arm near-surface tracer is 35 days, and for the Grove Arm near-bottom tracer it is 46 days. The corresponding dilution rates are  $3300$  and  $2500 \text{ m}^3 \text{ s}^{-1}$ , respectively.

The time series in Figure 3-24 for the Outer Queen Charlotte Sound and Tory Channel tracers lie well below the Grove Arm time series, indicating that these tracers are flushed out of the Sound more quickly. The Outer Queen Charlotte Sound (red) lines have a similar seasonal variation to the Grove Arm (blue) lines and the annual-average flushing times are lower at 16 days (near-surface) and 22 days (near-bottom). The Tory Channel (dark green) tracers are different in character again, in that the near-surface and near-bottom lines are very close to each other and there is not a strong seasonal variation. The annual-mean flushing time for these tracers is 10.9 days. Another feature of the Tory Channel time series is that there is no initial portion with a slope of 1, at least not one that is evident on this graph. This indicates that some of the tracer released at the Tory Channel source is taken outside the boundaries of Queen Charlotte Sound within a day or so of the release.

**Table 3-2: Equilibrium flushing times and dilution rates for Queen Charlotte Sound.** Flushing times and dilution rates evaluated from the data in Figure 3-24 averaged over the last 365 days of the 200 m flushing simulation.

Site	Volume ( $10^6 \text{ m}^3$ )	Flushing time $T_e$ (days)	Dilution rate $D_e$ ( $\text{m}^3 \text{ s}^{-1}$ )
Grove Arm near-surface	9923	34.9	3290
Grove Arm near-bottom		46.1	2490
Outer QCS near-surface		15.6	7393

Site	Volume ( $10^6 \text{ m}^3$ )	Flushing time $T_e$ (days)	Dilution rate $D_e$ ( $\text{m}^3 \text{ s}^{-1}$ )
Outer QCS near-bottom		22.0	5217
Tory Channel near-surface		10.9	10,530
Tory Channel near-bottom		10.9	10,570

It is also useful to compare the flushing behaviour between the 200 m model (which is used for production simulations in this project), the 400 m model (which is used for development) and the 100 m model (which is very expensive to run for periods of a year or more, but can be used to investigate the effect of resolution on the model's treatment of processes). This comparison is shown for the near-surface sources in Figure 3-25. The most noticeable feature of the comparison is the big difference between the 400 m and 200 m models for the Grove Arm and Tory Channel tracers: the flushing time for the 400 m model is much larger than for the 200 m. The obvious explanation is that the coarse resolution of the 400 m model causes it to underestimate tidal transport and stirring in Tory Channel. The 100 m model, which has been run for 200 days, matches the 200 m model to within 10-20%.

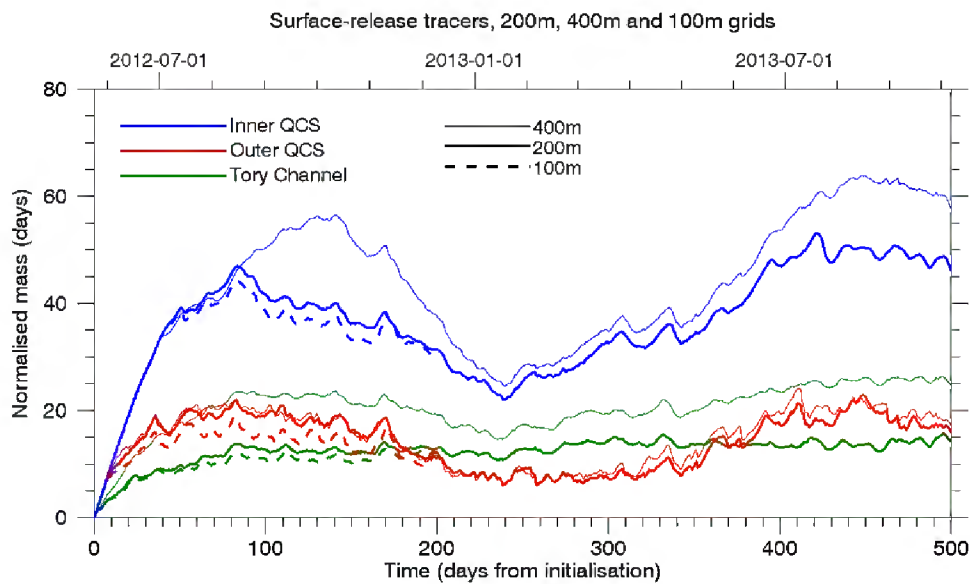


**Figure 3-25: Effect of model resolution on flushing.** Normalised mass of tracer within Queen Charlotte Sound versus time for the Grove Arm (blue), Outer Queen Charlotte Sound (red) and Tory Channel (dark green) near-surface tracers with the 400 m (thin), 200 m (thick) and 100 m (dashed) models.

It being quite clear that Queen Charlotte Sound is not generally well-mixed, the next 3 figures (Figure 3-26 to Figure 3-28) show the mean surface concentration for each tracer, normalised and expressed as a dilution rate as described above. For the Grove Arm source, the pattern for the near-surface source (Figure 3-26a) is very similar to the pattern for the near-bottom tracer (Figure 3-26b). Dilution rates are in the vicinity of  $400\text{--}800\text{ m}^3\text{ s}^{-1}$  (red) in Grove Arm and drop away to  $4000\text{--}12,000\text{ m}^3\text{ s}^{-1}$  (light and dark green) in Outer Queen Charlotte Sound and Tory Channel. The Cook Strait coastline is exposed to dilution rates in excess of  $40,000\text{ m}^3\text{ s}^{-1}$  (light grey). The small differences between the two panels in Figure 3-26 are instructive. There is a maximum in surface concentration (minimum in dilution rate) within a kilometre or two around the source for the near-surface tracer but not the near-bottom tracer, which is to be expected. It is notable however, that the surface concentration at the head of Grove Arm is higher for the near-bottom tracer than it is for the near-surface tracer: this suggests the existence of a (probably weak on average) estuarine circulation in Grove Arm, with surface water flowing out towards the outer sound and being replaced by upwelled deeper water.

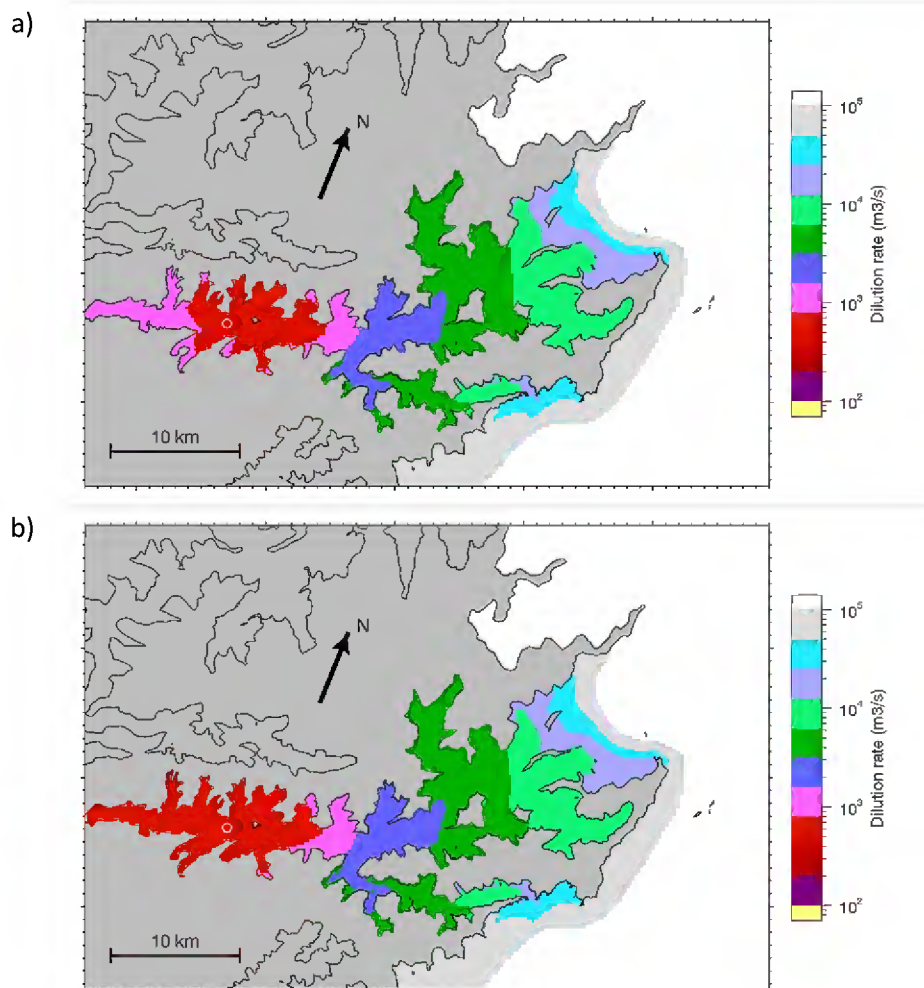


**Figure 3-26: Equilibrium concentration for Grove Arm tracers.** Surface concentration of tracers from Grove Arm (a) near-surface and (b) near-bottom tracer sources in the 200 m model, averaged over the final 365 days and expressed as a dilution rate. The source location is indicated by a white circle.

For the Outer Queen Charlotte Sound tracers (Figure 3-27), concentrations are highest (dilution rates lowest) in the area around the source and are in the range  $1700\text{--}3000\text{ m}^3\text{ s}^{-1}$  (dark blue), with a maximum in concentration around the near-surface source again. There is a definite horizontal shift

between the near-surface pattern (Figure 3-27a) and the near-bottom pattern (Figure 3-27b), with the direction of the shift again suggesting an estuarine circulation: surface water moving towards Cook Strait and deeper water moving towards the head of the Sound. Dilution rates in Grove Arm are quite high at  $12,000\text{--}25,000\text{ m}^3\text{ s}^{-1}$  for the near-surface source and  $6000\text{--}12,000\text{ m}^3\text{ s}^{-1}$  for the near-bottom source. Again, the difference suggests an estuarine circulation. Overall the results imply that surface water in Outer Queen Charlotte Sound tends not to move into Grove Arm.

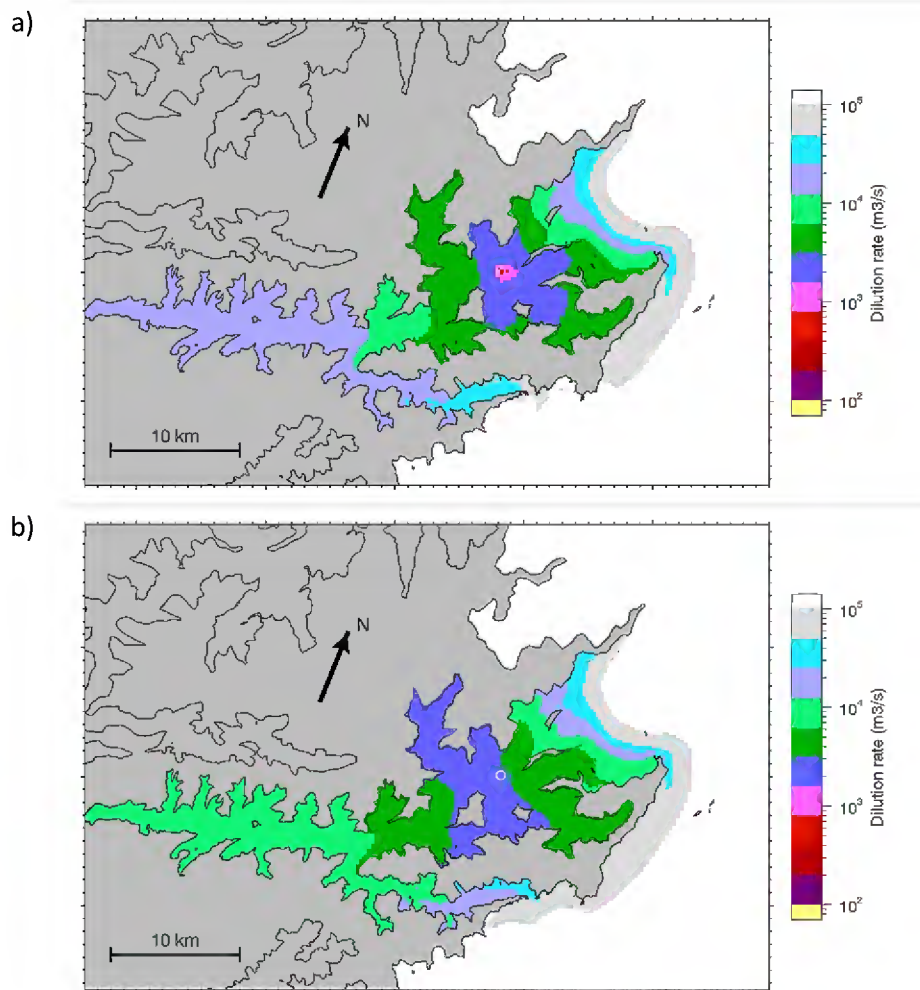


**Figure 3-27: Equilibrium concentration for Outer Queen Charlotte Sound tracers.** As Figure 3-26 but for tracers released at the Outer Queen Charlotte Sound location.

For the Tory Channel tracers (Figure 3-28), the surface dilution patterns for the near-surface and near-bottom sources are very similar to each other. A notable feature is that the concentration in Grove Arm (dilution rate  $3000\text{--}6000\text{ m}^3\text{ s}^{-1}$ ) is substantially higher than for the Outer Queen Charlotte Sound tracers. This suggests that Tory Channel is an effective conduit for exchanging material between Grove Arm and Cook Strait.

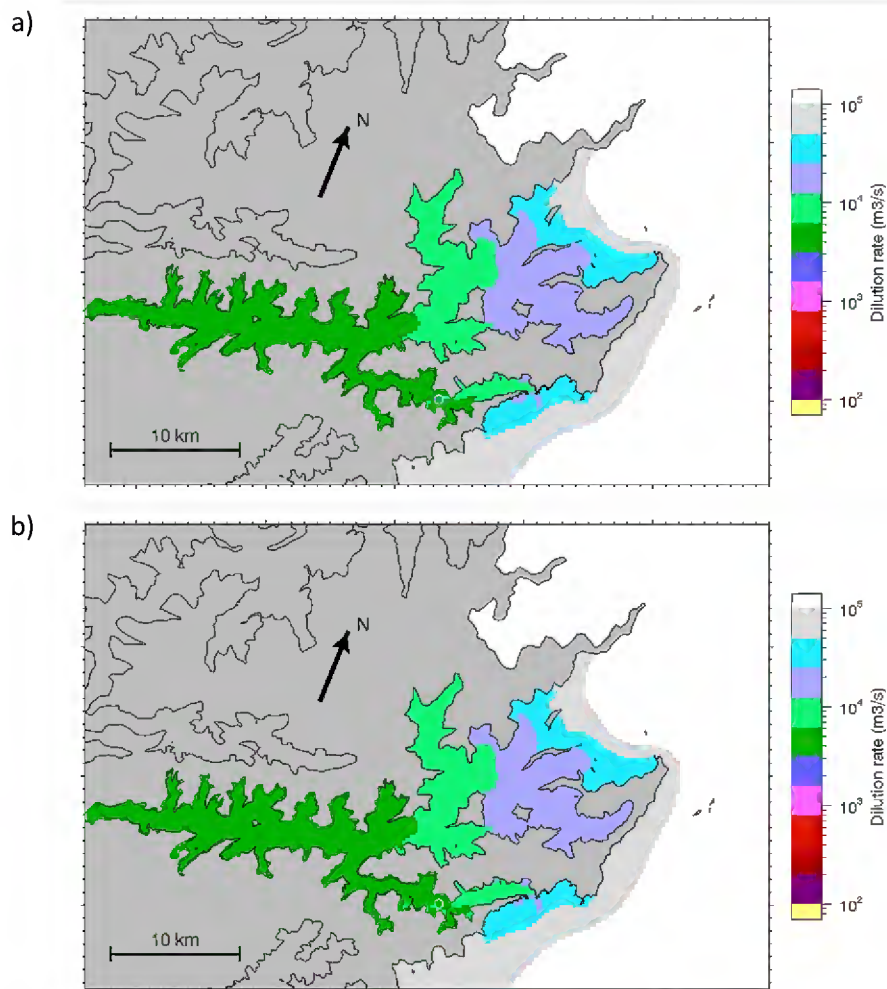


**Figure 3-28: Equilibrium concentration for Tory Channel tracers.** As Figure 3-26 but for tracers released from the Tory Channel location.

### 3.8 Hydrodynamic model summary

Grid resolutions from 50 m to 400 m were tested. The 200 m model reproduces the essential aspects of the hydrodynamics of Queen Charlotte Sound with acceptable accuracy and allows simulations with the full biological model for periods of over one year. Tory Channel is clearly not modelled well at 400 m resolution.

Given the large tidal currents in Tory Channel and the significant circulation patterns in the mean flow, generated by tidal rectification, modelling mean currents at a single point is a challenge. The Tory Channel ADCP data show a mean current  $\sim 0.08 \text{ m s}^{-1}$  directed towards west-southwest. The model shows a somewhat weaker current directed towards the southeast. This suggests that the model may be underestimating the inflow through the Channel (from Cook Strait to Queen Charlotte Sound). It is also possible, however, that the discrepancy arises because the model does not have the pattern of tidally generated mean flow exactly right, i.e. that the discrepancy is specific to the particular location where the measurements were made.

The model's temperature and salinity agree well with observations. The model reproduces the contrast between the seasonally stratified area in Queen Charlotte Sound on the one hand, and Tory Channel on the other. The model's representation of the freshwater input (via a combination of rainfall over the Sound plus small-catchment inflow distributed around the coastline) is simple, but apparently effective. The model produces a well-defined estuarine circulation in Queen Charlotte Sound (but not in Tory Channel) and the data from the Outer QCS ADCP confirms this.

The analysis of modelled currents and volume fluxes shows several features that are pertinent to the movement of dissolved material through the Sound.

- The tidal volume fluxes through Tory Channel are large, at around  $20,000 \text{ m}^3 \text{ s}^{-1}$  at neap tide and  $30,000 \text{ m}^3 \text{ s}^{-1}$  at spring tide.
- In addition there is a sub-tidal flow, typically inwards through Tory Channel and outwards through Outer QCS (i.e. clockwise around Arapawa Island) that varies from extremes of  $-2000 \text{ m}^3 \text{ s}^{-1}$  to  $+6000 \text{ m}^3 \text{ s}^{-1}$ . Short-term (5–10 day) fluctuations in this flow are largely driven by the surface stress (wind), with stresses directed towards NNE (i.e. winds from SSW) driving a positive flow.
- The sub-tidal flow averaged over the final year of the simulation is  $660 \text{ m}^3 \text{ s}^{-1}$  and there is a slow variation, from less than  $500 \text{ m}^3 \text{ s}^{-1}$  in winter to  $+1800 \text{ m}^3 \text{ s}^{-1}$  in early autumn. This variation does not appear to be related to the surface stress. It might be related to the seasonal variation in temperature and salinity.

The flushing behaviour of Queen Charlotte Sound has been investigated with idealised tracer sources in three locations. The flushing time in this framework is a function of the position of the tracer source. The flushing time (Table 3-2) varies from 35–46 days for tracer released in Grove Arm to only 10.9 days for tracer released in central Tory Channel. The flushing time for the tracers released in Inner QCS and Outer QCS varies seasonally, being larger in winter than summer. This may be related to seasonal variations in the flow in Queen Charlotte Sound.

The tidal excursion in Tory Channel is approximately 15 km, which is comparable to its length, i.e. material introduced at one end of Tory Channel can be transported to the other end within one tidal cycle, particularly at spring tide.

Based on the above information about flows and flushing, we suggest the following idealised picture of transport through Tory Channel and Queen Charlotte Sound:

- The large tidal flows through Tory Channel maintain a vertically well-mixed state and allow it to act as a “mixing pipe”, i.e. as a conduit for bi-directional exchange between central Queen Charlotte Sound and Cook Strait.
- The seasonally varying sub-tidal inflow through Tory Channel will aid the movement of water from Cook Strait into central Queen Charlotte Sound.
- Particularly in summer, Tory Channel water is cooler and more saline—and hence denser—than Queen Charlotte Sound surface water. Tory Channel water will therefore tend to move into the lower, inflowing branch of the estuarine circulation and move into Inner QCS before it is transported outwards at the surface through Inner and Outer QCS.



- The flushing calculations are consistent with this picture showing, for example, that material introduced into Tory Channel is present at higher mean concentrations (lower dilutions) in Inner QCS than material introduced at the same rate at the surface in Outer QCS.

Possible improvements to the hydrodynamic model include:

- Generating surface wind fields to drive the model with a higher-resolution atmospheric model.
- Embed a higher-resolution model of Tory Channel within the main model via ROMS nesting techniques. This has the potential to improve the representation of the tidal flows through Tory Channel and their interaction with sub-tidal flow.

## 4 Biophysical model: Methods

As described in the introduction, the biophysical model is comprised of several component ‘sub-models’:

- The ROMS hydrodynamic model
- A so-called nutrient/phytoplankton/zooplankton/detritus (NPZD) model. The particular model that we have adopted includes a simple description of the benthic mineralization of sedimented detritus. For that reason, we will refer to it as the *biogeochemical model*.
- A mussel farm model which focuses upon feeding, respiration and excretion
- A fish farm model which also focuses upon feeding, respiration and excretion

The hydrodynamic model component has been described in the previous sections. In this section, we describe the biogeochemical, mussel farm and fish farm model components.

### 4.1 Model description

The ROMS code includes several alternative *nutrient/phytoplankton/zooplankton/detritus (NPZD)* sub-models to describe water-column nutrient-plankton dynamics. We elected to base our biological modelling upon the Fennel sub-model (Fennel, K., Wilkin et al. 2006; Fennel, K., Wilkin et al. 2008; Fennel, K., Hetland et al. 2011). We made this choice for the following reasons. Firstly, the Fennel model is one of the simpler biogeochemical models that ships with ROMS. The more complex alternatives will impose an unacceptably high additional computational burden. Furthermore, the available field data would be insufficient to calibrate or validate these more complex models. Secondly, the Fennel model includes a simple description of benthic mineralization of sedimented detritus. Thirdly, we know that there is a more sophisticated benthic diagenesis (nutrient recycling) sub-model being developed by a group in the USA to accompany the Fennel model. We hope to be able to incorporate that model in the future. Since the Fennel model includes benthic mineralization, we will refer to it as a biogeochemical model.

Regardless of which biogeochemical sub-model is selected, it runs ‘in-line’ with the ROMS hydrodynamic simulation. That is, biogeochemical and hydrodynamic equations are solved simultaneously within the same code-base. The ‘in-line’ approach differs from the ‘off-line’ approach. In the latter, the hydrodynamic model is solved first, and the resulting time-series of water-temperature, salinity, and currents etc. are saved to file with (for example) 15 minute temporal resolution. The ‘in-line’ approach has two great advantages: (a) there is no need to save enormous (100s of GB) files of hydrodynamic results, and (b) the biogeochemical model is able to utilize the fundamental temporal resolution available from the hydrodynamic engine (approximately 12 seconds in our simulations using the 200 m grid).

The Fennel model assumes that nitrogen is the (only) element that might limit biological activity. Field data confirm that nitrogen is the limiting element in the Marlborough Sounds<sup>7</sup>. The Fennel

---

<sup>7</sup> The term nitrogen limitation implies that concentrations of inorganic nitrogen (primarily  $\text{NO}_3$  and  $\text{NH}_4^+$ ) are sufficiently low to constrain realizable individual phytoplankton cellular growth rates more than light intensity does. Theoretically, it is energetically less expensive to synthesize new nitrogenous tissues using ammonium rather than nitrate. Thus, it is common to assume that, given the choice, phytoplankton will consume  $\text{NH}_4^+$  in preference to  $\text{NO}_3$ . When the supply of ammonium is inadequate to meet growth demands, nitrate is

model has seven obligate state variables ( $\text{NO}_3$ ,  $\text{NH}_4^+$ , small and large (slow- and fast-sinking) detritus, phytoplankton nitrogen, phytoplankton chlorophyll and zooplankton nitrogen) and two optional ones (concentrations of dissolved oxygen and dissolved inorganic carbon). With the exceptions of these two optional state variables and chlorophyll, all the variables are measured in units of nitrogen concentration ( $\text{mmol N m}^{-3}$ ).

The full Fennel model is described in Appendix A. In brief, phytoplankton consume  $\text{NH}_4^+$  and/or  $\text{NO}_3$  as they grow. Zooplankton consume phytoplankton (and associated chlorophyll). In addition, phytoplankton can die of background processes such as entrapment into small detritus. Large and small organic detritus stems from zooplankton faeces as well as dying phytoplankton and zooplankton.  $\text{NH}_4^+$  stems from break-down of the detrital material. In turn,  $\text{NH}_4^+$  is oxidized into  $\text{NO}_3$ . The chlorophyll to phytoplankton nitrogen ratio evolves in response to the ratio of instantaneous photosynthetic rate relative to the local light-dependent maximum rate. The ratio tends to decline under nutrient-limiting conditions and increase under light-limiting ones. All else being equal, a high chlorophyll content permits greater phytoplankton growth than a low one.

In addition to the explicit coefficients of the Fennel model (Table 10-1), there are some features that are turned on/off by means of pre-processor switches when the model is run. Two of these switches influence the fate of particulate material which settles to the seabed. In our 'standard' runs we set them such that 25% of the material which settles on the sea-floor is immediately returned to the water-column as ammonium. The remaining 75% is assumed to be permanently lost through denitrification (Fennel et al. 2006)<sup>8</sup>. In our *worst case* simulations, we set these switches such that all of the sedimenting particulate organic nitrogen would be returned to the bottom-most layer of the water-column.

The Fennel model that ships with ROMS does not include mussel farms or fish-farms. NIWA has implemented appropriate mussel farm and fish-farm codes with funding from the Ministry of Business and Innovation and a predecessor body (Foundation for Research in Science and Technology).

The mussel code implements relevant parts of the mussel growth models described in Ren and Ross (2005) and Ren et al. (2010) (with some typographical errors in those papers amended in our code implementation). In particular, the rates of mussel induced particle capture, faecal (and pseudo-faecal) production,  $\text{NH}_4^+$  excretion,  $\text{O}_2$  uptake and  $\text{CO}_2$  production are all incorporated. Mussels are assumed to have the ability to capture all of the particulate materials in the Fennel model (phytoplankton, zooplankton, small and large detritus). The faeces and pseudo-faeces that they produce pass into the large detrital pool. On the other hand, the associated dynamic description of mussel growth (biovolume and weight) is not incorporated. Instead, the user supplies a time-series of mussel concentration (mussels  $\text{m}^{-3}$ ) for each of several mussel size-classes. A more detailed description of the ingestion/faeces/excretion components of the mussel model is provided in Appendix B whilst section 4.2 describes the manner in which the spatial distribution of the mussel crop was incorporated into the model.

---

used to meet the deficit. Whilst this certainly implies additional energy expenditure there is no reduction of realized phytoplankton growth rates in nitrogen-limited waters. This is because, by definition, the realized phytoplankton growth rate is nitrogen limited – they phytoplankton can accrue more than sufficient (non-nitrogenous) carbohydrates (by photosynthesis) to meet even the elevated energetic demands.

<sup>8</sup> The alternative choices were: (a) that the sedimenting material be permanently lost from the system (full denitrification of sedimenting material); or (b) that 100% of the sedimenting particulate nitrogen be instantly returned to the bottom-most layer of the water column as ammonium (no denitrification of sedimenting material).

The fish-farm sub-model works in a manner akin to that of the mussel farm. A detailed description of the uptake and release terms stemming from this model is provided in Appendix C. Section 4.3 describes the manner in which the spatial distribution of the fish crops were mapped onto the model grid.

The fish energetics model is based upon that of Stigebrandt (1999). The original Stigebrandt model is designed to conserve energy and contains descriptions of a maximal size-specific ingestion rate ( $J \text{ fish}^{-1} \text{ d}^{-1}$ ) from which ingestion (as  $\text{g food fish}^{-1} \text{ d}^{-1}$ ) can be calculated using a knowledge of the food composition, faecal production, ammonium production,  $\text{CO}_2$  production and  $\text{O}_2$  demand. As with the mussel model, we have not implemented the fish-growth component of the model. Instead, the user supplies time-series of fish abundance ( $\text{fish m}^{-3}$ ) for each of several fish size-classes. The user also specifies corresponding time-series of fish feed input rates ( $(\text{kg feed/kg fish live weight}) \text{ d}^{-1}$ ) for each fish size-class. If the implied feed input rate ( $\text{kg feed m}^{-3} \text{ d}^{-1}$ ) exceeds the implied maximal feed consumption rate, the excess food remains uneaten and its nitrogen content passes into the large detritus pool (as do fish faeces).

In the real world, mussels will put on weight over the course of a growth cycle. To achieve that, they must consume more nitrogen than they produce. Thus, in a time-average sense, they are a net sink for environmental nitrogen (though they may be temporary net sources during times when they are receiving insufficient food to offset their respiratory demands). Fish also put on weight over the course of a growth cycle, but they derive their nutrition from an exogenous source (fish feed) rather than from material that is already 'natively' present in the water-column. Any nitrogen that they lose to the environment (faeces and ammonium excretion) augments what is already in the environment. In contrast to mussel farms, fish-farms are a net source for environmental nitrogen.

## 4.2 Representing the spatial distribution of the mussel crop

Rather than representing each individual mussel line (or mussel farm) as a discrete entity within ROMS, we chose to represent the population of farmed mussels using the grid-structure (spatial resolution) adopted for the ROMS hydrodynamic and water-quality models.

Approximate concentrations of farmed mussels ( $\text{mussels m}^{-3}$ ) within each control-volume of the model domain were derived by adopting several assumptions.

- Since mussel feeding rates etc. are non-linear functions of individual size, we need to prescribe a realistic size-distribution for each population. We know of no data concerning seasonal changes in mussel size structure in the farms within Marlborough Sounds. Thus, we assumed that the size structure remains constant throughout the year, and that all farms share the same size structure. We used four size-classes: 32 mm, 47 mm, 72 mm, 100 mm). When required, these lengths were converted to weights using relationships from previous studies (Hickman 1979; Hickman and Illingworth 1980; Orban, Di Lena et al. 2002).
- We assumed that 10% of the length of each dropper was devoid of mussels, 20% was occupied by the smallest mussel size-class whilst the remaining size-classes each occupied 23.3%.

- On the occupied sections of dropper, we assumed that the respective mussel densities for the 32 mm, 47 mm, 72 mm and 100 mm size-classes were 170, 150, 130 and 110 mussels per metre length of dropper (dropper m)<sup>-1</sup>.
- We assumed that each long line supports 3750 m of dropper (110 m)<sup>-1</sup> of backbone ([www.NZMFA.co.nz/faq.asp](http://www.NZMFA.co.nz/faq.asp)).
- Droppers were assumed to extend from the sea-surface to the lesser of 3 m above the seabed or 12 m below the sea-surface. Time-varying sea-levels imply that the droppers may move into and out of layers of the spatial grid. Almost certainly, the depth to which droppers extend will not coincide with the interface between two model layers. Usually, one intermediate layer (with respect to ordering between sea-surface and sea-floor) will be only partially occupied by the droppers. Thus, the concentration of mussels within each control-volume was recalculated at every time-step of the simulation.
- Marlborough District Council provided us with a shape file that illustrates the locations of every backbone that existed in 2012 (digitized from aerial photographs). For our *existing farms* scenario, we deduced the mussel density within each water-column of the model from these backbones.
- For the *approved farms scenario*, we have no specific information on back-bone locations for farms which have been consented and/or occupied since the aerial survey but Marlborough District Council also provided us with a second shape-file. This shows a polygon for all marine farm licences together with additional information for each polygon (e.g. whether the license is approved, rejected or under-appeal). For the *approved farms scenario*, we populated the water-columns that contained aerial-survey backbones with mussels in the manner described for the *existing farms scenario*. We also populated any other water columns which contained polygons which are 'approved' but did not contain backbones during the aerial survey. For this latter set of water-columns, we calculated the relative area of mussel licence within the water-column (m<sup>2</sup> mussel licence m<sup>-2</sup> water-column) and assumed that they will contain 3 backbones (110 m long) ha<sup>-1</sup> of mussel-licence.

Collectively, the above assumptions imply that the size-class specific aerial densities of mussels within each licenced farming block are approximately 38, 34, 29 and 25 mussels m<sup>-2</sup> of licenced farm block for the 32, 47, 72 and 100 mm size classes respectively. Averaged across the surface area of a model water-column (*c.f.* surface area of a mussel farm license), the total mussel density is usually circa 60-80 mussels m<sup>-2</sup> (Figure 4-1).

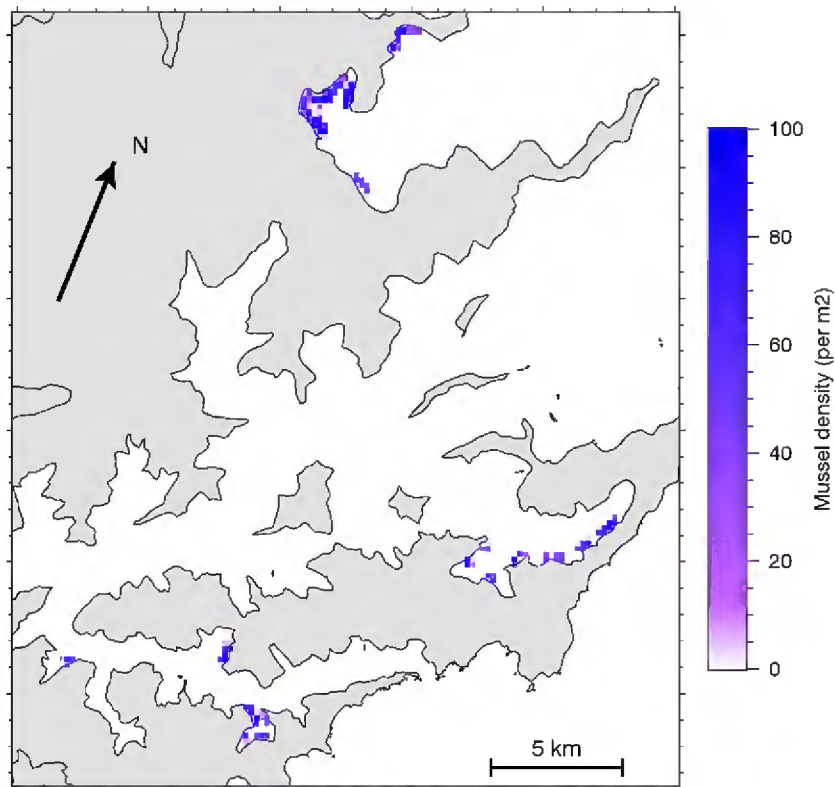


**Figure 4-1:** Map showing the depiction of mussel farms within the biophysical model grid. The colour indicates the mussel density (mussels  $\text{m}^{-2}$  summed over all size classes). White areas are those which contain no mussels.

### 4.3 Representing the spatial distribution of fish farms

As with the mussel-farms, individual fish-farms were not explicitly represented as discrete entities. Instead, we calculated time-series of farmed-fish concentrations (fish  $\text{m}^{-3}$ ) for each control volume of the model domain<sup>9</sup>. We did so in a manner similar to that for mussels.

- The consent conditions for each farm prescribe a maximum permissible annual feed discharge to the crop. We used that, together with information concerning the annual cycle of water temperature, the duration of the crop-cycle and a growth-model for salmon (akin to the one described earlier) to synthesize farm-specific time-series of:
  - (a) fish abundance within each of several size-classes (fish  $\text{farm}^{-1}$  by fish size-class),
  - (b) feed input rates ( $\text{kg feed kg}^{-1} \text{ fish d}^{-1}$  by fish size-class). This enabled us to calculate high temporal resolution time-series of population size-structure characteristics and feed input rates that are consistent with the prescribed annual-scale consent conditions and plausible farm management practices.
- For the purposes of this exercise, we partitioned each farm's crop into 14 size classes (individual fish live weight, g): 0–100, 100–200, 200–300, 300–400, 400–500,

<sup>9</sup> Given the scarcity of fish-farms within Marlborough Sounds relative to the spatial resolution of the model grid, most control-volumes contain no farmed-fish, and those which do contain farmed fish contain fish from only one farm

500–1000, 1000–1500, 1500–2000, 2000–2500, 2500–3000, 3000–3500, 3500–4000, 4000–4500, 4500–5000.

- Marlborough District Council provided us with shape files for each farm. In most cases, these included information on the perimeters of the pens. Where that information was not available, we approached NZKS Ltd. They made their engineering drawings available to us and we digitized the locations of the pen perimeters from these.
- We assumed that cages extend to 20 m below the sea-surface.
- We overlaid the farm perimeters upon the model grid to calculate the fractional area of farm within each water-column of the model grid.
- We assumed that the fish crop associated with each farm was evenly distributed throughout the implied farm-volume (and that feed inputs were evenly distributed across its horizontal surface-area).
- NZKS also provided us with schedules (time-series) of cohort-and-farm-specific: fish abundance, mean live weight and feed-input rates.
- For the purposes of modelling, we assumed that each fish farm was entirely enclosed within a single water-column of the model and calculated fish densities accordingly (Figure 4-2). We recalculated the total concentration of fish (of each size-class contained within the control-volume) within each control-volume at every time-step. We also calculated control-volume-specific feed input rates at every time-step.

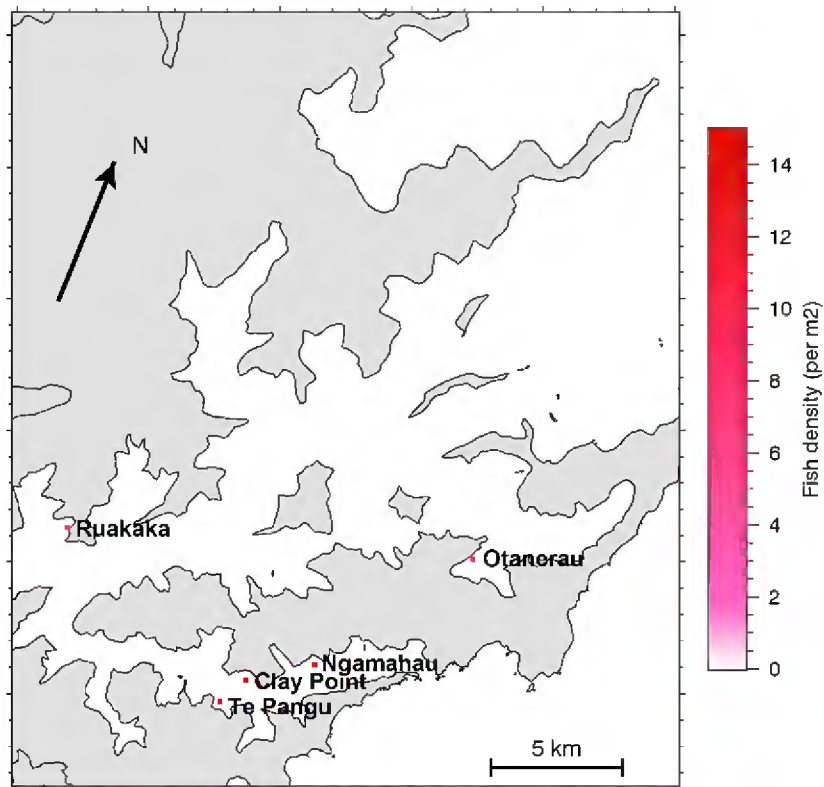


**Figure 4-2:** Map showing the locations of the five fish farms. The colour indicates the fish density (fish  $m^{-2}$  summed over all size classes) averaged over the  $200 \times 200$  m grid cell around each fish farm during the final 12 months of the simulation.

#### 4.4 Water quality data

Marlborough District Council collect water samples at five stations (QCS-1, QCS-2, QCS-3, QCS-4 and QCS-5, Figure 4-3) using a Van Dorn sampler. Sampling began in July 2011 and has continued at approximately monthly intervals since then. At each station, near-surface water is collected from 1 m below the sea-surface<sup>10</sup> and a near-bed sample is collected from approximately 1 m above the seabed. Each water-sample was held within an ice-packed chilly-bin and shipped to the NIWA chemistry laboratory in Hamilton within 24 hours of collection. Upon arrival at the laboratory, a small volume of each sample was preserved with Lugols (for subsequent plankton counts). The remainder was frozen until needed for nutrient analysis etc. Table 4-1 provides details of the water-quality variables that are measured. Quantities measured include: nitrate, ammoniacal nitrogen, dissolved reactive phosphorus, total dissolved nitrogen, total dissolved phosphorus, chlorophyll, suspended solids, volatile suspended solids, particulate carbon, particulate organic nitrogen and counts of phytoplankton and zooplankton individuals by species<sup>11</sup>. Phytoplankton and zooplankton carbon concentration was derived from the cell counts using measurements of the sizes of individual

<sup>10</sup> From July 2014, the near-surface sample will be taken using a hose-sampler to collect a depth-averaged water-sample from the upper 10 m of the water-column.

<sup>11</sup> The counts were made only for the near-surface water-samples. Furthermore, the counts will yield only qualitative abundance information for the larger (scarcer and more mobile) zooplankton.



plankton and published length-weight relationships. In addition, Secchi disk depth, near-surface water temperature and near-surface dissolved oxygen were measured.

**Table 4-1: Water-quality variables measured for Marlborough District Council.** Phytoplankton and zooplankton counts are made only on the near-surface water samples.

Property	Description	Detection limit	Method or comment
Ammonium Nitrogen	DRP,NH4-N,NO3-N, Simultaneous Auto-analysis	1 mg N m <sup>-3</sup>	Astoria
Dissolved Reactive Phosphorus	DRP,NH4-N,NO3-N, Simultaneous Auto-analysis	1 mg P m <sup>-3</sup>	Astoria
Nitrate + Nitrite Nitrogen	DRP,NH4-N,NO3-N, Simultaneous Auto-analysis	1 mg N m <sup>-3</sup>	Astoria
Volatile Suspended Solids	Filtration, drying at 104 C, followed by furnacing at 400 C	0.5 mg m <sup>-3</sup>	APHA 2540D
Inorganic Suspended Solids	Filtration, drying at 104 C, followed by furnacing at 400 C	0.5 mg m <sup>-3</sup>	APHA 2540D
Suspended Solids	Filtration, drying at 104 C, followed by furnacing at 400 C	0.5 mg m <sup>-3</sup>	APHA 2540D
Turbidity	Turbidimeter rated against Formazin standards	0.1 NTU	APHA 2130B
Chlorophyll a	Acetone pigment extraction, spectrofluorometric measurement.	0.1 mg Chla m <sup>-3</sup>	A*10200H
Dissolved Reactive Silicon	Molybdosilicate / ascorbic acid reduction.	1 mg Si m <sup>-3</sup>	APHA4500Si
Salinity	Salinometer, calibrated against seawater standard	0.1 ppt	YSI
Total Dissolved Nitrogen	Persulphate digest, auto cadmium reduction, FIA	10 mg N m <sup>-3</sup>	Lachat
Total Dissolved Phosphorus	Persulphate digest, molybdenum blue, FIA	1 mg P m <sup>-3</sup>	Lachat
Particulate Organic Carbon	Catalytic comb @900°C, sep, TCD, Elementar C/N analyser	0.1 mg C m <sup>-3</sup>	MAM, 01-1090
Particulate Organic Nitrogen	Catalytic comb @900°C, sep, TCD, Elementar C/N analyser	0.1 mg N m <sup>-3</sup>	MAM, 01-1090
Phytoplankton abundance	Water samples fixed with Lugols upon arriving at Hamilton labs. Subsequently, cells settled onto graticule slide. Cells within random fields identified (to lowest practical taxonomic resolution), measured and counted under microscope	-	Cell carbon estimated from cell dimensions and taxon-specific conversion factors

Property	Description	Detection limit	Method or comment
Zooplankton abundance	Counted, as for phytoplankton but no size determinations	-	Niskin bottle samples combined with cell counting are not well suited to capturing larger/more mobile zooplankton in sufficient numbers to permit robust abundance estimates. The counts and derived biomass estimates provide only very imprecise estimates of zooplankton abundance.

The Fennel model was calibrated to the field-data by eye rather than by automated fitting procedures. We set the attenuation coefficient for photosynthetically active radiation to  $0.22 \text{ m}^{-1}$  (based upon measurements of PAR attenuation made during CTD casts). We then calibrated the model by varying only the initial slope of the phytoplankton photosynthesis-irradiance curve (coefficient PhyIS).

#### 4.5 Initial conditions

At the start of each simulation, the initial values of all biogeochemical variables were horizontally and vertically uniform at values representative of winter conditions in Queen Charlotte Sound. The model then spun up its own equilibrium over a period of 50–100 days.

#### 4.6 Model calibration

The coefficients of the Fennel biogeochemical model, the mussel model and the salmon model are listed in Table 10-1, Table 10-2 and Table 10-3. Almost all of the coefficients were left at their default values. Only the background attenuation coefficient for photosynthetically active radiation (PAR), and the initial slope of the half-saturation constant for light-limited growth were modified. The former was set equal to the mean value derived from measurements made with a PAR sensor during CTD casts on each of the monthly sampling visits made by MDC during July 2011-December 2013. The latter was chosen by informal ('by eye') calibration of the *existing* situation scenario variant of the model to the MDC water-quality data (section 4.4).

#### 4.7 Cook Strait boundary data

There are few historical measurements of water-quality in Cook Strait. Indeed, the only publicly available water quality data that we know of for Cook Strait are those published in Bradford et al. (1986); i.e., three summertime surveys during 1980 & 1981. Fortunately, New Zealand King Salmon measured water-quality (nutrients, phytoplankton, chlorophyll, particulate nitrogen, but *not* zooplankton) at five stations around Port Gore monthly from July 2012-April 2013. One of these stations is mid-way across the Port Gore mouth of Cook Strait (Figure 4-3). Earlier numerical modelling (Knight 2012) suggests that this location will have Cook Strait water-characteristics. Furthermore, the water-quality at this station is markedly different from that of the other four stations (which are well within the bay). It also differs from that of outer Pelorus (PLS7/NZKS7) and

outer Queen Charlotte (QCS5) and outer Tory Channel (NZKS22). The natures of the differences are consistent with our belief that the outer Port Gore station is sampling Cook Strait water.

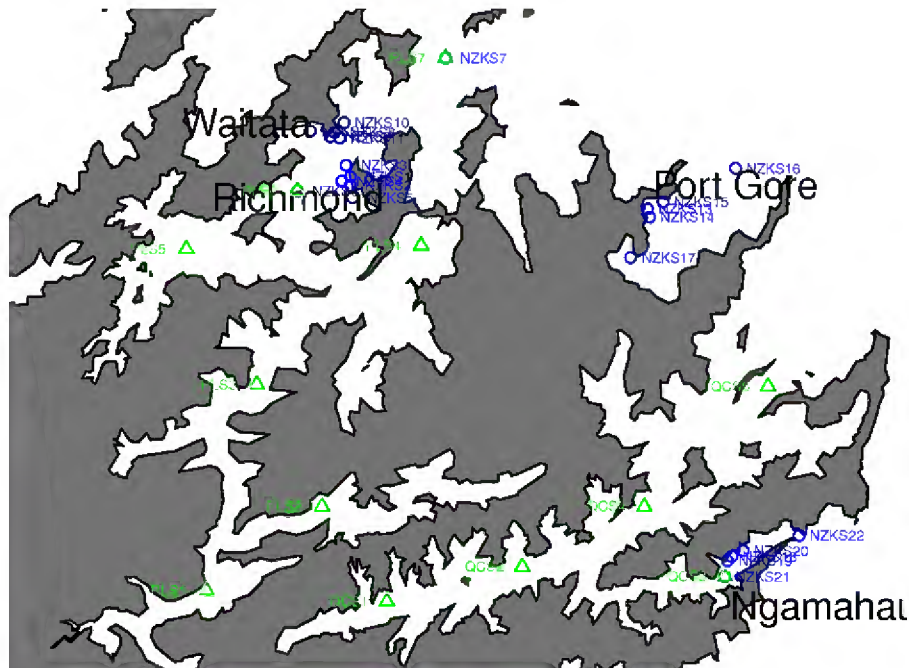


**Figure 4-3:** Map illustrating the locations of Marlborough District Council (green) and New Zealand King Salmon (blue) water-quality sampling sites. Data from NZKS16 were used to construct the Cook Strait boundary conditions for the NPZD-model.

New Zealand King Salmon Ltd ceased sampling at Port Gore shortly after the Supreme Court upheld the appeal against the Port Gore salmon farm that NZKS had been seeking, but Marlborough District Council continued to sample outer-most Port Gore station (NZKS16) for a further two months. Thus, we have access to one years' worth of monthly data at that station. We generated nominal time-series of sea-surface properties from a 3 month time-centred smoothing curve through the 12 months' worth of near-surface data. We used the corresponding near-bed data to generate a time series which we assumed to be typical of water at 50 m depth. For the upper 50 m of the water-column, we then used linear interpolation (in the vertical) to derive layer-specific boundary conditions from the smoothed data. Below 50 m, we assumed concentrations were depth invariant (equal to the prescribed values at 50 m).

Boundary conditions for zooplankton were based upon the zooplankton data that Marlborough District Council have gathered at their outer most Queen Charlotte station (station 5). As the zooplankton biomass estimates are imprecise (Table 4-1), we used the time-averaged value from the field data as a temporally invariant boundary condition.

For our modelling, we chose to assume that all DON is 'old, refractory/inert' material, that is, biologically inactive on the time-scales of interest.

## 4.8 Catchment Boundary Conditions

Picton waste-water discharge was a point source of nutrient, dissolved oxygen, dissolved inorganic carbon, and particulate detritus but not phytoplankton or zooplankton. Details of flow and water-quality characteristics were provided by Marlborough District Council. The Picton wastewater data included flow, nitrate+nitrite nitrogen, ammoniacal nitrogen, total nitrogen and volatile suspended solids and dissolved oxygen (one record only). We assumed that detrital nitrogen could be equated to the difference between total nitrogen and the dissolved inorganic nitrogen constituents (implicitly ignoring the reality that some of this difference may be contributed by dissolved organic nitrogen rather than particulate organic nitrogen).

Nutrient inputs from other catchment sources were excluded. Marlborough District Council have collected monthly water-quality data in three (of the many small) streams that drain into Queen Charlotte (Duncan, Waitohi and Graham). Those data indicate that the nitrate and ammonium concentrations are generally lower than those in the seawater of Queen Charlotte. In effect, the stream inputs operate to 'dilute' the nutrient-concentrations in the Sound. Paradoxically, by excluding them from our model, we will have rendered our model more prone to nitrogen enrichment. In that sense, it is therefore 'worst-case' – albeit that the effect is very small because streams contribute very little water (but even less nutrient) in comparison with the nutrient exchange across the Cook Strait boundaries.

## 4.9 Simulation scenarios

Whilst the contract calls for three specific scenarios to be simulated (that we dub *existing situation*, *approved farms*, *worst case*, see section 1.3), we felt that it would be helpful to present several additional simulations as precursors.

- *No farms*: in this simulation there were no mussel or fish farms present within the domain.
- *Existing mussel farms only*.

All of the simulations were run on the 200 meter resolution grid.

We choose to use the results from our *no farms* simulation as the baseline against which to assess the influence of aquaculture activities and sensitivity to benthic denitrification. Whilst the *existing farms* scenario provides a better analogue of the present day situation, choosing the *no farms* scenario as our baseline enables us to better distinguish the differing effects of mussel farms and fish farms. Without the *no farms* simulation, our baseline simulation would be the *existing conditions*. Since the mussel-farming activities in the *approved farms* scenario are very similar to those of the *existing farms* scenario, we would have only very limited ability to distinguish the influence of mussel farming (*c.f.* fish farming) if we used the *existing conditions* as the baseline.

## 4.10 Analysis and presentation of biophysical model simulation results

We made our biophysical simulations on the 200 m resolution horizontal grid. Whilst we have finer resolution grids, the model becomes too computationally expensive to permit annual scale simulations at those finer resolutions (Table 2-1). At 200 m resolution, the detailed structures of

individual fish farms and mussel farms are not resolved. However beyond, say, 1 km, natural mixing will have eroded the farm-derived steep gradients to sufficient degree that the grid spacing ceases to be significant. Thus, in the far-field the simulated concentrations will be much less subject to bias. In short, the model has been designed with the intent that it be used to derive an understanding of the regional (and large-bay scale) influences of farming rather than the farm-scale/small bay-scale influences.

Simulation results at the locations of each of the five Marlborough District Council sampling sites were stored at approximately 6 minute resolution. In addition, the 24 hour averaged concentrations for every control-volume were saved once per simulated day.

For the most part, each model state-variable has an unequivocal analogue in the field data, but the situation for model ammonium and model detrital nitrogen is more complex.

Firstly, in reality, non-living organic nitrogen is comprised of both dissolved organic nitrogen (DON) and non-living particulate organic nitrogen (non-living PON). Whilst we have field determinations of DON, the model has no explicit DON pool. Rather a fraction of any newly dead living matter passes into one or other of the two particulate detrital pools whilst the remainder passes directly into the so-called ammonium pool. Thus, the question arises: 'how should we apportion real-world DON between modelled ammoniacal nitrogen and the two modelled particulate detrital classes'? Whilst real-world DON concentrations are moderately high (see section 5), the majority of marine DON is usually considered to be 'old, refractory' material that is almost inert on the time-scales of interest. We therefore chose to ignore the real world DON when setting our boundary and initial conditions.

Secondly, our direct field determinations of PON measure total (living and non-living) particulate organic nitrogen whereas the model draws distinctions between (living) particulate phytoplankton N, (living) particulate zooplankton N and two classes (small, slow-sinking and large, faster-sinking) of non-living particulate detrital nitrogen.

Plankton nitrogen biomass is known only roughly: from the microscope counts and measurements of individuals and literature estimates for the volume-specific nitrogen contents of different taxa. Table 4-2 describes the means by which analogues to the model state-variables were derived from the field data. In short, (i) we assume that field- and modelled ammoniacal nitrogen are direct analogues of one-another, (ii) we derive approximate estimates of living particulate nitrogen from the microscope based counts of phytoplankton and zooplankton and measurements of the dimensions of these plankton, (iii) we use the field determinations of PON as a lower bound for the sum of simulated abundances of large detrital N, small detrital N and living particulate N, (iv) we use the sum of the field determinations of PON and DON as an upper bound for the sum of simulated abundances of large detrital N, small detrital N and living particulate N.

**Table 4-2: Means by which the field-data were used to derive analogue values for the model state-values.**

Model State-variable	Derivation from field data	Comment
"Nitrate"	$\text{NO}_3^+ + \text{NO}_2$	
"Ammonium"	$\text{NH}_4^+ + \text{NH}_3$	The model has no explicit DON pool. We choose to lump real-world DON into the model detrital pool (see below)
Chlorophyll-a	Chlorophyll-a	GFC filter (approx. 2 $\mu\text{m}$ pore size)

Model State-variable	Derivation from field data	Comment
Phytoplankton carbon concentration	Microscope counts of cells combined with measurements of cell dimensions and literature values for C:volume ratios	
Zooplankton carbon concentration	Microscope counts of cells combined with measurements of cell dimensions and literature values for C:volume ratios	
Total detrital nitrogen (LDetN + SDetN)	(a) PON – phytoplankton N – zooplankton N	given our decision to lump real-world DON into the model detrital pool, (a) & (b) provide lower and upper bounds upon the plausible range of concentrations for the sum of the two model detrital classes. Since we have chosen to ignore real-world DON when setting our initial and boundary conditions, we anticipate that the model should produce PON concentrations that are closer to those of measured PON than those of measured (PON+DON).
	(b) PON + DON - phytoplankton N – zooplankton N	

For the purposes of illustrating how well the model reproduces the historical field data, we will present time-series plots which show the field data (symbols) and corresponding simulation results (4.5 minute resolution, from the ‘existing conditions’ scenario). We will present the results as a series of five figures. Each figure corresponds to one of the five Marlborough District Council monitoring stations. Each figure will contain six panels (one each for nitrate, ammonium, chlorophyll, phytoplankton carbon, zooplankton carbon and particulate nitrogen). Each panel will show: (a) time-series of field measurements at the near-surface location (red circles), (b) time-series of field measurements at the near-bed location (blue triangles), (c) corresponding simulated time-series at the net-surface (red-line) and near-bed (blue line) locations.

We illustrate the predicted influences which the various alternative scenarios have upon water quality (relative to the *existing scenario*), in three ways. Firstly, we present five figures akin to those described above, but in this case, each panel will show six curves (being the simulated near-surface and near-bed properties under each of the three different scenarios). These figures indicate how water-quality at the five Marlborough District Council stations is predicted to behave under the various scenarios.

Secondly, we will show a series of false-colour figures. The figure will contain six rows and each row will contain three panels (maps). Each panel is a false colour map of the model domain. Pixel colour at any location in the map is indicative of the numerical value of the property<sup>12</sup> in question at the pixel-location (yellow/red being ‘high’, and blue being ‘low’). The colour-scheme is designed to yield ‘pleasing’ colours that allow differences to be distinguished readily. The colours should not be interpreted as indicative of whether or not the magnitude of change might be deemed ‘acceptable’. For example, ‘green’ should not be deemed to imply ‘safe/acceptable’ and ‘red’ should not be interpreted as meaning ‘unsafe/unacceptable’. The numerical range spanned by the colour-scale differs for each variable that we plot. Thus, when comparing maps of different properties, one must

<sup>12</sup> In this context, *property* is used as a convenient short-hand to refer to the time-averaged absolute or relative concentration for a particular state-variable.

recognise that any specific colour does not necessarily equate to the same numerical value in both maps.

Each row corresponds to a different model state-variable (i.e., ammonium, nitrate, etc). Within a row, the left-hand most panel will show a time-averaged concentration for the state-variable under the *no farms scenario*. The central and right-hand columns panel will illustrate the time-averages of relative concentration  $RC_p$  for other scenarios. For example, the central column may show results from the *existing conditions* scenario relative to the *no farms* one and the right-hand panel may illustrate  $RC_p$  for the *future scenario 1* relative to the *no farms* scenario. The time-average of relative concentration is calculated as:

**Equation 4-1: Definition of relative concentration**

$$RC_p = 1 + \frac{1}{N} \sum_{n=1}^N \frac{P_n^f - P_n^e}{\varepsilon + P_n^e}$$

in which  $N$  is the number of time-levels involved in the time-average,  $\varepsilon=10^{-100}$  (present to avoid the possibility of a division by zero), while  $P_n^e$  and  $P_n^f$  represent the simulated 12-hour average concentration  $P$  at time-level  $n$  in the baseline and alternative scenarios respectively.  $RC_p$  takes the value 1 if the time-average of the differences is zero. If, on time-average, the alternative scenario yields lower concentrations than the baseline scenario,  $RC_p$  will take a value less than 1. Conversely, if the alternative scenario tends to yield higher concentrations than the baseline scenario,  $RC_p$  will take a value greater than 1.

Our third (and final) means of representing the influences of different scenarios is similar to the second. Rather than maps of relative change, we present maps of absolute change, or concentration difference. Zero indicates no change, negative values indicate that the alternative scenario is yielding lower concentrations than the baseline simulation (left-hand most image) and positive values indicate the alternative simulation is yielding larger concentrations. Furthermore, rather than presenting the images for all state-variables within a 6×3 matrix of maps (all on the one page), we present the as a 1×3 matrix per page. This enables the individual maps to be larger such that fine spatial detail can be better discerned.

The first two analyses are presented in Section 5 and the third is presented in Appendix G.

## 5 Biophysical model: Results

### 5.1 Biophysical results: existing conditions

Marlborough District Council's water-quality sampling data showed that near-surface and near-bed surface nutrient water quality values tend to diverge during the spring/summer/autumn months at stations QCS1, 2, 4 & 5 (i.e. those in the main-stem of Queen Charlotte) (Figures 5.1 – 5.5). This vertical stratification seems stronger and long-lasting in inner Queen Charlotte (stations 1 & 2) than outer Queen Charlotte (stations 4 & 5). In contrast, at QCS-3 (Tory channel), near-surface and near-bed characteristics remain very similar throughout the year. In the main-stem of Queen Charlotte, the water-column becomes thermally stratified during the summer months, but in Tory Channel, the stronger tidal currents (and resultant vertical mixing) dissipate the solar heat input throughout the water-column so quickly that a stable, buoyant layer of warm surface water cannot form.

Near-surface nitrate concentrations are low for much of the year at the inner Queen Charlotte stations, but drop to low levels for only the two-three months of summer at the outer stations. At all Queen Charlotte stations, near-bed nitrate concentrations are 'high' for the majority of months, but they do drop for two-three months during summer – and they drop to markedly lower concentrations at the inner stations. In Tory Channel, the near-surface and near-bed nitrate dynamics are both similar to those of near-bed nitrate at the Queen Charlotte stations.

The dynamics of ammonium are qualitatively similar to those of nitrate. Near-bed ammonium concentrations tend to be higher and temporally more stable than near-surface concentrations. Furthermore, near-surface ammonium concentrations tend to be 'low' for a larger fraction of the spring/summer/autumn period at the inner Queen Charlotte stations. It is worth noting that the ammonium concentrations are usually not sufficiently high to fully satisfy the phytoplankton nitrogen demand. Thus, they have to resort to consuming  $\text{NO}_3$ . In summer, light is plentiful and the phytoplankton have the potential to grow rapidly (if they can secure sufficient nutrient). Thus, the nitrate demand is high and nitrate concentrations are drawn down. In winter, light is scarce and phytoplankton have a lower growth potential. Nonetheless, growing cells will still exert a  $\text{NO}_3$  demand because  $\text{NH}_4$  concentrations are insufficient to meet their demands.

The field data indicate that phytoplankton (whether measured by chlorophyll concentration or inferred carbon abundance) tend to be more abundant near-surface than near-bed. The annual maximum abundances are markedly greater at the two inner-most Queen Charlotte stations than at the other three stations. At the two inner stations, concentrations tend to be greatest in late winter/early spring and in autumn. At the two outer stations of Queen Charlotte and in Tory channel, they tend to be greatest during the summer months. Near-surface phytoplankton abundance tends to be lower at the Tory Channel station than at the other four stations.

Zooplankton biomass has usually been below  $10 \text{ mg C m}^{-3}$ , but there have been occasions on which it exceeded  $30 \text{ mg C m}^{-3}$  (maximum  $>150 \text{ mg C m}^{-3}$ ). Abundances tend to be a bit higher during summer than winter and they tend to be higher in inner and central Queen Charlotte than in outer Queen Charlotte or Tory Channel.

Time-averaged PON concentrations are greatest at the two inner Queen Charlotte stations (QCS-1 & QCS-2) and lowest at the Tory Channel station (QCS-3). At all stations, PON concentrations tended to be lower during the early/mid 2012 to mid-2013 period than they were during the prior 12 months or subsequent 12 months. We do not know what drives this difference – phytoplankton standing



stocks were not markedly lower during the early/mid 2012 – mid 2013 period and monitoring by NZKS at the Cook Strait mouths of Tory Channel and Port Gore (July 2013-June 2014 only) reveal PON concentrations which were generally lower than those measured at Queen Charlotte stations 1-5. We infer that the high PON concentrations measured inside Queen Charlotte/Tory during the latter part of 2013 and early part of 2014 were not driven directly by increased PON concentrations within imported Cook Strait water.

In comparison with the aforementioned inter-annual variability, the PON concentrations show only a weak annual cycle (being slightly more abundant during summer). DON and PON concentrations are usually similar (within a factor of 2-3) to one another.

## 5.2 Comparisons of simulation results with calibration field data

In this section, we compare results from the *existing farms* scenario (run on the 200 m resolution hydrodynamic grid) with the water quality data that Marlborough District Council have been gathering from Queen Charlotte Sound and Tory Channel. We used these field data to calibrate two (only) of the model coefficients. Thus, this comparison cannot be regarded as a validation test. Unfortunately, independent field data from Queen Charlotte are too scarce to permit a validation. It is true that New Zealand King Salmon made monthly measurements of water-quality in Tory Channel during July 2013- June 2014, but sampling was at the same time and location as the MDC sampling<sup>13,14</sup>. Thus, those data are not sufficiently independent to qualify as validation data.

At station QCS-3 (Tory Channel), the model consistently over-predicts phytoplankton carbon and chlorophyll concentrations (Figure 5-3). It also yields nitrate concentrations which are consistently at or below the lower bounds of the measured values. Simulated ammonium, zooplankton and PON concentrations are consistent with the measured values.

Elsewhere (i.e., at QCS stations 1 to 2 and 4 to 5), the model's performance is better in the sense that it does not consistently over- or under-predict the concentrations of any water-quality variables. That is not to say that the model does not yield some marked discrepancies relative to the field data. During the summer period, simulated nearbed  $\text{NO}_3$  concentrations are often too low at the two inner-most stations (QCS-1 and QCS-2, Figure 5-1 & Figure 5-2). This probably reflects the fact that the model over-predicts summertime phytoplankton abundance at these stations. Indeed, the model suggests that phytoplankton tend to be most abundant during the summer months at these stations – whereas the field data suggest that phytoplankton are most abundant during late winter/early spring and during autumn at these stations.

The model performs best at the two outer Queen Charlotte sites (QCS-4 and QCS-5). At these sites, it gets the timing of the phytoplankton maximum correct (mid/late summer). The winter minima of phytoplankton and the summer maxima are also of the correct magnitudes. Similarly, the dynamics (mean, amplitude and phase) of near-surface and near-bed  $\text{NO}_3$  and  $\text{NH}_4^+$  concentrations are reproduced well, as are those of PON and zooplankton (with the exception of a marked two-month 'bloom' in late summer 2013 at site QCS-4).

---

<sup>13</sup> However, the NZKS surface samples were depth-averages over approximately the upper 10 m of the water-column cf. point samples at 1 m depth by MDC.

<sup>14</sup> In addition, NZKS gathered water-quality samples in the immediate vicinity of the planned Ngamahau farm, but that is very close to, and has similar water quality to MDC station QCS-3. Inspection of Figure 5-10 and Figure 5-11 suggests that the model will reproduce the water-quality at these stations as well as it reproduces QCS-3 water-quality.

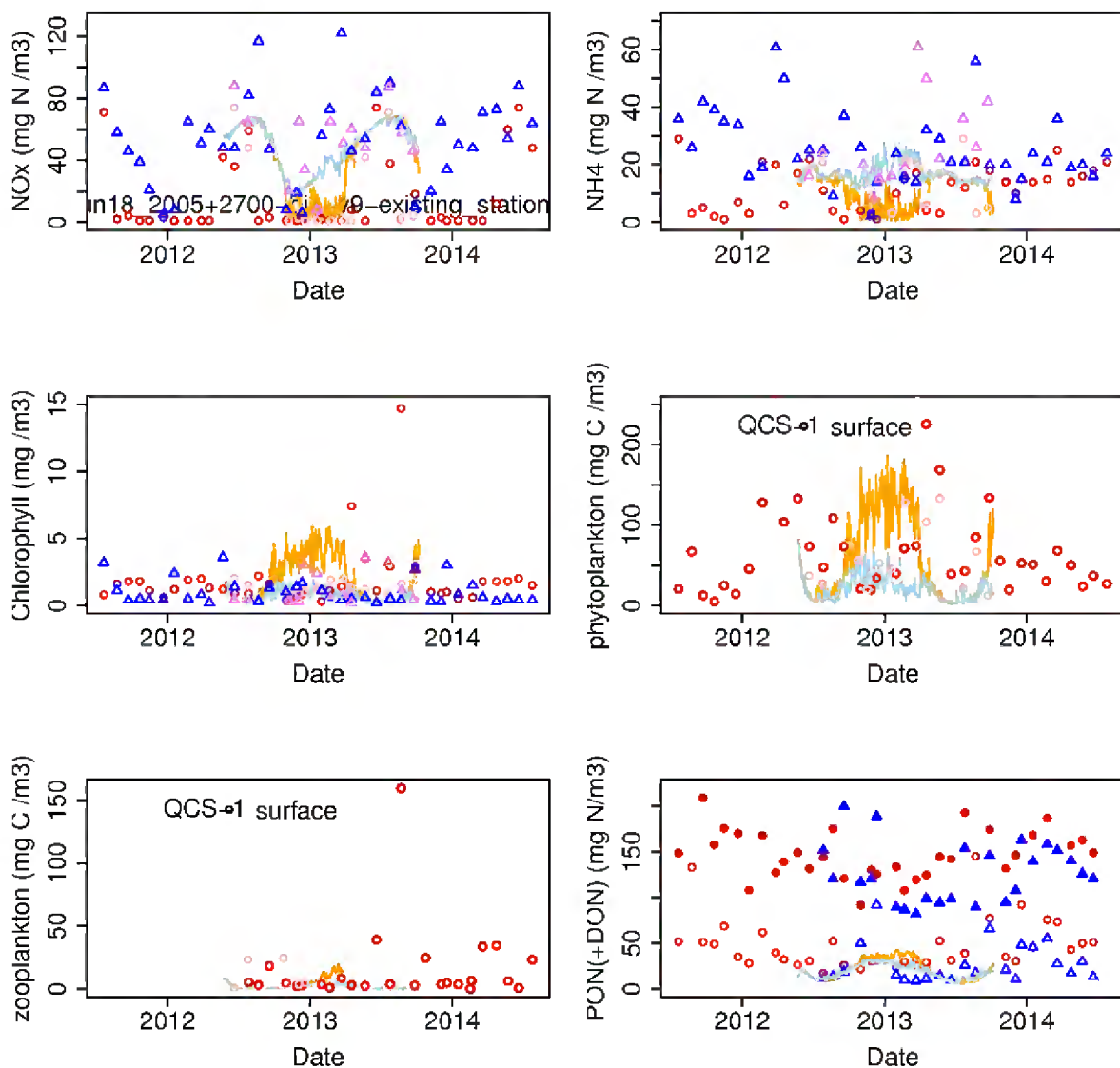


**Figure 5-1: Time-series of measured and simulated water-quality characteristics at station QCS-1.** Circles denote near-surface field-measurements. Triangles denote near-bed field measurements. Red and blue symbols are the raw field data. Pink and violet symbols also present the field data, but measurements made outside the simulation dates have been transposed to the corresponding day-of-year within the simulation period. Orange line: near-surface simulation; pale blue line: near-bed simulation. In the bottom, right hand image, open symbols represent PON concentration whilst filled symbols represent the sum of PON and DON concentrations.

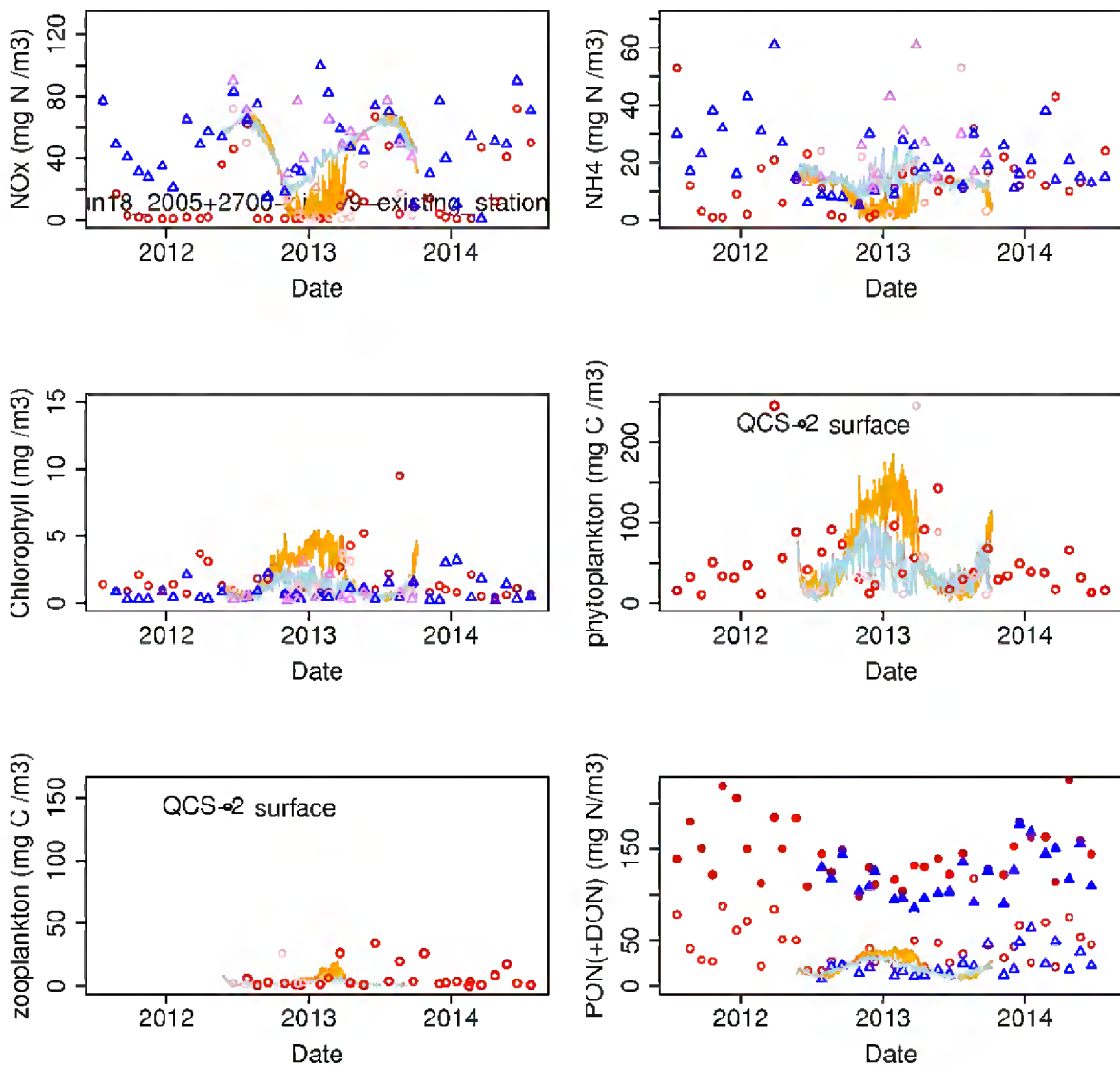


**Figure 5-2: Time-series of measured and simulated water-quality characteristics at station QCS-2.** Rest of caption as for Figure 5-1.

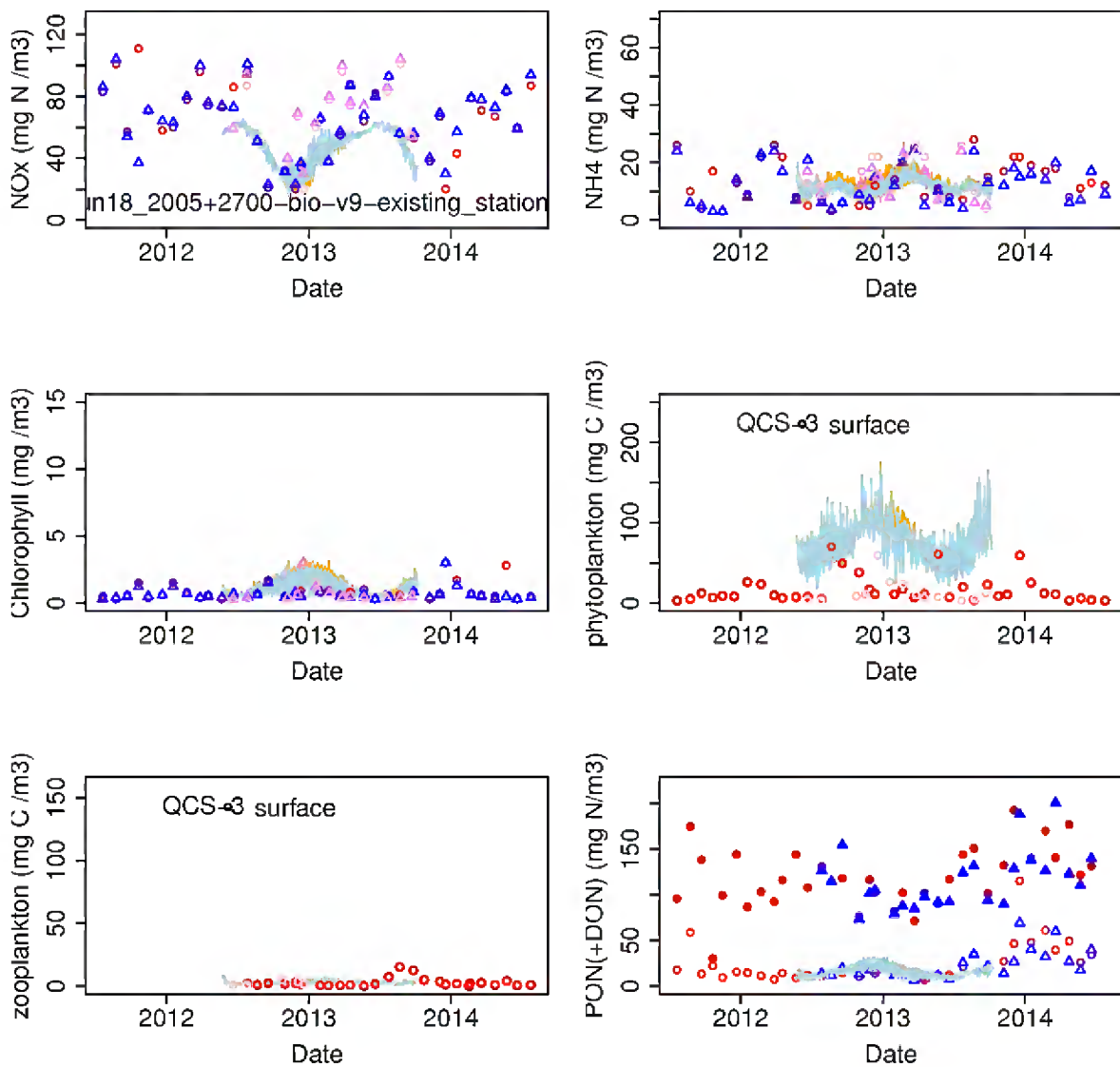


**Figure 5-3: Time-series of measured and simulated water-quality characteristics at station QCS-3.** Rest of caption as for Figure 5-1.

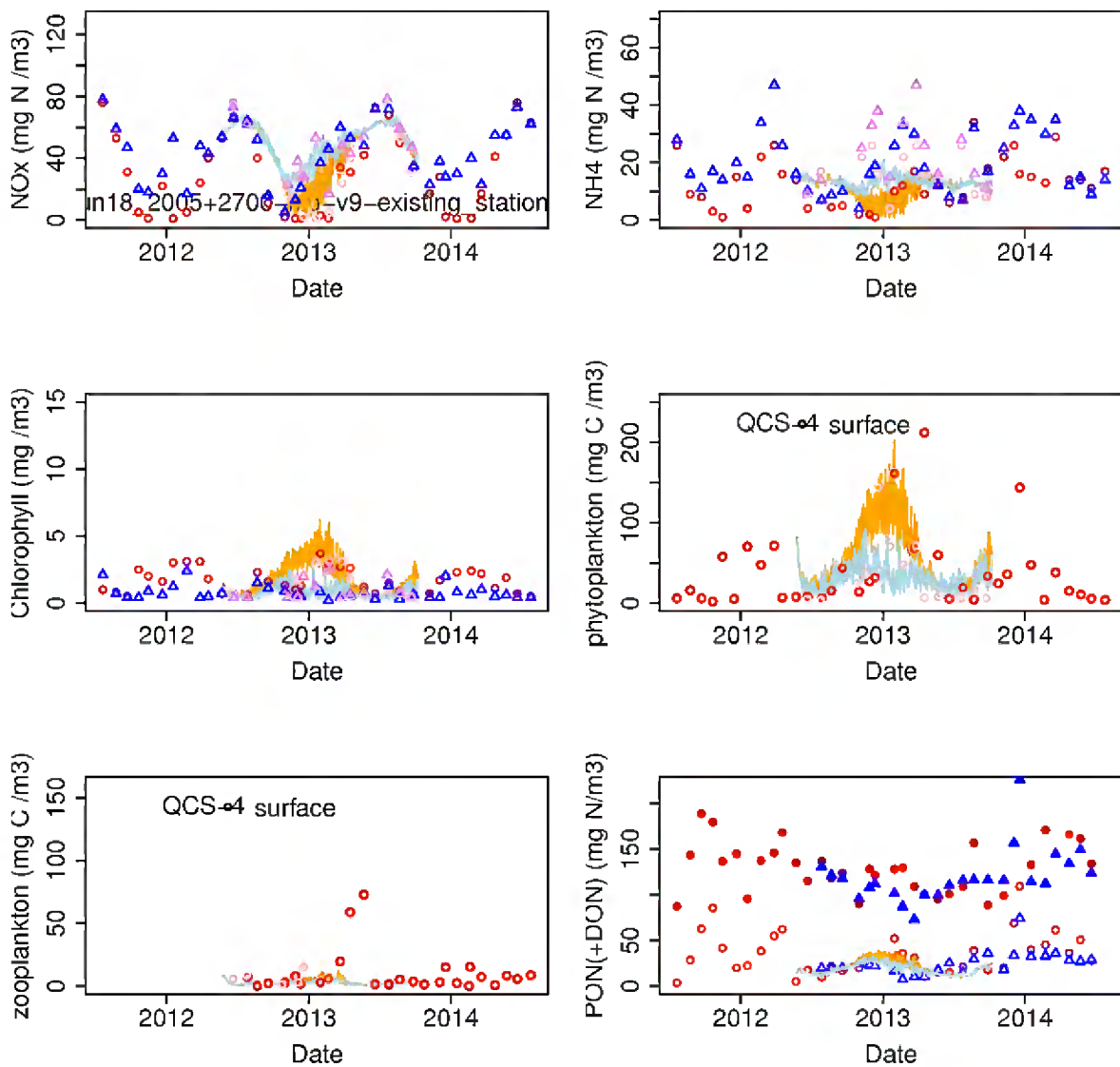


**Figure 5-4: Time-series of measured and simulated water-quality characteristics at station QCS-4.** Rest of caption as for Figure 5-1. .

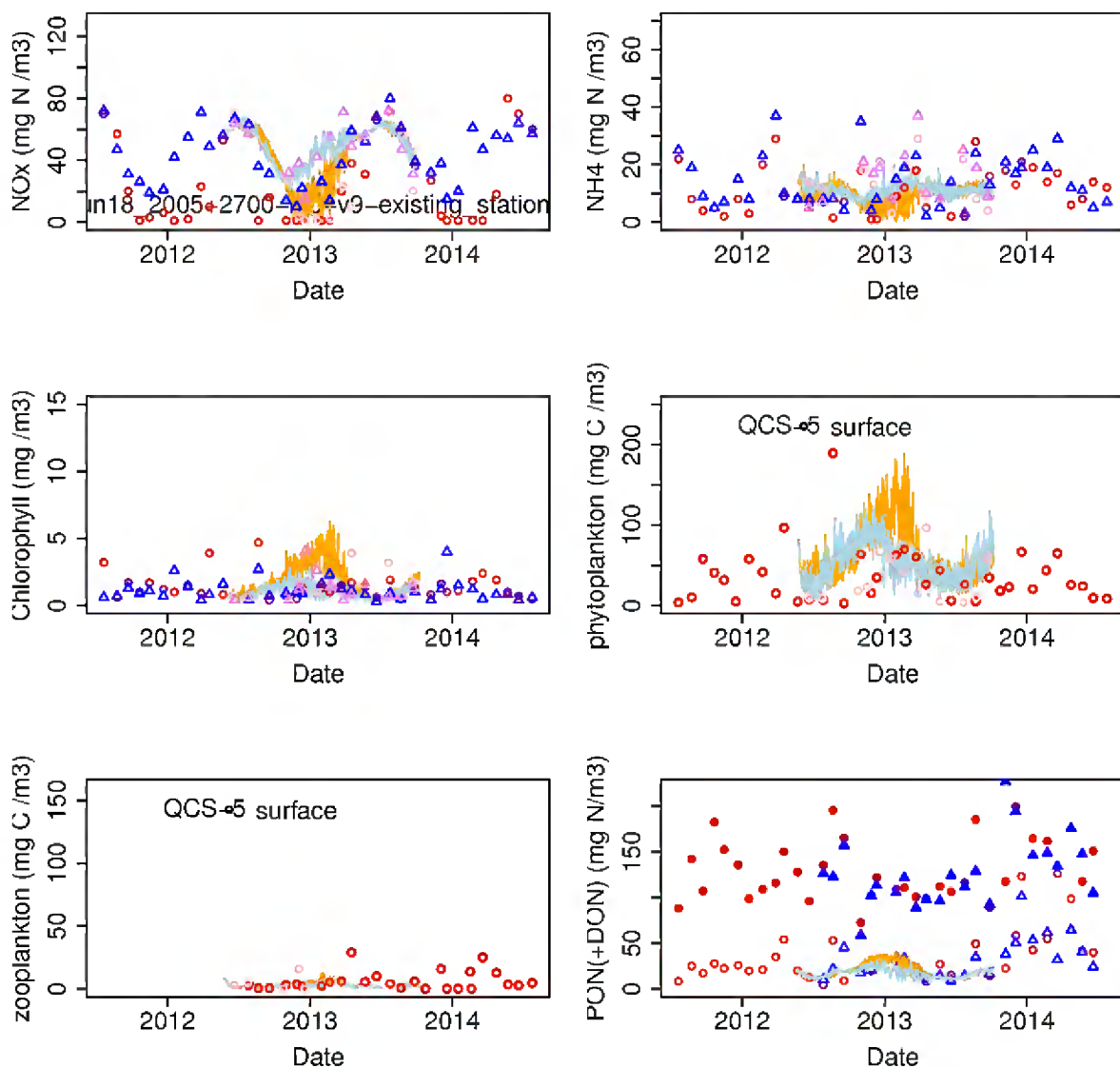


**Figure 5-5: Time-series of measured and simulated water-quality characteristics at station QCS-5.** Rest of caption as for Figure 5-1.

### 5.3 Simulations of the influence of existing mussel farming and existing mussel+fish farming (with benthic denitrification)

We will start by comparing the simulation results from the *no farms* scenario with those stemming from the *existing mussel farms only* scenario and the *existing fish farms* scenario. In the simulations presented within this section denitrification was permitted. These simulations were made on the 200 m resolution hydrodynamic grid. Rather than presenting time-series of simulation results at specific locations (as in Section 5.2), we present maps of time-averaged patterns. Specifically, we choose two time averaging periods. The first (2012-09-15 to 2013-02-28) is a period of spring/summer-time nutrient limitation, whilst the second (2013-05-01 to 2013-08-01) is a period of winter nutrient excess. The summer period begins approximately 110 days after the start of the simulation. Thus, the

model will have had plenty of time to forget the prescribed initial conditions. We also choose to show the time averages for the '1 m below sea-surface' layer. This corresponds to the near-surface region sampled by Marlborough District Council.

In the remainder of this section, we present maps of relative concentration (dimensionless units). The same underlying data are presented as maps of concentration change in Appendix G.

## Winter

Simulated concentrations of ammonium and small detritus are greatest in inner and central/outer Queen Charlotte (Figure 5-6). In contrast, concentrations of nitrate and large detritus are greater in Cook Strait and Tory Channel. Chlorophyll (and phytoplankton N) is markedly more abundant throughout Queen Charlotte Sound and Tory Channel than in Cook Strait. To a lesser extent, the same is also true of zooplankton.

The majority of mussel farms within this domain are in East Bay and Port Gore. There are no fish farms in Port Gore, and the flow in Cook Strait makes flow of Queen Charlotte water into Port Gore very unlikely. Inspection of the relative concentration plots for the mussel farms scenario (central column of images in Figure 5-10) suggests that mussel farming has an almost imperceptible influence upon winter-time nitrate concentrations, but that ammonium concentrations are increased by 20–30% within the environs of the mussel farms (e.g. at the bay-scale in Otanerau/East Bay and in Port Gore). On the other hand, consumption of particulate organic matter (phytoplankton, zooplankton, small and large detritus) by the mussels induces reductions of ~10–15% in these bays.

The model suggests that, during the winter period, the fish farm nutrients induce localized increases in the concentration of ammonium and large detritus (up to doubling the concentration in the immediate environs of the farm) and a small influence (2–5% increase) upon the concentration of small detritus in the far-field (notably, inner Queen Charlotte). The fish farm nutrients induce only a barely perceptible (on the chosen colour-scale) influence upon the concentrations of phytoplankton or zooplankton. Given the colour-scale, this implies that the changes are less than about 2% relative to the *no farms* scenario.

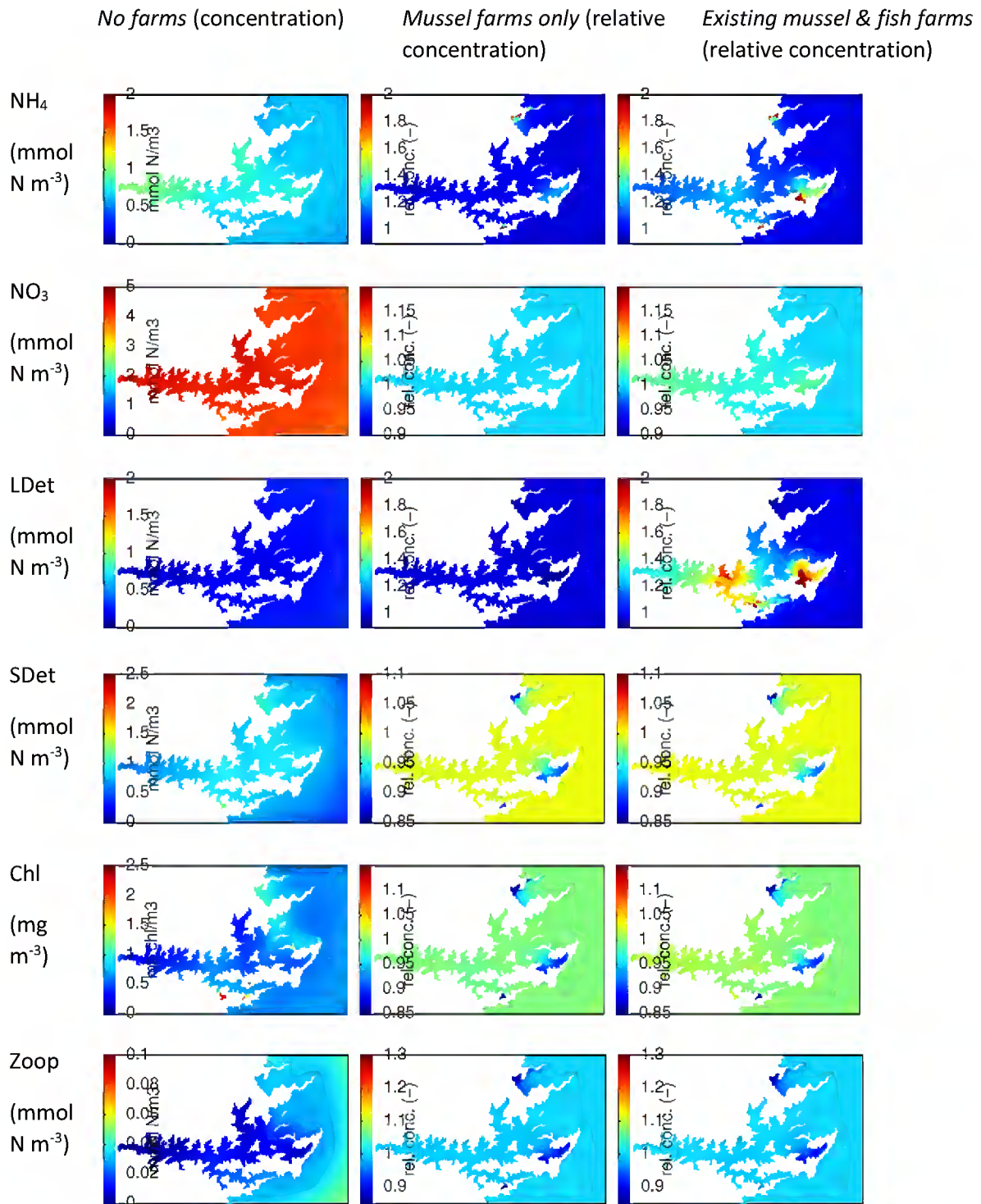


**Figure 5-6: Winter-period time averaged absolute and relative concentration for the no farms, existing mussel farms and existing mussel+fish farms scenarios.** The left hand column shows the time-averaged concentration for the no farms scenario for the indicated variables. The central column shows the time-averaged relative concentration for the existing mussel farm scenario and the right hand column shows the time-averaged relative concentration for the existing mussel+fish farm scenario. All simulations were run on the 200 m resolution grid. Concentrations are all shown in terms of nitrogen. LDet refers to large detritus, SDet is the small detritus class, and Zoop is zooplankton.



## Summer

In the absence of any farms, summer-time concentrations of ammonium and nitrate are lower than the winter-time concentrations, detrital concentrations are similar whilst phytoplankton and zooplankton concentrations are higher.

In Port Gore and Otanerau/East Bay, the presence of mussel farms increases concentrations of near-surface ammonium (up to 200% increase) and nitrate (circa 20% increase) relative to the no farms situation. The concentrations of near-surface detritus are reduced by about 5% in these bays, those of phytoplankton are reduced by approximately 5% in Otanerau/East Bay and up to 15% in inner Port Gore. Zooplankton concentrations are predicted to be reduced by up to approximately 15% in Otanerau/East Bay and in Port Gore. Whilst the mussels ingest phytoplankton just as readily as they ingest zooplankton and detritus, they also mineralise a fraction of the ingested detritus and zooplankton to inorganic nutrient. In effect, the mussels serve to fertilize the surface waters during summer by speeding the mineralization process. The combination of reduced zooplankton grazing pressure and more fertile waters enables those phytoplankters which are not ingested to grow more rapidly than they would in the absence of the mussels. Thus, the phytoplankton population recovers more rapidly – such that it exhibits lesser depletion than zooplankton.

During the summer period, the presence of fish farms leads to dramatic (up to 200%) increases in the concentration of ammonium and large detritus in the immediate environs of the fish-farms. The far-field effects are of a much lesser magnitude (but evident throughout Queen Charlotte, and to a lesser extent Tory Channel). In the far-field, near-surface concentrations of ammonium (increase of 10-20% relative to the *no farms* situation), nitrate (0–10% increase), large detritus (10–20% increase), small detritus (0–5%, increase), chlorophyll (0–10%, increase) and zooplankton (0–15%, increase). The largest far-field increases tend to occur in inner Queen Charlotte Sound, whilst the smallest changes are in outer Tory channel.

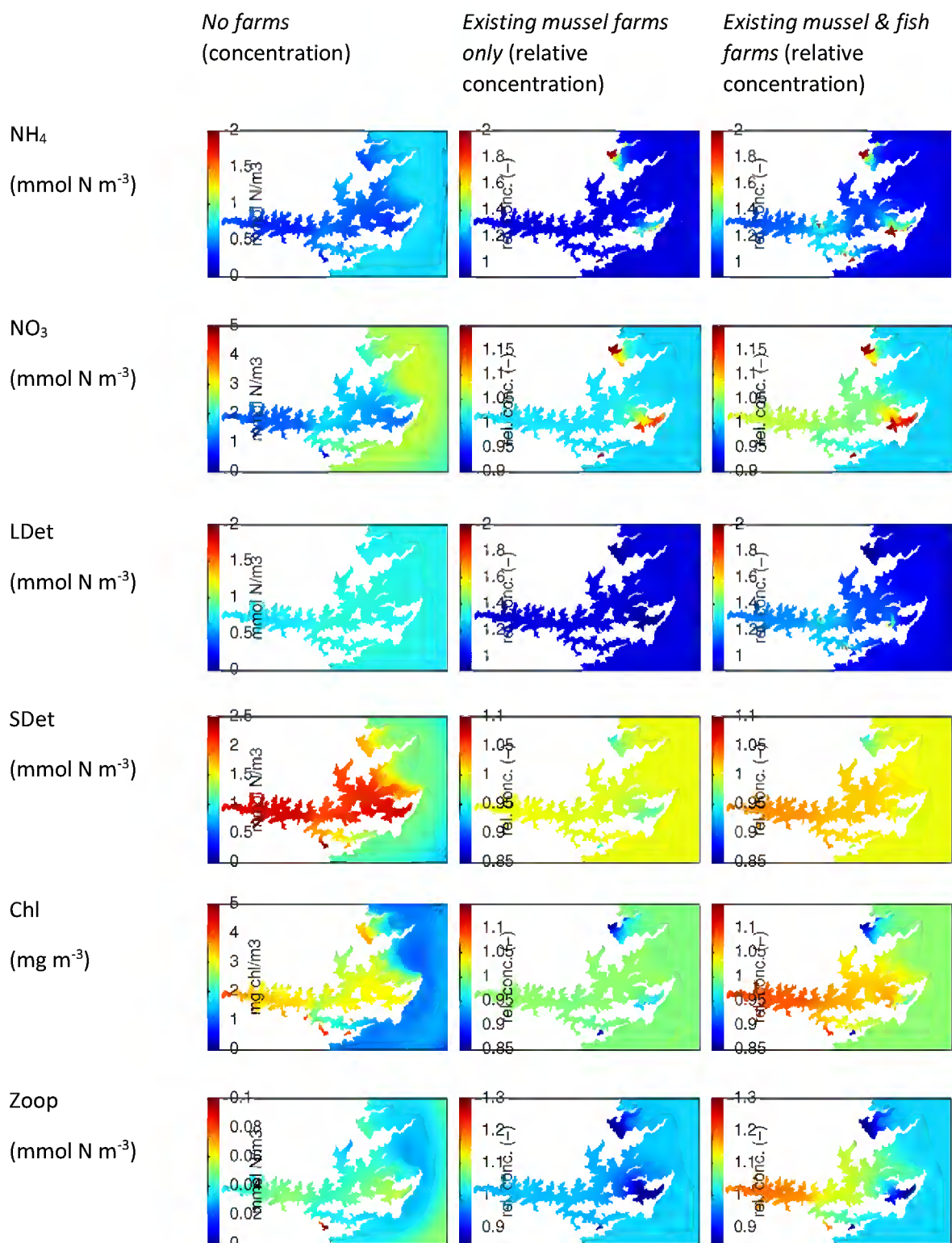


**Figure 5-7: Summer-period time averaged absolute and relative concentration for the no farms, existing mussel farms and existing mussel+fish farms scenarios.** Rest of caption as for Figure 5-6.

## 5.4 Simulations of the influence of combined mussel & fish farming activities under 2012 occupation and approved occupation

In the previous section we examined the influence which mussel farming (at 2012 development levels) and the joint influence of mussel (2012 development) and fish farming (2012/2013 feed input levels) upon the water quality of Queen Charlotte Sound. In this section we use the model to examine the influence of further mussel and fish farm expansion. Specifically, we compare some of the earlier simulation results with those from a new scenario in which:

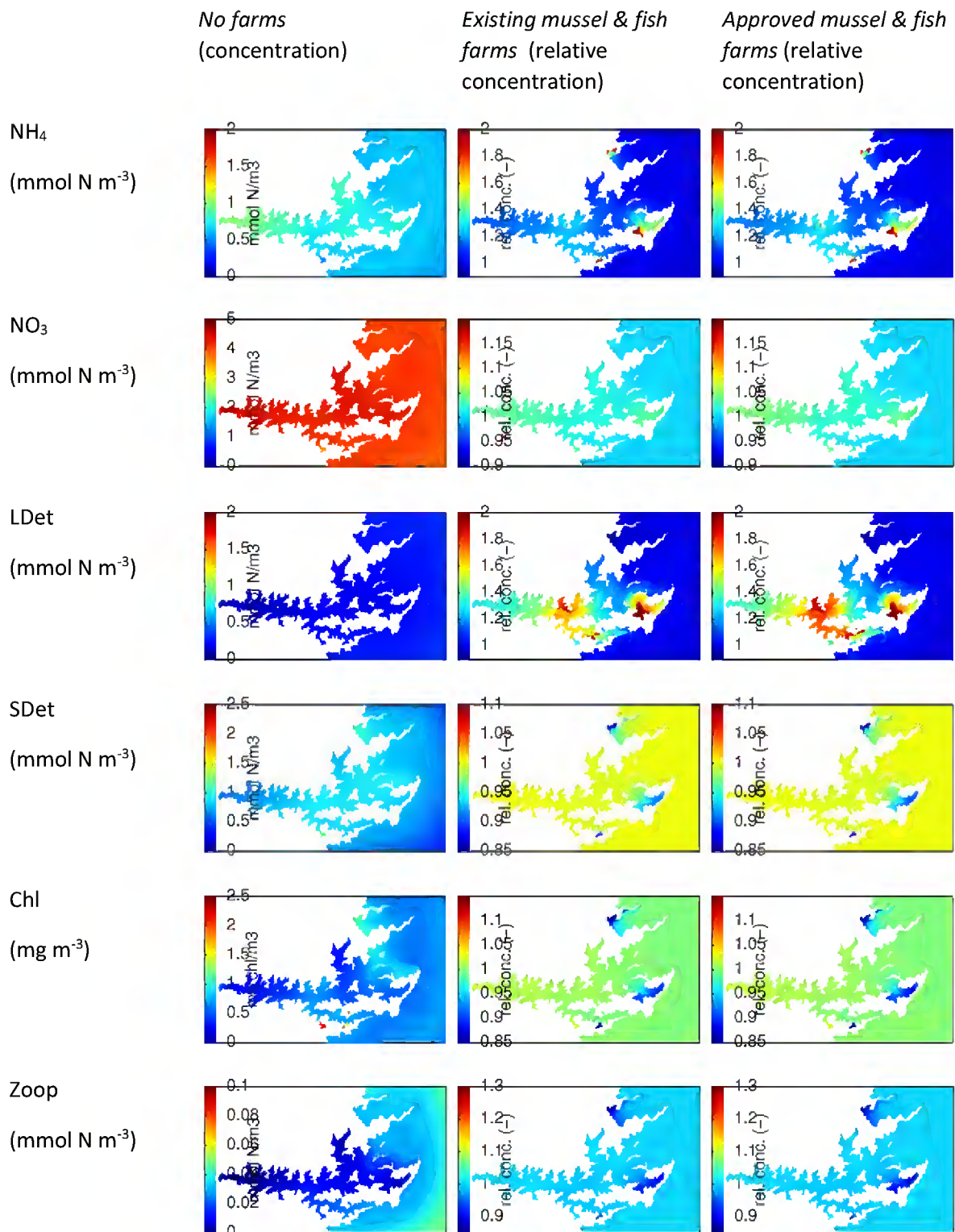
- The mussel farms that were visible in the 2012 aerial survey are augmented with all other blocks of water space that have been approved for mussel farming since then (and/or which were approved but not yet occupied at the time of the 2012 aerial survey)
- The four existing salmon farms (Ruakaka, Otanerau, Te Pangu, Clay Point) were assumed to be stocked in a manner that would cause them to fully utilize the maximum annual feed input rates stipulated in their licensing conditions<sup>15</sup>.
- The recently approved Ngamahau salmon farm was added into the system. We assumed that it would operate at its maximum annual feed input rate and that the cohort structure (proportions of fish within each size-class) would be the same as that in Te Pangu during the 2012/13 year<sup>15</sup>.

Figure 5-8 and Figure 5-9 show time-averaged results for the winter and summer periods respectively. (Note that relative to Figures 5-6 and 5-7 only the right hand columns of these figures are new.) The key point is that, the images in the right hand columns of Figure 5-8 and Figure 5-9 are not dramatically different from those in the central columns. This implies that the model predicts that the additional mussel farms and the additional fish-farm inputs will have only a relatively small incremental influence upon water quality. During the winter, the additional fish farm inputs appear to cause a slightly greater (a further 1% or so on top of that due to the *existing farms*) NO<sub>3</sub> enrichment in inner Queen Charlotte and greater (a further 5–10% or so) large detritus enrichment in inner Tory Channel and central Queen Charlotte but effects upon other components of the food web are barely perceptible.

During the summer, one sees a new spot of elevated ammonium around the new Ngamahau farm, and NO<sub>3</sub> concentrations are elevated by a further 1-2% (on top of that due to the *existing farms*) in inner Queen Charlotte. Concentrations of phytoplankton, small detritus and zooplankton also increase by a further 1–2% (on top of that due to *existing farms*) throughout inner and central Queen Charlotte.

---

<sup>15</sup> For each farm, we applied a temporally constant scale factor to the 2012/13 fish stock and feed input details provided by NZKS such that the annual feed input limits were attained. The scaling factor was (licenced maximum annual feed input/realized 2012/13 annual feed input).



**Figure 5-8: Winter-period time averaged absolute and relative concentration for the no farms, existing mussel+fish farms and the approved mussel+fish farms scenarios.** The left hand column shows the time-averaged concentration for the no farms scenario. The central column shows the time-averaged relative concentration for the existing mussel+fish farm scenario and the right hand column shows the time-averaged relative concentration for the approved mussel+fish farm scenario. All simulations were run on the 200 m resolution grid.

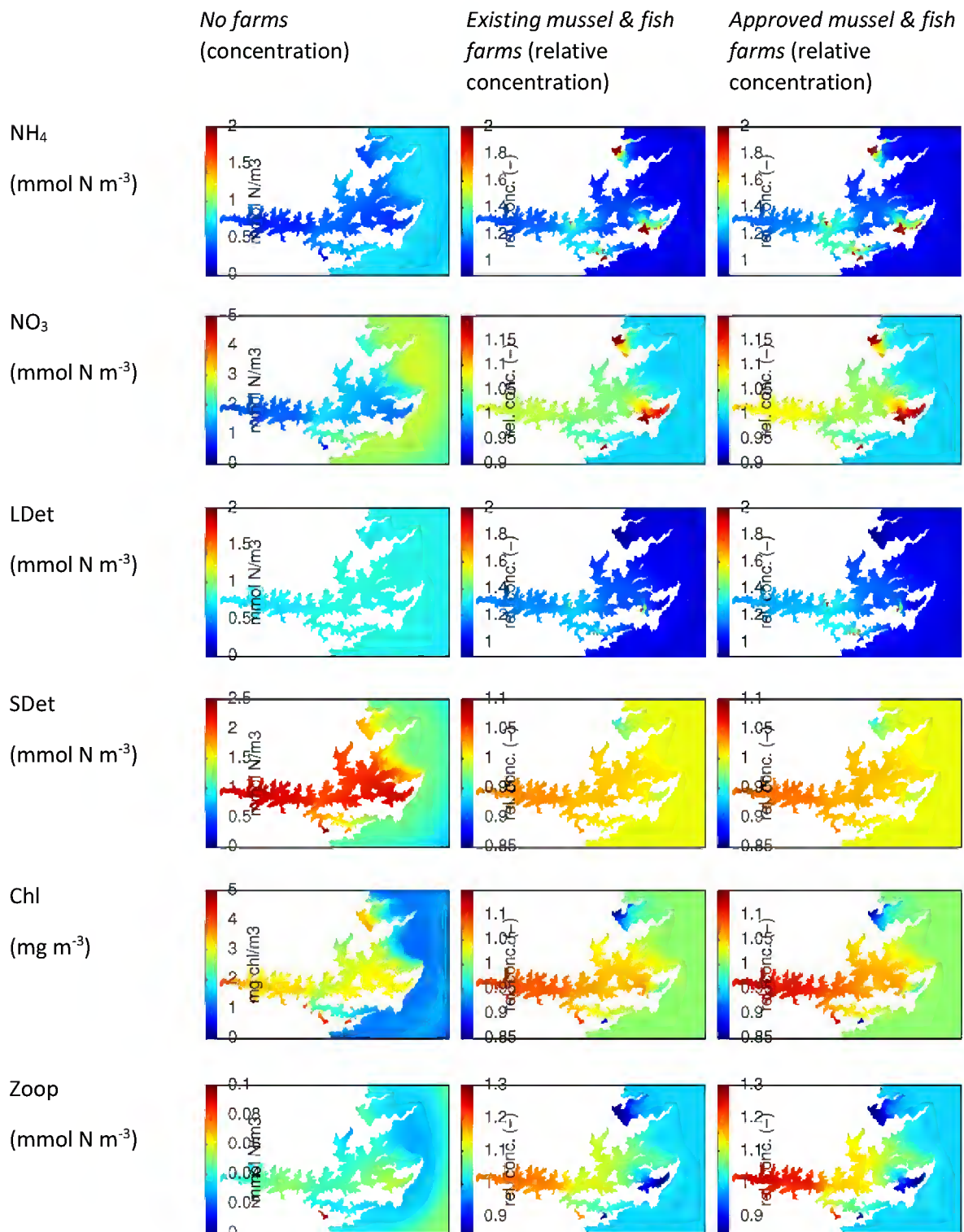


**Figure 5-9: Summer-period time averaged absolute and relative concentration for the no farms, existing mussel+fish farms and the approved mussel+fish farms scenarios. Rest of caption as for Figure 5-8.**

### 5.4.1 Instantaneous dynamics

Sections 5.3 and 5.4 presented maps of time-averaged results spanning all of the Sound. An alternative way of viewing the data is to inspect time-series of instantaneous values at specific locations. The images in Appendix F illustrate the time-series of simulated near-surface water-quality variables at the five Marlborough District Council water quality stations. The key points are:

- The phase of the seasonal cycle does not change in response to changes in the extent of mussel and fish farming
- Addition of the Ngamahau fish farm (together with expansion of the already existing fish-farms such that they operate at their maximum permitted feed input rates) induces predicted incremental changes which are small relative to those which are predicted to have been associated with the development of the mussel and fish farms presently in existence.
- The figures serve to demonstrate that the magnitudes of farm induced change are small relative to the natural variability.

## 5.5 Influence of denitrification

Fish farms are a source of nitrogen for the system (the catchment is another source) and the Cook Strait boundaries may be a net source at times. Nitrogen may be lost from the system by only two means: export across the Cook Strait boundaries or denitrification at the seabed. The Fennel model has only a relatively crude description of denitrification. Specifically, 75% of any particulate nitrogen that settles to the seabed is lost to denitrification and the remaining 25% returns to the bottom-most water-column as ammonium. The model predicts denitrification rates vary from about  $0.2 \text{ mmol N m}^{-2} \text{ d}^{-1}$  to about  $1.2 \text{ mmol N m}^{-2} \text{ d}^{-1}$  in Queen Charlotte and Tory Channel at sites well removed ( $>2 \text{ km}$ ) from fish farms. We know of no measurements of sediment denitrification rates in Queen Charlotte Sound but Kaspar, Gillespie et al. (1985) measured rates of  $0.1\text{--}0.9 \text{ mmol N m}^{-2} \text{ d}^{-1}$  at control sites in Keneperu ( $0.7\text{--}6.1 \text{ mmol N m}^{-2} \text{ d}^{-1}$  under mussel farms). In another study Christensen et al. (2003) measured denitrification rates of  $0.4\text{--}0.7 \text{ mmol N m}^{-2} \text{ d}^{-1}$  under mussel farms in Beatrix Bay. Beyond the immediate environs of the fish-farms, the model is yielding denitrification rates which are similar to those control site values. We infer that the model is producing plausible denitrification rates throughout most of Queen Charlotte and Tory Channel. Under the fish-farms, the model is yielding denitrification rates approaching  $3 \text{ mmol N m}^{-2} \text{ d}^{-1}$ , but these high rates are restricted to within a few hundred meters (at most) of the farm perimeter.

Summed over Tory Channel and Queen Charlotte Sounds, and averaged over a year, the incremental denitrification flux (in the *existing farms* simulation relative to the *no farms* one) is approximately  $0.3 \text{ tonne N d}^{-1}$ . In comparison the input of nitrogen from the fish-farms is approximately  $3 \text{ tonne N d}^{-1}$ . Thus, denitrification removes about 10% of the fish-farm derived nitrogen. The remaining  $2.7 \text{ tonne}$  is exported into Cook Strait, apart from that harvested in mussels and fish.

The nitrogen withdrawn from the system when mussels are harvested is not explicitly modelled, but it is implicitly included by the assumption that the user-prescribed time-series of mussel abundance implies constant biomass within each class size. The model indicates that the mussels will, for the most part, be growing (as they do in reality). Therefore the model implicitly assumes a continuous mussel harvest during the year. In evidence to the NZKS Board of Inquiry (Knight 2011), it was

calculated that nitrogen losses to denitrification are about 30 times greater than losses to mussel harvest in Queen Charlotte Sound.

For the preceding simulations we assumed that 75% of the particulate organic nitrogen that settles to the seabed denitrifies. Whilst the resultant denitrification rates are consistent with those measured in the Sounds, the model's description of denitrification processes is very crude. Fish farms introduce nitrogen into the system. Denitrification removes at least some of this nitrogen (thereby buffering the system against fish-farm impacts). It is therefore appropriate to determine how sensitive the model's dynamics (and, more importantly, the inferences that we might draw with respect to fish-farming influences) are to denitrification. We therefore made two further simulations. In both, denitrification was turned off. Thus, all sedimenting particulate organic nitrogen returns to the bottom-most layer of the water-column as ammonium. In the first of the two new simulations, there were no mussel or fish farms present. The second had both mussel farms and fish-farms. All blocks licensed for mussel farms were assumed to be occupied and all fish farms (including Ngamahau) were assumed to be introducing feed at the maximum rates permitted by their consents.

Figure 5-9 and Figure 5-10 show time-averaged results for the winter and summer periods respectively. During winter (and in the absence of farming) surface water ammonium concentrations rise by 20% (outer Queen Charlotte) to 30% (inner Queen Charlotte) when denitrification is turned off in the model. Nitrate concentrations rise by 3% (outer Queen Charlotte) to 7% (inner Queen Charlotte). There are also very small (~1%) increases in the concentrations of phytoplankton, zooplankton and detritus in inner Queen Charlotte.

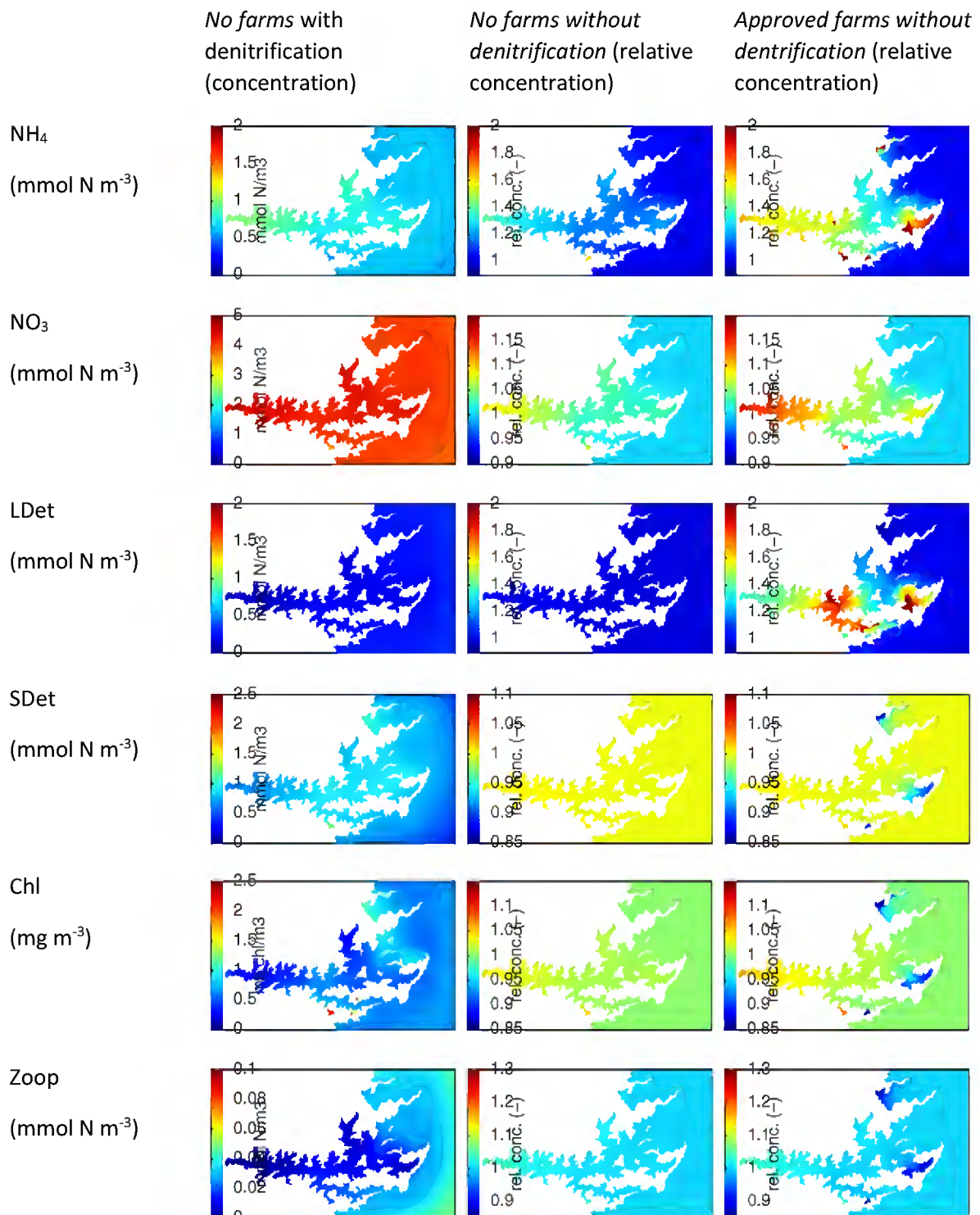
When the *approved* mussel and fish farms are added into the *no denitrification* simulation, the model predicts ammonium increases (relative to *no farms with denitrification*) of 40–60%, nitrate increases of 2–12%, increases of 20–80% for large detritus (most of this is the increment that is unsettled fish faeces and waste food), increases of small detritus amounting to 0–2% (inner Queen Charlotte only) and phytoplankton and zooplankton increases of ~5% in inner Queen Charlotte. The images in the right hand column of Figure 5-10 may also be compared with those in the right hand column of Figure 5-8 or the central column of Figure 5-10. Both comparisons provide means of determining how much of the changes evident in the right-hand column of Figure 5-10 can be attributed to the aquaculture activities rather than to the imposed loss of denitrification function. The vast majority of the increments in the concentration of large detritus can be ascribed to unsettled faeces and uneaten food, but for the other constituents, it appears that denitrification (or its absence) is almost as important as the presence or absence of aquaculture (particularly fish farming) in determining the magnitudes of far-field change. This is especially true in the (shallower) side bays and inner Queen Charlotte.

Figure 5-11 is similar to Figure 5-10 but shows results for the summer time-averages. It is clear that when denitrification is turned off the enhancement of ammonium, small detritus and plankton is greater during the summer than during the winter. Conversely, there is less enhancement of nitrate and large detritus. Comparing the right-hand and central columns of Figure 5-11, we again infer that the magnitudes of far-field change arising from presence/absence of benthic denitrification are similar (albeit that the aquaculture effects are a little larger).

The consent conditions for the new fish farm at Ngamahau stipulate that the farm should not cause the system to move significantly towards a eutrophic state. Evidence presented at the hearings implies that annual- and space averaged chlorophyll concentrations in excess of 5 mg Chl m<sup>-3</sup> are indicative of a eutrophic state. It is therefore worth noting that even under the combination of *no*

*benthic denitrification* and *approved farms*, winter time-averaged chlorophyll concentrations remain well below 5 mg Chl m<sup>-3</sup>. Even during summer, time-averaged chlorophyll concentrations remain below this threshold – albeit that they are circa 4 mg m<sup>-3</sup> in some side bays and do exceed that threshold intermittently.





**Figure 5-10: Winter-period time averaged absolute and relative concentration for the *no farms with denitrification*, *no farms without denitrification* and *approved farms without denitrification* scenarios. The left hand column shows the time-averaged concentration for the *no farms with denitrification* scenario. The central column shows the time-averaged relative concentration for the *no farms without denitrification* scenario and the right hand column shows the time-averaged relative concentration for the *approved farms without denitrification* scenario. All simulations were run on the 200 m resolution grid.**

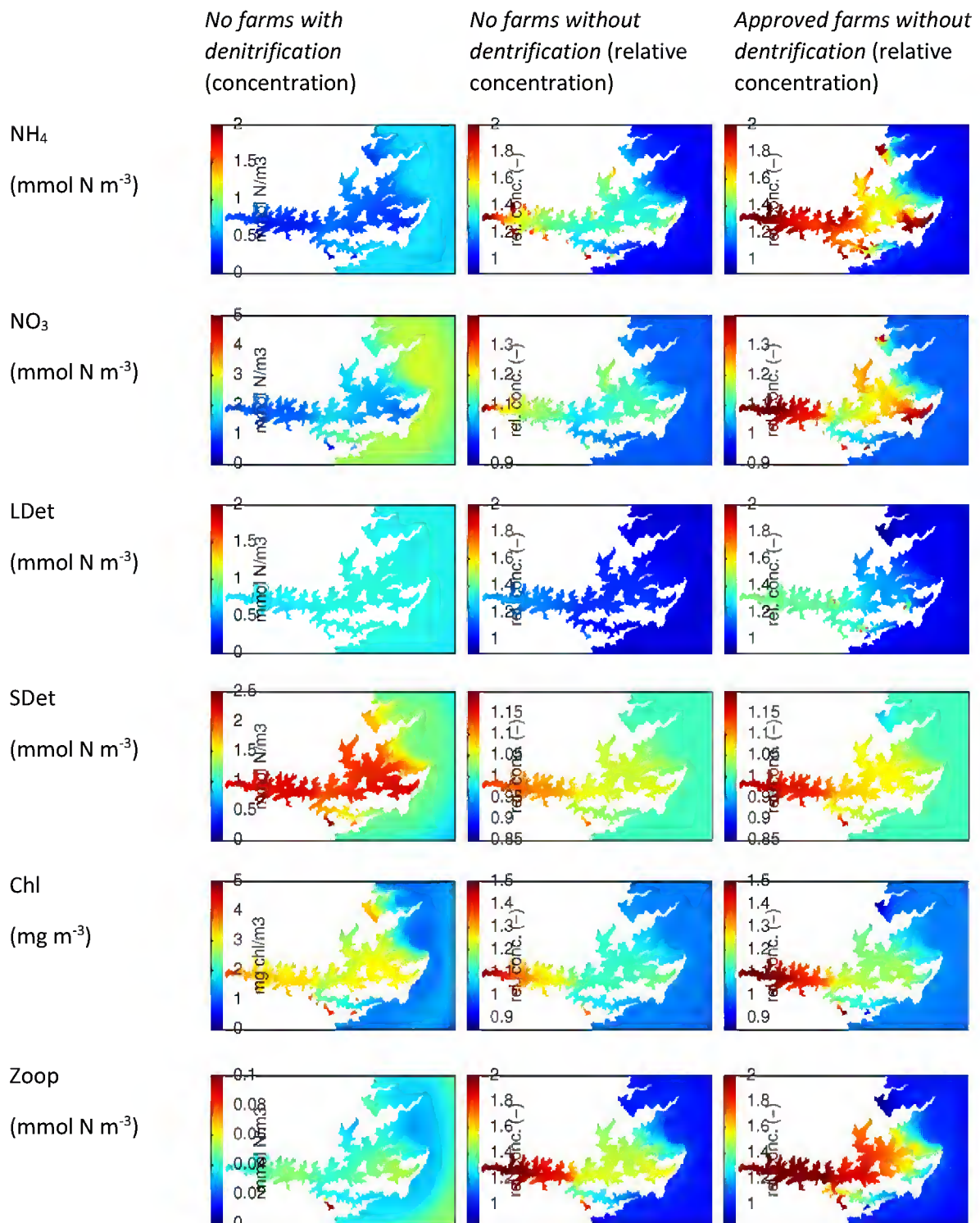


**Figure 5-11: Summer-period time averaged absolute and relative concentration for the *no farms with denitrification*, *no farms without denitrification* and *approved farms without denitrification* scenarios.** Rest of caption as for Figure 5-10.

## 5.6 Total nitrogen under each scenario

In the preceding sections we presented results concerning individual components of the Fennel water quality model and, when discussing farm (or denitrification) induced change, we presented results in terms of relative concentration. In this section, we will examine the results (from a subset of the simulations that we have already presented) as an aggregate measure (total nitrogen, or TN) and express change as concentration increment rather than relative change. Total nitrogen is a derived quantity. Within the model, it corresponds to the sum of nitrogen within ammonium, nitrate, the two detritus fractions, phytoplankton and zooplankton. This quantity is not directly equivalent to a field measurement of total nitrogen (which would include dissolved organic nitrogen).

The results show that when denitrification is permitted, the greatest changes in TN ( $2\text{--}3\text{ mmol N m}^{-3}$ ) are restricted to the immediate environs of the fish farms (Figure 5-12). Given that fish-food inputs are greater in the summer, it is a little surprising that the modelled near-field TN increases are greater in the winter than in the summer. We speculate that flushing and/or specific rates of denitrification are sufficiently greater in the summer that they can more than offset the increased feed inputs. In the *with denitrification* scenarios, the predicted far-field TN concentration increment due to the farming activities is circa  $0.5\text{ mmol N m}^{-3}$  in the winter. This increment does not increase dramatically with the shift from *existing* to *approved* farms. Comparing the *no farms with denitrification* and *no farms without denitrification* results, benthic denitrification has the effect of reducing water column TN by up to  $1\text{ mmol N m}^{-3}$  in the winter and up to  $2\text{ mmol N m}^{-3}$  in the summer. Benthic denitrification is more influential in the shallow side bays and shallow, less well flushed inner Queen Charlotte. Addition of *approved* farms into the *no denitrification* scenario induces further increments to the TN concentrations (relative to the *no farms with denitrification* scenario: circa  $1.0\text{--}1.5\text{ mmol N m}^{-3}$  throughout much of inner Queen Charlotte during the winter, and up to about  $2.5\text{ mmol N m}^{-3}$  in the summer. This magnitude of TN increment amounts to 20-50% of the predicted *no farms, with denitrification* background level. Comparing the magnitudes of change (relative to *no farms with denitrification*) arising in the *no farms without denitrification* and *approved farms without denitrification* scenarios, we deduce that the model implies that farming induces a TN increment that is a little greater than that which would arise if all benthic denitrification were to cease.

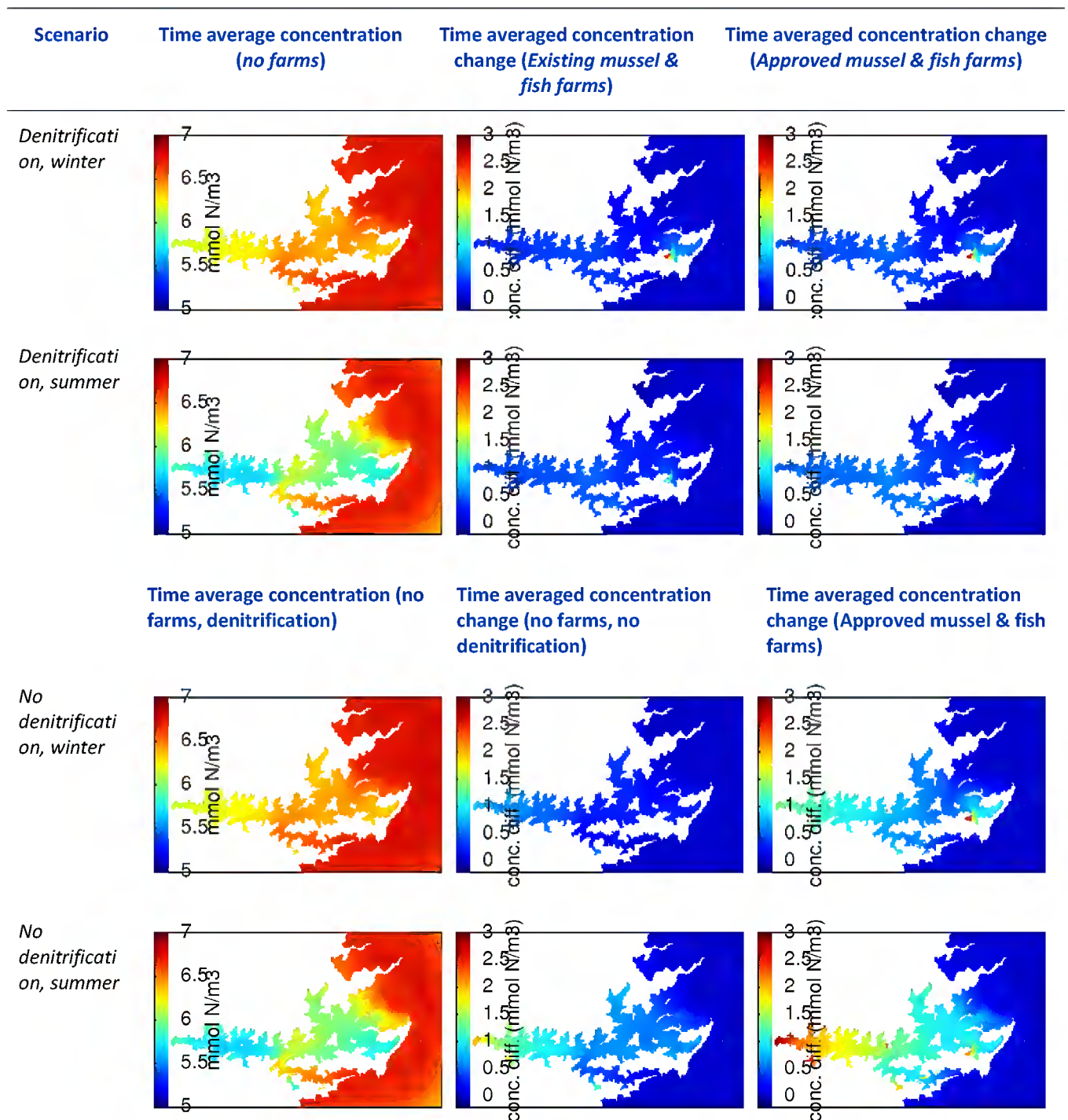


**Figure 5-12: Time averaged concentration of total nitrogen TN under some of the scenarios that we have simulated.** TN is calculated as the sum of modelled ammonium, nitrate, detritus, phytoplankton and zooplankton nitrogen concentrations ( $\text{mmol N m}^{-3}$ ). In all rows, the left-most image is the time-averaged concentration for the *no farms with denitrification* scenario. In the upper two rows, the central image is the time-averaged concentration change (relative to the *no farms with denitrification* scenario) for the *existing farms with denitrification* scenario. In the lower two rows, the central image is the concentration change for the *no farms without denitrification* scenario (rel to the *no farms with denitrification* scenario). The right-hand images are concentration changes for the *approved farms* scenario (with or without denitrification) relative to the *no farms with denitrification* one. Note that the colour-scale for TN (left-most images) does not extend to zero.

## 6 Biophysical model: Discussion

### 6.1 Performance of the biophysical model

No specific numerical criteria have been set by which to assess the performance of the biophysical model. Furthermore, we have resorted to making use of the Marlborough District Council water-quality data in the (informal, 'by eye') calibration process. Since there are insufficient independent data to permit a validation of the model, it is only possible to judge its performance by reference to the calibration data. It is clear that the model reproduces the mean annual abundance of all state-variables at all locations fairly well (in comparison with the calibration data). It also reproduces the amplitude of seasonal fluctuations fairly well. In Tory Channel and outer Queen Charlotte it reproduces the phase of seasonal fluctuations well, but in inner Queen Charlotte it fails to reproduce the bimodal phytoplankton dynamics (peaks of abundance in late winter/early spring and late summer/early autumn).

In the context of this work, we are endeavouring to determine the relative changes induced by shellfish farming and fish-farming. With that in mind, it is appropriate to ask: 'does it matter that the model fails to reproduce the timing of the phytoplankton peaks in inner Queen Charlotte?'. We believe the answer is 'not greatly'.

Firstly, the mussel farms and fish farms are located in Tory Channel and outer Queen Charlotte. Furthermore, at least during winter, the model suggests that their influences upon living components of the foodweb (the plankton) are expressed only in outer Queen Charlotte. Fortunately, the calibration exercise yielded a much better fit to the data from central and outer Queen Charlotte and Tory Channel than it did for inner Queen Charlotte. This is by good fortune rather than by design—we did not consciously favour fitting the outer Queen Charlotte/Tory channel data over the inner Queen Charlotte data.

Secondly, shellfish filter particulate matter out of the water column. The mussel model explicitly assumes that the quantity of water that each mussel pumps across its gills (the filtration apparatus) is independent of seston concentration. Thus, the daily specific gross capture rate for seston is not influenced by the absolute quantity of seston in the water. On the other hand, the fraction of the captured seston that passes into the gut (rather than being rejected in pseudo-faeces) is assumed to decline as the capture rate increases. That is, the relative quantity of captured seston that is rejected as pseudofaeces (hence, returned to seston) increases with seston concentration. Thus, the net specific seston removal rate declines as seston concentration rises. Fortunately, the decline is almost negligibly small across the seston concentrations found in the Sounds. Consequently, we infer that the model should be capable of adequately predicting near-field seston depletion levels if the near-field hydrodynamics are correct. Far-field change will be determined by a combination of many factors (hydrodynamics, plankton growth rates, detrital remineralization and settling rates etc). The data do not allow us to determine whether the individual rates are close to being correct, but the fact that the far-field standing stocks are 'about right' on average offers some encouragement.

In the context of this model, fish farms are a source of nitrogen (as ammonium and particulate organic detritus). The rates of ammonium and detritus input are strongly correlated with the user-supplied fish-feed input rates, but also influenced by the parameterisation of the fish-physiology model. Those fish-feed input rates were based upon monthly rates provided to us by New Zealand King Salmon. We have recorded (but not reported) the derivative ammonium and detritus input rates calculated by our model and they are consistent with the prescribed inputs. It is worth emphasizing

that the fish feed input rates reported by NZKS for the 2012/13 year were lower than they had been in earlier years. Consequently, the nitrogen input rates for our *existing farms* scenario were lower than the maximum permitted by the consent conditions. By definition, that is appropriate for the *existing situation* simulation, but for the *approved farms* simulation (with and without denitrification) we chose to assume that the fish farms would operate in a manner that enabled them to fully utilize their maximum discharge limits.

The location (spatial and foodweb-level) and magnitudes of fish-farm induced change are dictated by myriad processes (currents, mixing, detrital sinking and mineralization rates, kinetics of plankton growth etc.). The hydrodynamic model has been shown to reproduce currents in the main stems of Queen Charlotte and Tory moderately well (section 3). The key biological processes governing how quickly (and how much) farm-derived nutrient is incorporated into the food chain are:

- Detrital denitrification rates
- Detrital mineralization rates
- Phytoplankton growth rates (particularly under nutrient-limiting conditions)

We have already established (section 4.10) that the denitrification rates are consistent with those measured elsewhere in the Sounds (Pelorus Sound). We do not have data with which to validate any of the other biogeochemical rates predicted by our model but the coefficients that we have adopted to describe the various rate processes are typical of those seen in the water-column modelling literature. That said, though the specific detrital decay rates ( $0.01 \text{ d}^{-1}$ ) that we have adopted are typical of fresh plankton-derived material in the water-column (Enríquez, Duarte et al. 1993), they are high relative to those adopted when modelling the decay of fish-faeces in the seabed. For example, Brigolin, Pastres et al. (2009) adopted a value of  $0.0027 \text{ d}^{-1}$ . Since the bulk of farm-derived faeces will tend to arise in the summer, the implication is that too much of the farm-derived faecal nutrient will be mineralized during the summer (nutrient months). Thus, the model may be over-estimating summertime fertilization potential.

## 6.2 Limitations of the biophysical model

Perhaps the most obvious deficiency in the biophysical model (cf particle-tracking deposition model described in section 7) is that we assumed that faeces from fish and mussels (and pseudo-faeces from mussels) all pass into the large detritus pool. We retained the default sinking speed for this pool ( $3 \text{ m d}^{-1}$ ). In reality, faeces and pseudo-faeces sink at speeds of a few centimetres per second ( $100\text{--}1000 \text{ m d}^{-1}$ ). The implication must be that faeces etc. emanating from fish- and mussel farms travel too far horizontally before hitting the seabed. Once on the seabed, this material becomes subject to denitrification processes. Denitrification renders nitrogen nutrient biologically unavailable. Given that faecal material remains in the water-column too long, one might legitimately argue that the model is permitting too much fish-farm derived nitrogen to remain bio-available. This suggests that the model may be over-estimating the degree to which fish-farm derived nitrogen can enhance plankton standing stocks during the summer period. On the other hand, denitrification rates can become suppressed when the organic loading is too high. The Fennel model does not include this detail, but it is possible that, in reality, this is occurring under the fish farms. If so, the Fennel model will over-estimate near-field removal of farm-derived particulate nitrogen. We have tracked the rates of denitrification etc. in our *with denitrification* simulations and we estimate that denitrification

removes approximately 10% of the fish-farm derived nitrogen inputs. Thus, the water-column is responding to the remaining 90%. One might infer that, even if none of the farm-derived nitrogen (faecal or ammoniacal) were ever to be denitrified, the changes in water-column water-quality would not be very much larger than the model already predicts. Our *without denitrification* simulations tend to support that conclusion.

The model has some other subtleties. The foodweb is truncated. The highest explicit trophic group is zooplankton. The influence of predators of zooplankton is represented by imposing a specific mortality rate ( $d^{-1}$ ) upon the zooplankton. In particular, the Fennel model assumes that the specific mortality rate increases linearly with rising zooplankton abundance. This assumption is not atypical of NPZD models, but Steele, Henderson (1992) and Edwards, Yool (2000) have shown that the dynamics of a nutrient-phytoplankton-zooplankton model can be very sensitive to the form (and parameterization) of this top-level predatory closure term. Under some situations, the system can be induced to exhibit high frequency oscillations (alternating booms and busts) even in an otherwise constant environment. The fact that the Fennel model assumes that the specific mortality rate increases linearly with rising zooplankton abundance reduces the likelihood of such oscillations. The implication is that it is possible that the Fennel model may under-estimate the frequency and/or extent of short-lived algal blooms. We have chosen to focus our attention upon time-averages. These are less sensitive to the form of the mortality closure term. Time averages are also more relevant when it comes to assessing the magnitudes of farm induced change relative to those permitted by the consent conditions associated with Ngamahau farm.

The truncated foodweb is deliberately simple. It does not include higher trophic levels. Perhaps more importantly, it does not include bacteria or macroalgae. Like the phytoplankton, these will consume farm-derived nutrients. Since the model lacks these two groups, the phytoplankton have exclusive access to the farm derived nutrient. This implies that the model probably over-estimates the extent to which the phytoplankton community may change (increase) in response to farm-derived nutrient.

Photosynthetically active radiation is almost entirely restricted to the visible spectrum, but this is composed of light of many wave-lengths. Even pure water absorbs some wave-lengths of visible light (e.g. red) much more strongly than others (e.g. green). The PAR attenuation coefficient represents an empirical measure of PAR absorption. Because it is PAR-based (rather than wave-length specific), its value tends to decline with increasing depth (as the residual PAR becomes increasingly concentrated in the weakly absorbed wave-lengths). The Fennel model does not break PAR down into multiple wave-length bands. Thus, it cannot take account of this subtlety. Our estimate of the PAR attenuation coefficient is based upon PAR measurements made from more than 8 m below the sea-surface. By this depth, all the strongly absorbed PAR wavelengths (which make up about 50% of the visible spectrum at the sea surface) have disappeared. The implication is that we are probably over-estimating the quantity of PAR which penetrates to 8 m and deeper. To some extent, this can be (has been) accommodated through calibration of the initial slope of the photosynthesis-irradiance curve, but it is possible that this weakness in the model is responsible for some of its deficiencies with respect to reproducing the field data. Specifically, the model tends to over-predict summertime near-bed phytoplankton concentrations (and under-predict corresponding  $\text{NO}_3$  concentrations) in inner Queen Charlotte. We suspect that, in part at least, this reflects inaccurate reproduction of the pattern of PAR decline with respect to depth.

Whilst the model reproduces both the annual average and the annual amplitude of fluctuations in the state-variables moderately well, it performs less well in terms of reproducing the phase of the annual cycle. Possible explanations for this include:

- The timing of phytoplankton blooms is strongly influenced by vertical mixing. It is possible that seemingly minor discrepancies between simulated and real-world vertical mixing could induce the phase errors.
- The Marlborough Sounds are narrow and bounded by steep and relatively high hills. A significant fraction of the sea-surface will be shaded from the sun for several hours in the morning or evening. The model takes no account of this. Whilst phytoplankton photosynthetic rates become saturated at relatively low light intensities, it is probable that daily primary production is over-estimated by the model – particularly during the winter period when the sun does not rise so high. The absence of this topographic shading may contribute to the model’s tendency to over-estimate phytoplankton standing stocks and mis-represent the phase of the annual cycle of phytoplankton abundance. Additional shade would extend (probably only slightly) the period during which phytoplankton are light limited (rather than nutrient limited). This provides another reason to suggest that the model may over-estimate the influence which exogenous nutrients (be they from fish farms or catchment) may have upon water-quality.
- Inadequacy of our Cook Strait boundary conditions. These are based upon scarce field data. In the case of zooplankton, we used a temporally constant boundary condition (i.e., we removed all seasonal variability that may genuinely be present). In the case of other variables, we applied a 3 month smoothing window to the field data when generating the boundary conditions. Our intent was to buffer the simulations against one-off extremes (whether genuine or sampling error) in the field data, but an inevitable corollary is that we may will damped out genuine seasonal scale variability that may influence dynamics within the Sounds.

Finally, we have chosen to make long-term simulations on a grid having 200 m horizontal resolution. Long term simulations would have been prohibitively expensive on a finer grid (Table 2-1). 200 m resolution is approximately the size of the collective pen structure of a fish farm. The biophysical model does not have sufficient resolution to properly represent the steep concentration gradients of (for example, ammonium and large detritus) that will exist in the immediate environs of a farm. Specifically, it will exhibit excessive numerical dispersion such that it will tend to under-estimate concentrations very close to the farm, but over-estimate them slightly further afield. At greater distances (perhaps, >1 km), natural dispersion will have eroded the steep gradients so the excessive numerical dispersion is of lesser import and the simulated concentrations will be more reliable. If near-field concentrations are to be examined using this model, we would need to adopt one of the finer grids (e.g. 50 m) and restrict ourselves to simulating shorter calendar periods.

### 6.3 Implications of the biophysical modelling results: putting the changes in context

The MDC monitoring data indicate that near-surface nitrate concentrations vary more than ten-fold through the course of the seasons (Figure 5-1 to Figure 5-5). Ammonium concentrations vary more than two-fold, phytoplankton and zooplankton concentrations vary five- to ten-fold and particulate detrital concentrations vary more than three-fold. Even if one restricts attention to any one calendar month (taken from different years), the fluctuations can be substantial (compare pink and red circles



and pink and blue triangles in Figure 5-1 to Figure 5-5). Unpublished historical data which NIWA gathered in Pelorus Sound indicates that a similar level of variability is also present there at a fortnightly time-scale.

Clearly, the predicted magnitudes of farm-induced (or *denitrification associated*) change (relative to the *no farms* situation) are small relative to present-day natural variability. Furthermore, whilst we have chosen to focus upon seasonal-scale averages, inspection of time-series of instantaneous water-quality characteristics at a few specific locations have not revealed any relative changes which are dramatically larger than are evident in the seasonal averages (Appendix F). That is, the time-averaging is not obviously masking any alarming, but short-lived events that are driven by the farms.

Whilst the fish farms are predicted to increase summertime near-surface phytoplankton standing stocks by 5–10%, the resultant phytoplankton concentrations remain unexceptional by the standards of New Zealand coastal waters. The time-averaged predicted concentrations are certainly not high enough to turn the water noticeably green or to be indicative of possible eutrophication.

In comparison with the magnitudes of natural variability, it is tempting to argue that 5-15% changes in (for example) phytoplankton standing stock are negligibly small — even when they persist for an entire season and over a large fraction of the Sound. That may be slightly naïve. Given sufficient time, a 5% increase in resource availability could, in theory, permit a disproportionate change in consumer abundance. Certainly, a correlation between annual-scale average seston abundance and mussel yields has been found in Pelorus Sound (Zeldis, J.R., Howard-Williams et al. 2008; Zeldis, J.R., Hadfield et al. 2013). In that case there was a roughly two-fold difference between the maximum and minimum annual average particulate N abundances and that was associated with a yield difference of approximately 30% (of the long term average). If we make a leap of faith and assume that the correlation is indicative of causation, this opens the possibility that fish-farming could be beneficial to mussel farmers – however, the benefit will be marginal. Our model predicts that seston concentrations will increase by only a few percent during the summer months. Furthermore, in inner Queen Charlotte and Tory Channel, they revert to farm-free levels during the winter months. This regular ‘reset’ may introduce a ‘bottleneck’ that would limit the extent to which populations of short-lived organisms can develop a multi-annual response to regular summer-time enhancement.

There are no definitive/universal standards which state what an acceptable quantum of change might be for any water-column property in the context of aquaculture. In the Firth of Thames, a negotiation process led to agreement that, averaged over a year, mussel farming in the Wilson Bay Aquaculture Management Area A (Zeldis, J., Felsing et al. 2005):

- should not induce phytoplankton depletion that exceeded 25% over an area twice that of the AMA (the AMA has an area of approx. 1200 ha)
- should not induce phytoplankton depletion that exceeds 20% over more than 10% of the Firth’s surface area

The AMA concept has no direct equivalent in Queen Charlotte/Tory Channel but time-averaged phytoplankton depletion does not exceed 25% anywhere.

The New Zealand King Salmon Board of Inquiry stipulated several water quality standards that must not be broken (Final report Appendices 4-7). For example Appendix 4 section 51 stipulates:

*51 The farm shall be operated at all times in such a way as to achieve the following qualitative Water Quality Standards in the water column:*

- a To not cause an increase in the frequency or duration of phytoplankton blooms (i.e. chlorophyll a concentrations  $\geq 5 \text{ mg/m}^3$ ) [Note: water clarity as affected by chlorophyll a concentrations is addressed by this objective];*
- b To not cause a change in the typical seasonal patterns of phytoplankton community structure (i.e. diatoms vs. dinoflagellates), and with no increased frequency of harmful algal blooms (HAB"s) (i.e. exceeding toxicity thresholds for HAB species);*
- c To not cause reduction in dissolved oxygen concentrations to levels that are potentially harmful to marine biota [Note: Near bottom dissolved oxygen under the net pens is addressed separately through the EQS – Seabed Deposition];*
- d To not cause elevation of nutrient concentrations outside the confines of established natural variation for the location and time of year, beyond 250m from the edge of the net pens;*
- e To not cause a persistent shift from a mesotrophic to a eutrophic state;*
- f To not cause an obvious or noxious build-up of macroalgal (eg sea lettuce) biomass [Note to be monitored in accordance with Condition 80h].*

Three of these (a, d, e) can be addressed with our present model. First, we note that the Board appears to have adopted a threshold of  $5 \text{ mg chl a m}^{-3}$  as indicative of eutrophy. The Consent Conditions do not make it clear, but referring back to the underlying evidence<sup>16</sup>, it is clear that this should be interpreted as an annual average. The mere fact that one (or even several) samples yield chlorophyll concentrations in excess of  $5 \text{ mg chl a m}^{-3}$  need not indicate that the system is in a eutrophied state.

Whilst the biophysical modelling indicates that a time-averaged threshold of  $5 \text{ mg chl a m}^{-3}$  may be approached (even exceeded) at some locations during the summer period, it certainly doesn't indicate that it will be exceeded over a large fraction of Queen Charlotte/Tory Channel during the summer period. Furthermore, it will not be exceeded on a year-round basis (the relevant time-scale for this threshold). Our modelling spans a period of 500 days. It suggests that, over that time-span, fish farming (including Ngamahau) in Queen Charlotte/Tory Channel will not cause the system to shift into a eutrophied state. We cannot entirely refute the possibility of a longer-term evolution towards eutrophy (whether exhibited as persistently and substantially increased phytoplankton or substantial change elsewhere in the foodweb). Nonetheless, it is our current opinion that the combination of winter-time light limitation, relatively rapid flushing and benthic denitrification make it unlikely that the system will undergo extreme change in response to the levels of farming presently permitted in this system.

## 6.4 Biophysical modelling: summary of conclusions

- The model predicts that mussel farming induces bay-scale effects which amount to a few percent of background concentrations. These are small relative to natural variability.
- The model predicts that fish farming induces effects which extend through the entire Queen Charlotte/Tory channel system. Except very close to the farms, the effects do

---

<sup>16</sup> The figure of  $5 \text{ mg chl a m}^{-3}$  appears to stem from evidence put forward by (Gillespie, P., Knight, B., MacKenzie, L. (2011) The New Zealand King Salmon Company Limited: assessment of environmental effects - water column: 79. citing Smith, V., Tilman, G., Nekola, J. (1999) Eutrophication: impacts of excess nutrient inputs on freshwater, marine, and terrestrial ecosystems. *Environmental Pollution*, 100(1-3): 179-196. and Wild-Allen, K., Herzfeld, M., Thomsen, P.A., Rosebrock, U., Parslow, J., Volkman, J.K. (2010) Applied coastal biogeochemical modelling to quantify the environmental impact of fish farm nutrients and inform managers. *Journal of Marine Systems*, 81: 134-147. 10.1016/j.marsys.2009.12.013).

not exceed 20% of background in summer (30% in winter). These are smaller than seasonal-scale natural variability, but are chronic in nature.

- Wintertime light limitation acts as a 'bottleneck' which limits the response of short-lived organisms to the increased nutrient concentrations.
- The absolute concentrations of nutrient and phytoplankton associated with the fish-farming scenarios are not alarmingly high. They are not atypical of New Zealand coastal waters.
- The majority of the farm derived nutrient is predicted to be lost from the system by export to Cook Strait, rather than by denitrification in the seabed.
- Whilst we believe that the inferences that we draw from our modelling are robust, we caution that almost no sensitivity trials have been undertaken to justify that belief. We therefore recommend that further sensitivity trials be undertaken to determine the degree to which the model predictions are robust against assumptions regarding:
  - Sinking speed of fish and mussel faeces (introduce a third detrital class specifically for these very fast sinking materials)
  - Denitrification potential (what happens if denitrification of fish faeces, but not other detritus, is prohibited?)
  - Light attenuation (what happens if we take better account of the differential attenuation of different wavelengths?; what happens if topographic shading is introduced)
  - Formulation of the zooplankton mortality term
  - The role of dissolved organic nitrogen (by how much would the system's dynamics change if we assumed that catchment- and ocean-derived DON was biologically active rather than inert)
  - Sensitivity to Cook Strait boundary conditions (potential inter-annual variability in the extent to which Cook Strait water intrudes into Queen Charlotte/Tory and/or in the water-quality characteristics of the intruding Cook Strait water).

## 7 Deposition modelling

### 7.1 Methods

We simulated the first-time deposition foot-prints of farm waste (faeces + uneaten food) using a particle-tracking model. Particles represent ‘parcels’ of waste material (measured as grams of carbon). Particles were released on a continuous basis from random horizontal locations within the pen-perimeter of each farm. At release, each particle was also assigned a random initial depth between the sea-surface and 20 m below the surface. Subsequently, each particle moves under the influence of local-to-particle-currents, the intrinsic particle sinking velocity and turbulence.

The instantaneous local-to-particle currents were interpolated from an archive of 15 minute resolution hydrodynamic results generated by the 100 m resolution ROMS model. We adopted a sinking velocity of  $5 \text{ cm s}^{-1}$  (Brigolin, Pastres et al. 2009, and unpublished NIWA data). Turbulence was incorporated by adding a random velocity increment into each particle’s equation of motion. The maximum absolute magnitude of this random term is proportional to the square-root of the estimated local dispersion coefficient. We assumed a horizontal dispersion coefficient of  $1 \text{ m}^2 \text{ s}^{-1}$ . Vertical dispersion was derived from the shear, with a Richardson Number correction term. This yielded dispersion coefficients in the range  $10^{-5} - 10^{-1} \text{ m}^2 \text{ s}^{-1}$ . We solved the resultant stochastic differential equation for particle motion by adopting Stratonovich Calculus and a second order Runge-Kutta method (Heun coefficients). For stochastic systems, this method is first-order strong convergent with respect to time-step. We adopted a time-step of 0.0005 d. This ensures that particles cannot pass through more than three layers within a single time-step, so get to experience much (but not necessarily all) of any vertical variations in currents and mixing during their passage to the sea-bed.

At each farm, particles were released one at a time. The interval between particle releases was determined by the estimated daily rate of waste production ( $\text{g C farm}^{-1} \text{ d}^{-1}$ ) and the nominal ‘size’ ( $\text{g C}$ ) of each particle. The ‘size’ was chosen such that each farm generated between approximately 15,000 (Ngamahau) and 50,000 (Te Pangu) particles over the course of a simulation. Each simulation spanned 20 simulated days. The farm-specific waste production rates were derived from monthly feed input rates ( $\text{tonne feed farm}^{-1} \text{ month}^{-1}$ ), and an estimated carbon:feed weight fraction. This was derived from the C:dry weight ratios of protein, lipid and carbohydrate, and the typical proximate composition of salmon feed (Buschmann, Costa-Pierce et al. 2007). Refer to Table 7-1 for further details.

**Table 7-1: Assumptions regarding composition of fish feed and assimilation of fish feed for deposition modelling.**

Quantity	units	Value	Source
Fraction of ingested protein that is assimilated across gut wall	$\text{g assimilated g}^{-1}$ ingested	0.90	(Buschmann, Costa-Pierce et al. 2007)
Fraction of ingested lipid that is assimilated across gut wall	$\text{g assimilated g}^{-1}$ ingested	0.95	(Buschmann, Costa-Pierce et al. 2007)

Quantity	units	Value	Source
Fraction of ingested carbohydrate that is assimilated across gut wall	g assimilated g <sup>-1</sup> ingested	0.60	(Buschmann, Costa-Pierce et al. 2007)
Feed protein fraction	g protein g <sup>-1</sup> feed	0.45	(Buschmann, Costa-Pierce et al. 2007)
Feed lipid fraction	g lipid g <sup>-1</sup> feed	0.35	(Buschmann, Costa-Pierce et al. 2007)
Feed carbohydrate fraction	g carbohydrate g <sup>-1</sup> feed	0.14	(Buschmann, Costa-Pierce et al. 2007)
Implied carbon content of feed	g C g <sup>-1</sup> feed	0.47	
Implied assimilation efficiency for carbon	g assimilated g <sup>-1</sup> ingested	0.82	
Assumed monthly feed input rate (Clay Point)	tonne	280	Based upon NZKS records
Assumed monthly feed input rate (Te Pangu)	tonne	280	Based upon NZKS records
Assumed monthly feed input rate (Otanerau)	tonne	120	Based upon NZKS records
Assumed monthly feed input rate (Ruakaka)	tonne	200	Based upon NZKS records
Ngamahau	tonne	280	Based upon NZKS records

## 7.2 Analysis and presentation of deposition model results

The location at which each particle first settled onto the seabed was recorded during the course of the simulation. Subsequently, all settlement locations were binned onto a 20 m resolution grid. This yields a bit-map of location-specific mass-accrual over the course of the 20 d simulation. Daily settlement rates are easily derived from that by dividing by the simulation period (20 d). We present the results as false-colour maps in which colour is indicative of the daily settlement rate.

## 7.3 Deposition modelling: Results

Figure 7-1 presents false colour maps to show the simulated patterns of deposition around each farm. At all farms, the majority of particles settle within a small distance of the pens. At the three farms in Tory Channel (Clay Point, Te Pangu and Ngamahau) a minority of particles travel several hundred (more than 1000 m in the case of Ngamahau) from the pens, but most settle within 200 m of the pens. At Ruakaka and Otanerau all particles settle within 120 m of the pens. Deposition rates immediately under the pens range between 15-20 g C m<sup>-2</sup> d<sup>-1</sup> (Te Pangu) and 25-30 g C m<sup>-2</sup> d<sup>-1</sup>

(Otanerau). At the pen edges they range around  $10\text{--}20 \text{ g C m}^{-2} \text{ d}^{-1}$ . There have been no measurements of deposition rates around these farms<sup>17</sup>, however rates of  $5\text{--}45 \text{ g C m}^{-2} \text{ d}^{-1}$  have been measured at the edge of the pen at Waihinau in Pelorus Sound (D. Morrissey, NIWA, unpublished data). Keeley et al. (2013) used the DEPOMOD particle-tracking tool to simulate deposition under these farms. At the pen edges, their modelled deposition rates (as  $\text{kg solids m}^{-2} \text{ y}^{-1}$ ) equate to approximately  $12\text{--}25 \text{ g C m}^{-2} \text{ d}^{-1}$  (Ruakaka). It is encouraging that the two models yield similar near pen deposition rates, despite being driven by differing hydrodynamics having been parameterized independently of one another. Visual comparison of our deposition plots with their maps (their Figures 6, 7 & 8) of predicted benthic environmental footprint (which they derive from their modelled deposition rates) leads us to infer that both models predict footprints which are only subtly different. They also present maps of observed environmental footprint (again, their Figures 6 – 8). On the basis of a superficial inspection, we suggest that the extents and crescentic shapes of the observed footprints at Te Pangu and Clay Point are better reproduced by our model than by DEPOMOD. A more formal statistical comparison is not possible without access to their raw data. If our model is, indeed, better reproducing the footprints, we believe that it will be because our model incorporates horizontally (as well as vertically) varying currents (with 100 m horizontal resolution) whereas DEPOMOD lacks any horizontal resolution.

Observations elsewhere suggest that the structure of the benthic faunal community can be expected to change when deposition rates exceed about  $1\text{--}5 \text{ g C m}^{-2} \text{ d}^{-1}$ . Clearly, one should expect the communities under the four existing farms and the forthcoming Ngamahau farm to differ from those which would exist at these sites in the absence of the farms. Benthic monitoring by the Cawthron Institute (undertaken on behalf of New Zealand King Salmon Ltd) confirms that this is the case (Keeley et al. 2013).

---

<sup>17</sup> NIWA are currently endeavouring to measure deposition rates around Te Pangu farm but no results are available yet.

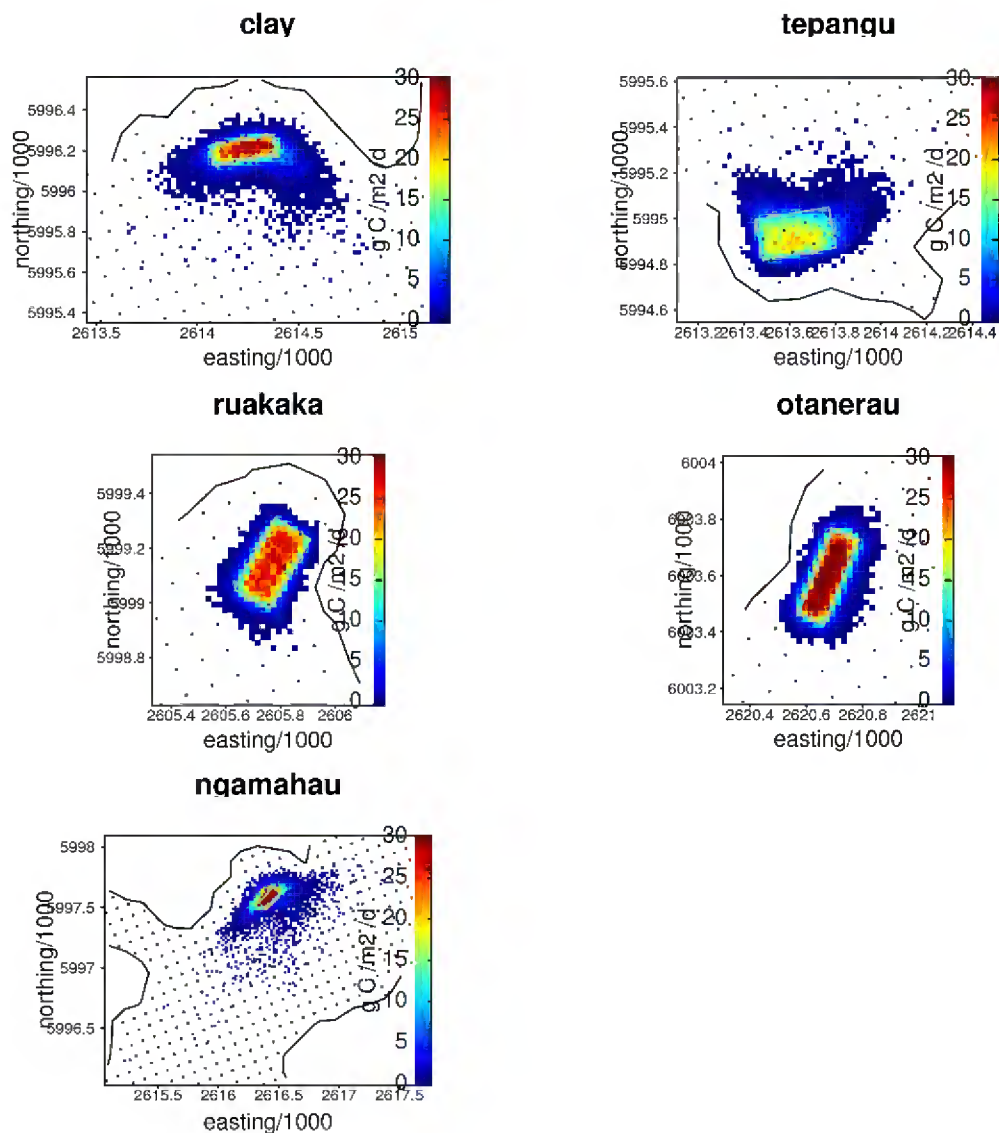


**Figure 7-1:** False colour plots of the simulated rates of fish faeces deposition ( $\text{g C m}^{-2} \text{d}^{-1}$ ) around each farm. The grey polygons denote the pen perimeter of each farm. The black curve indicates the location of the coastline in the simulation model. The black dots indicate the locations of the centroids of each wet grid-cell in the hydrodynamic model that provided the currents for the particle tracking. The colour-scale is the same in each image but the horizontal scales differ.

## 7.4 Summary & Conclusions

- The simulated deposition footprints are in close agreement with the DEPOMOD simulation tool for these farms. We believe that our results better agree with observational data than the DEPOMOD results do. We believe that this is because our simulation model incorporates spatial variability in currents (a feature that DEPOMOD lacks).
- They are also consistent with measurements of deposition rates made at the salmon farm in Waihinau Bay (Pelorus Sound)

## 8 Acknowledgements

We are grateful for the support that we have received from the staff of Marlborough District Council – notably: Alan Johnson, Fleur Tiernan, Mike Ede and Steve Ulrich. We are also grateful for the support that New Zealand King Salmon Ltd (notably Mark Gillard and Mark Preece) have provided. In particular, we thank them for providing detailed information about the historical feed input and stocking characteristics of each their existing farms.



## 9 Glossary of abbreviations and terms

ADCP	Acoustic Doppler current profiler: an instrument for measuring velocity profiles
bathymetry	The process of measuring and analysing seafloor depth. A bathymetric data set is often informally called a bathymetry.
denitrification	A bacterially mediated process through which nitrate ( $\text{NO}_3^-$ ) is converted to nitrous oxide gas ( $\text{N}_2\text{O}$ ) and, in some circumstances, free nitrogen gas ( $\text{N}_2$ ). Denitrification occurs under anoxic conditions. It tends to occur most rapidly in zones where oxic and anoxic areas are in close proximity to one another.
light-limited	The realizable phytoplankton growth rate is limited by low intensities of ambient photosynthetically available radiation (PAR). The term is usually applied when considering growth averaged over a 24 hour period. Since PAR intensity declines with increasing distance below the sea-surface, near-bed waters are more likely to be light-limited than near-surface waters. Similarly, light-limitation is more likely during the winter than summer.
nitrification	A bacterially mediated process by which ammonium is converted to nitrate via nitrite. Nitrification requires the presence of free oxygen and is suppressed by PAR.
nutrient-limited	The realizable phytoplankton growth rate is limited by low concentrations of nutrient in the water-column. The term is usually applied when considering growth averaged over a 24 hour period.
PAR	<u>Photosynthetically active radiation</u> : that part of the solar spectrum that plants (including phytoplankton) can harvest and utilize to drive photosynthesis.
stratified	When the water column is stratified, a surface layer of lower density water floats above a sub-surface layer of higher density water. The surface layer can be less dense because it is cooler or more salty than the sub-surface water, or a combination of both.

## 10 References

- Beckmann, A., Haidvogel, D.B. (1993) Numerical Simulation of Flow around a Tall Isolated Seamount. Part I: Problem Formulation and Model Accuracy. *Journal of Physical Oceanography*, 23(8): 1736-1753. doi: 10.1175/1520-0485(1993)023<1736:NSOFAA>2.0.CO;2
- Beers, J.R. (1966) Studies on the chemical composition of the major zooplankton groups in the Sargasso sea of Bermuda. *Limnology & Oceanography*, 11(4): 520-528.
- Bowie, G.L., Mills, W.B., Porcella, D.B., Campbell, C.L., Pagenkopf, J.R., Rupp, G.L., Johnson, K.M., Chan, P.W.H., Gherini, S.A., Chamberlin, C.E. (1985) *Rates, constants, and formulations in surface water quality modelling*. United States Environmental Protection Agency, Athens, Georgia: 455.
- Bradford, J.M., Lapennas, P.P., Murtagh, R.A., Chang, F.H., Wilkinson, V. (1986) Factors controlling summer phytoplankton production in greater Cook Strait, New Zealand. *New Zealand Journal of Marine & Freshwater Research*, 20(2): 253-279.
- Brigolin, D., Pastres, R., Nickell, T.D., Cromey, C.J., Aguilera, D.R., Regnier, P. (2009) Modelling the impact of aquaculture on early diagenetic processes in sea loch sediments. *Marine Ecology Progress Series*, 388: 63-80. 10.3354/meps08072
- Buschmann, A.H., Costa-Pierce, B.A., Cross, S., Iriarte, J.L., Olsen, Y., Reid, G. (2007) Nutrient impacts of farmed Atlantic Salmon (*Salmo salar*) on pelagic ecosystems and implications for carrying capacity. *World Wildlife Fund Salmon Aquaculture Dialogue by the Technical Working Group on nutrients and carrying capacity* 68.  
<http://www.worldwildlife.org/what/globalmarkets/aquaculture/WWFBinaryitem8844.pdf>
- Christensen, P.B., Glud, R.N., Dalsgaard, T., Gillespie, P.A. (2003) Impacts of longline mussel farming on oxygen and nitrogen dynamics and biological communities of coastal sediments. *Aquaculture*, 218: 567-588. file:///H:/was\_p/pdf\_reprints/christensen\_et\_al2003\_aquaculture218\_567.pdf
- Edwards, A.M., Yool, A. (2000) The role of higher predation in plankton population models. *Journal of Plankton Research*, 22(6): 1085-1112.
- Enders, E.C., Scruton, D.A. (2006) Potential application of bioenergetics models to habitat modeling and importance of appropriate metabolic rate estimates with special consideration for Atlantic Salmon. *Canadian Technical Report of Fisheries and Aquatic Sciences*, 2641: 40. <http://www.dfo-mpo.gc.ca/Library/321568.pdf>
- Enríquez, S., Duarte, C.M., Sand-Jensen, K. (1993) Patterns in decomposition rates among photosynthetic organisms: the importance of detritus C:N:P content. *Oecologia*, 94: 457-471.
- Fennel, K., Hetland, R., Feng, Y., Di Marco, S. (2011) A coupled physical-biological model of the Northern Gulf of Mexico shelf: model description, validation and analysis of phytoplankton variability. *Biogeosciences*, 8: 1881-1899. 10.5194/bg-8-1881-2011
- Fennel, K., Wilkin, J., Levin, J., Moisan, J., O'Reilly, J., Haidvogel, D. (2006) Nitrogen cycling in the Middle Atlantic Bight: results from a three-dimensional model and implications for the North Atlantic nitrogen budget. *Global Biogeochemical Cycles*, 20: GB3007. 10.1029/2005GB002456

Fennel, K., Wilkin, J., Previdi, M., Najjar, R. (2008) Dentrification effects on air-sea CO<sub>2</sub> flux in the coastal ocean: simulations for the northwest North Atlantic. *Geophysical Research Letters*, 35: L24608. 10.1029/2008GL036147

Gillespie, P., Knight, B., MacKenzie, L. (2011) The New Zealand King Salmon Company Limited: assessment of environmental effects - water column: 79.

Hadfield, M.G. (2013) South Taranaki Bight Iron Sand Extraction Sediment Plume Modelling: Phase 3 studies. *NIWA Client Report WLG2013-36*: 86.  
[http://www.epa.govt.nz/Publications/NIWA\\_sediment\\_plume\\_modelling\\_report.pdf](http://www.epa.govt.nz/Publications/NIWA_sediment_plume_modelling_report.pdf)

Hadfield, M.G., Zeldis, J.R. (2012) Freshwater dilution and transport in Canterbury Bight. *NIWA Client Report*, WLG2011-54: 39. <http://ecan.govt.nz/publications/Pages/fresh-water-canterbury-bight.aspx>

Haidvogel, D.B., Arango, H.G., Budgell, W.P., Cornuelle, B.D., Curchitser, E., Di Lorenzo, E., Fennel, K., Geyer, W.R., Hermann, A.J., Lanerolle, L., Levin, J., McWilliams, J.C., Miller, A.J., Moore, A.M., Powell, T.M., Shchepetkin, A.F., Sherwood, C.R., Signell, R.P., Warner, J.C., Wilkin, J. (2008) Ocean forecasting in terrain-following coordinates: Formulation and skill assessment of the Regional Ocean Modeling System. *Journal of Computational Physics*, 227(7): 3595-3624. doi: 10.1016/j.jcp.2007.06.016

Heath, R.A. (1974) Physical oceanographic observations in Marlborough Sounds. *New Zealand Journal of Marine and Freshwater Research*, 8(4): 691-708. 10.1080/00288330.1974.9515538

Hickman, R.W. (1979) Allometry and growth of the Green-Lipped Mussel *Perna canaliculus* in New Zealand. *Marine Biology*, 51(4): 311-327.

Hickman, R.W., Illingworth, J. (1980) Condition cycle of the Green-Lipped Mussel *Perna canaliculus* in New Zealand. *Marine Biology*, 60(1): 27-38.

Kalnay, E., Kanamitsu, M., Kistler, R., Collins, W., Deaven, D., Gandin, L., Iredell, M., Saha, S., White, G., Woollen, J., Zhu, Y., Chelliah, M., Ebisuzaki, W., Higgins, W., Janowiak, J., Mo, K.C., Ropelewski, C., Wang, J., Leetmaa, A., Reynolds, R., Jenne, R., Joseph, D. (1996) The NCEP/NCAR 40-year reanalysis project. *Bulletin of the American Meteorological Society*, 77(3): 437-471. 10.1175/1520-0477(1996)077<0437:tnyrp>2.0.co;2

Kaspar, H.F., Gillespie, P.A., Boyer, I.C., MacKenzie, A.L. (1985) Effects of mussel aquaculture on the nitrogen cycle and benthic communities in Kenepuru Sound, Marlborough Sounds, New Zealand. *Marine Biology*, 85(2): 127-136.

Keeley, N.B., Cromey, C.J., Goodwin, E.O., Gibbs, M.T., Macleod, C.M. (2013) Predictive depositional modelling (DEPOMOD) of the interactive effect of current flow and resuspension on ecological impacts beneath salmon farms. *Aquaculture Environment Interactions*, 3: 275-291. 10.3354/aei00068

Knight, B.J. (2011) The New Zealand King Salmon Company Ltd: Assessment of Environmental Effects - Water Column, Cawthron Report # 1985.

Knight, B.J. (2012) Supplementary document of figures and tables - for evidence provided by Benjamin Robert Knight in relation to water column effects for the New Zealand King Salmon Co. Ltd. *Board of Inquiry appointed under section 149J of the Resource Management Act 1991 to consider The New Zealand King Salmon Co. Limited's private plan change requests to the Marlborough Sounds*

*Resource Management Plan and resource consent applications for marine farming at nine sites located in the Marlborough Sounds: 28.*

Monsen, N.E., Cloern, J.E., Lucas, L.V., Monismith, S.G. (2002) A comment on the use of flushing time, residence time, and age as transport time scales. *Limnology & Oceanography*, 47(5): 1545-1553.

Orban, E., Di Lena, G., Navigato, T., Cassini, I., Marzetti, A., Caproni, R. (2002) Seasonal changes in meat content, condition index and chemical composition of mussels (*Mytilus galloprovincialis*) cultured in two different Italian sites. *Food Chemistry*, 77(1): 57-65.

Petrell, R.J., Jones, R.E. (2000) Power requirement of swimming in chinook salmon and Atlantic salmon and implications for food conversion and growth performance. *Aquaculture Engineering*, 22: 225-239.

Ren, J.S., Ross, A.H. (2005) Environmental influence on mussel growth: a dynamic energy budget model and its application to the greenshell mussel *Perna canaliculus*. *Ecological Modelling*, 189: 347-362. file:///H:/was\_p/pdf\_reprints/ren\_and\_ross2005\_ecol\_modelling189\_p347\_362.pdf

Ren, J.S., Ross, A.H., Hadfield, M.G., Hayden, B.J. (2010) An ecosystem model for estimating potential shellfish culture production in sheltered coastal waters. *Ecological Modelling*, 221: 527-539. 10.1016/j.ecolmodel.2009.11.003

Reynolds, R.W., Smith, T.M., Liu, C., Chelton, D.B., Casey, K.S., Schlax, M.G. (2007) Daily high-resolution-blended analyses for sea surface temperature. *Journal of Climate*, 20(22): 5473-5496. 10.1175/2007jcli1824.1

Schmidt-Nielsen, K. (1982) *Animal Physiology*. Cambridge University Press, Cambridge: 560.

Shearer, K.D., Åsgård, T., Andorsdóttir, G., Aas, G.H. (1994) Whole body elemental and proximate composition of Atlantic salmon (*Salmo salar*) during life cycle. *Journal of Fish Biology*, 44: 785-797.

Smith, S.D. (1988) Coefficients for sea surface wind stress, heat flux, and wind profiles as a function of wind speed and temperature. *Journal of Geophysical Research*, 93(C12): 15467-15472. doi: 10.1029/JC093iC12p15467

Smith, V., Tilman, G., Nekola, J. (1999) Eutrophication: impacts of excess nutrient inputs on freshwater, marine, and terrestrial ecosystems. *Environmental Pollution*, 100(1-3): 179-196.

Steele, J.H., Henderson, E.W. (1992) The role of predation in plankton models. *Journal of Plankton Research*, 14: 157-172.

Stigebrandt, A. (1999) Turnover of energy and matter by fish - a general model with application to salmon, 5: 28. <http://www.biaoqiang.org/default.aspx?event=vd&docid=209>

Thompson, R.O.R.Y. (1983) Low-Pass Filters to Suppress Inertial and Tidal Frequencies. *Journal of Physical Oceanography*, 13(6): 1077-1083. 10.1175/1520-0485(1983)013<1077:LPFTSI>2.0.CO;2

Vincent, W.F., Howard-Williams, C., Downes, M., Dryden, S. (1989) Underwater light and photosynthesis at three sites in Pelorus Sound, New Zealand. *New Zealand Journal of Marine & Freshwater Research*, 23(1): 79-91. <http://dx.doi.org/10.1080/00288330.1989.9516343>

Walters, R.A., Goring, D.G., Bell, R.G. (2001) Ocean tides around New Zealand. *New Zealand Journal of Marine and Freshwater Research*, 35: 567-579.

Wild-Allen, K., Herzfeld, M., Thomsen, P.A., Rosebrock, U., Parslow, J., Volkman, J.K. (2010) Applied coastal biogeochemical modelling to quantify the environmental impact of fish farm nutrients and inform managers. *Journal of Marine Systems*, 81: 134-147. 10.1016/j.marsys.2009.12.013

Zeldis, J., Felsing, M., Wilson, J. (2005) Limits of acceptable change. *Coastal news*, 30: 1-3.

Zeldis, J.R., Hadfield, M.G., Booker, D.J. (2013) Influence of climate on Pelorus Sound mussel aquaculture yields: predictive models and underlying mechanisms. *Aquaculture Environment Interactions*, 4(1): 1-15. 10.3354/aei00066

Zeldis, J.R., Howard-Williams, C., Carter, C.M., Schiel, D.R. (2008) ENSO and riverine control of nutrient loading, phytoplankton biomass and mussel aquaculture yield in Pelorus Sound, New Zealand. *Marine Ecology Progress Series*, 371: 131-142.

Zeldis, J.R., Robinson, K., Ross, A.H., Hayden, B.J. (2004) First observations of predation by New Zealand Greenshell<sup>®</sup> mussels (*Perna canaliculus*) on zooplankton. *Journal of Experimental Marine Biology and Ecology*, 311: 287-299. file:///h:/was\_p/pdf\_reprints/zeldis/mussel\_predation\_final.pdf

Zimmerman, J.T.F. (1988) Estuarine residence times. In: B. Kjerfve (Ed). *Hydrodynamics of Estuaries*. CRC Press, Boca Raton, Florida: 75-84.

## Appendix A Mathematical description of the Fennel NPZD model

$$\frac{\partial Phy}{\partial t} = \mu Phy - g_{Zoo} Zoo - m_{Phy} (Phy - PhyMIN)^+ - \tau (SDet + Phy) Phy - w_{Phy} \frac{\partial Phy}{\partial z} - \sum_{i=1}^{N_{muss}} Mus_i V_i Phy \psi_{Phy}$$

The term  $\sum_{i=1}^{N_{muss}} Mus_i V_i Phy \psi_{Phy}$  denotes the total local phytoplankton biomass loss rate ( $\text{mmol N m}^{-3} \text{ d}^{-1}$ ) due to the mussels of each size-class  $i$ .  $Mus_i$  denotes the local concentration of mussels (mussels of size  $i$  class  $\text{m}^{-3}$ ).  $V_i$  ( $\text{m}^3 \text{ d}^{-1} \text{ mussel}^{-1}$ ) denotes the volume of water filtered across the gills and  $\psi_{Phy}$  ( $0 < \psi_{Phy} \leq 1$ ) denotes the relative efficiency with which phytoplankton in the water passing over the gills is captured.

$$\mu = 0.59 \mu_0 1.066^T \frac{\alpha I}{\sqrt{(0.59 \mu_0 1.066^T)^2 + (\alpha I)^2}} \left( \frac{NO3}{k_{NO3} + NO3} \right) \left( \frac{PhyIP}{k_{NH4} + NH4} \right) \left( \frac{NH4}{k_{NH4} + NH4} \right)$$

$$I = I_0 \text{ par } e^{-z \left( K_w + \frac{K_{Chl} \int_0^z Chl(\zeta) d\zeta}{z} \right)}$$

$$g_{Zoo} = g_{max} \frac{Phy^2}{k_{Phy} + Phy^2}$$

$$\frac{\partial Chl}{\partial t} = \rho_{Chl} \mu Chl - g_{Zoo} Zoo \frac{Chl}{Phy} - m_p (Chl - ChlMIN) - \tau (SDet + Phy) Chl - w_{Phy} \frac{\partial Chl}{\partial z} - \sum_{i=1}^{N_{muss}} Mus_i V_i Chl \psi_{Phy}$$

$$\rho_{Chl} = \frac{\Theta_{max} \mu Phy}{\alpha I Chl}$$

$$\frac{\partial Zoo}{\partial t} = g_{Zoo} \beta Zoo - l_{bm} (Zoo - ZooMin)^+ - l_E \frac{Phy^2}{k_p + Phy^2} \beta Zoo - m_{Zoo} Zoo^2 - \sum_{i=1}^{N_{muss}} Mus_i V_i Zoo \psi_{Zoo}$$

$$\frac{\partial SDet}{\partial t} = g_{Zoo} (1 - \beta) Zoo + m_{Zoo} Zoo^2 + m_{Phy} Phy - \tau (SDet + Phy) SDet - r_{SDet} SDet - w_{SDet} \frac{\partial SDet}{\partial z} - \sum_{i=1}^{N_{muss}} Mus_i V_i SDet \psi_{SDet}$$

$$\frac{\partial LDet}{\partial t} = \tau(SDet + Phy)^2 - r_{LDet}LDet - w_{LDet} \frac{\partial LDet}{\partial z} \sum_{i=1}^{N_{muss}} Mus_i V_i LDet \psi_{LDet} + \sum_{i=1}^{N_{fish}} faeces_i + uneatenfeed_i$$

$$\frac{\partial NO_3}{\partial t} = -\mu_{max}f(I)L_{NO_3}Phy + nNH_4$$

$$n = n_{max} \left( 1 - \frac{I - I_0}{k_I + I - I_0} \right)^+$$

$$\frac{\partial NH_4}{\partial t} = -\mu_{max}f(I)L_{NH_4}Phy - nNH_4 + l_{BMZoo} + l_E \frac{Phy^2}{k_P + Phy^2} \beta Z_{Zoo} + r_{SDet}SDet + r_{LDet}LDet + \sum_{i=1}^{N_{muss}} excretion_i + \sum_{i=1}^{N_{fish}} excretion_i$$

**Table 10-1: Coefficients of the Fennel module.** Unless otherwise noted, the values are those specified in the code that forms a part of the ROMS distribution. The coefficients are listed by both their Fennel-paper and ROMS-code names. A few coefficients are present only in the ROMS-code. A little additional explanation for those is presented in the Comment column.

Coefficient (Fennel 2006)	Coefficient (ROMS code)	Description	Units	Value	Comment
$K_w$	AttSW	Light attenuation coefficient due to seawater and components other than chlorophyll	$m^{-1}$	0.21	MDC data for Secchi disk depth in Queen Charlotte converted to a diffuse light attenuation coefficient using a correlation between attenuation and Secchi disk depth established with data from Pelorus Sound (Vincent, Howard-Williams et al. 1989) and applying discount of approx. $0.2 m^{-1}$ to avoid 'double counting' of attenuation due to chlorophyll
$K_{chl}$	AttChl	Light attenuation coefficient for chlorophyll	$m^2 mg^{-1} chl$	0.02486	
$par$	PARfrac	Fraction of incident shortwave radiation that is photosynthetically active	-	0.43	
$\mu_0$	Vp0	Temperature limited phytoplankton growth parameter	-	1.0	
$I_0$	I_thNH4	Radiation threshold for nitrification inhibition	$W m^{-2}$	0.0095	
$k_I$	D_p5NH4	Half saturation radiation for nitrification inhibition	$W m^{-2}$	0.1	

Coefficient (Fennel 2006)	Coefficient (ROMS code)	Description	Units	Value	Comment
$n_{max}$	NitriR	Maximum rate of nitrification	d <sup>-1</sup>	0.05	
$1/k_{NO_3}$	K_NO3	Inverse half saturation for phytoplankton NO <sub>3</sub> uptake	m <sup>3</sup> mmol <sup>-1</sup> N	2	
$1/k_{NH_4}$	K_NH4	Inverse half saturation for phytoplankton NH <sub>4</sub> uptake	m <sup>3</sup> mmol <sup>-1</sup> N	2	
$k_{Phy}$	K_Phy	Half saturation constant (squared) for zooplankton ingestion	(mmol N m <sup>-3</sup> ) <sup>2</sup>	2	
$\theta_{max}$	Chl2C_m	Maximum Chl:phytoplankton carbon ratio	mg Chl mg <sup>-1</sup> C	0.0535	
NA	ChlMin	Minimum Chl:phytoplankton carbon ratio	mg Chl mg <sup>-1</sup> C	0.001	Additional coefficient present within ROMS. Chlorophyll background mortality falls to zero when the phytoplankton abundance falls below this value.
NA	PhyCN	Phytoplankton C:N ratio	mmol C mmol <sup>-1</sup> N	6.625	Additional coefficient present within ROMS. Required there for modelling of dissolved inorganic carbon and utilized in the mussel feeding model
$1/k_{NH_4}$	PhyIP	Phytoplankton, coeff governing NH <sub>4</sub> dependent inhibition of NO <sub>3</sub> uptake	mmol <sup>-1</sup> N	1.5	Note that the ROMS implementation of the Fennel model distinguishes two coefficients (K_NH4, PhyIP) that correspond to two different usages of the original Fennel model's coefficient $k_{NH_4}$
$\alpha$	PhyIS	Initial slope of photosynthesis/irradiance curve	(W m <sup>-2</sup> d) <sup>-1</sup>	0.0125	In the code, PhyIS is defined in the manner of (Fennel, K., Hetland et al. 2011) rather than that of (Fennel, K., Wilkin et al. 2006). The numeric value that we have adopted was derived by calibration. It is half of the ROMS-default, but the ROMS default value is towards the upper end of the (large) range cited in the literature (Fennel, K., Wilkin et al. 2006)
NA	PhyMin	Phytoplankton mortality guard threshold	mmol N m <sup>-3</sup>	0.001	Additional coefficient present within ROMS. Phytoplankton background mortality falls to zero when the phytoplankton abundance falls below this value.
$m_{phy}$	PhyMR	Phytoplankton specific 'background' mortality rate	d <sup>-1</sup>	0.15	
$\beta$	ZooAE_N	Zooplankton assimilation efficiency for ingested nitrogen	-	0.75	



Coefficient (Fennel 2006)	Coefficient (ROMS code)	Description	Units	Value	Comment
$l_{bm}$	ZooBM	Zooplankton specific basal metabolic rate	$d^{-1}$	0.1	
NA	ZooCN	Zooplankton C:N ratio	$mmol\ C\ mmol^{-1}\ N$	6.625	Additional coefficient present within ROMS. Required there for modelling of dissolved inorganic carbon and utilized in the mussel feeding model
$l_E$	ZooER	Zooplankton specific excretion rate	$d^{-1}$	0.1	
$g_{max}$	ZooGR	Zooplankton maximum specific ingestion rate	$d^{-1}$	0.6	
NA	ZooMin	Zooplankton guard threshold for basal metabolism	$mmol\ N\ m^{-3}$	0.001	Additional coefficient present within ROMS. Zooplankton respiratory losses when zooplankton concentration falls below this threshold.
$m_{Zoo}$	ZooMR	Zooplankton specific mortality rate	$d^{-1}$	0.025	
$R_{LDet}$	LDERRN	Specific mineralization rate for N within large detritus	$d^{-1}$	0.01	Additional coefficient present within ROMS. Required there for modelling of dissolved inorganic carbon.
NA	LDERRC	Specific mineralization rate for C within large detritus	$d^{-1}$	0.01	
$\tau$	CoagR	Specific rate for coagulation of small detritus and phytoplankton to large detritus	$d^{-1}$	0.005	
$R_{SDet}$	SDeRRN	Specific mineralization rate for N within small detritus	$d^{-1}$	0.01	
NA	SDeRRC	Specific mineralization rate for C within small detritus	$d^{-1}$	0.01	Additional coefficient present within ROMS. Required there for modelling of dissolved inorganic carbon
$w_{phy}$	wPhy	Sinking velocity for phytoplankton	$m\ d^{-1}$	0.1	
$w_{LDet}$	wLDet	Sinking velocity for large detritus	$m\ d^{-1}$	1.0	
$w_{SDet}$	wSDet	Sinking velocity for small detritus	$m\ d^{-1}$	0.1	

**Table 10-2: Coefficients required to link the Fennel NPZD model and the Ren mussel physiology model.** The coefficients in this Table are not found in either of the original Fennel or Ren models but they are required in order to allow the models to be coupled. The coefficients used in our implementation of the mussel physiology are those specified within Ren & Ross (2005) or Ren et al. (2010).

Coefficient	Description	Units	Value	Comment
LDeCN	C:N ratio for large detritus	mmol C mmol <sup>-1</sup> N	6.625	Assumed, but consistent with Fennel model C:N ratios of zooplankton and phytoplankton and the assumption that detrital C & N mineralize at the same rates
SDeCN	C:N ratio for small detritus	mmol C mmol <sup>-1</sup> N	6.625	Assumed, but consistent with Fennel model C:N ratios of zooplankton and phytoplankton and the assumption that detrital C & N mineralize at the same rates
SIS	Concentration of suspended inorganic sediment	mg ash weight m <sup>-3</sup>	2000	Marlborough District Council water quality samples from Queen Charlotte Sound
$\psi_{Phy}$	Relative search volume of mussels for phytoplankton	-	1.0	By definition
$\psi_{Zoo}$	Relative search volume of mussels for zooplankton	-	1.0	(Zeldis, J.R.,; Robinson et al. 2004)
$\psi_{LDet}$	Relative search volume of mussels for large detritus	-	1.0	Assumed, but consistent with (Zeldis, J.R.,; Robinson et al. 2004)
$\psi_{SDet}$	Relative search volume of mussels for small detritus	-	1.0	Assumed, but consistent with (Zeldis, J.R.,; Robinson et al. 2004)
PhyDWN	Dry weight to nitrogen ratio for phytoplankton	g DW mmol <sup>-1</sup> N	1.02	(Bowie, Mills et al. 1985)
ZooDWN	Dry weight to nitrogen ratio for phytoplankton	g DW mmol <sup>-1</sup> N	0.89	(Beers 1966)
LDeDWN	Dry weight to nitrogen ratio for large detritus	g DW mmol <sup>-1</sup> N	1.0	Assumed, chosen to lie between the corresponding ratios for phytoplankton and zooplankton (closer to the former)
SDeDWN	Dry weight to nitrogen ratio for small detritus	g DW mmol <sup>-1</sup> N	1.0	Assumed, chosen to lie between the corresponding ratios for phytoplankton and zooplankton (closer to the former)

## Appendix B Mathematical description of the mussel farm model

The full Ren et al. (2010) mussel growth model includes explicit dynamic descriptions of the rates of change of mussel energy reserves and structural volume. In his model, the reserve:structure ratio can vary through time (it provides an index of mussel condition or level of starvation). Some of the physiological rates are influenced by the ratio. We do not go to these lengths. The mussels of our population are described only in terms of numbers per length class). Length and structural volume are closely related, but instantaneous length provides no information about mussel condition. For the purposes of calculating all physiological rates, we assume that our mussels have replete reserves.

An individual mussel is defined by its shell length ( $M_L$ , mm). In turn, this defines various body-weight characteristics. The whole animal wet-weight (inclusive of shell, gram) is denoted  $M_{WW+S}$ :

$$M_{WW+Shell} = 0.00025 M_L^{2.726}$$

The wet-weight exclusive of shell (gram) is:

$$M_{WW} = 0.32 M_{WW+Shell}$$

The dry weight (exclusive of shell, gram) is:

$$M_{DW} = 0.2 M_{WW}$$

We assume that our mussels have replete reserves, and that reserves amount to 40% of the dry body mass (exclusive of the shell). Thus, the dry weight mass (gram) of structural tissue (ie proteins, carbohydrates etc., which once laid down, cannot be remobilized to meet energetic demands etc.) is:

$$M_S = 0.6 M_{DW}$$

and, the dry weight mass (gram) of mussel reserve materials is:

$$M_R = M_{DW} - M_S = 0.4 M_{DW}$$

The energy content (J) of these reserves is

$$E = \frac{1000 M_R}{\mu_E}$$

The biovolume ( $M_V$ ) of the structural material is

$$M_V = \frac{M_S}{\rho}$$

In the original Ren model, the maximum energy reserves (J cm<sup>-3</sup>) are denoted  $[E_m]$ . In our derivation of this model, we assume  $E = [E_m] M_V$ .

$$M_V = \frac{M_{DW}}{0.2} = M_{WW}$$

The energy content of the mussel (Joules, exclusive of shell) is

$$M_J = 1000(M_S \mu_S + M_R \mu_R)$$

As noted previously, we assume the mussels have replete reserves, so

$$M_R \mu_R = \frac{M_J - 1000 M_S \mu_S}{1000} = 2600 M_V$$

Mussels are assumed to consume seston. We measure its abundance (as perceived by the mussels) as: carbon ( $S_C$ , mg C m<sup>-3</sup>), nitrogen ( $S_N$ , mg N m<sup>-3</sup>) and dry weight ( $S_{DW}$ , mg dry weight m<sup>-3</sup>). Seston is assumed to comprise of small and large detritus, phytoplankton and zooplankton and suspended inorganic matter. The carbon ( $S_C$ , mmol C m<sup>-3</sup>), nitrogen ( $S_N$ , mmol N m<sup>-3</sup>), dry-weight ( $S_{DW}$ , mg m<sup>-3</sup>) and energy concentrations ( $S_J$ , J m<sup>-3</sup>) of perceived seston are given by:

$$S_C = Phy. \varphi_{C:N}^{Phy} \psi_{Phy} + Zoo. \varphi_{C:N}^{Zoo} \psi_{Zoo} + LDet. \varphi_{C:N}^{LDet} \psi_{LDet} + SDet. \varphi_{C:N}^{SDet} \psi_{SDet}$$

$$S_N = Phy \psi_{Phy} + Zoo \psi_{Zoo} + LDet \psi_{LDet} + SDet \psi_{SDet}$$

$$S_{DW} = Phy. \varphi_{DW:N}^{Phy} \psi_{Phy} + Zoo. \varphi_{DW:N}^{Zoo} \psi_{Zoo} + LDet. \varphi_{DW:N}^{LDet} \psi_{Zoo} + SDet. \varphi_{DW:N}^{SDet} \psi_{Zoo} + SIS$$

$$S_J = Phy. \varphi_{C:N}^{Phy} \cdot \varphi_{J:C}^{Phy} \psi_{Phy} + Zoo. \varphi_{C:N}^{Zoo} \cdot \varphi_{J:C}^{Zoo} \psi_{Zoo} + LDet. \varphi_{C:N}^{LDet} \cdot \varphi_{J:C}^{LDet} \psi_{LDet} + SDet. \varphi_{C:N}^{SDet} \cdot \varphi_{J:C}^{SDet} \psi_{SDet}$$

The volume of water pumped across the mussel gill surface is:

$$V = U_{mm} M_V^{2/3} f(K)$$

Where  $f(K)$  denotes the temperature dependence function (temperature in Kelvin)

$$f(K) = k_{T0} e^{\left(\frac{T_A - T_0}{T_0 K}\right)} \left[ 1 + e^{\left(\frac{T_{AL} - T_{AL}}{K - T_L}\right)} + e^{\left(\frac{T_{AH} - T_{AH}}{T_H - K}\right)} \right]^{-1}$$

The quantities of phytoplankton, zooplankton, large detritus, small detritus and energy captured on the gills are:

$$C_{Phy} = V Phy \psi_{Phy}$$

$$C_{Zoo} = V Zoo \psi_{Zoo}$$

$$C_{LDet} = V LDet \psi_{LDet}$$

$$C_{SDet} = V SDet \psi_{SDet}$$

$$C_J = V \left( Phy \psi_{Phy} \varphi_{C:N}^{Phy} \varphi_{J:C}^{Phy} + Zoo \psi_{Zoo} \varphi_{C:N}^{Zoo} \varphi_{J:C}^{Zoo} + LDet \psi_{LDet} \varphi_{C:N}^{LDet} \varphi_{J:C}^{LDet} + SDet \psi_{SDet} \varphi_{C:N}^{SDet} \varphi_{J:C}^{SDet} \right)$$

Of this material, a fraction is lost as pseudo-faeces. The remainder passes into the gut. The fraction passing into the gut is given by:

The rate at which energy is assimilated across the gut wall is

$$A_J = V \frac{S_C}{S_C + H_{pm}} p_{A_{max}}$$

The rates of carbon and nitrogen assimilation are:

$$A_C = \frac{V(\text{Phy}\psi_{\text{Phy}}\varphi_{\text{C:N}}^{\text{Phy}} + \text{Zoo}\psi_{\text{Zoo}}\varphi_{\text{C:N}}^{\text{Zoo}} + \text{LDet}\psi_{\text{LDet}}\varphi_{\text{C:N}}^{\text{LDet}} + \text{SDet}\psi_{\text{SDet}}\varphi_{\text{C:N}}^{\text{SDet}})}{C_J} I_J$$

$$A_N = \frac{V(\text{Phy}\psi_{\text{Phy}} + \text{Zoo}\psi_{\text{Zoo}} + \text{LDet}\psi_{\text{LDet}} + \text{SDet}\psi_{\text{SDet}})}{C_J} I_J$$

Material which is not assimilated across the gut wall is lost as faeces and pseudo-faeces and passes into the large-detrital pool.

The mussel energy expenditure rate ( $J \text{ mussel}^{-1} \text{ d}^{-1}$ ) is made up of a basal term ( $p_M$ ) and a growth-and-filtration-related term ( $p_g$ ).

$$p_M = \left( \frac{[E]}{[E_G] + \kappa[E]} \right) f(K)[p_m]M_V$$

$$p_g = \left( \frac{[E]}{[E_G] + \kappa[E]} \right) [E_G]p_{A_{\max}}M_V^{2/3}$$

The mussel carbon respiration rate ( $E_C$ ,  $\text{mmol CO}_2\text{-C mussel}^{-1} \text{ d}^{-1}$ ) is:

$$E_C = \max \left[ A_C - \frac{p_M + p_g}{\mu_R}, A_C - A_N\varphi_{\text{C:N}}^{\text{Mus}} \right]$$

The mussel nitrogen excretion rate ( $E_N$ ,  $\text{mmol NH}_4\text{-N mussel}^{-1} \text{ d}^{-1}$ ) rate is:

$$E_N = A_N - \frac{1}{\varphi_{\text{C:N}}^{\text{Mus}}} \left[ A_C - \frac{p_M + p_g}{\mu_R} \right]$$

Symbol	Description	Units	Value	Comment
	Scaling coefficient relating whole animal wet weight (incl. of shell) to shell length	$\text{g mm}^{-2.726}$	0.00025	(Hickman 1979)
	Exponent in wet-weight:length relationship	-	2.76	(Hickman 1979)
	Fraction of whole animal wet weight that is not shell	-	0.32	
	dry weight: wet weight ratio of mussel soft tissue	-	0.2	
	Structural tissue dry weight mass/soft tissue dry weight mass for a well fed mussel	-	0.6	
$\mu_S$	Energy density of mussel structural tissue	$\text{J mg}^{-1}$ structural dry weight		
$\mu_R$	Energy density of mussel reserve tissue	$\text{J mg}^{-1}$ reserve dry weight		

Symbol	Description	Units	Value	Comment
$\varphi_{C:N}^{Phy}$	C:N ratio of phytoplankton	mol C / mol N		
$\varphi_{C:N}^{Zoo}$	C:N ratio of zooplankton	mol C / mol N		
$\varphi_{C:N}^{LDet}$	C:N ratio of large detritus	mol C / mol N		
$\varphi_{C:N}^{SDet}$	C:N ratio of small detritus	mol C / mol N		
$\varphi_{DW:N}^{Phy}$	C:N ratio of phytoplankton	g dry weight / mol N		
$\varphi_{DW:N}^{Zoo}$	C:N ratio of zooplankton	g dry weight / mol N		
$\varphi_{DW:N}^{LDet}$	C:N ratio of large detritus	g dry weight / mol N		
$\varphi_{DW:N}^{SDet}$	C:N ratio of small detritus	g dry weight / mol N		
$\varphi_{J:C}^{Phy}$	Energy density of phytoplankton	J / mmol C		
$\varphi_{J:C}^{Zoo}$	Energy density of zooplankton	J / mmol C		
$\varphi_{J:C}^{LDet}$	Energy density of large detritus	J / mmol C		
$\varphi_{J:C}^{SDet}$	Energy density of small detritus	J / mmol C		
$\psi^{Phy}$	Mussel filtration efficiency for phytoplankton	$m^3 m^{-3}$		
$\psi^{Zoo}$	Mussel filtration efficiency for zooplankton	$m^3 m^{-3}$		
$\psi^{LDet}$	Mussel filtration efficiency for large detritus	$m^3 m^{-3}$		
$\psi^{SDet}$	Mussel filtration efficiency for small detritus	$m^3 m^{-3}$		
$H_{pm}$	Half saturation seston concentration	mmol C $m^{-3}$	295/12	
$p_{A_{max}}$	Maximum surface area specific assimilation rate	J $cm^{-2} d^{-1}$		
$\rho$	Biovolume-specific concentration of structural materials	g structural $cm^{-3}$ biovolume	0.2	

## Appendix C Mathematical description of the fish farm model

Stigebrandt derived a model for salmon growth that is based upon energy conservation. Fish size is expressed as live weight ( $W$ , gram), and energy content ( $Q$ , Joules). The energy density of fish flesh ( $C_{fi}$ , J g<sup>-1</sup> live weight) is assumed to be constant.

$$Q = WC_{fi}$$

The maximal fish growth rate ( $G_{\max}$ , g live weight fish<sup>-1</sup> d<sup>-1</sup>) is assumed to scale allometrically with fish weight and exponentially with temperature ( $T$ , Celsius).

$$G_{\max} = aW^b e^{\tau T}$$

The realized ingestion rate ( $Q_r$ , J fish<sup>-1</sup> d<sup>-1</sup>) is the lesser of the per-capita feed provision rate ( $Q_{feed}$ , J fish<sup>-1</sup> d<sup>-1</sup>) or the maximal ingestion rate ( $Q_{r\max}$ , J fish<sup>-1</sup> d<sup>-1</sup>, to be defined in greater detail later)

$$Q_r = \min(Q_{feed}, Q_{r\max}) aW^\gamma e^{\tau T}$$

The feed is deemed to consist of a water fraction ( $F_w$ , g water g<sup>-1</sup> feed), a protein fraction ( $F_p$ , g protein g<sup>-1</sup> feed), a lipid fraction ( $F_l$ , g lipid g<sup>-1</sup> feed) and a carbohydrate fraction ( $F_c$ , g carbohydrate g<sup>-1</sup> feed). The energy densities (J g<sup>-1</sup> substrate) for lipid and carbohydrate are denoted  $C_l$  and  $C_c$  respectively. For protein, we define two energy densities.  $C_p^{NO_3}$  denotes the energy density if the protein is fully catabolised to yield NO<sub>3</sub> as the nitrogenous end-product.  $C_p^{NH_4}$  denotes the (smaller) energy density that arises when protein is catabolised to yield ammonium as an end-product. The energy density of food is defined to be:

$$\delta = F_p C_p^{NO_3} + F_l C_l + F_c C_c$$

The fractional contributions of protein, lipid and carbohydrate to the total ingested energy are:

$$E_p^{NO_3} = \frac{F_p C_p^{NO_3}}{\delta}, E_p^{NH_4} = \frac{F_p C_p^{NH_4}}{\delta}, E_l = \frac{F_l C_l}{\delta} \text{ and } E_c = \frac{F_c C_c}{\delta}$$

A fraction of the ingested energy is lost in faeces. The loss rate ( $Q_f$ , J fish<sup>-1</sup> d<sup>-1</sup>) is determined by the assimilation efficiencies for protein ( $A_p$ , dimensionless), carbohydrate ( $A_c$ ) and lipid ( $A_l$ ) and by the fractional contributions which each makes to total energy ingestion.

$$Q_f = Q_r \left( (1 - A_p) E_p^{NO_3} + (1 - A_l) E_l + (1 - A_c) E_c \right)$$

The process of breaking proteins, lipids and carbohydrates into simpler molecules and assimilating those across the gut wall incurs an energy expenditure (so-called specific dynamic action, ( $Q_{SDA}$ , J fish<sup>-1</sup> d<sup>-1</sup>). The SDA for protein amounts to 30% of the assimilated protein energy whilst the SDAs for lipid and carbohydrate amount to 5% of their respective energy assimilation rates:

$$Q_{SDA} = Q_r \left( 0.3 A_p E_p^{NO_3} + 0.05 (A_c E_c + A_l E_l) \right)$$

A fish is assumed to use dietary lipid and carbohydrate preferentially to fuel its energy demands (thereby conserving as much nitrogen as possible to synthesize new proteins). Nonetheless, when a fish assimilates more nitrogen than it requires to meet the nitrogen demands associated with building new flesh, it uses the excess protein to meet energetic expenditure. Similarly, when the total energy assimilation rate is insufficient to meet the basal energy demand, the fish is assumed to

meet the deficit by catabolising lipid, carbohydrate and protein at rates which maintain a fixed proximate body composition.  $E_p^{NO_3}$  is based upon full oxidation to  $NO_3$ , but fish catabolise proteins only to  $NH_4^+$ . Thus, account must be taken of the energy that is lost as  $NH_4^+$  when protein is catabolised. The result is an additional growth-related energy loss ( $Q_N$ , J fish<sup>-1</sup> d<sup>-1</sup>)

$$Q_N = \frac{E_p^{NO_3} - E_p^{NH_4}}{E_p^{NO_3}} C_p \left( F_p A_p \frac{Q_r}{\delta} - P_p \frac{dW}{dt} \right)$$

The energetic cost of growth (net accrual of new fish flesh;  $Q_g$ , J fish<sup>-1</sup> d<sup>-1</sup>) is assumed to be proportional to the rate of growth.

$$Q_g = C_{fi} \left[ \frac{dW}{dt} \right]^+$$

Basal energetic costs ( $Q_s$ , J fish<sup>-1</sup> d<sup>-1</sup>) are assumed to scale allometrically with fish weight and exponentially with temperature.

$$Q_s = \alpha W^\gamma e^{\tau T}$$

In the original Stigebrandt model, locomotory costs ( $Q_l$ , J fish<sup>-1</sup> d<sup>-1</sup>) were set to zero because basal metabolism was explicitly assumed to include a locomotory component. In our implementation, we have retained an explicit locomotory term (set proportional to the basal respiration – which explicitly excludes locomotion)

$$Q_l = \vartheta Q_s$$

Since farmed salmon are usually harvested before reaching sexual maturity, we assume that the energetic costs of gamete synthesis ( $Q_p$ , J fish<sup>-1</sup> d<sup>-1</sup>) are zero.

Collectively, the expressions for basal metabolism, maximal growth rate, maximal ingestion rate, digestive efficiencies, specific dynamic action, and protein catabolism efficiency imply an expression for the maximum ingestion rate (J fish<sup>-1</sup> d<sup>-1</sup>)

$$Q_{r_{\max}} = \frac{\left[ \alpha W^\gamma + a W^b \left( C_{fi} - \frac{E_p^{NO_3} - E_p^{NH_4}}{E_p^{NO_3}} C_p P_p \right) \right] e^{\tau T}}{1 - \left( (1 - A_p) E_p + (1 - A_l) E_l + (1 - A_c) E_c \right) - \left( 0.3 A_p E_p^{NO_3} + 0.05 (A_c E_c + A_l E_l) \right) - \frac{E_p^{NO_3} - E_p^{NH_4}}{E_p^{NO_3}} A_p E_p}$$

The rate of change of energy content  $\frac{dQ}{dt}$  (J fish<sup>-1</sup> d<sup>-1</sup>) is given by the difference between the rates of energy ingestion ( $Q_r$ ) and energy loss through: faeces  $Q_f$ , catabolism of protein ingested in excess of growth requirements ( $Q_N$ ), basal metabolism ( $Q_s$ ), locomotory metabolism ( $Q_l$ ), specific dynamic action, energy expended in synthesis of new flesh ( $Q_g$ ) and energy expended in synthesis of gametes ( $Q_p$ ).

$$\frac{dQ}{dt} = Q_r - Q_f - Q_N - Q_s - Q_l - Q_{SDA} - Q_g - Q_p = C_{fi} \frac{dW}{dt}$$



Since  $Q_N$  and  $Q_g$  are dependent upon  $\frac{dW}{dt}$ , the equation does not have an analytic solution. We use the bisection method to calculate a realized instantaneous value for  $\frac{dQ}{dt}$  that satisfies this equation. Conceptually similar equations can be set up for carbon. Again, we use the bisection method to solve that equation. The final realized growth rate (which may be negative) is the lesser of the two growth rates (expressed in energy units). Realized carbon, nitrogen etc. uptake and release fluxes are then calculated on the basis of that growth rate. Oxygen demand can be derived from the calculated assimilation rates of protein, carbohydrate and lipid, the realized fish growth rate and the respiratory quotient of each substrate. (Buschmann, Costa-Pierce et al. 2007)

**Table 10-3: Coefficients for the fish physiology module.** WW: wet weight

Coefficient (Stigebrandt 1999)	Coefficient (ROMS code)	Description	Units (Stigebrandt) [ROMS]	Value	Comment
$C_p^{NO_3}$		Energy protein when fully oxidized to nitrate	J g <sup>-1</sup>	23.0x10 <sup>3</sup>	<a href="http://www.fao.org/docrep/003/aa040e/aa040e08.htm">http://www.fao.org/docrep/003/aa040e/aa040e08.htm</a>
$C_p^{NH_4}$		Energy density of protein when catabolized to ammonium	J g <sup>-1</sup>	19.0x10 <sup>3</sup>	(Schmidt-Nielsen 1982)
$C_l$		Energy density of lipid	J g <sup>-1</sup>	39.33x10 <sup>3</sup>	(Schmidt-Nielsen 1982)
$C_c$		Energy density of carbohydrate	J g <sup>-1</sup>	17.57x10 <sup>3</sup>	(Schmidt-Nielsen 1982)
	FeedWaterFrac	Energy density of ingested carbohydrate	g water g <sup>-1</sup> feed	0.085	(Buschmann, Costa-Pierce et al. 2007)
$F_p$	FeedProteinFrac	Protein content of the fish feed	g protein g <sup>-1</sup> feed	0.45	(Buschmann, Costa-Pierce et al. 2007); <a href="http://en.wikipedia.org/wiki/Chinook_salmon">http://en.wikipedia.org/wiki/Chinook_salmon</a>
$F_l$	FeedLipidFrac	Lipid content of the fish feed	g lipid g <sup>-1</sup> feed	0.22	<a href="http://en.wikipedia.org/wiki/Chinook_salmon">http://en.wikipedia.org/wiki/Chinook_salmon</a> ; but see (Buschmann, Costa-Pierce et al. 2007) – which suggests 0.35
$F_c$	FeedCarbFrac	Carbohydrate content of fish feed	g carbohydrate g <sup>-1</sup> feed	0.14	<a href="http://en.wikipedia.org/wiki/Chinook_salmon">http://en.wikipedia.org/wiki/Chinook_salmon</a> ; but see (Buschmann, Costa-Pierce et al. 2007) – which suggests 0.10
	FishWaterFrac	Water content of the fish feed	g water g <sup>-1</sup> fish	0.75	(Shearer, Åsgård et al. 1994)
$P_p$	FishProteinFrac	Protein content of the fish	g protein g <sup>-1</sup> fish	0.14	(Shearer, Åsgård et al. 1994)
$P_l$	FishLipidFrac	Lipid content of the fish	g lipid g <sup>-1</sup> fish	0.10	(Shearer, Åsgård et al. 1994)
$P_c$	FishCarbFrac	Carbohydrate content of fish	g carbohydrate g <sup>-1</sup> fish	0.015	(Shearer, Åsgård et al. 1994)
$\delta$	Derived property (see right)	Energy density of fish feed	J g <sup>-1</sup>	$\delta$ $= F_p C_p^{NO_3}$ $+ F_l C_l$ $+ F_c C_c$	$1 \leq F_p + F_l + F_c$ , allowing that fish feed may have a small water content

Coefficient (Stigebrandt 1999)	Coefficient (ROMS code)	Description	Units (Stigebrandt) [ROMS]	Value	Comment
$C_{fi}$	Derived property (see right)	Energy density of live fish	J g <sup>-1</sup>	$C_{fi}$ = $P_p C_p^{NO_3}$ + $P_l C_l$ + $P_c C_c$	
$A_p$	FishAssimEfficProt	Assimilation efficiency for protein content of fish feed	-	0.9	(Buschmann, Costa-Pierce et al. 2007)
$A_l$	FishAssimEfficLipid	Assimilation efficiency for lipid content of fish feed	-	0.95	(Buschmann, Costa-Pierce et al. 2007)
$A_c$	FishAssimEfficCarbo	Assimilation efficiency for carbohydrate content of fish feed	-	0.6	(Buschmann, Costa-Pierce et al. 2007)
	SDAProt	Specific dynamic action for digestion of protein	J expended J <sup>-1</sup> protein assimilated across gut wall	0.3	(Stigebrandt 1999)
	SDALipid	Specific dynamic action for digestion of lipid	J expended J <sup>-1</sup> lipid assimilated across gut wall	0.05	(Stigebrandt 1999)
	SDACarbo	Specific dynamic action for digestion of carbohydrate	J expended J <sup>-1</sup> carbohydrate assimilated across gut wall	0.05	(Stigebrandt 1999)
NA	W <sub>L</sub> s	Scale coefficient in fish weight:length allometry	kg WW mm <sup>-1/WLe</sup> fork length	2.84627x10 <sup>-9</sup>	(Petrell and Jones 2000)
NA	W <sub>Le</sub>	Exponent in fish weight:length allometry	-	3.27	(Petrell and Jones 2000)
$a$	G <sub>W</sub> s	Exponent in fish allometric relation between maximal growth rate and live weight	(g WW) <sup>1-GWe</sup> d <sup>-1</sup>	0.038	(Petrell and Jones 2000)
$b$	G <sub>We</sub>	Exponent in fish allometric relation between maximal growth rate and live weight	-	0.667	(Petrell and Jones 2000)
$\alpha$	resps	Exponent in fish allometric relation between basal respiration rate and live weight	J (g WW) <sup>-</sup> $\gamma$ d <sup>-1</sup>	46.024	(Stigebrandt 1999)

Coefficient (Stigebrandt 1999)	Coefficient (ROMS code)	Description	Units (Stigebrandt) [ROMS]	Value	Comment
$\gamma$	respe	Exponent in fish allometric relation between basal respiration rate and live weight	-	0.74	(Enders and Scruton 2006) but see (Stigebrandt 1999) who suggests 0.8
	Tmptrs	Scale coefficient in exponential relationship governing fish maximal growth and basal respiration	-	1.0	(Stigebrandt 1999). The reference temperature is 0 °C
$\tau$	Tmptre	Exponent coefficient in exponential relationship governing fish maximal growth and basal respiration	°C <sup>-1</sup>	0.08	(Stigebrandt 1999)
	SwimCostFrac	Energy expended in swimming relative to basal energy expenditure	J J <sup>-1</sup>	1.1	(Petrell and Jones 2000)
	Nresid	Fraction of the protein energy assimilated across the gut wall which is lost as ammonium during protein catabolism	J J <sup>-1</sup>	$\frac{E_p^{NO_3} - E_p^{NH_4}}{E_p^{NO_3}}$	(Stigebrandt 1999). Careful reading of (Stigebrandt 1999) reveals that his value for the energy content of protein is based upon complete oxidation. He introduces Nresid=0.15 to account for the energy that is lost because fish oxidize protein only to a NH <sub>4</sub> <sup>+</sup> endpoint. That is a little smaller than the value derived from our chosen values for $E_p^{NO_3}$ and $E_p^{NH_4}$

## Appendix D Fish feed inputs

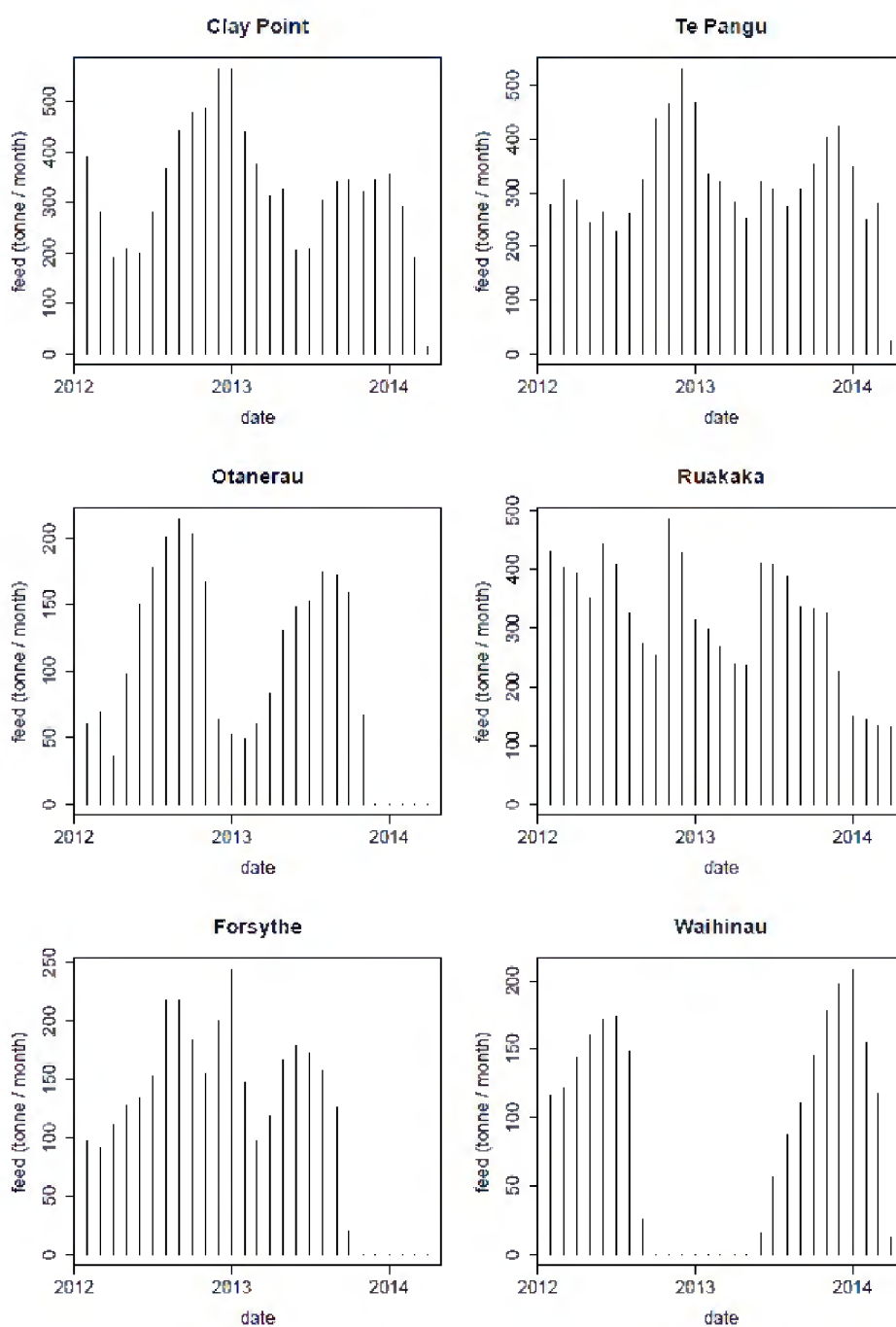


**Figure D-1: Histogram of monthly feed inputs provided by New Zealand King Salmon for their existing farms.** Forsythe and Waihinau farms are outside the Queen Charlotte Sound model domain and were not included in the simulations.

## Appendix E Hydrodynamic model vs observations: additional graphs and tables

### Temperature and salinity scatter plots

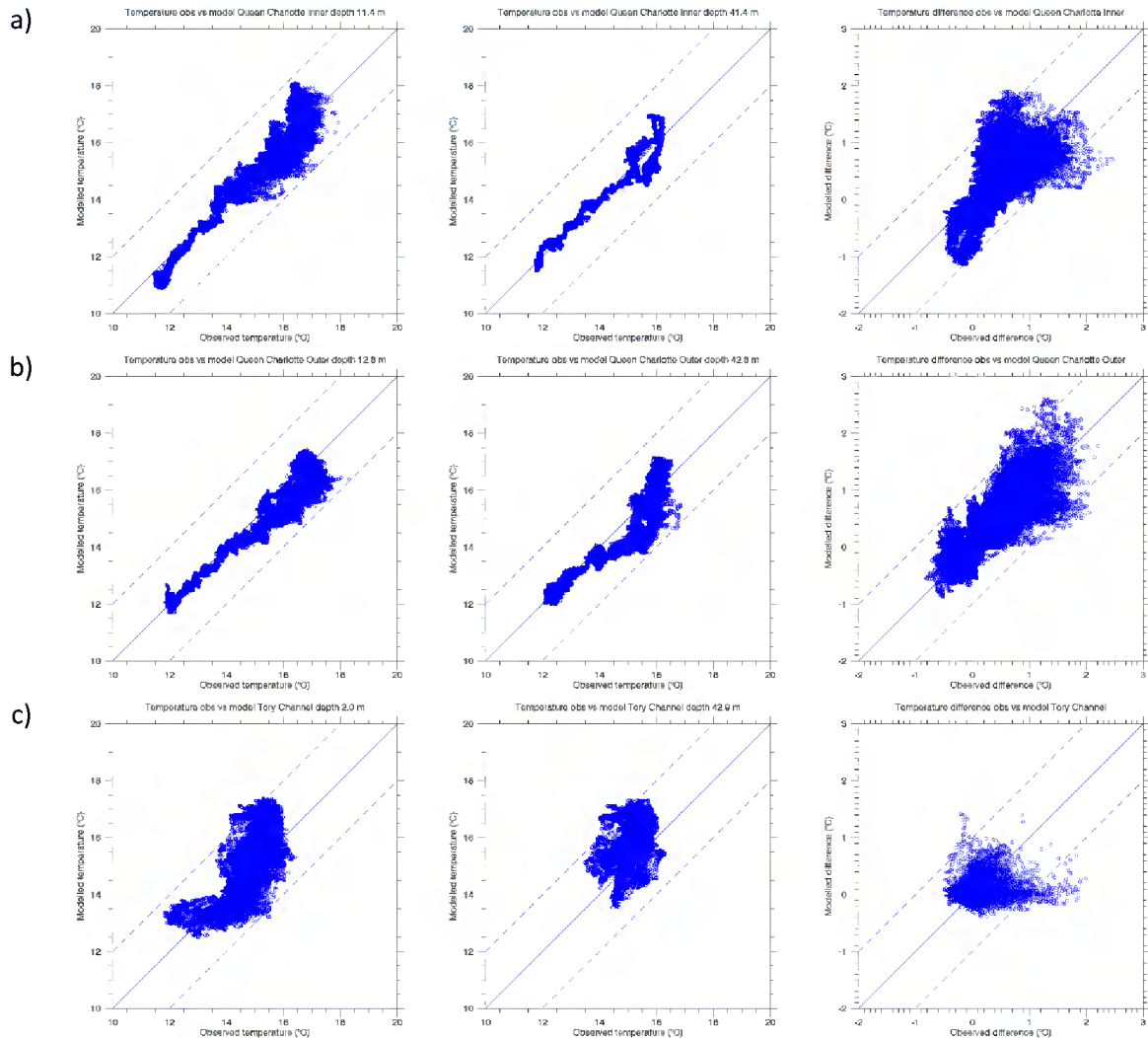


**Figure E-1: Temperature comparison.** Scatter-plot comparison of observed and modelled temperature time series for: a) QCS Inner; b) QCS Outer; c) Tory Channel. The panels show the upper (left) and lower (middle) sensors, plus the difference, upper minus lower (right).

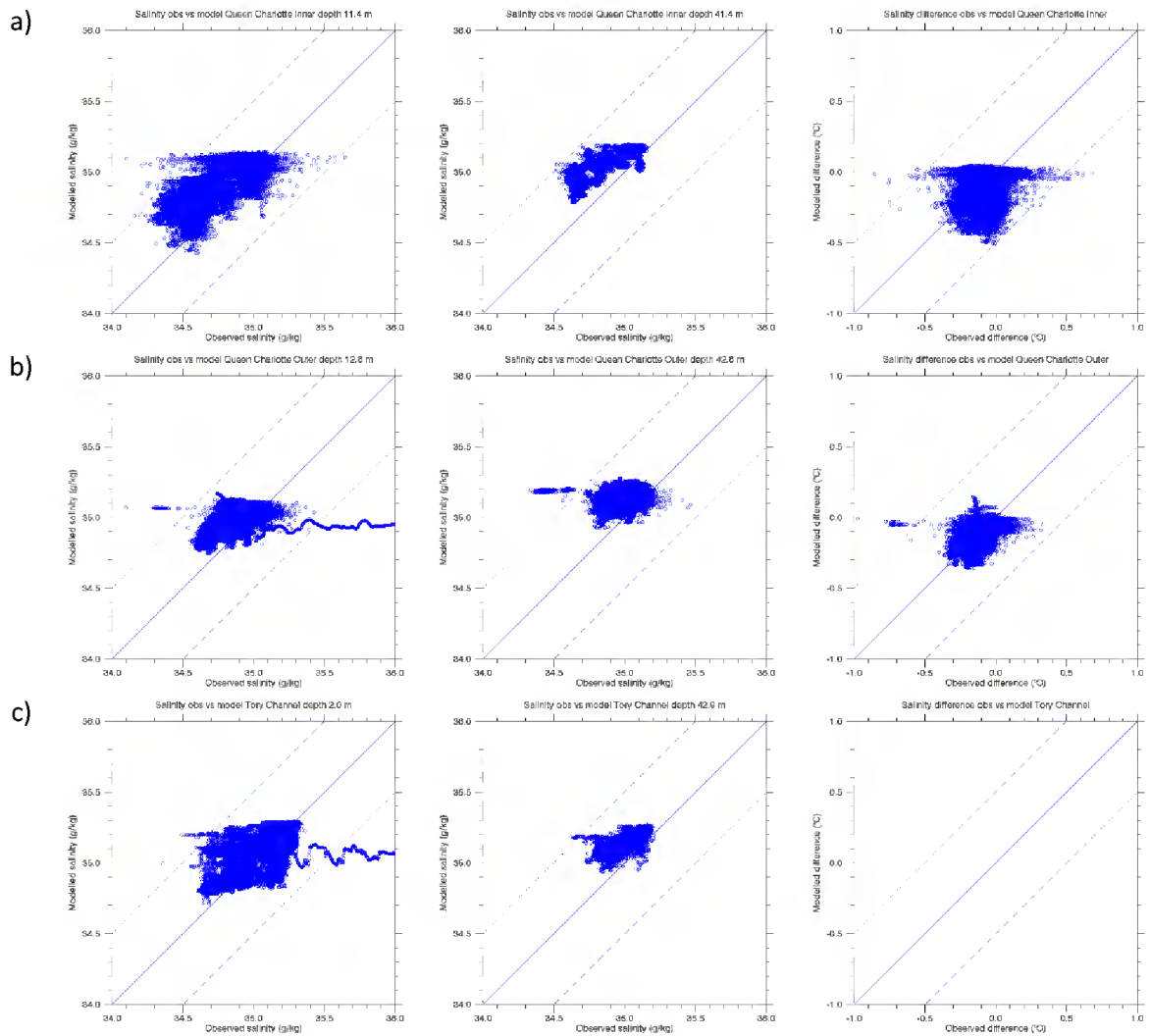


**Figure E-2: Salinity comparison.** Scatter-plot comparison of observed and modelled salinity time series for: a) QCS Inner; b) QCS Outer; c) Tory Channel. The panels show the upper (left) and lower (middle) sensors, plus the difference, upper minus lower (right).

## Tidal height tabulated parameters

**Table E-1: S2 tidal height parameters.** S2 tidal height parameters from ADCP pressure data and model. Here “ratio” means model value divided by observed value and “diffce” means model value minus observed value.

ADCP Site/Deployment	Amplitude (m)			Phase (°)		
	Obs.	Model	Ratio	Meas.	Model	Diffce
QCS Outer Deployment 1	0.239	0.262	<b>1.10</b>	37.1	29.7	<b>-7.5</b>
QCS Outer Deployment 2	0.221	0.241	<b>1.09</b>	42.5	42.1	<b>-0.5</b>
Tory Channel Deployment 1	0.197	0.228	<b>1.16</b>	32.9	26.6	<b>-6.3</b>
Tory Channel Deployment 2	0.176	0.208	<b>1.18</b>	38.5	39.8	<b>1.4</b>

**Table E-2: N2 tidal height parameters.** As Table E-1 but for the N2 constituent.

ADCP Site/Deployment	Amplitude (m)			Phase (°)		
	Obs.	Model	Ratio	Meas.	Model	Diffce
QCS Outer Deployment 1	0.031	0.053	<b>1.73</b>	170.6	135.9	<b>-34.7</b>
QCS Outer Deployment 2	0.056	0.092	<b>1.64</b>	139.7	117.9	<b>-21.8</b>
Tory Channel Deployment 1	0.050	0.078	<b>1.55</b>	152.1	127.9	<b>-24.3</b>
Tory Channel Deployment 2	0.092	0.134	<b>1.45</b>	125.2	110.0	<b>-15.2</b>

**Table E-3: O1 tidal height parameters.** As Table E-1 but for the O1 constituent.

ADCP Site/Deployment	Amplitude (m)			Phase (°)		
	Obs.	Model	Ratio	Meas.	Model	Diffce
QCS Outer Deployment 1	0.023	0.026	<b>1.10</b>	95.1	96.8	<b>1.7</b>
QCS Outer Deployment 2	0.034	0.022	<b>0.66</b>	126.1	103.6	<b>-22.5</b>
Tory Channel Deployment 1	0.024	0.027	<b>1.14</b>	119.4	98.4	<b>-21.0</b>
Tory Channel Deployment 2	0.019	0.024	<b>1.24</b>	128.0	106.0	<b>-22.0</b>



## Tidal velocity graphs

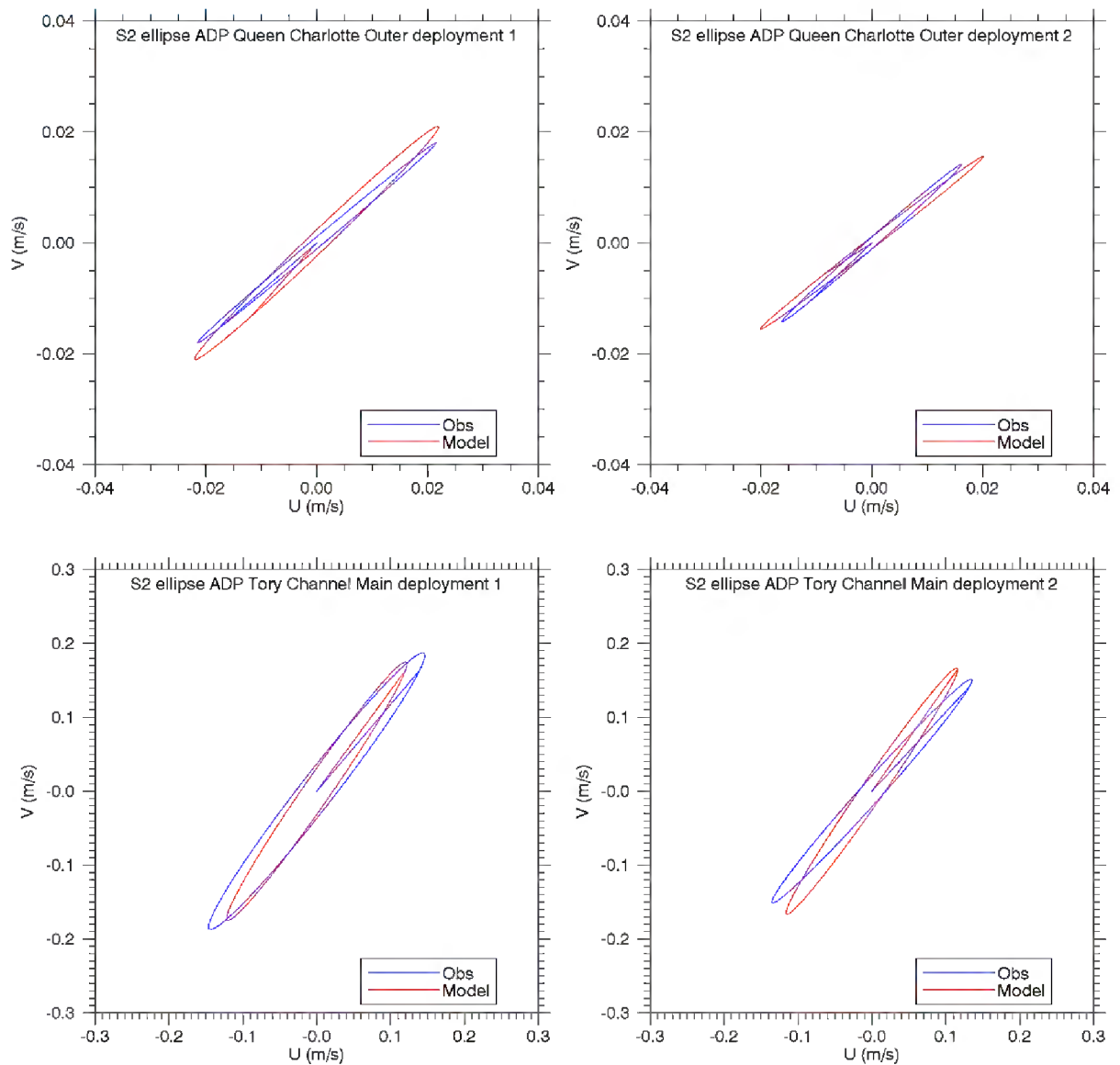


**Figure E-3: S2 tidal velocity comparison.** Mid-depth S2 tidal ellipses from ADCP (blue) and model (red) for Queen Charlotte Outer (upper) and Tory Channel (lower) sites. The format of the graphs follows Figure 3-5 and Figure 3-6.

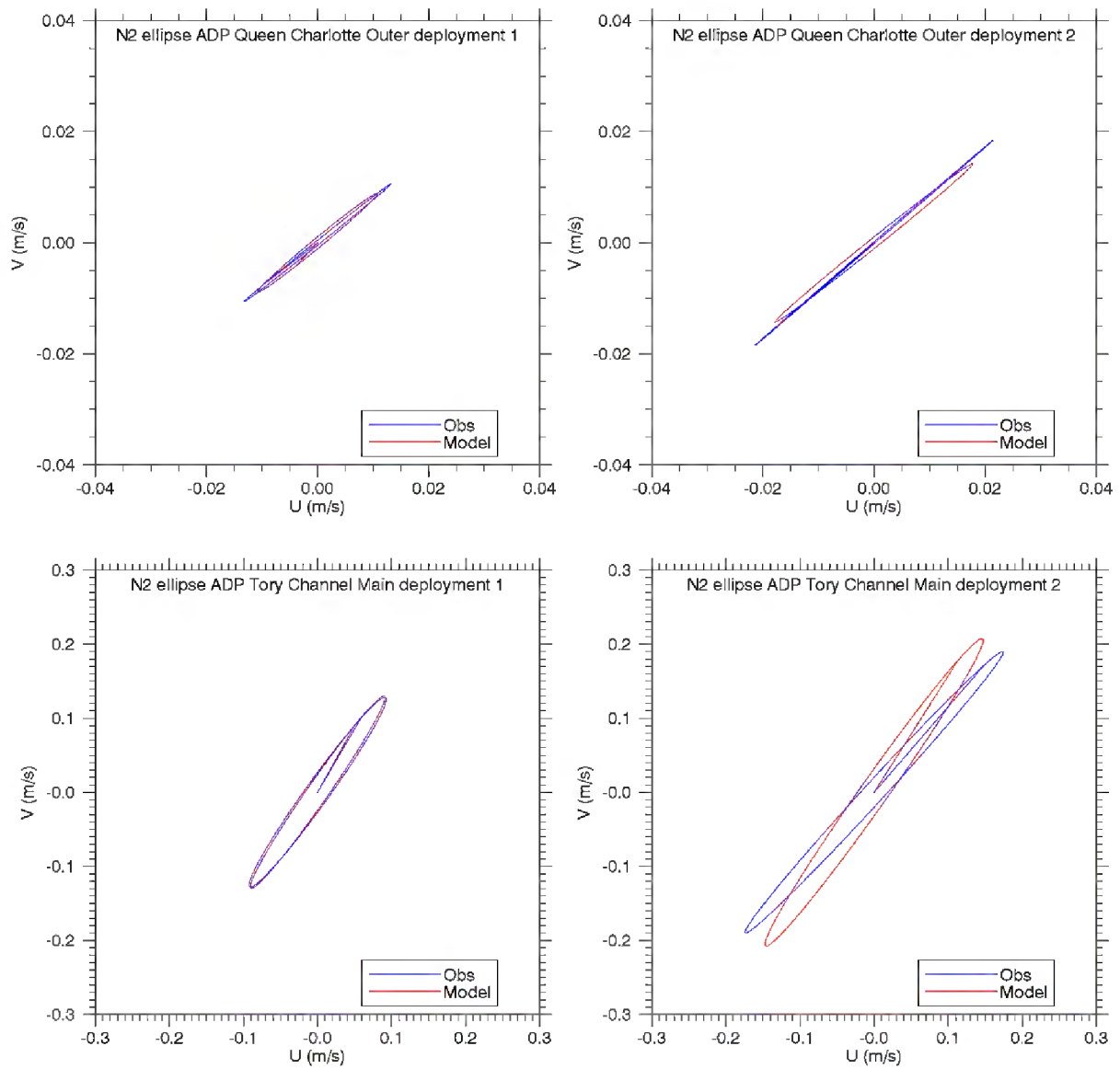


**Figure E-4: N<sub>2</sub> tidal velocity comparison.** As Figure E-3 but for the N<sub>2</sub> constituent.

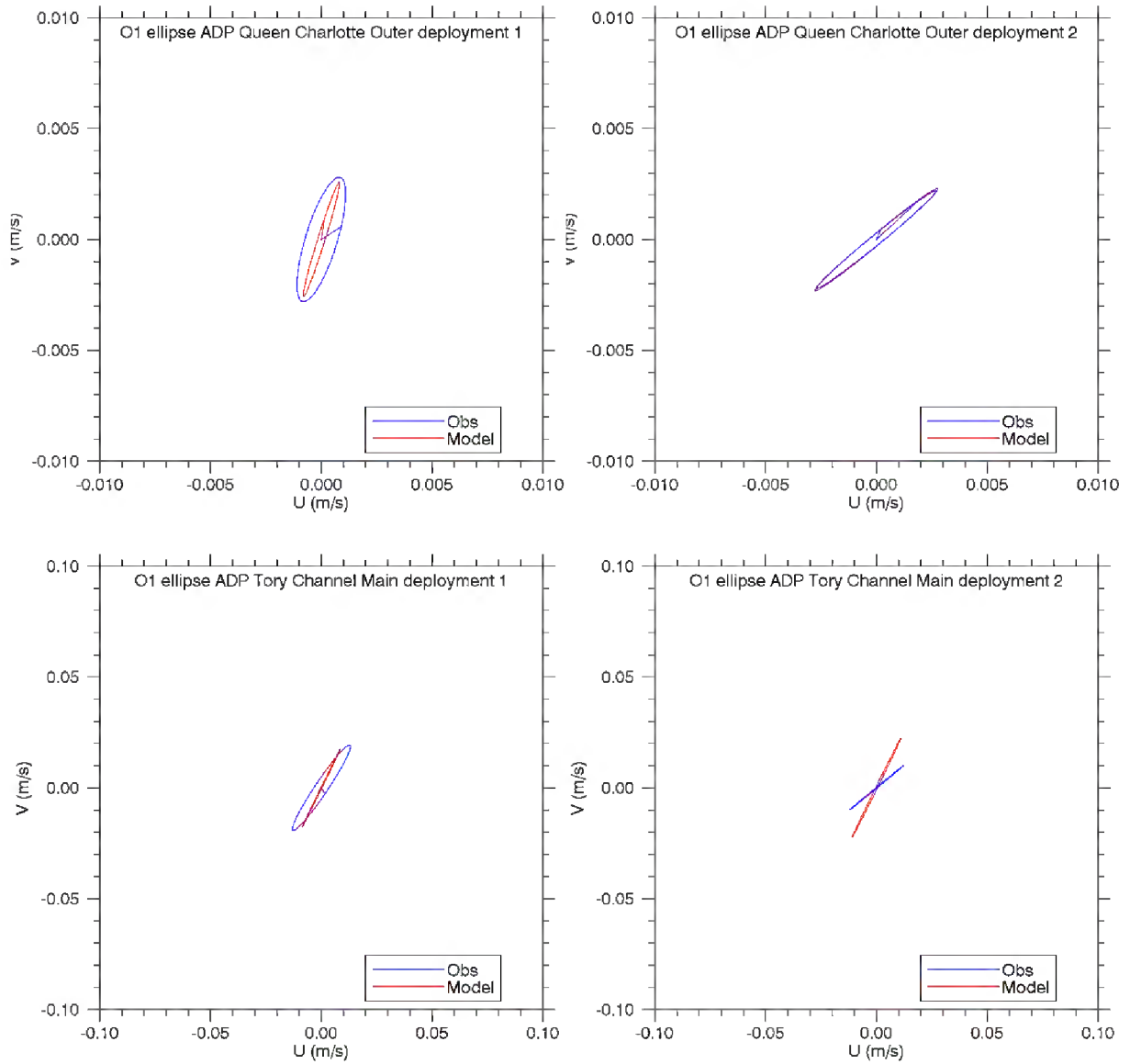


**Figure E-5: O<sub>1</sub> tidal velocity comparison.** As Figure E-3 but for the O<sub>1</sub> constituent.

## Tidal velocity tabulated parameters

**Table E-4: Comparison of M2 tidal ellipse parameters.** M2 tidal ellipse parameters from ADCP measurements and model. Here “ratio” means model value divided by measured value and “diffce” means model value minus measured value.

ADCP Site/Deployment	Semi-major axis (m/s)			Eccentricity			Inclination (°T)			Phase (°)		
	Meas.	Model	Ratio	Meas.	Model	Diffce	Meas.	Model	Diffce	Meas.	Model	Diffce
QCS Outer Deployment 1	0.085	0.070	<b>0.82</b>	-0.04	0.01	<b>0.04</b>	51.8	50.2	<b>-1.5</b>	174.8	153.7	<b>-21.1</b>
QCS Outer Deployment 2	0.085	0.068	<b>0.80</b>	-0.02	0.03	<b>0.05</b>	50.6	50.8	<b>0.1</b>	172.1	156.1	<b>-16.0</b>
Tory Channel Deployment 1	0.948	0.975	<b>1.03</b>	0.07	0.09	<b>0.02</b>	39.7	36.1	<b>-3.6</b>	356.8	350.5	<b>-6.3</b>
Tory Channel Deployment 2	0.941	0.975	<b>1.04</b>	0.06	0.09	<b>0.03</b>	43.9	36.1	<b>-7.9</b>	355.3	349.7	<b>-5.6</b>

**Table E-5: Comparison of S2 tidal ellipse parameters.** As Table E-4 but for the S2 constituent.

ADCP Site/Deployment	Semi-major axis (m/s)			Eccentricity			Inclination (°T)			Phase (°)		
	Meas.	Model	Ratio	Meas.	Model	Diffce	Meas.	Model	Diffce	Meas.	Model	Diffce
QCS Outer Deployment 1	0.028	0.030	<b>1.08</b>	0.03	0.06	<b>0.03</b>	50.2	46.3	<b>-3.9</b>	145.3	125.5	<b>-19.8</b>
QCS Outer Deployment 2	0.021	0.025	<b>1.18</b>	0.04	-0.04	<b>-0.07</b>	48.8	52.7	<b>3.8</b>	137.0	115.3	<b>-21.8</b>
Tory Channel Deployment 1	0.237	0.212	<b>0.90</b>	0.10	0.09	<b>-0.01</b>	37.9	34.7	<b>-3.1</b>	24.8	17.4	<b>-7.4</b>
Tory Channel Deployment 2	0.203	0.203	<b>1.00</b>	0.07	0.07	<b>0.00</b>	41.8	34.8	<b>-7.0</b>	17.8	4.6	<b>-13.2</b>

**Table E-6: Comparison of N2 tidal ellipse parameters.** As Table E-4 but for the N2 constituent.

ADCP Site/Deployment	Semi-major axis (m/s)			Eccentricity			Inclination (°T)			Phase (°)		
	Meas.	Model	Ratio	Meas.	Model	Diffce	Meas.	Model	Diffce	Meas.	Model	Diffce
QCS Outer Deployment 1	0.017	0.014	<b>0.81</b>	-0.02	0.06	<b>0.07</b>	51.6	50.3	<b>-1.3</b>	138.3	114.6	<b>-23.7</b>
QCS Outer Deployment 2	0.028	0.023	<b>0.82</b>	0.01	0.04	<b>0.03</b>	49.4	51.2	<b>1.9</b>	153.6	134.0	<b>-19.5</b>
Tory Channel Deployment 1	0.157	0.158	<b>1.00</b>	0.10	0.09	<b>-0.01</b>	35.7	34.8	<b>-0.8</b>	317.2	310.8	<b>-6.4</b>
Tory Channel Deployment 2	0.257	0.254	<b>0.99</b>	0.05	0.07	<b>0.02</b>	42.5	35.2	<b>-7.3</b>	332.0	326.4	<b>-5.6</b>

**Table E-7: Comparison of O1 tidal ellipse parameters.** As Table E-4 but for the O<sub>1</sub> constituent.

ADCP Site/Deployment	Semi-major axis (m/s)			Eccentricity			Inclination (°T)			Phase (°)		
	Meas.	Model	Ratio	Meas.	Model	Diffce	Meas.	Model	Diffce	Meas.	Model	Diffce
QCS Outer Deployment 1	0.023	0.019	<b>0.84</b>	0.12	-0.01	<b>-0.14</b>	33.9	26.1	<b>-7.8</b>	93.1	78.3	<b>-14.7</b>
QCS Outer Deployment 2	0.016	0.025	<b>1.56</b>	0.01	0.02	<b>0.00</b>	50.6	26.2	<b>-24.4</b>	79.7	94.3	<b>14.6</b>
Tory Channel Deployment 1	0.003	0.003	<b>0.96</b>	-0.23	0.09	<b>0.33</b>	16.9	17.6	<b>0.8</b>	286.7	290.6	<b>3.9</b>
Tory Channel Deployment 2	0.003	0.003	<b>1.01</b>	0.08	0.06	<b>-0.02</b>	47.7	46.3	<b>-1.4</b>	281.9	317.1	<b>35.2</b>

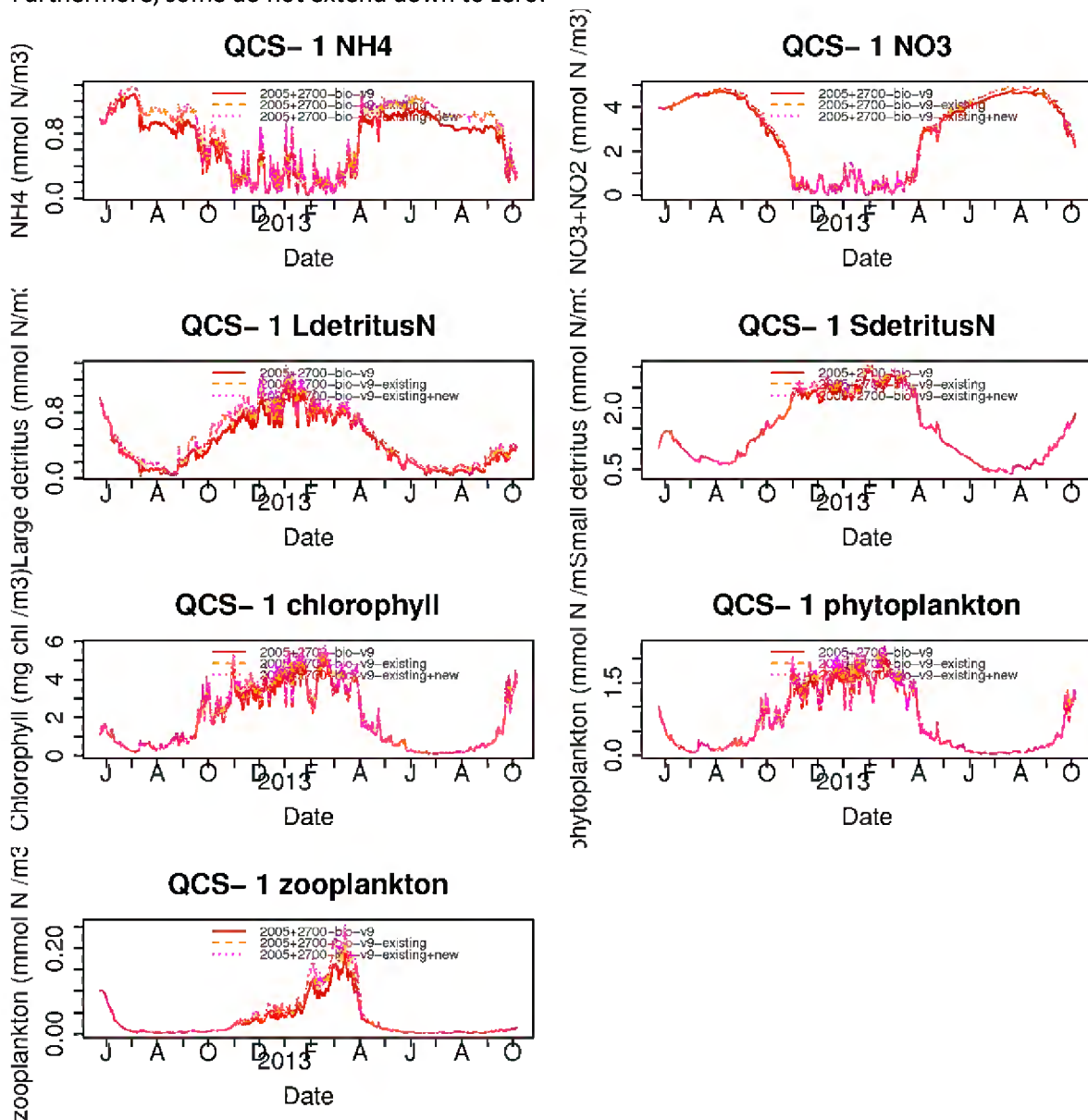
## Sub-tidal velocity tabulated parameters

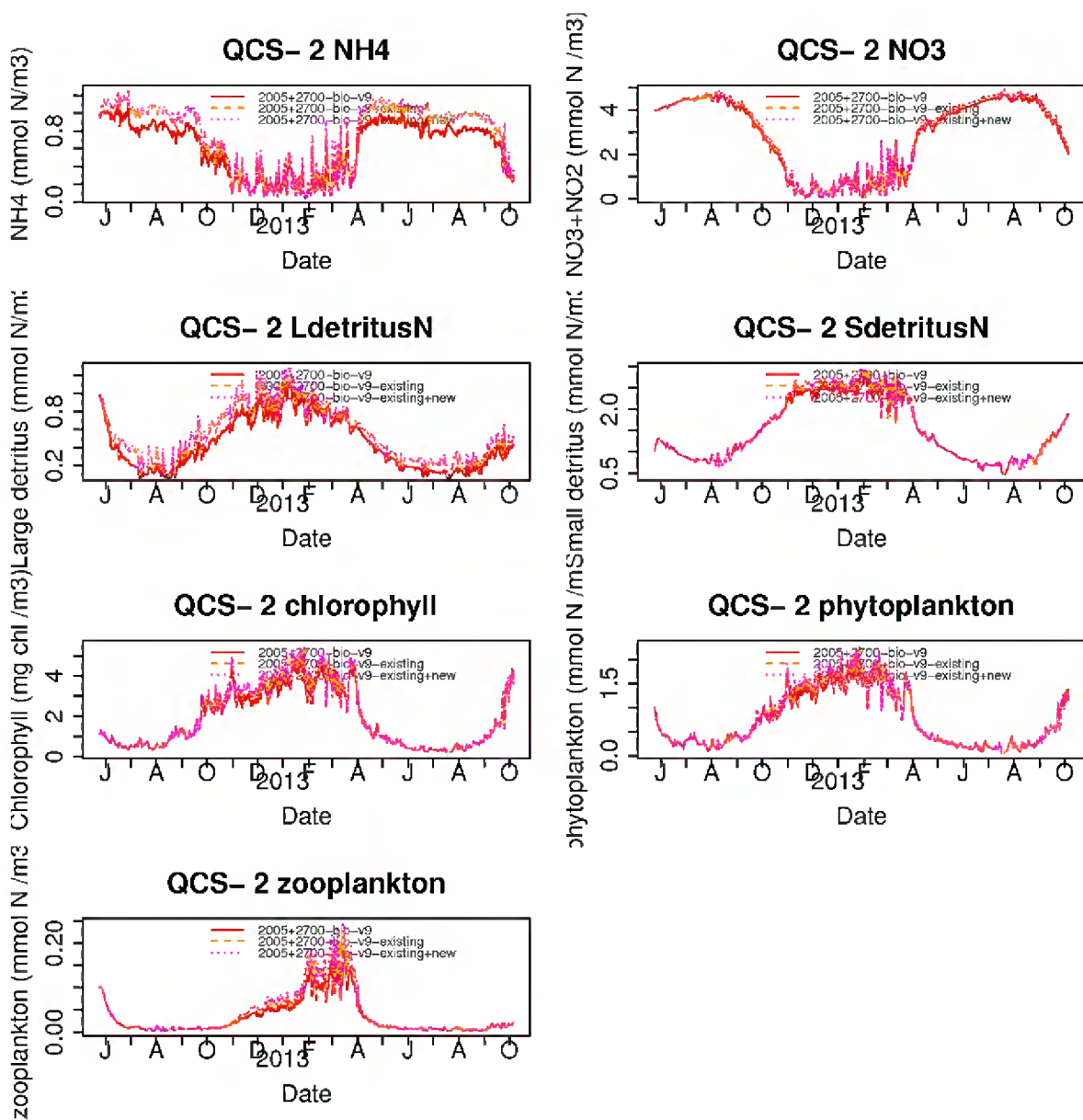
**Table E-8: Sub-tidal velocity comparison.** Sub-tidal mean and variance ellipse parameters from ADCP measurements and model, and temporal correlations between measured and modelled time series. Here “ratio” means model value divided by measured value and “diffce” means model value minus measured value.

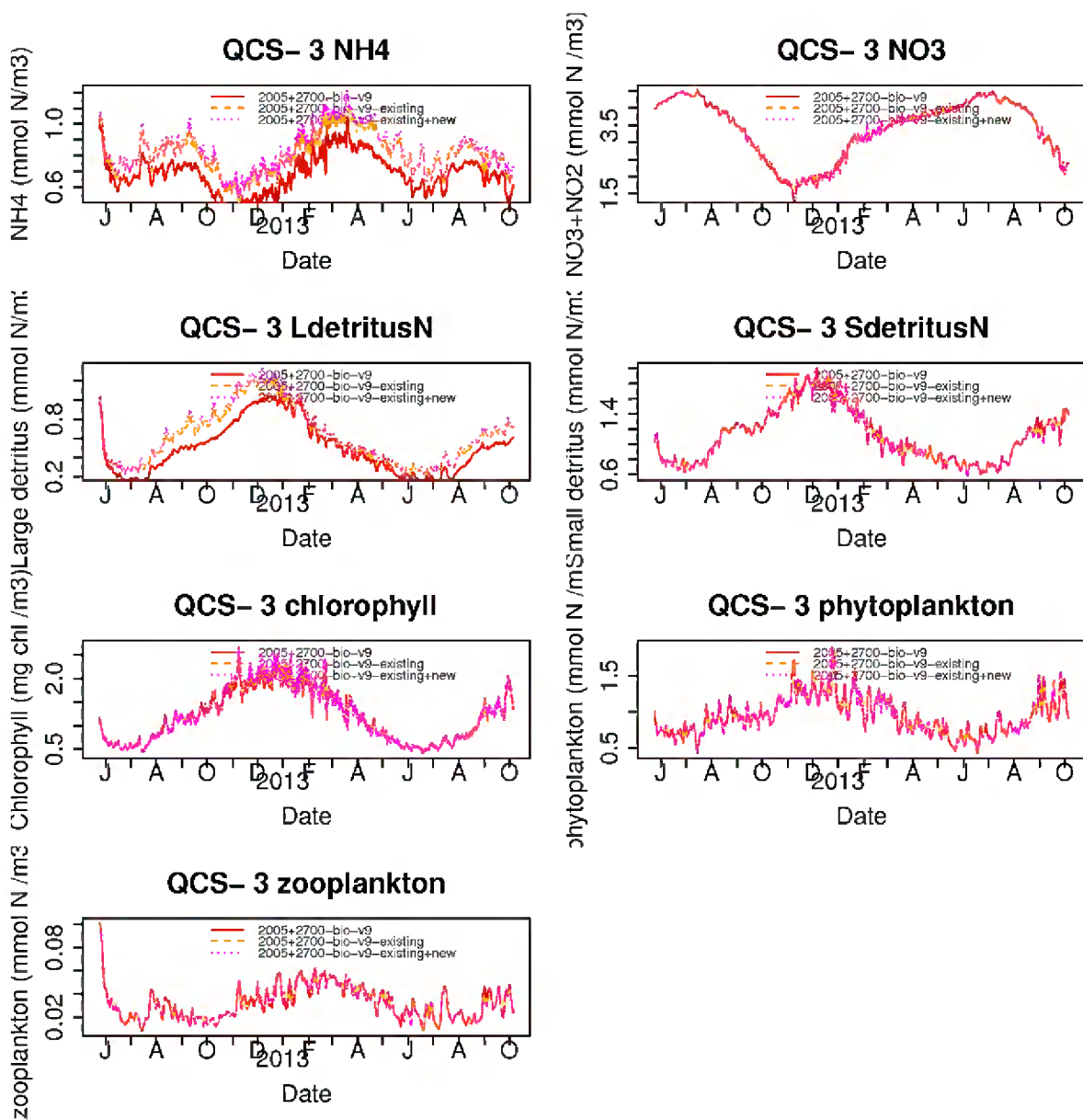
ADCP Site & Deployment	Mean magnitude (m/s)			Mean direction (°T)			Semi-major axis (m/s)			Eccentricity			Inclination (°T)			Correlation	
	Meas.	Model	Diffce	Meas.	Model	Diffce	Meas.	Model	Ratio	Meas.	Model	Diffce	Meas.	Model	Diffce	Along-axis	Across-axis
QCS Outer Dep. 1	0.009	0.008	<b>-0.001</b>	353.1	332.6	<b>-20.5</b>	0.011	0.014	<b>1.18</b>	0.64	0.66	<b>0.02</b>	74.9	35.6	<b>-39.4</b>	-0.14	0.49
QCS Outer Dep. 2	0.015	0.013	<b>-0.002</b>	0.1	29.2	<b>29.0</b>	0.012	0.017	<b>1.33</b>	0.64	0.47	<b>-0.17</b>	58.4	64.6	<b>6.2</b>	0.60	0.58
Tory Channel Dep. 1	0.066	0.045	<b>-0.020</b>	253.1	118.2	<b>-134.9</b>	0.046	0.044	<b>0.95</b>	0.24	0.27	<b>0.03</b>	34.1	26.7	<b>-7.3</b>	0.83	0.47
Tory Channel Dep. 2	0.089	0.060	<b>-0.029</b>	246.8	164.2	<b>-82.6</b>	0.037	0.044	<b>1.19</b>	0.28	0.26	<b>-0.02</b>	34.2	31.4	<b>-2.7</b>	0.72	0.38

## Appendix F Time-series of simulated water quality at the Marlborough District Council sampling sites under differing scenarios.

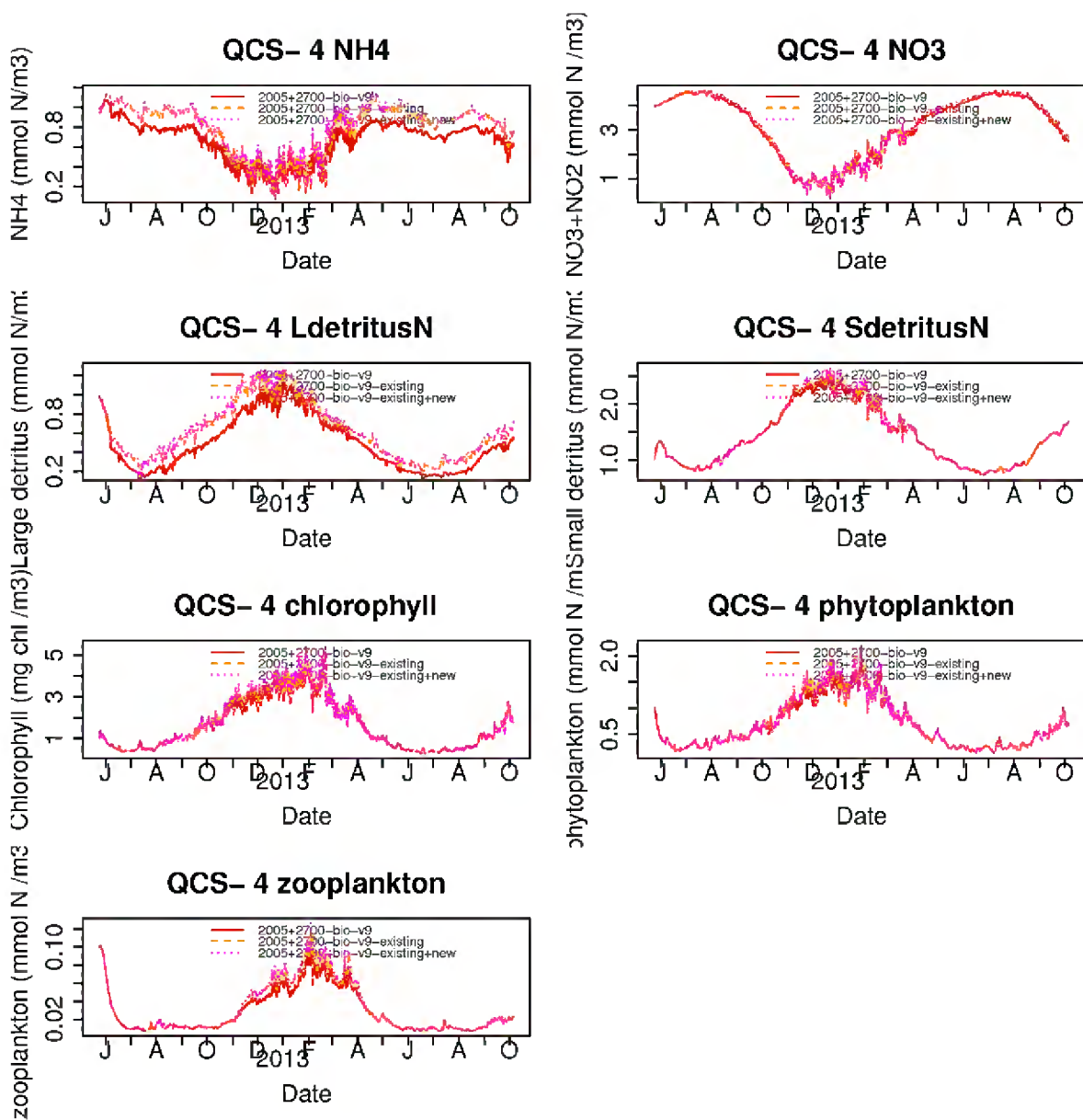
The solid red lines (2005+2700-bio-v9) are results from the *no farms* scenario. The dashed lines (2005+2700-bio-v9-existing) are from the *existing farms* scenario. The dotted lines (2005+2700-bio-v9-new) are from the *approved farms* scenario. Denitrification was operating in all the simulations. Note that, to maximise the detail that can be resolved within the plots, the numerical scales on the y-axes differ across variables. For some of the variables, the scales also differ across stations. Furthermore, some do not extend down to zero.

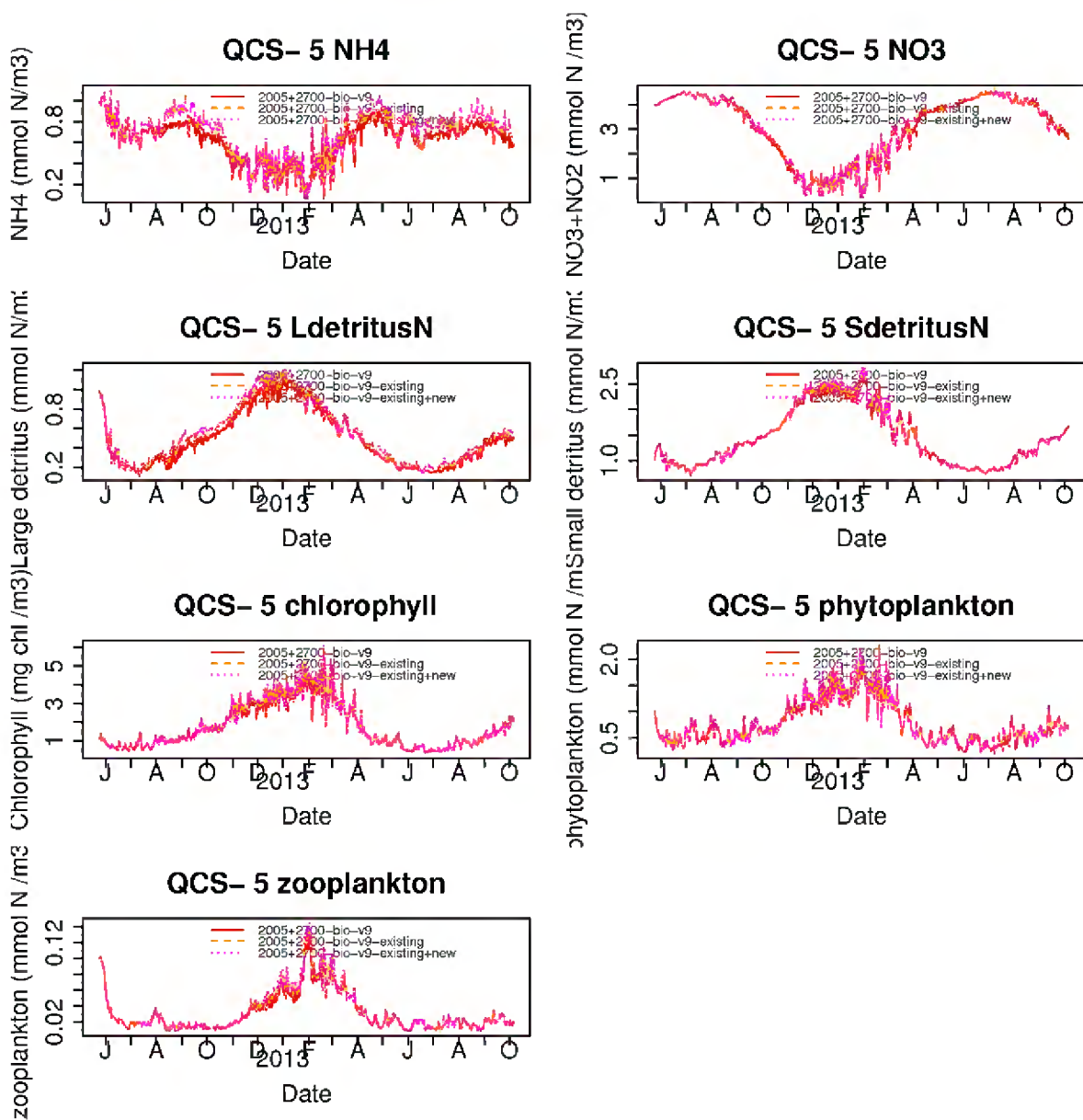












## Appendix G Enlarged images of simulation results

In this appendix, we present the simulation results in a larger format. Specifically, on each page, we present results for just one state-variable. Each page contains three images. The left-hand most is the time-averaged concentration for the state variable under the baseline scenario. The remaining two are concentration differences under an alternative scenario. The inset text within each figure provides the information with which to interpret the figure:

Row	Explanation
1	The state variable and layer being plotted (layer 20 is the surface most layer)
2	The base path where plots are to be found
3	The results file used to construct the baseline concentration plot (left- hand image)
4	The results used to construct the central image
5	The results used to construct the right-hand image
6	The time-period being plotted (seconds from 1 Jan 2005)
7	Is the colour-scale scale logarithmic or linear
8	Number of time-levels contributing to the time-average

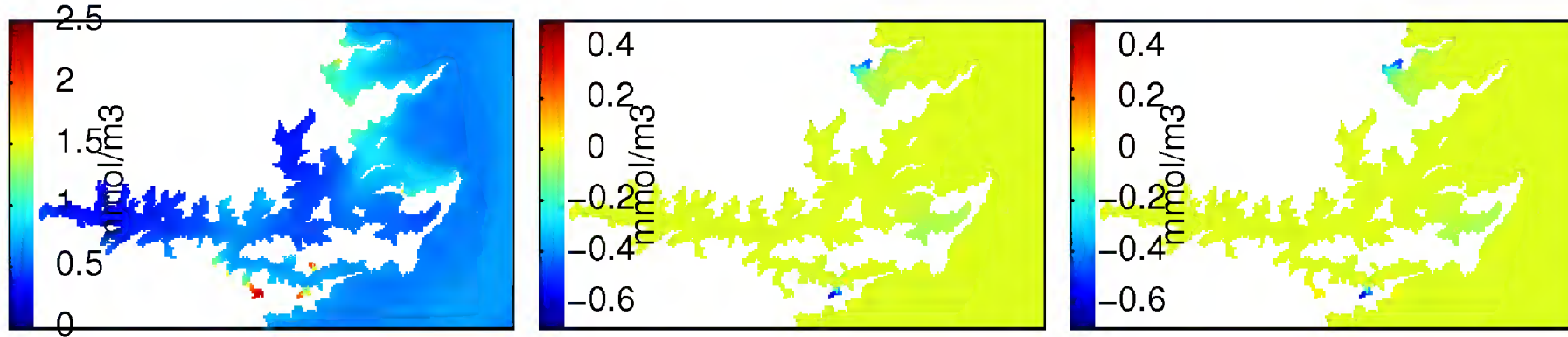
The scenarios associated with each image can be inferred using the information in this table:

Path	Explanation
Run18/2005+2700-bio-v9	The <i>nofarms+denitrification</i> simulation: our baseline
Run18/2005+2700-bio-v9-existing-mussels	The <i>existing mussel farms + denitrification</i> simulation (no fish farms)
Run18/2005+2700-bio-v9-existing	The <i>existing mussel and fish farms with denitrification</i> simulation
Run18/2005+2700-bio-v9-existing+new	The <i>approved farms + denitrification</i> simulation

Path	Explanation
Run18/2005+2700-bio-v9nd	The <i>no farms, no denitrification</i> simulation
Run18/2005+2700-bio-v9nd-existing+new	The <i>approved farms without denitrification</i> simulations
	262850400–273391200: the winter period
	243151200–257493600: the summer period

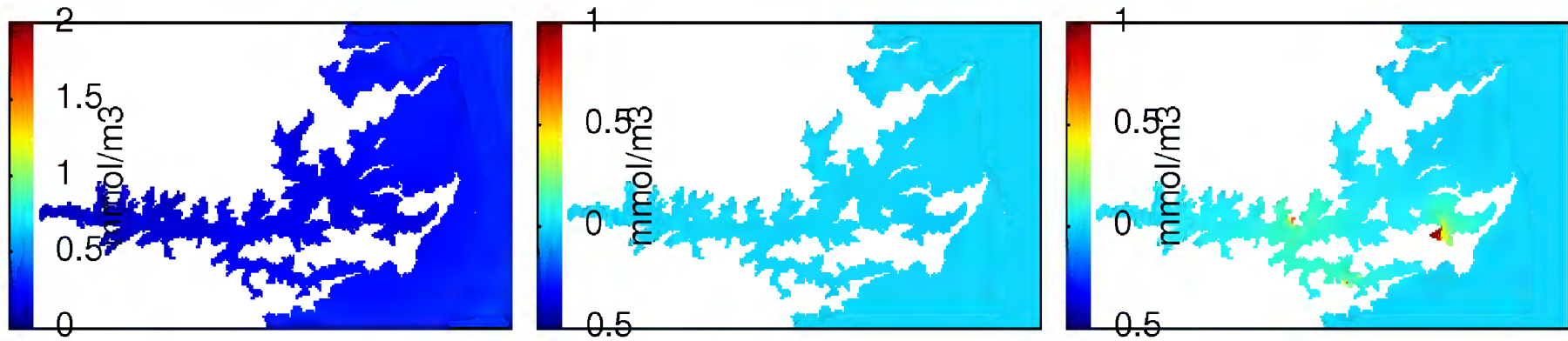
# Comparison of *no farms*, *existing mussel farms* and *existing mussel+fish farms* (with denitrification)

Winter



```
+chlorophyll in layer 20
/mnt/projects_welwfs07/MDC13301/Working/niall/hpcf/R

/mnt/projects_welwfs07/MDC13301/Working/Mark/Data/Model output/run18/2005+2700-bio-v9/roms_avg_0001.nc
/mnt/projects_welwfs07/MDC13301/Working/Mark/Data/Model output/run18/2005+2700-bio-v9-existing-mussels/roms_avg_0001.nc
/mnt/projects_welwfs07/MDC13301/Working/Mark/Data/Model output/run18/2005+2700-bio-v9-existing/roms_avg_0001.nc
time range: 262850400 273391200
[log(conc)?, log(change)]=[ FALSE , FALSE ] is.rel.conc= FALSE
n.sample= 245
```

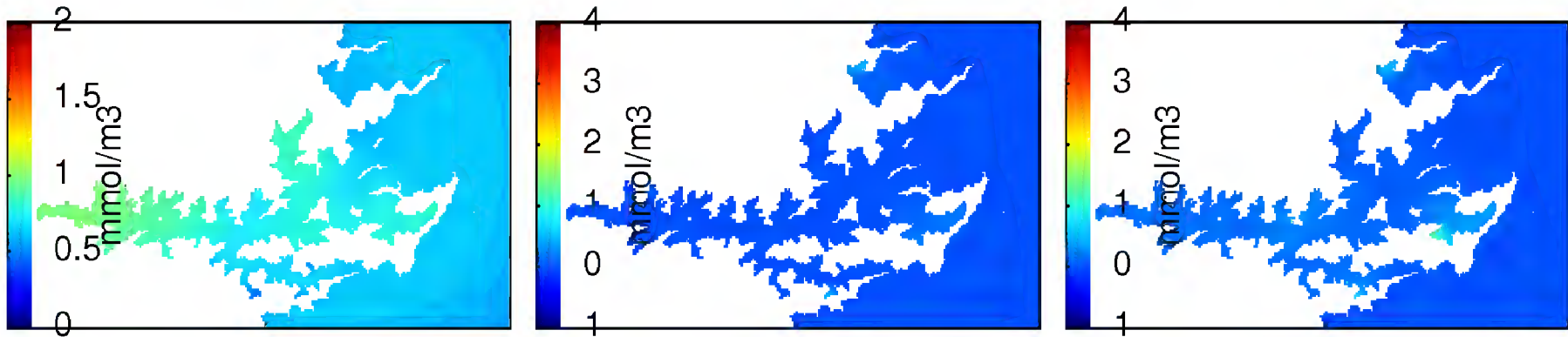


```

+LdetritusN in layer 20
/mnt/projects_welwfs07/MDC13301/Working/niall/hpcf/R

/mnt/projects_welwfs07/MDC13301/Working/Mark/Data/Model output/run18/2005+2700-bio-v9/roms_avg_0001.nc
/mnt/projects_welwfs07/MDC13301/Working/Mark/Data/Model output/run18/2005+2700-bio-v9-existing-mussels/roms_avg_0001.nc
/mnt/projects_welwfs07/MDC13301/Working/Mark/Data/Model output/run18/2005+2700-bio-v9-existing/roms_avg_0001.nc
time range: 262850400 273391200
[log(conc)?, log(change)]=[ FALSE , FALSE ] is.rel.conc= FALSE
n.sample= 245

```

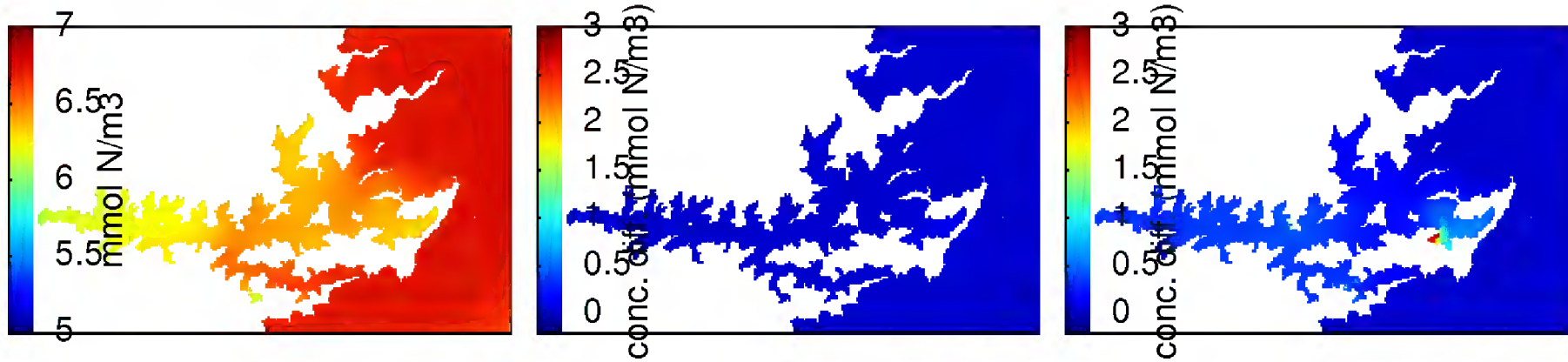


```

+NH4 in layer 20
/mnt/projects_welwfs07/MDC13301/Working/niall/hpcf/R

/mnt/projects_welwfs07/MDC13301/Working/Mark/Data/Model output/run18/2005+2700-bio-v9/roms_avg_0001.nc
/mnt/projects_welwfs07/MDC13301/Working/Mark/Data/Model output/run18/2005+2700-bio-v9-existing-mussels/roms_avg_0001.nc
/mnt/projects_welwfs07/MDC13301/Working/Mark/Data/Model output/run18/2005+2700-bio-v9-existing/roms_avg_0001.nc
time range: 262850400 273391200
[log(conc)?, log(change)]=[ FALSE , FALSE ] is.rel.conc= FALSE
n.sample= 245

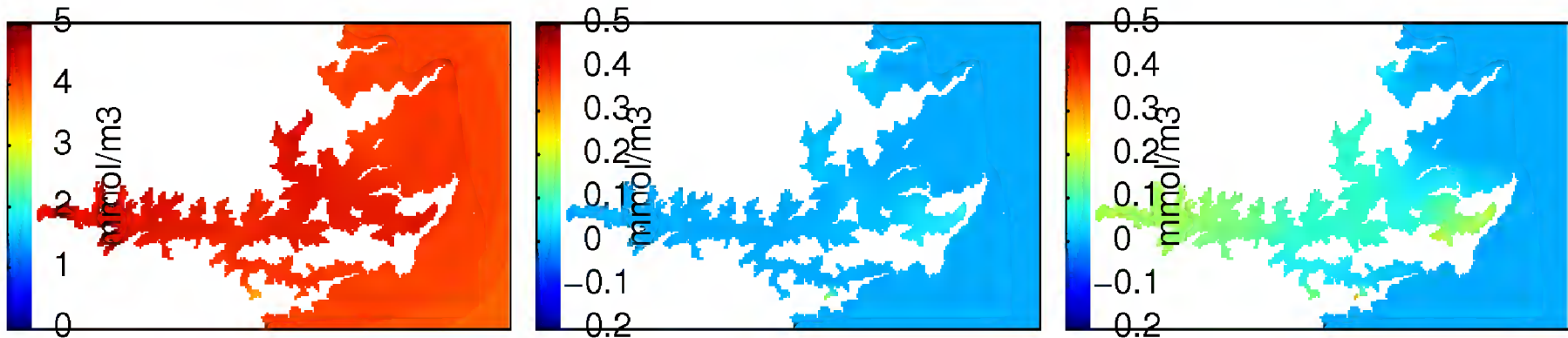
```



+NH4+NO3+SdetritusN+LdetritusN+phytoplankton+zooplankton in layer 20  
 /mnt/projects\_welwfs07/MDC13301/Working/niall/hpcf/R

/mnt/projects\_welwfs07/MDC13301/Working/Mark/Data/Model output/run18/2005+2700-bio-v9/roms\_avg\_0001.nc  
 /mnt/projects\_welwfs07/MDC13301/Working/Mark/Data/Model output/run18/2005+2700-bio-v9-existing-mussels/roms\_avg\_0001.nc  
 /mnt/projects\_welwfs07/MDC13301/Working/Mark/Data/Model output/run18/2005+2700-bio-v9-existing/roms\_avg\_0001.nc  
 time range: 262850400 273391200  
 [log(conc)?, log(change)]=[ FALSE , FALSE ] is.rel.conc= FALSE  
 n.sample= 245



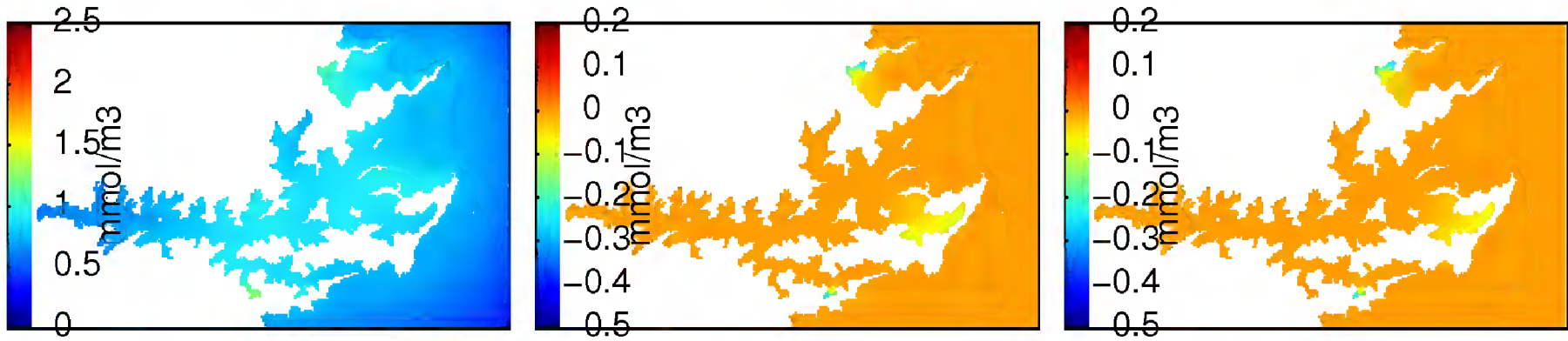


```

+NO3 in layer 20
/mnt/projects_welwfs07/MDC13301/Working/niall/hpcf/R

/mnt/projects_welwfs07/MDC13301/Working/Mark/Data/Model output/run18/2005+2700-bio-v9/roms_avg_0001.nc
/mnt/projects_welwfs07/MDC13301/Working/Mark/Data/Model output/run18/2005+2700-bio-v9-existing-mussels/roms_avg_0001.nc
/mnt/projects_welwfs07/MDC13301/Working/Mark/Data/Model output/run18/2005+2700-bio-v9-existing/roms_avg_0001.nc
time range: 262850400 273391200
[log(conc)?, log(change)]=[ FALSE , FALSE ] is.rel.conc= FALSE
n.sample= 245

```

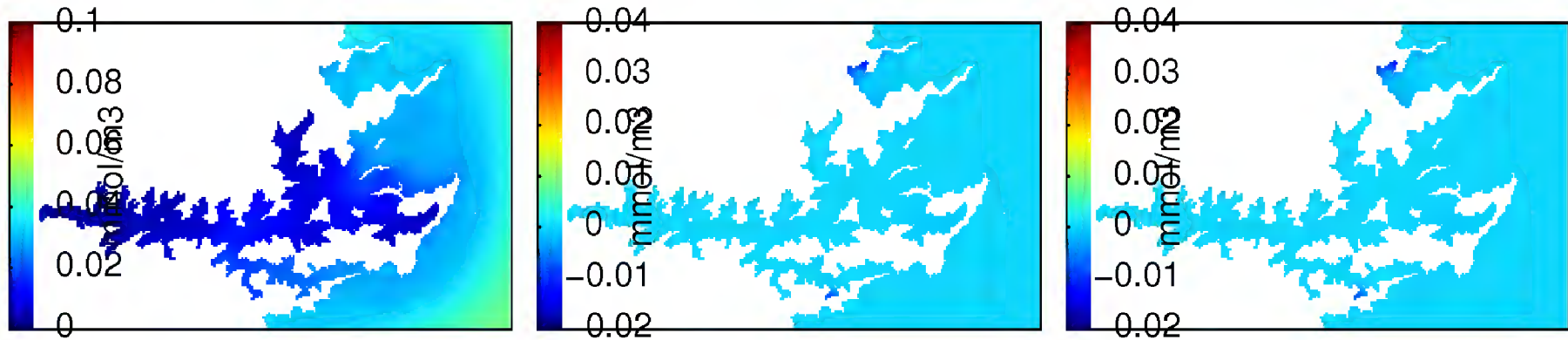


```

+SdetritusN in layer 20
/mnt/projects_welwfs07/MDC13301/Working/niall/hpcf/R

/mnt/projects_welwfs07/MDC13301/Working/Mark/Data/Model output/run18/2005+2700-bio-v9/roms_avg_0001.nc
/mnt/projects_welwfs07/MDC13301/Working/Mark/Data/Model output/run18/2005+2700-bio-v9-existing-mussels/roms_avg_0001.nc
/mnt/projects_welwfs07/MDC13301/Working/Mark/Data/Model output/run18/2005+2700-bio-v9-existing/roms_avg_0001.nc
time range: 262850400 273391200
[log(conc)?, log(change)]=[ FALSE , FALSE ] is.rel.conc= FALSE
n.sample= 245

```



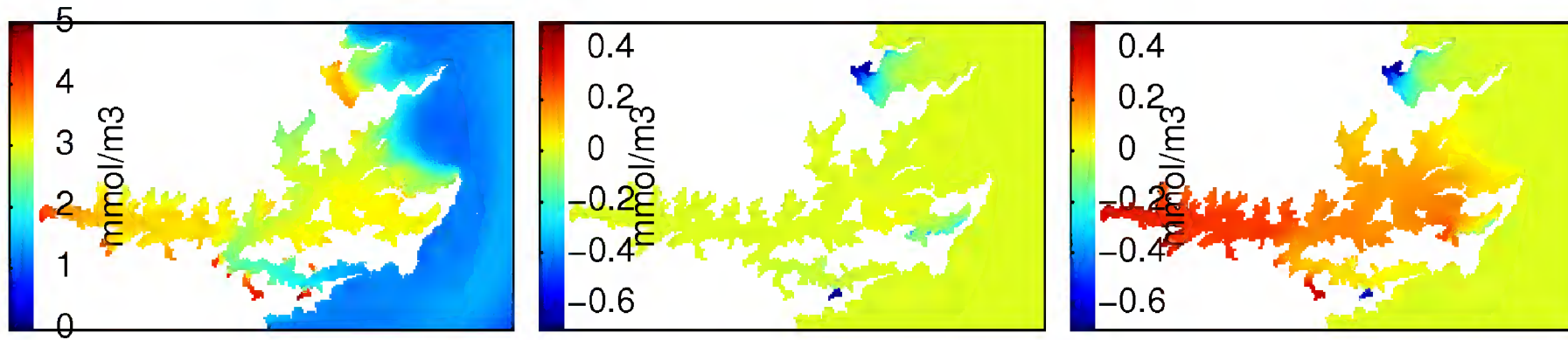
```

+zooplankton in layer 20
/mnt/projects_welwfs07/MDC13301/Working/niall/hpcf/R

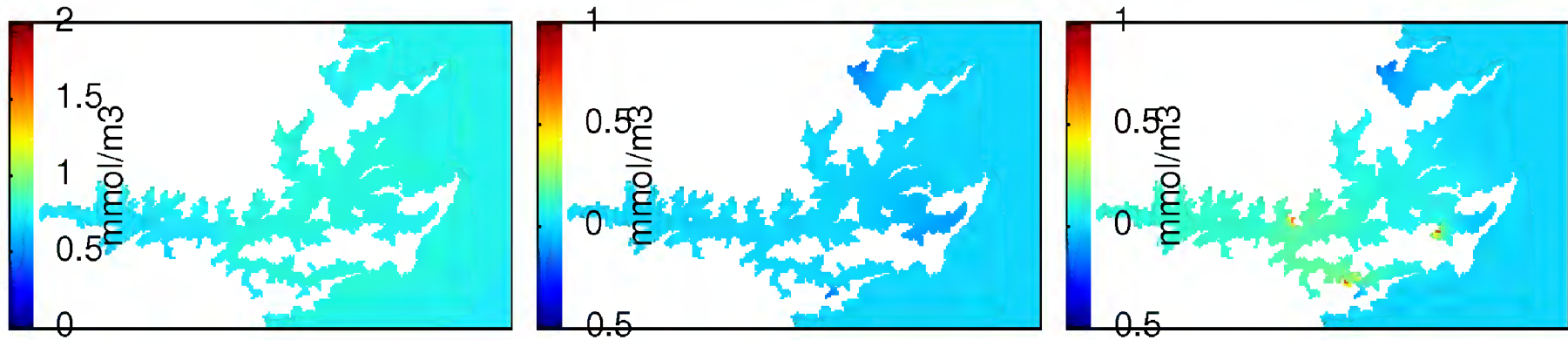
/mnt/projects_welwfs07/MDC13301/Working/Mark/Data/Model output/run18/2005+2700-bio-v9/roms_avg_0001.nc
/mnt/projects_welwfs07/MDC13301/Working/Mark/Data/Model output/run18/2005+2700-bio-v9-existing-mussels/roms_avg_0001.nc
/mnt/projects_welwfs07/MDC13301/Working/Mark/Data/Model output/run18/2005+2700-bio-v9-existing/roms_avg_0001.nc
time range: 262850400 273391200
[log(conc)?, log(change)]=[ FALSE , FALSE ] is.rel.conc= FALSE
n.sample= 245

```

Summer



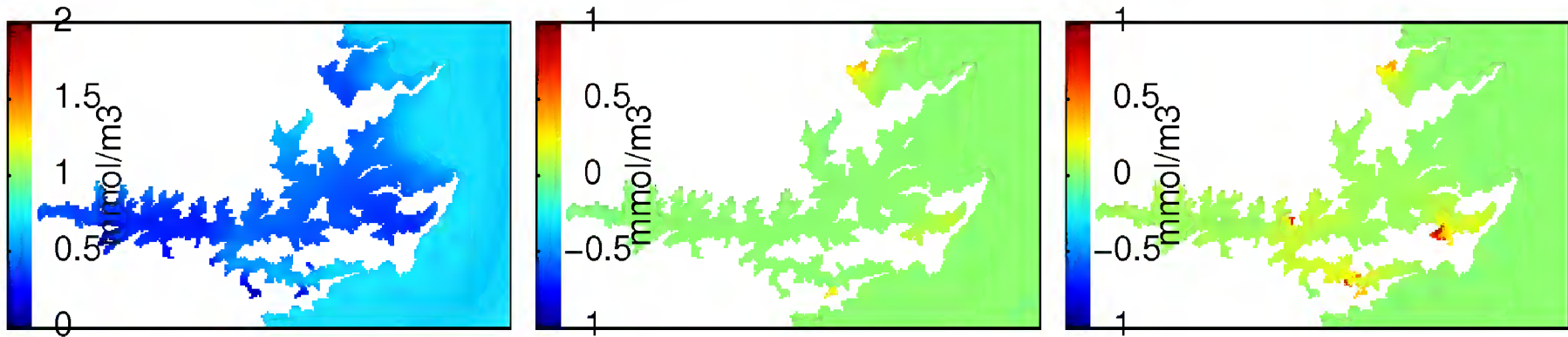
```
+chlorophyll in layer 20
/mnt/projects_welwfs07/MDC13301/Working/niall/hpcf/R
/mnt/projects_welwfs07/MDC13301/Working/Mark/Data/Model output/run18/2005+2700-bio-v9/roms_avg_0001.nc
/mnt/projects_welwfs07/MDC13301/Working/Mark/Data/Model output/run18/2005+2700-bio-v9-existing-mussels/roms_avg_0001.nc
/mnt/projects_welwfs07/MDC13301/Working/Mark/Data/Model output/run18/2005+2700-bio-v9-existing/roms_avg_0001.nc
time range: 243151200 257493600
[log(conc)?, log(change)]=[ FALSE , FALSE ] is.rel.conc= FALSE
n.sample= 333
```



+LdetritusN in layer 20  
 /mnt/projects\_welwfs07/MDC13301/Working/niall/hpcf/R

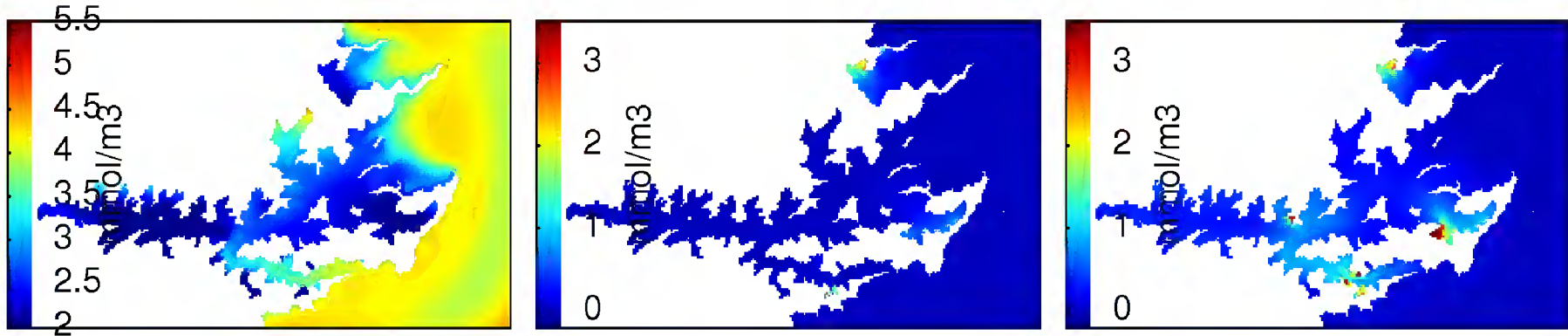
/mnt/projects\_welwfs07/MDC13301/Working/Mark/Data/Model output/run18/2005+2700-bio-v9/roms\_avg\_0001.nc  
 /mnt/projects\_welwfs07/MDC13301/Working/Mark/Data/Model output/run18/2005+2700-bio-v9-existing-mussels/roms\_avg\_0001.nc  
 /mnt/projects\_welwfs07/MDC13301/Working/Mark/Data/Model output/run18/2005+2700-bio-v9-existing/roms\_avg\_0001.nc

time range: 243151200 257493600  
 [log(conc)?, log(change)]=[ FALSE , FALSE ] is.rel.conc= FALSE  
 n.sample= 333



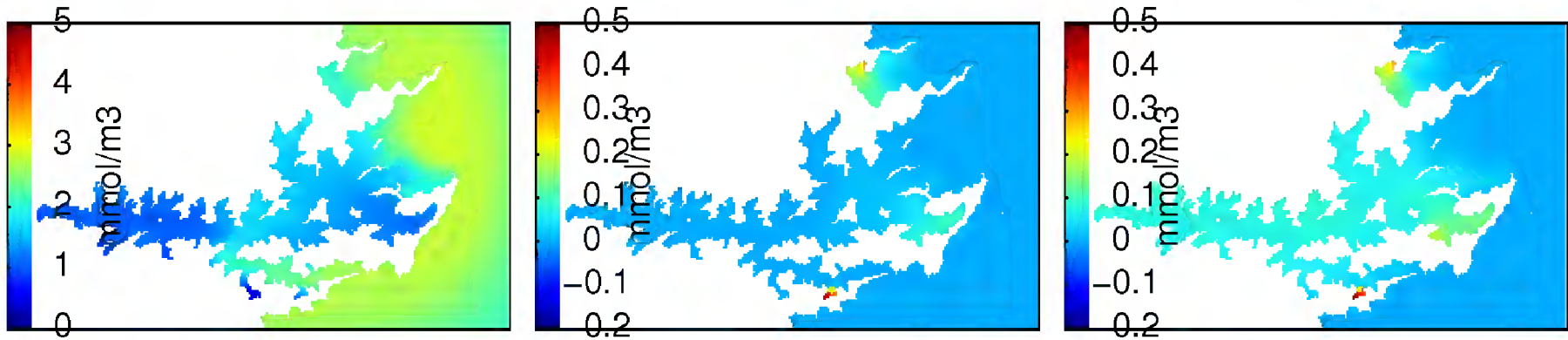
+NH4 in layer 20  
 /mnt/projects\_welwfs07/MDC13301/Working/niall/hpcf/R

/mnt/projects\_welwfs07/MDC13301/Working/Mark/Data/Model output/run18/2005+2700-bio-v9/roms\_avg\_0001.nc  
 /mnt/projects\_welwfs07/MDC13301/Working/Mark/Data/Model output/run18/2005+2700-bio-v9-existing-mussels/roms\_avg\_0001.nc  
 /mnt/projects\_welwfs07/MDC13301/Working/Mark/Data/Model output/run18/2005+2700-bio-v9-existing/roms\_avg\_0001.nc  
 time range: 243151200 257493600  
 [log(conc)?, log(change)]=[ FALSE , FALSE ] is.rel.conc= FALSE  
 n.sample= 333



+NH4+NO3+SDetN+LDetN+phytoplankton+zooplankton in layer 20  
 /mnt/projects\_welwfs07/MDC13301/Working/niall/hpcf/R

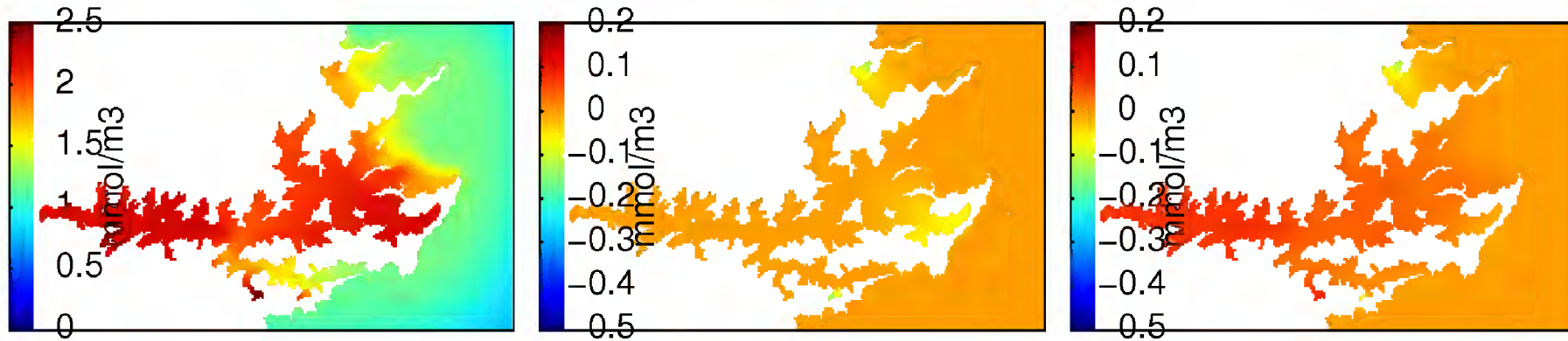
/mnt/projects\_welwfs07/MDC13301/Working/Mark/Data/Model output/run18/2005+2700-bio-v9/roms\_avg\_0001.nc  
 /mnt/projects\_welwfs07/MDC13301/Working/Mark/Data/Model output/run18/2005+2700-bio-v9-existing-mussels/roms\_avg\_0001.nc  
 /mnt/projects\_welwfs07/MDC13301/Working/Mark/Data/Model output/run18/2005+2700-bio-v9-existing/roms\_avg\_0001.nc  
 time range: 243151200 257493600  
 [log(conc)?, log(change)]=[ FALSE , FALSE ] is.rel.conc= FALSE  
 n.sample= 333



+NO3 in layer 20  
 /mnt/projects\_welwfs07/MDC13301/Working/niall/hpcf/R

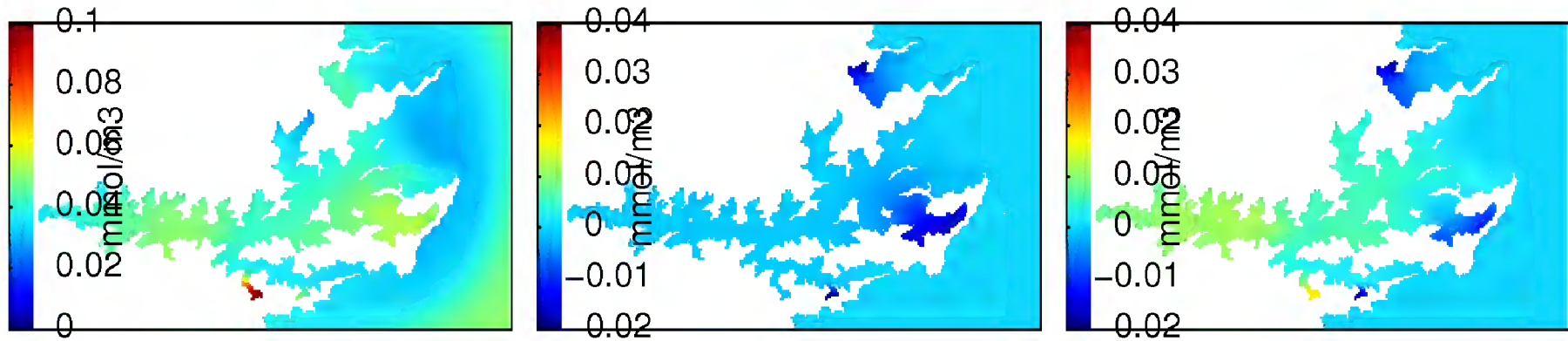
/mnt/projects\_welwfs07/MDC13301/Working/Mark/Data/Model output/run18/2005+2700-bio-v9/roms\_avg\_0001.nc  
 /mnt/projects\_welwfs07/MDC13301/Working/Mark/Data/Model output/run18/2005+2700-bio-v9-existing-mussels/roms\_avg\_0001.nc  
 /mnt/projects\_welwfs07/MDC13301/Working/Mark/Data/Model output/run18/2005+2700-bio-v9-existing/roms\_avg\_0001.nc  
 time range: 243151200 257493600  
 [log(conc)?, log(change)]=[ FALSE , FALSE ] is.rel.conc= FALSE  
 n.sample= 333





+SdetritusN in layer 20  
 /mnt/projects\_welwfs07/MDC13301/Working/niall/hpcf/R

/mnt/projects\_welwfs07/MDC13301/Working/Mark/Data/Model output/run18/2005+2700-bio-v9/roms\_avg\_0001.nc  
 /mnt/projects\_welwfs07/MDC13301/Working/Mark/Data/Model output/run18/2005+2700-bio-v9-existing-mussels/roms\_avg\_0001.nc  
 /mnt/projects\_welwfs07/MDC13301/Working/Mark/Data/Model output/run18/2005+2700-bio-v9-existing/roms\_avg\_0001.nc  
 time range: 243151200 257493600  
 [log(conc)?, log(change)]=[ FALSE , FALSE ] is.rel.conc= FALSE  
 n.sample= 333



```

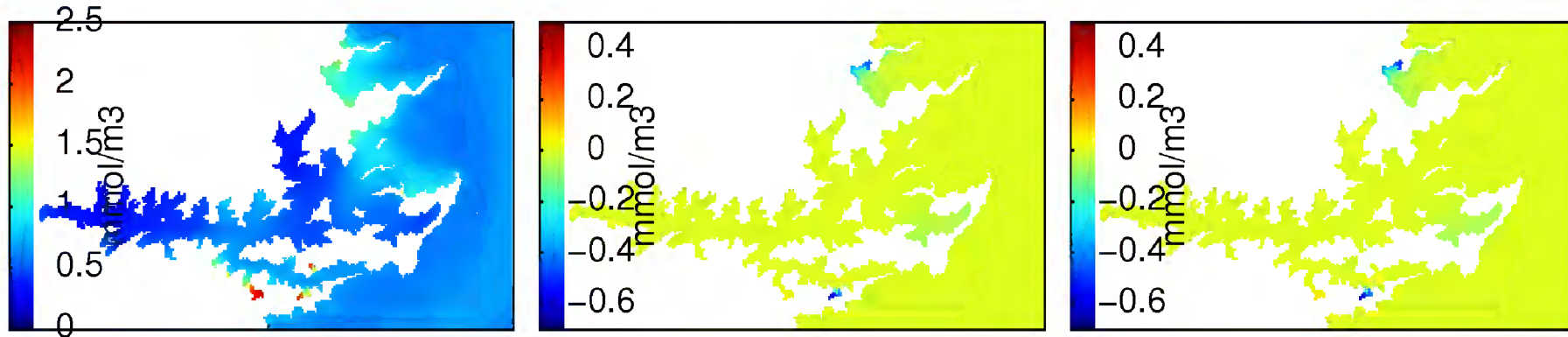
+zooplankton in layer 20
/mnt/projects_welwfs07/MDC13301/Working/niall/hpcf/R

/mnt/projects_welwfs07/MDC13301/Working/Mark/Data/Model output/run18/2005+2700-bio-v9/roms_avg_0001.nc
/mnt/projects_welwfs07/MDC13301/Working/Mark/Data/Model output/run18/2005+2700-bio-v9-existing-mussels/roms_avg_0001.nc
/mnt/projects_welwfs07/MDC13301/Working/Mark/Data/Model output/run18/2005+2700-bio-v9-existing/roms_avg_0001.nc
time range: 243151200 257493600
[log(conc)?, log(change)]=[ FALSE , FALSE ] is.rel.conc= FALSE
n.sample= 333

```

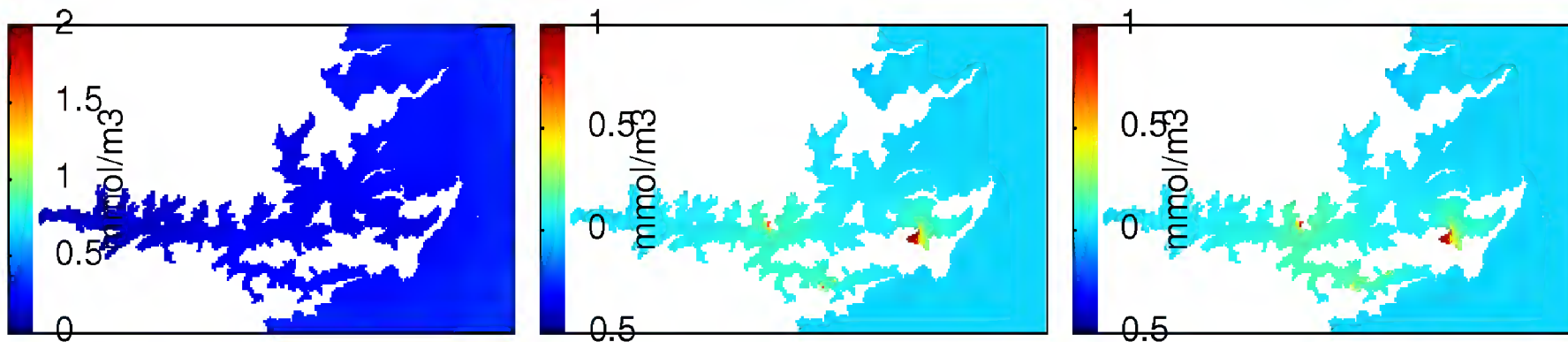
## Comparison of *no farms*, *existing farms* and *approved mussel+fish farms* (with denitrification)

Winter



```
+chlorophyll in layer 20
/mnt/projects_welwfs07/MDC13301/Working/niall/hpcf/R

/mnt/projects_welwfs07/MDC13301/Working/Mark/Data/Model output/run18/2005+2700-bio-v9/roms_avg_0001.nc
/mnt/projects_welwfs07/MDC13301/Working/Mark/Data/Model output/run18/2005+2700-bio-v9-existing/roms_avg_0001.nc
/mnt/projects_welwfs07/MDC13301/Working/Mark/Data/Model output/run18/2005+2700-bio-v9-existing+new/roms_avg_0001.nc
time range: 262850400 273391200
[log(conc)?, log(change)]=[ FALSE , FALSE ] is.rel.conc= FALSE
n.sample= 245
```

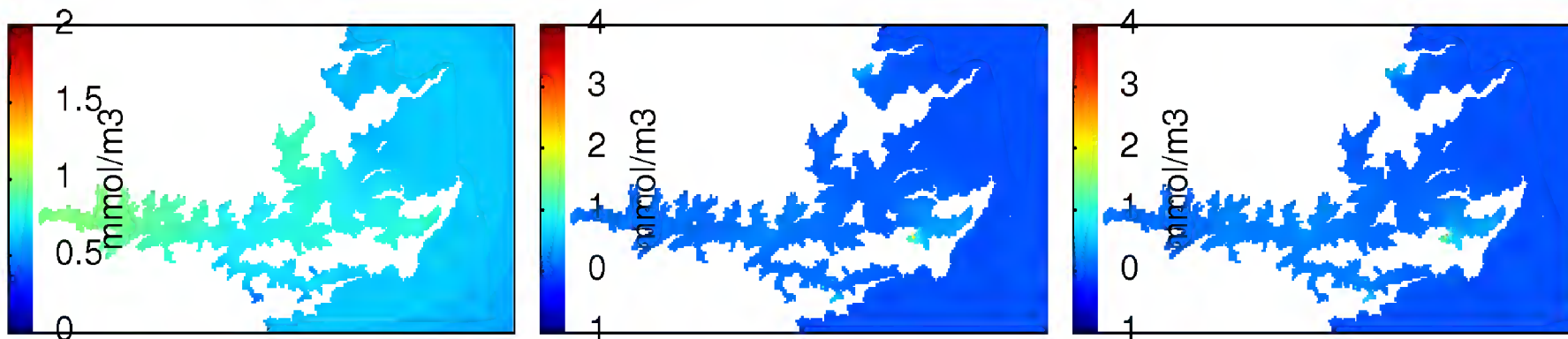


```

+LdetritusN in layer 20
/mnt/projects_welwfs07/MDC13301/Working/niall/hpcf/R

/mnt/projects_welwfs07/MDC13301/Working/Mark/Data/Model output/run18/2005+2700-bio-v9/roms_avg_0001.nc
/mnt/projects_welwfs07/MDC13301/Working/Mark/Data/Model output/run18/2005+2700-bio-v9-existing/roms_avg_0001.nc
/mnt/projects_welwfs07/MDC13301/Working/Mark/Data/Model output/run18/2005+2700-bio-v9-existing+new/roms_avg_0001.nc
time range: 262850400 273391200
[log(conc)?, log(change)]=[ FALSE , FALSE ] is.rel.conc= FALSE
n.sample= 245

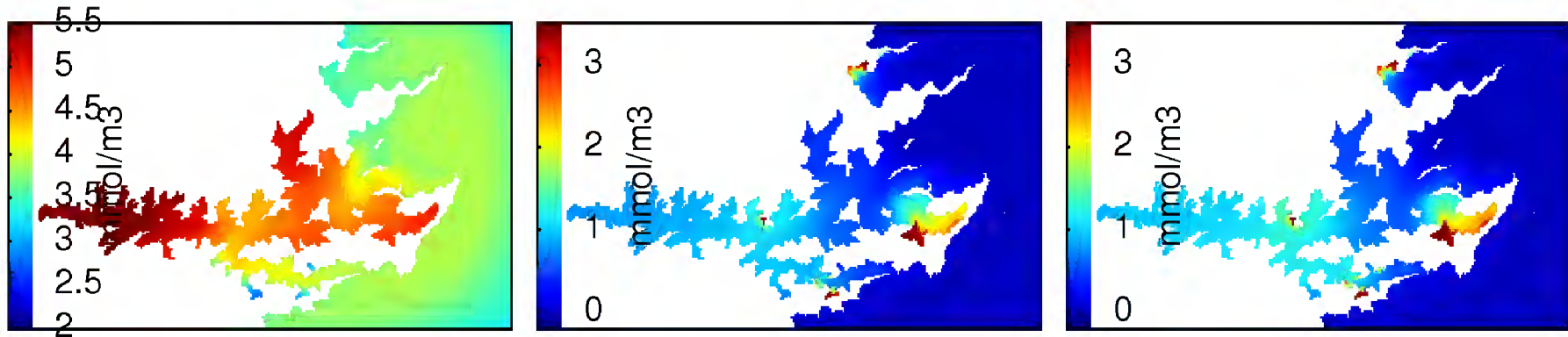
```



```

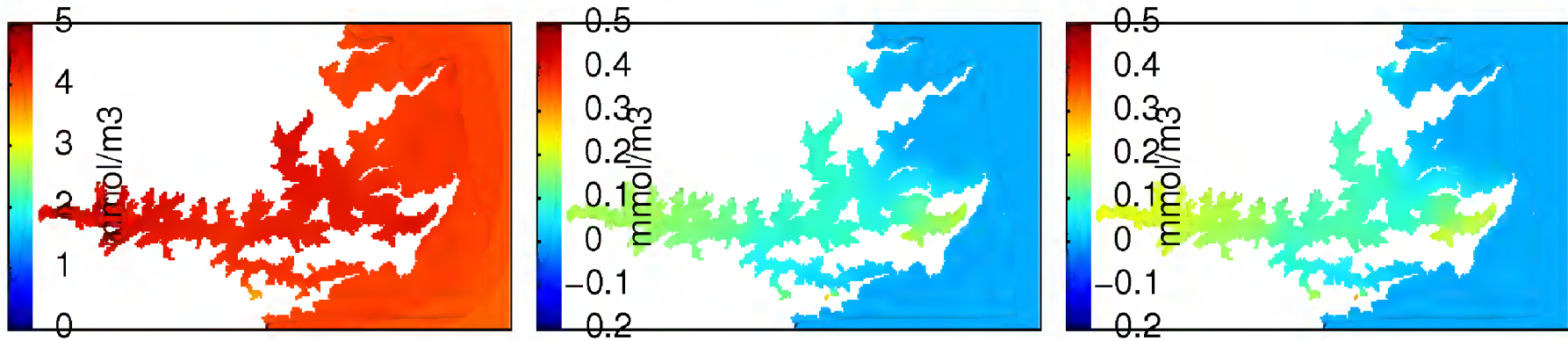
+NH4 in layer 20
/mnt/projects_welwfs07/MDC13301/Working/niall/hpcf/R
/mnt/projects_welwfs07/MDC13301/Working/Mark/Data/Model output/run18/2005+2700-bio-v9/roms_avg_0001.nc
/mnt/projects_welwfs07/MDC13301/Working/Mark/Data/Model output/run18/2005+2700-bio-v9-existing/roms_avg_0001.nc
/mnt/projects_welwfs07/MDC13301/Working/Mark/Data/Model output/run18/2005+2700-bio-v9-existing+new/roms_avg_0001.nc
time range: 262850400 273391200
[log(conc)?, log(change)]=[ FALSE , FALSE ] is.rel.conc= FALSE
n.sample= 245

```



+NH4+NO3+SDetN+LDetN+phytoplankton+zooplankton in layer 20  
 /mnt/projects\_welwfs07/MDC13301/Working/niall/hpcf/R

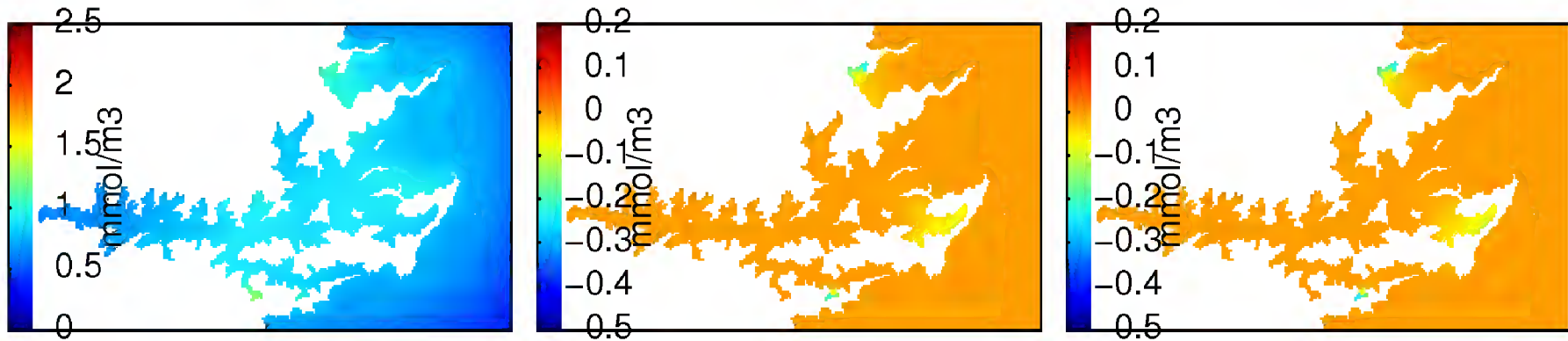
/mnt/projects\_welwfs07/MDC13301/Working/Mark/Data/Model output/run18/2005+2700-bio-v9/roms\_avg\_0001.nc  
 /mnt/projects\_welwfs07/MDC13301/Working/Mark/Data/Model output/run18/2005+2700-bio-v9-existing/roms\_avg\_0001.nc  
 /mnt/projects\_welwfs07/MDC13301/Working/Mark/Data/Model output/run18/2005+2700-bio-v9-existing+new/roms\_avg\_0001.nc  
 time range: 262850400 273391200  
 [log(conc)?, log(change)]=[ FALSE , FALSE ] is.rel.conc= FALSE  
 n.sample= 245



```

+NO3 in layer 20
/mnt/projects_welwfs07/MDC13301/Working/niall/hpcf/R
/mnt/projects_welwfs07/MDC13301/Working/Mark/Data/Model output/run18/2005+2700-bio-v9/roms_avg_0001.nc
/mnt/projects_welwfs07/MDC13301/Working/Mark/Data/Model output/run18/2005+2700-bio-v9-existing/roms_avg_0001.nc
/mnt/projects_welwfs07/MDC13301/Working/Mark/Data/Model output/run18/2005+2700-bio-v9-existing+new/roms_avg_0001.nc
time range: 262850400 273391200
[log(conc)?, log(change)]=[ FALSE , FALSE ] is.rel.conc= FALSE
n.sample= 245

```



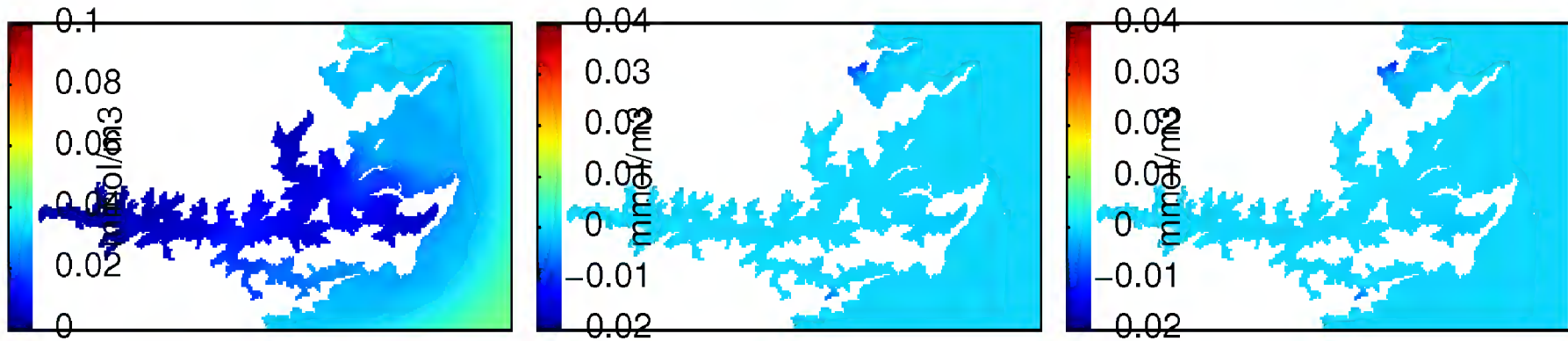
```

+SdetritusN in layer 20
/mnt/projects_welwfs07/MDC13301/Working/niall/hpcf/R

/mnt/projects_welwfs07/MDC13301/Working/Mark/Data/Model output/run18/2005+2700-bio-v9/roms_avg_0001.nc
/mnt/projects_welwfs07/MDC13301/Working/Mark/Data/Model output/run18/2005+2700-bio-v9-existing/roms_avg_0001.nc
/mnt/projects_welwfs07/MDC13301/Working/Mark/Data/Model output/run18/2005+2700-bio-v9-existing+new/roms_avg_0001.nc
time range: 262850400 273391200
[log(conc)?, log(change)]=[ FALSE , FALSE ] is.rel.conc= FALSE
n.sample= 245

```





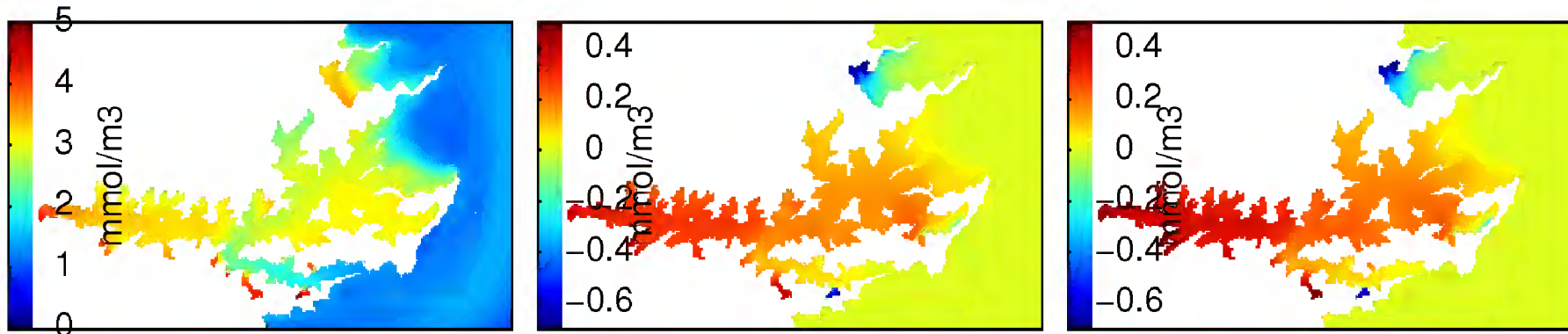
```

+zooplankton in layer 20
/mnt/projects_welwfs07/MDC13301/Working/niall/hpcf/R

/mnt/projects_welwfs07/MDC13301/Working/Mark/Data/Model output/run18/2005+2700-bio-v9/roms_avg_0001.nc
/mnt/projects_welwfs07/MDC13301/Working/Mark/Data/Model output/run18/2005+2700-bio-v9-existing/roms_avg_0001.nc
/mnt/projects_welwfs07/MDC13301/Working/Mark/Data/Model output/run18/2005+2700-bio-v9-existing+new/roms_avg_0001.nc
time range: 262850400 273391200
[log(conc)?, log(change)]=[ FALSE , FALSE ] is.rel.conc= FALSE
n.sample= 245

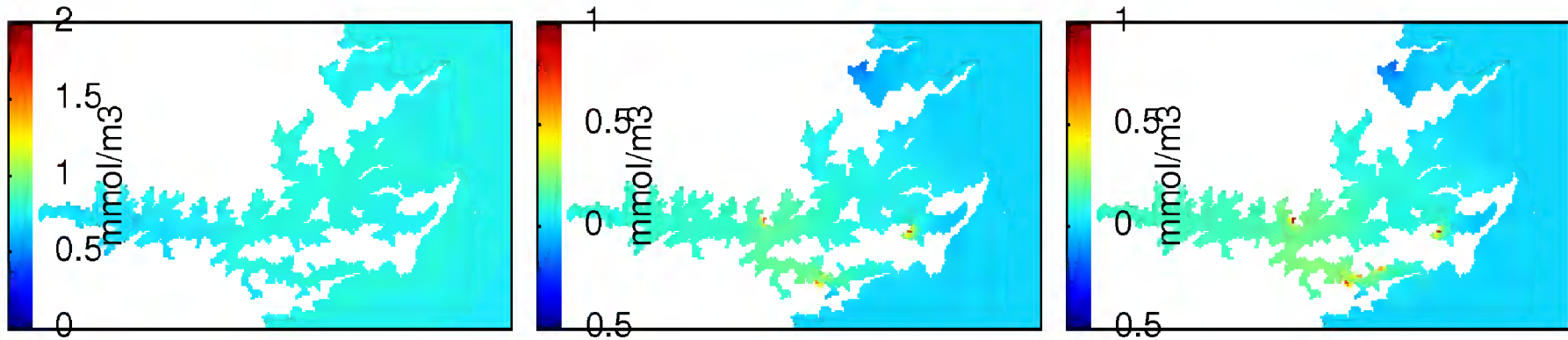
```

Summer



```
+chlorophyll in layer 20
/mnt/projects_welwfs07/MDC13301/Working/niall/hpcf/R

/mnt/projects_welwfs07/MDC13301/Working/Mark/Data/Model output/run18/2005+2700-bio-v9/roms_avg_0001.nc
/mnt/projects_welwfs07/MDC13301/Working/Mark/Data/Model output/run18/2005+2700-bio-v9-existing/roms_avg_0001.nc
/mnt/projects_welwfs07/MDC13301/Working/Mark/Data/Model output/run18/2005+2700-bio-v9-existing+new/roms_avg_0001.nc
time range: 243151200 257493600
[log(conc)?, log(change)]=[ FALSE , FALSE ] is.rel.conc= FALSE
n.sample= 333
```

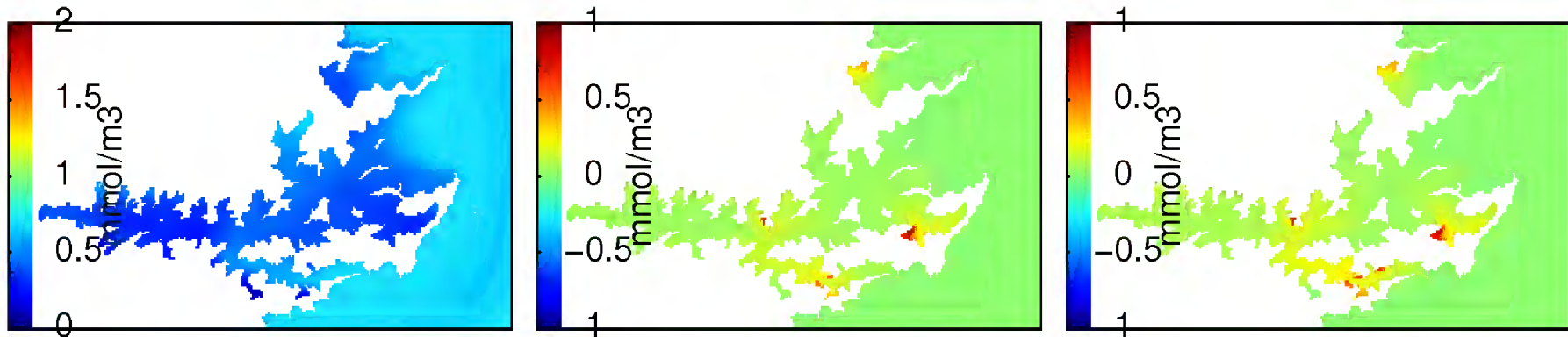


```

+LdetritusN in layer 20
/mnt/projects_welwfs07/MDC13301/Working/niall/hpcf/R

/mnt/projects_welwfs07/MDC13301/Working/Mark/Data/Model output/run18/2005+2700-bio-v9/roms_avg_0001.nc
/mnt/projects_welwfs07/MDC13301/Working/Mark/Data/Model output/run18/2005+2700-bio-v9-existing/roms_avg_0001.nc
/mnt/projects_welwfs07/MDC13301/Working/Mark/Data/Model output/run18/2005+2700-bio-v9-existing+new/roms_avg_0001.nc
time range: 243151200 257493600
[log(conc)?, log(change)]=[ FALSE , FALSE ] is.rel.conc= FALSE
n.sample= 333

```

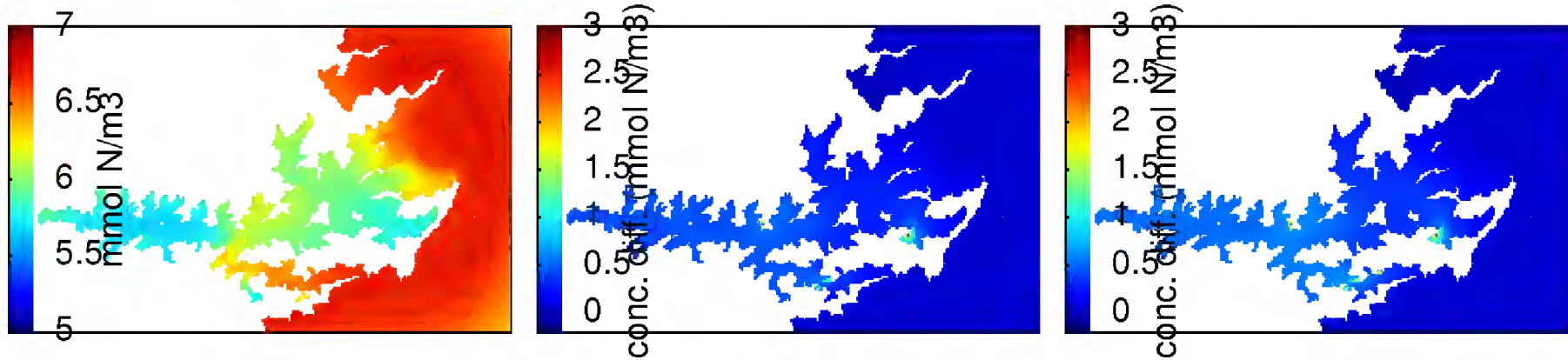


```

+NH4 in layer 20
/mnt/projects_welwfs07/MDC13301/Working/niall/hpcf/R

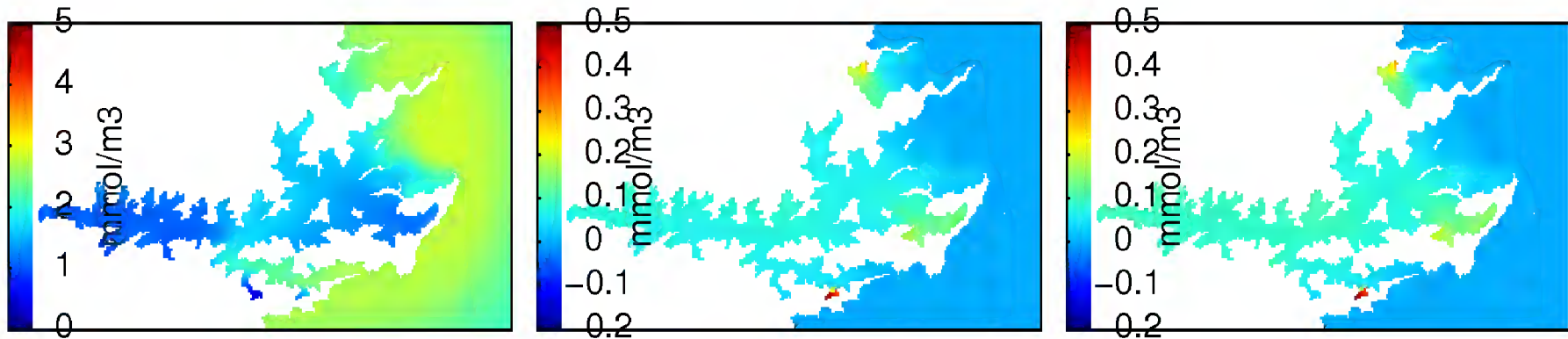
/mnt/projects_welwfs07/MDC13301/Working/Mark/Data/Model output/run18/2005+2700-bio-v9/roms_avg_0001.nc
/mnt/projects_welwfs07/MDC13301/Working/Mark/Data/Model output/run18/2005+2700-bio-v9-existing/roms_avg_0001.nc
/mnt/projects_welwfs07/MDC13301/Working/Mark/Data/Model output/run18/2005+2700-bio-v9-existing+new/roms_avg_0001.nc
time range: 243151200 257493600
[log(conc)?, log(change)]=[ FALSE , FALSE ] is.rel.conc= FALSE
n.sample= 333

```



+NH4+NO3+SdetritusN+LdetritusN+phytoplankton+zooplankton in layer 20  
 /mnt/projects\_welwfs07/MDC13301/Working/niall/hpcf/R

/mnt/projects\_welwfs07/MDC13301/Working/Mark/Data/Model output/run18/2005+2700-bio-v9/roms\_avg\_0001.nc  
 /mnt/projects\_welwfs07/MDC13301/Working/Mark/Data/Model output/run18/2005+2700-bio-v9-existing/roms\_avg\_0001.nc  
 /mnt/projects\_welwfs07/MDC13301/Working/Mark/Data/Model output/run18/2005+2700-bio-v9-existing+new/roms\_avg\_0001.nc  
 time range: 243151200 257493600  
 [log(conc)?, log(change)]=[ FALSE , FALSE ] is.rel.conc= FALSE  
 n.sample= 333

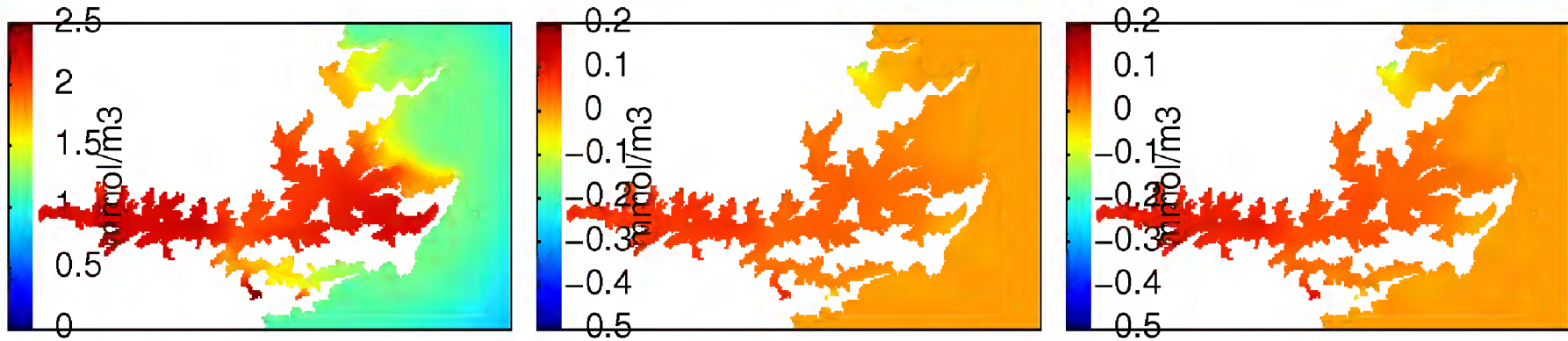


```

+NO3 in layer 20
/mnt/projects_welwfs07/MDC13301/Working/niall/hpcf/R

/mnt/projects_welwfs07/MDC13301/Working/Mark/Data/Model output/run18/2005+2700-bio-v9/roms_avg_0001.nc
/mnt/projects_welwfs07/MDC13301/Working/Mark/Data/Model output/run18/2005+2700-bio-v9-existing/roms_avg_0001.nc
/mnt/projects_welwfs07/MDC13301/Working/Mark/Data/Model output/run18/2005+2700-bio-v9-existing+new/roms_avg_0001.nc
time range: 243151200 257493600
[log(conc)?, log(change)]=[ FALSE , FALSE ] is.rel.conc= FALSE
n.sample= 333

```

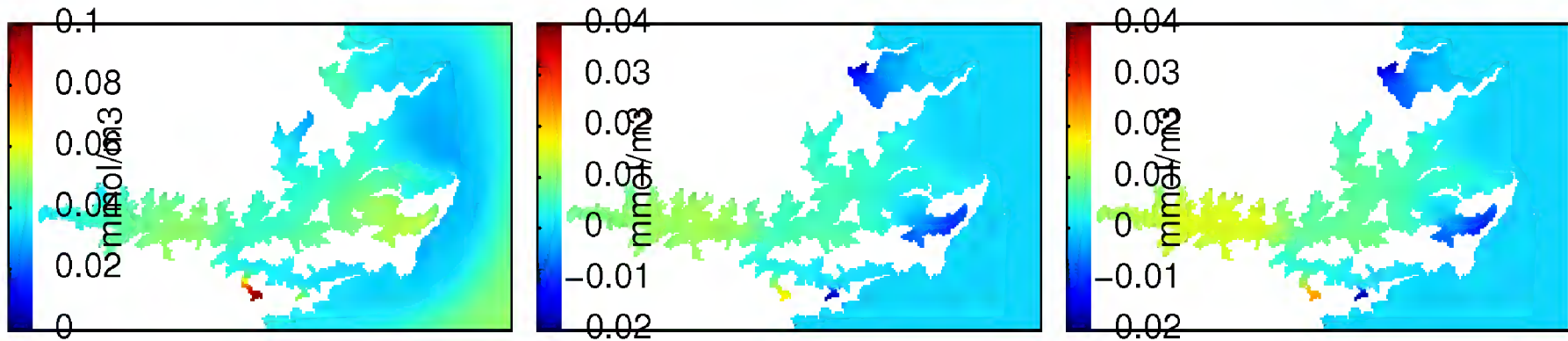


```

+SdetritusN in layer 20
/mnt/projects_welwfs07/MDC13301/Working/niall/hpcf/R

/mnt/projects_welwfs07/MDC13301/Working/Mark/Data/Model output/run18/2005+2700-bio-v9/roms_avg_0001.nc
/mnt/projects_welwfs07/MDC13301/Working/Mark/Data/Model output/run18/2005+2700-bio-v9-existing/roms_avg_0001.nc
/mnt/projects_welwfs07/MDC13301/Working/Mark/Data/Model output/run18/2005+2700-bio-v9-existing+new/roms_avg_0001.nc
time range: 243151200 257493600
[log(conc)?, log(change)]=[ FALSE , FALSE ] is.rel.conc= FALSE
n.sample= 333

```



```

+zooplankton in layer 20
/mnt/projects_welwfs07/MDC13301/Working/niall/hpcf/R

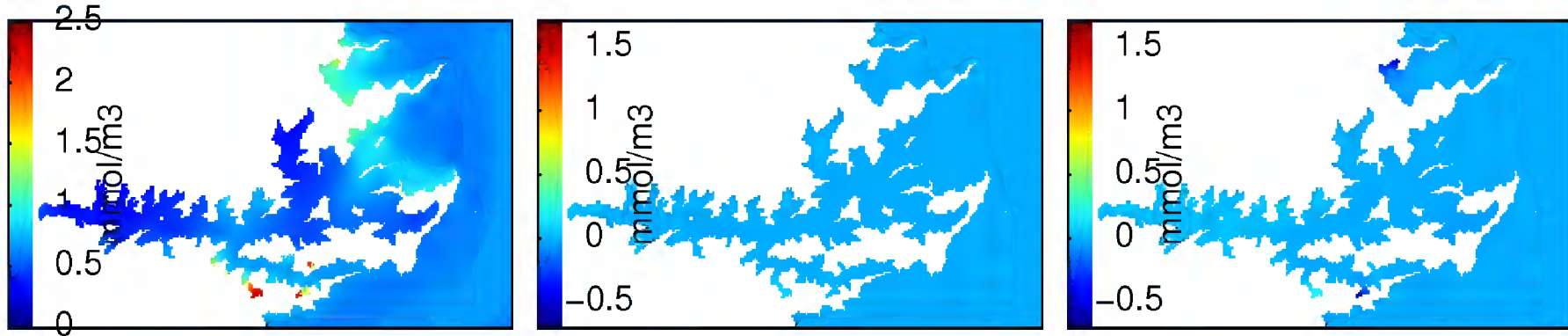
/mnt/projects_welwfs07/MDC13301/Working/Mark/Data/Model output/run18/2005+2700-bio-v9/roms_avg_0001.nc
/mnt/projects_welwfs07/MDC13301/Working/Mark/Data/Model output/run18/2005+2700-bio-v9-existing/roms_avg_0001.nc
/mnt/projects_welwfs07/MDC13301/Working/Mark/Data/Model output/run18/2005+2700-bio-v9-existing+new/roms_avg_0001.nc
time range: 243151200 257493600
[log(conc)?, log(change)]=[ FALSE , FALSE ] is.rel.conc= FALSE
n.sample= 333

```

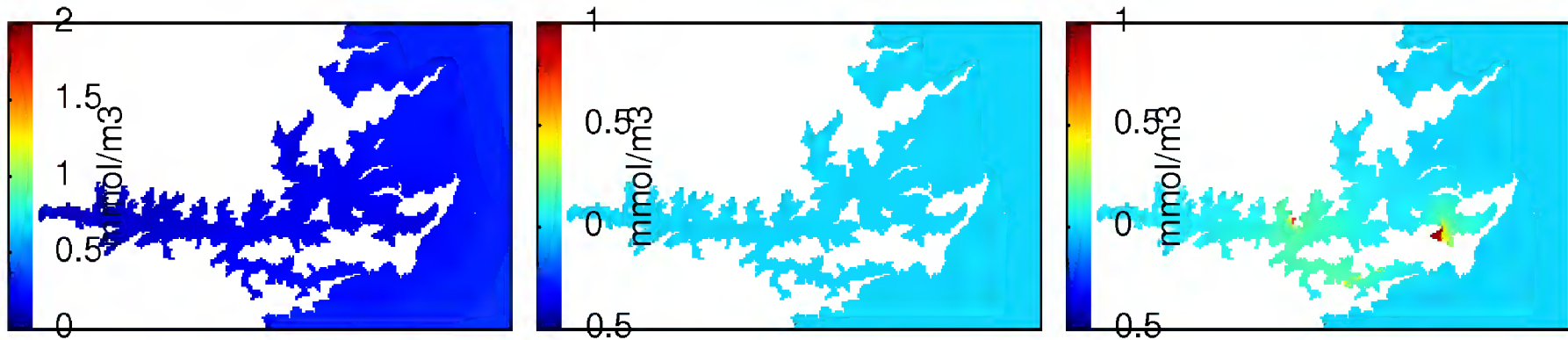


## Comparison of *no farms*, *existing farms* and *approved farms* (without denitrification)

Winter



```
+chlorophyll in layer 20
/mnt/projects_welwfs07/MDC13301/Working/niall/hpcf/R
/mnt/projects_welwfs07/MDC13301/Working/Mark/Data/Model output/run18/2005+2700-bio-v9/roms_avg_0001.nc
/mnt/projects_welwfs07/MDC13301/Working/Mark/Data/Model output/run18/2005+2700-bio-v9nd/roms_avg_0001.nc
/mnt/projects_welwfs07/MDC13301/Working/Mark/Data/Model output/run18/2005+2700-bio-v9nd-existing+new/roms_avg_0001.nc
time range: 262850400 273391200
[log(conc)?, log(change)]=[ FALSE , FALSE ] is.rel.conc= FALSE
n.sample= 245
```

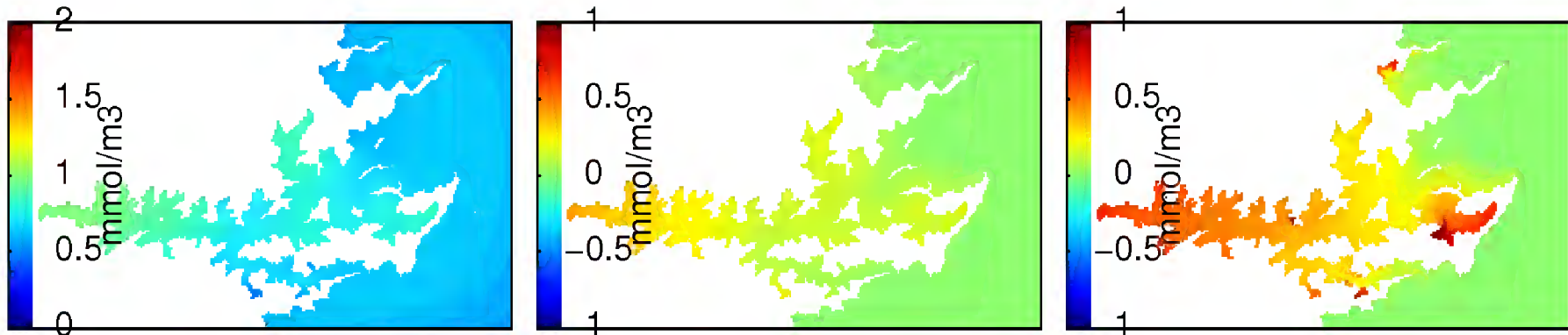


```

+LdetritusN in layer 20
/mnt/projects_welwfs07/MDC13301/Working/niall/hpcf/R

/mnt/projects_welwfs07/MDC13301/Working/Mark/Data/Model output/run18/2005+2700-bio-v9/roms_avg_0001.nc
/mnt/projects_welwfs07/MDC13301/Working/Mark/Data/Model output/run18/2005+2700-bio-v9nd/roms_avg_0001.nc
/mnt/projects_welwfs07/MDC13301/Working/Mark/Data/Model output/run18/2005+2700-bio-v9nd-existing+new/roms_avg_0001.nc
time range: 262850400 273391200
[log(conc)?, log(change)]=[ FALSE , FALSE ] is.rel.conc= FALSE
n.sample= 245

```

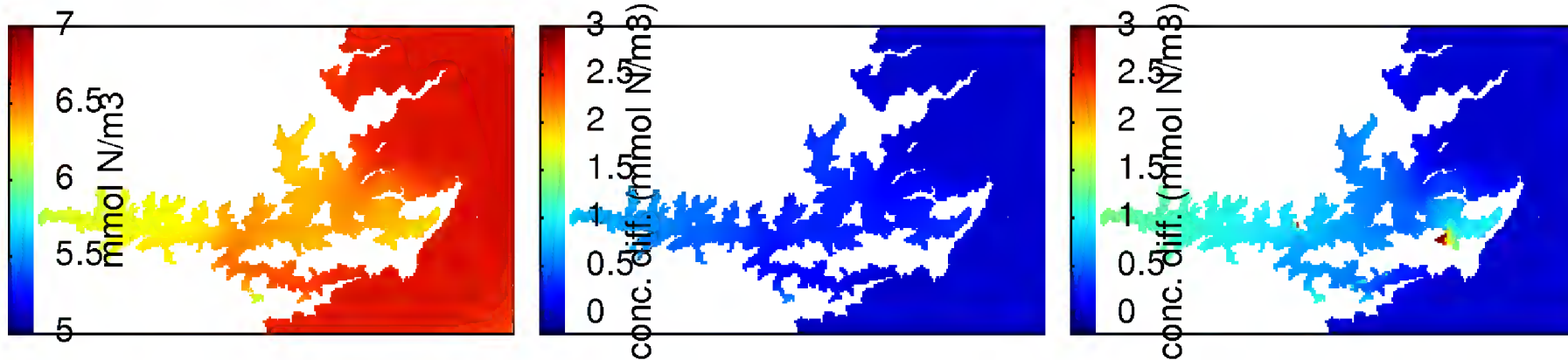


```

+NH4 in layer 20
/mnt/projects_welwfs07/MDC13301/Working/niall/hpcf/R

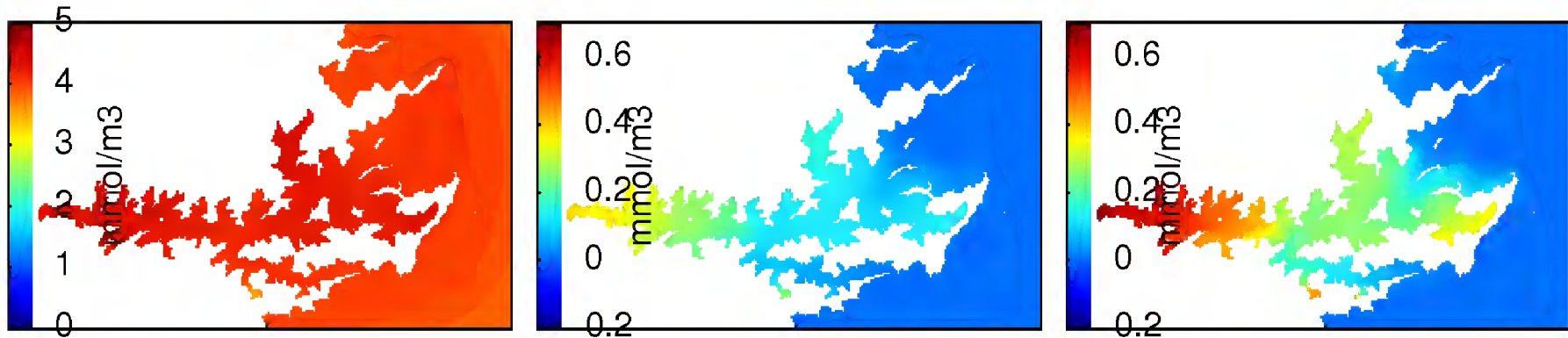
/mnt/projects_welwfs07/MDC13301/Working/Mark/Data/Model output/run18/2005+2700-bio-v9/roms_avg_0001.nc
/mnt/projects_welwfs07/MDC13301/Working/Mark/Data/Model output/run18/2005+2700-bio-v9nd/roms_avg_0001.nc
/mnt/projects_welwfs07/MDC13301/Working/Mark/Data/Model output/run18/2005+2700-bio-v9nd-existing+new/roms_avg_0001.nc
time range: 262850400 273391200
[log(conc)?, log(change)]=[ FALSE , FALSE ] is.rel.conc= FALSE
n.sample= 245

```



```
+NH4+NO3+SdetritusN+LdetritusN+phytoplankton+zooplankton in layer 20
/mnt/projects_welwfs07/MDC13301/Working/niall/hpcf/R
```

```
/mnt/projects_welwfs07/MDC13301/Working/Mark/Data/Model output/run18/2005+2700-bio-v9/roms_avg_0001.nc
/mnt/projects_welwfs07/MDC13301/Working/Mark/Data/Model output/run18/2005+2700-bio-v9nd/roms_avg_0001.nc
/mnt/projects_welwfs07/MDC13301/Working/Mark/Data/Model output/run18/2005+2700-bio-v9nd-existing+new/roms_avg_0001.nc
time range: 262850400 273391200
[log(conc)?, log(change)]=[ FALSE , FALSE ] is.rel.conc= FALSE
n.sample= 245
```

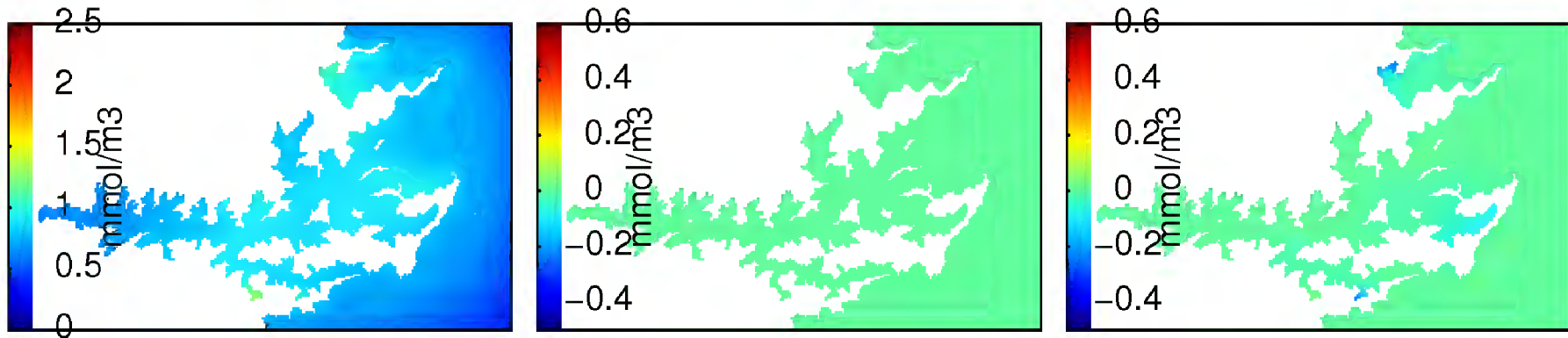


```

+NO3 in layer 20
/mnt/projects_welwfs07/MDC13301/Working/niall/hpcf/R

/mnt/projects_welwfs07/MDC13301/Working/Mark/Data/Model output/run18/2005+2700-bio-v9/roms_avg_0001.nc
/mnt/projects_welwfs07/MDC13301/Working/Mark/Data/Model output/run18/2005+2700-bio-v9nd/roms_avg_0001.nc
/mnt/projects_welwfs07/MDC13301/Working/Mark/Data/Model output/run18/2005+2700-bio-v9nd-existing+new/roms_avg_0001.nc
time range: 262850400 273391200
[log(conc)?, log(change)]=[ FALSE , FALSE ] is.rel.conc= FALSE
n.sample= 245

```

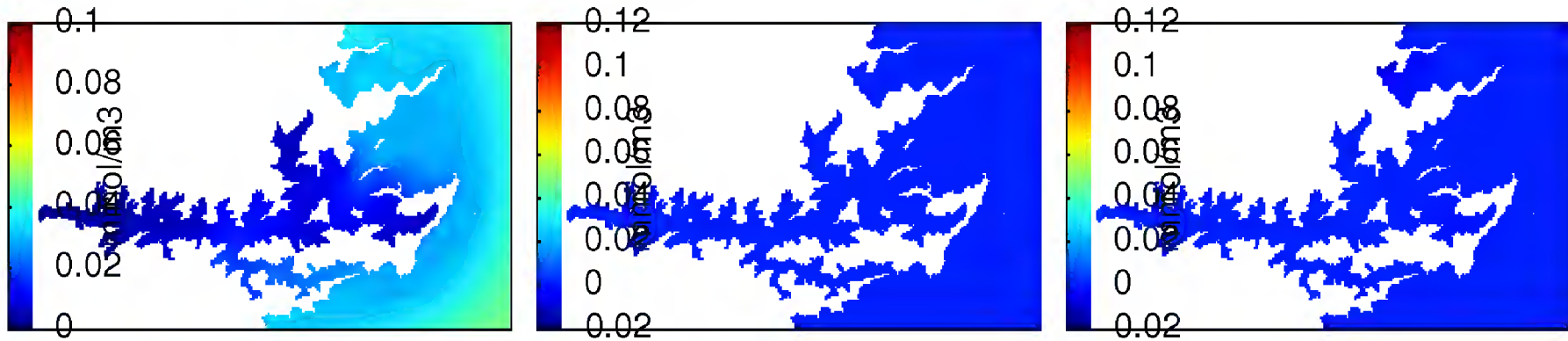


```

+SdetritusN in layer 20
/mnt/projects_welwfs07/MDC13301/Working/niall/hpcf/R

/mnt/projects_welwfs07/MDC13301/Working/Mark/Data/Model output/run18/2005+2700-bio-v9/roms_avg_0001.nc
/mnt/projects_welwfs07/MDC13301/Working/Mark/Data/Model output/run18/2005+2700-bio-v9nd/roms_avg_0001.nc
/mnt/projects_welwfs07/MDC13301/Working/Mark/Data/Model output/run18/2005+2700-bio-v9nd-existing+new/roms_avg_0001.nc
time range: 262850400 273391200
[log(conc)?, log(change)]=[ FALSE , FALSE ] is.rel.conc= FALSE
n.sample= 245

```



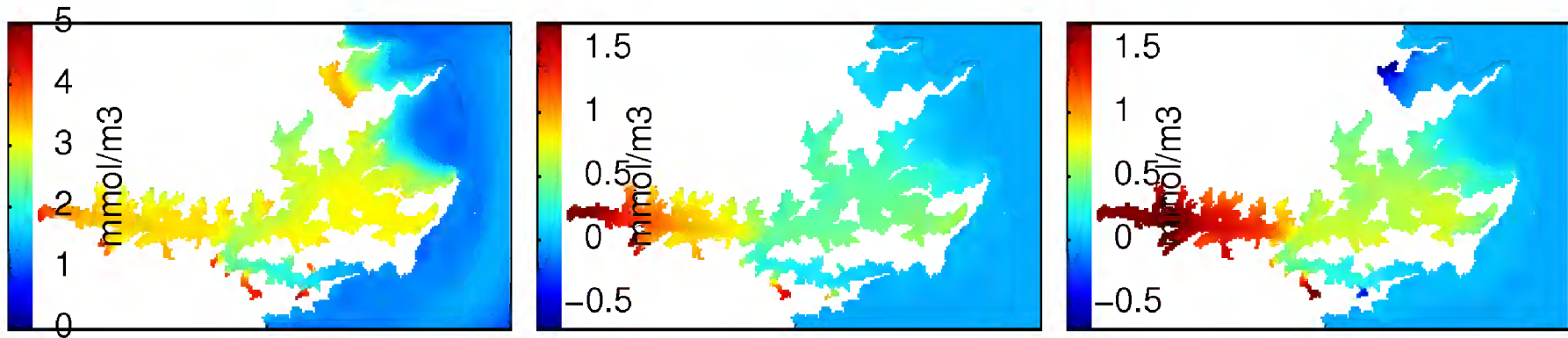
```

+zooplankton in layer 20
/mnt/projects_welwfs07/MDC13301/Working/niall/hpcf/R

/mnt/projects_welwfs07/MDC13301/Working/Mark/Data/Model output/run18/2005+2700-bio-v9/roms_avg_0001.nc
/mnt/projects_welwfs07/MDC13301/Working/Mark/Data/Model output/run18/2005+2700-bio-v9nd/roms_avg_0001.nc
/mnt/projects_welwfs07/MDC13301/Working/Mark/Data/Model output/run18/2005+2700-bio-v9nd-existing+new/roms_avg_0001.nc
time range: 262850400 273391200
[log(conc)?, log(change)]=[ FALSE , FALSE ] is.rel.conc= FALSE
n.sample= 245

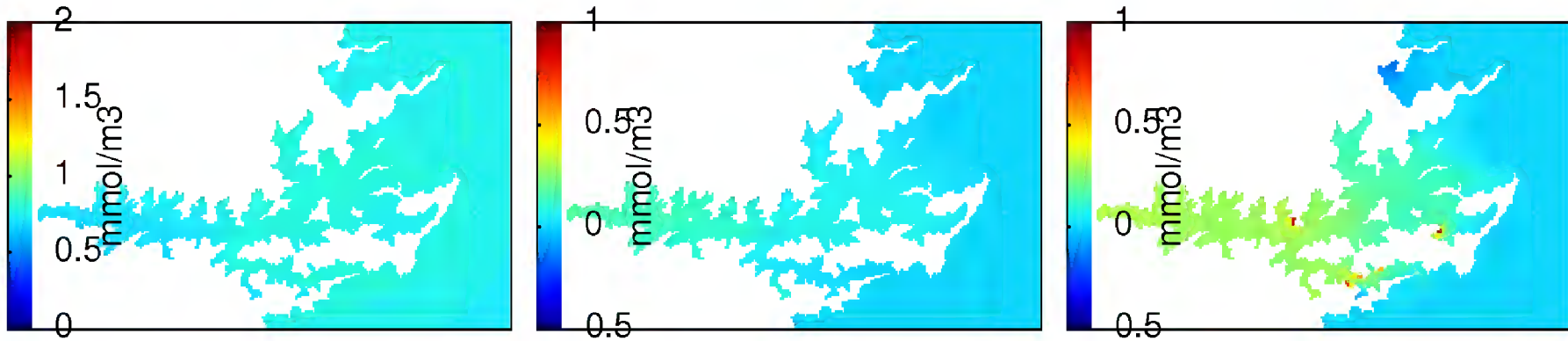
```

Summer



```
+chlorophyll in layer 20
/mnt/projects_welwfs07/MDC13301/Working/niall/hpcf/R
/mnt/projects_welwfs07/MDC13301/Working/Mark/Data/Model output/run18/2005+2700-bio-v9/roms_avg_0001.nc
/mnt/projects_welwfs07/MDC13301/Working/Mark/Data/Model output/run18/2005+2700-bio-v9nd/roms_avg_0001.nc
/mnt/projects_welwfs07/MDC13301/Working/Mark/Data/Model output/run18/2005+2700-bio-v9nd-existing+new/roms_avg_0001.nc
time range: 243151200 257493600
[log(conc)?, log(change)]=[ FALSE , FALSE ] is.rel.conc= FALSE
n.sample= 333
```



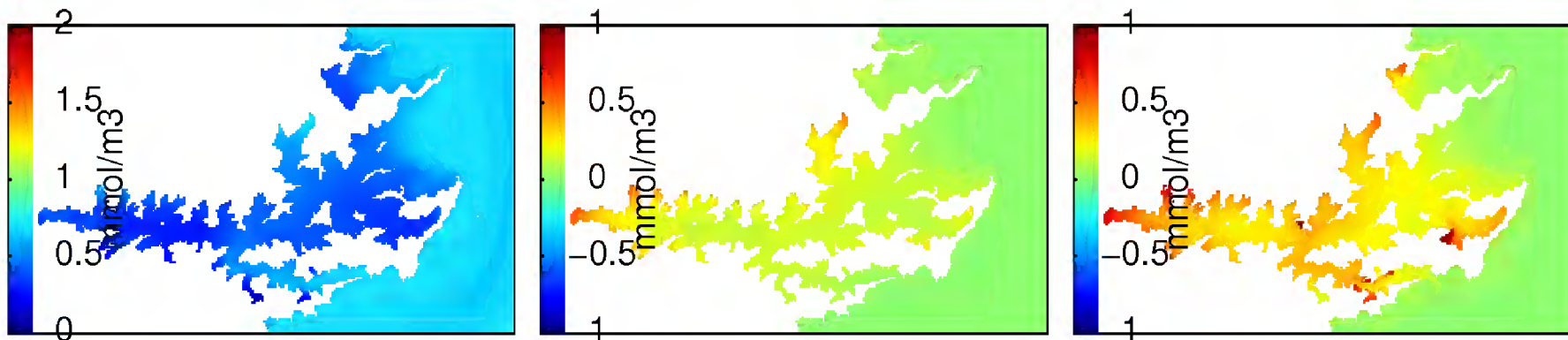


```

+LdetritusN in layer 20
/mnt/projects_welwfs07/MDC13301/Working/niall/hpcf/R

/mnt/projects_welwfs07/MDC13301/Working/Mark/Data/Model output/run18/2005+2700-bio-v9/roms_avg_0001.nc
/mnt/projects_welwfs07/MDC13301/Working/Mark/Data/Model output/run18/2005+2700-bio-v9nd/roms_avg_0001.nc
/mnt/projects_welwfs07/MDC13301/Working/Mark/Data/Model output/run18/2005+2700-bio-v9nd-existing+new/roms_avg_0001.nc
time range: 243151200 257493600
[log(conc)?, log(change)]=[ FALSE , FALSE ] is.rel.conc= FALSE
n.sample= 333

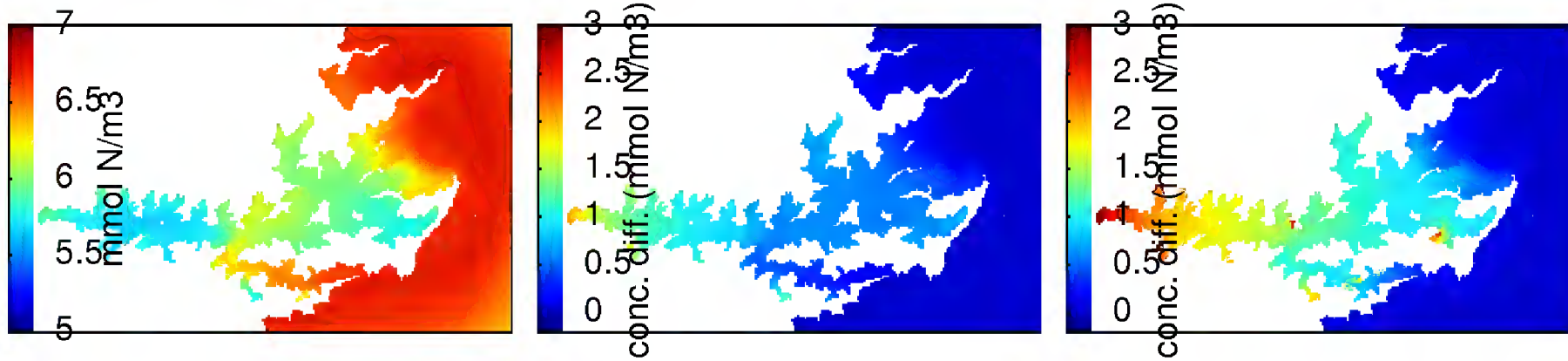
```



```

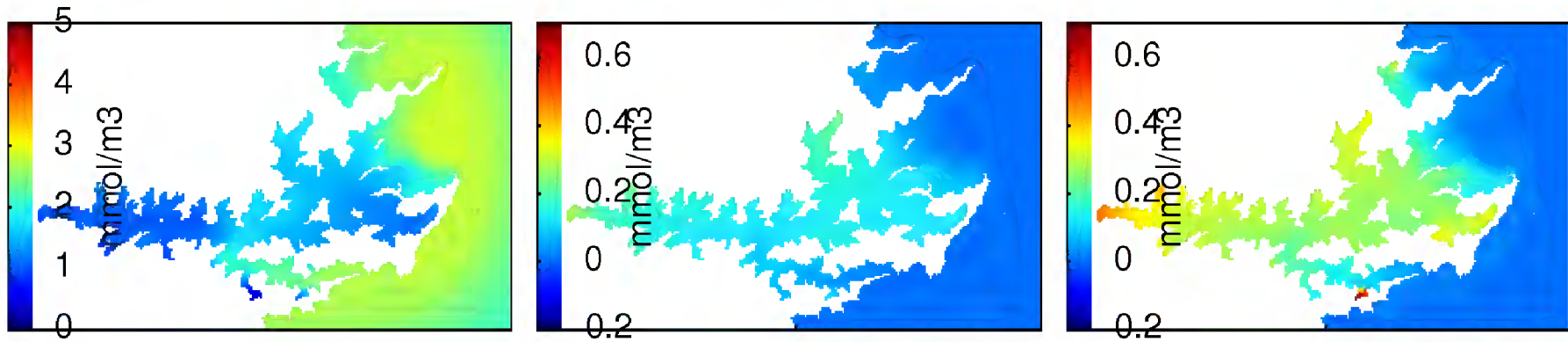
+NH4 in layer 20
/mnt/projects_welwfs07/MDC13301/Working/niall/hpct/R
/mnt/projects_welwfs07/MDC13301/Working/Mark/Data/Model output/run18/2005+2700-bio-v9/roms_avg_0001.nc
/mnt/projects_welwfs07/MDC13301/Working/Mark/Data/Model output/run18/2005+2700-bio-v9nd/roms_avg_0001.nc
/mnt/projects_welwfs07/MDC13301/Working/Mark/Data/Model output/run18/2005+2700-bio-v9nd-existing+new/roms_avg_0001.nc
time range: 243151200 257493600
[log(conc)?, log(change)]=[ FALSE , FALSE ] is.rel.conc= FALSE
n.sample= 333

```



+NH4+NO3+SdetritusN+LdetritusN+phytoplankton+zooplankton in layer 20  
 /mnt/projects\_welwfs07/MDC13301/Working/niall/hpcf/R

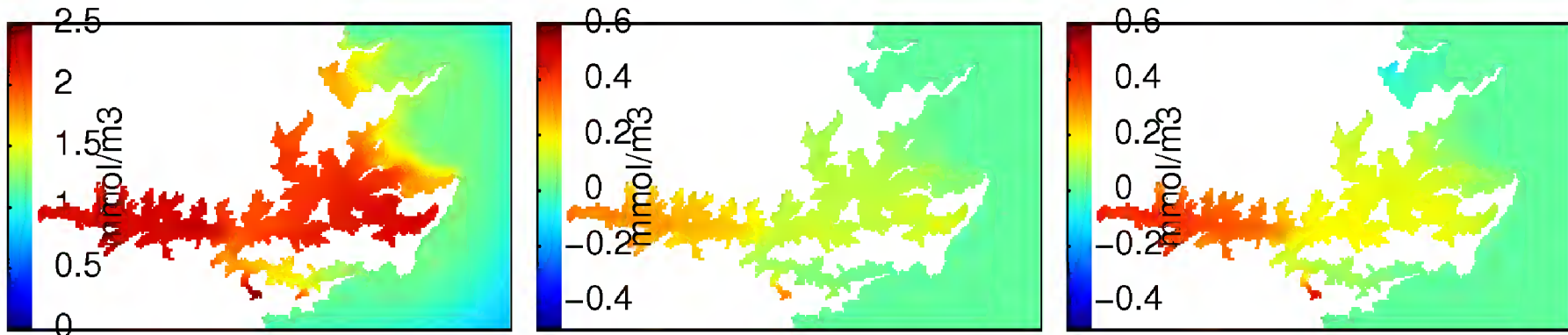
/mnt/projects\_welwfs07/MDC13301/Working/Mark/Data/Model output/run18/2005+2700-bio-v9/roms\_avg\_0001.nc  
 /mnt/projects\_welwfs07/MDC13301/Working/Mark/Data/Model output/run18/2005+2700-bio-v9nd/roms\_avg\_0001.nc  
 /mnt/projects\_welwfs07/MDC13301/Working/Mark/Data/Model output/run18/2005+2700-bio-v9nd-existing+new/roms\_avg\_0001.nc  
 time range: 243151200 257493600  
 [log(conc)?, log(change)]=[ FALSE , FALSE ] is.rel.conc= FALSE  
 n.sample= 333



```

+NO3 in layer 20
/mnt/projects_welwfs07/MDC13301/Working/niall/hpcf/R
/mnt/projects_welwfs07/MDC13301/Working/Mark/Data/Model output/run18/2005+2700-bio-v9/roms_avg_0001.nc
/mnt/projects_welwfs07/MDC13301/Working/Mark/Data/Model output/run18/2005+2700-bio-v9nd/roms_avg_0001.nc
/mnt/projects_welwfs07/MDC13301/Working/Mark/Data/Model output/run18/2005+2700-bio-v9nd-existing+new/roms_avg_0001.nc
time range: 243151200 257493600
[log(conc)?, log(change)]=[ FALSE , FALSE ] is.rel.conc= FALSE
n.sample= 333

```

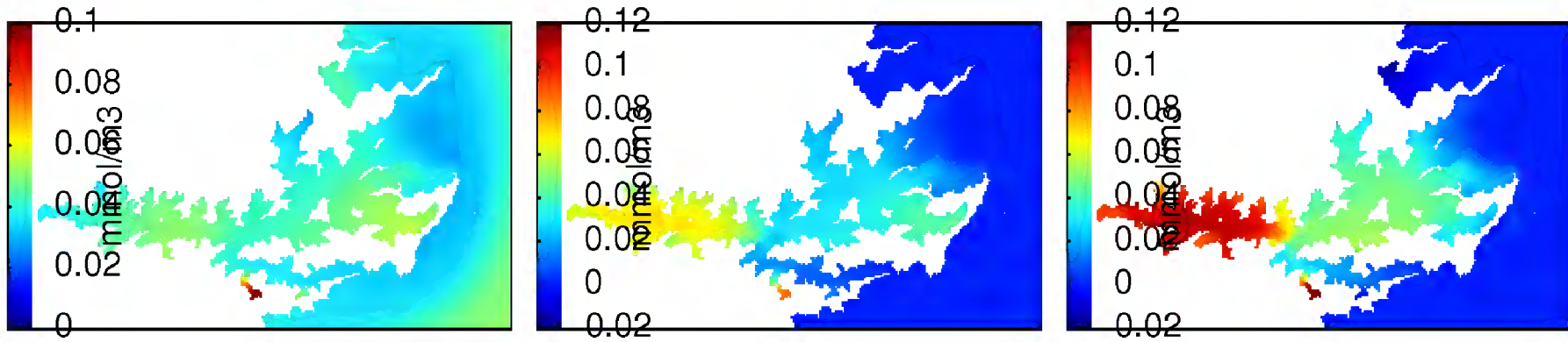


```

+SdetritusN in layer 20
/mnt/projects_welwfs07/MDC13301/Working/niall/hpcf/R

/mnt/projects_welwfs07/MDC13301/Working/Mark/Data/Model output/run18/2005+2700-bio-v9/roms_avg_0001.nc
/mnt/projects_welwfs07/MDC13301/Working/Mark/Data/Model output/run18/2005+2700-bio-v9nd/roms_avg_0001.nc
/mnt/projects_welwfs07/MDC13301/Working/Mark/Data/Model output/run18/2005+2700-bio-v9nd-existing+new/roms_avg_0001.nc
time range: 243151200 257493600
[log(conc)?, log(change)]=[ FALSE , FALSE ] is.rel.conc= FALSE
n.sample= 333

```



```

+zooplankton in layer 20
/mnt/projects_welwfs07/MDC13301/Working/niall/hpcf/R

/mnt/projects_welwfs07/MDC13301/Working/Mark/Data/Model output/run18/2005+2700-bio-v9/roms_avg_0001.nc
/mnt/projects_welwfs07/MDC13301/Working/Mark/Data/Model output/run18/2005+2700-bio-v9nd/roms_avg_0001.nc
/mnt/projects_welwfs07/MDC13301/Working/Mark/Data/Model output/run18/2005+2700-bio-v9nd-existing+new/roms_avg_0001.nc
time range: 243151200 257493600
[log(conc)?, log(change)]=[ FALSE , FALSE ] is.rel.conc= FALSE
n.sample= 333

```

